

A NEW TECHNIQUE FOR CALIBRATING STRAPDOWN  
INERTIAL REFERENCE UNITS WITH LARGE ERRORS

by

HOWARD MUSOFF

B.E.E., City College of New York  
(1960)

M.S., Northeastern University  
(1966)

SUBMITTED IN PARTIAL FULFILLMENT  
OF THE REQUIREMENTS FOR THE  
DEGREE OF DOCTOR OF SCIENCE  
IN INSTRUMENTATION

at the

MASSACHUSETTS INSTITUTE OF TECHNOLOGY

February, 1979

Signature of Author \_\_\_\_\_  
Department of Aeronautics & Astronautics

Certified by \_\_\_\_\_ Thesis Supervisor

Certified by \_\_\_\_\_ Thesis Supervisor

Approved by \_\_\_\_\_ Technical Supervisor, CSDL

Accepted by \_\_\_\_\_ Chairman, Departmental Graduate Committee  
ARCHIVES

Massachusetts Institute of Technology

1979

A NEW TECHNIQUE FOR CALIBRATING STRAPDOWN  
INERTIAL REFERENCE UNITS WITH LARGE ERRORS

by

Howard Musoff

Submitted to the Department of  
Aeronautics and Astronautics on November 7, 1978  
in partial fulfillment of the requirements for  
the degree of Doctor of Science

ABSTRACT

A set of techniques is originated for calibration of the inertial reference unit of a Low Cost Inertial Guidance System (LCIGS). Very large instrument error parameters are estimated without the need for external precise knowledge of the system orientation with respect to the earth rate and gravity vectors. This is made possible by utilizing the known non-linear relations between the components of earth rate and gravity sensed by the instruments and the respective magnitudes of earth rate and gravity at the system test location in addition to the known relations between the error parameters and measurements to allow solution of the parameters from complete sets of simultaneous equations. A linear extrapolation method for reducing accelerometer quantization in order to speed up the calibration process is also presented.

Thesis Supervisor: Wallace E. VanderVelde  
Title: Professor of Aeronautics and  
Astronautics

Thesis Supervisor: Walter M. Hollister  
Title: Associate Professor of  
Aeronautics and Astronautics

Thesis Supervisor: Ricahrd A. McKern  
Title: Inertial System Analysis Section  
Chief  
Charles Stark Draper Laboratory

## ACKNOWLEDGMENT

I would like to express my gratitude to Prof. Wallace VanderVelde, my Doctoral Committee chairman, for his invaluable guidance throughout the research and writing of this thesis. I am also grateful to Mr. Richard McKern, a member of the Doctoral Committee and my technical supervisor at the Draper Laboratory, for his important advice. My appreciation is extended to Prof. Walter Hollister, also a member of my Doctoral Committee, for his continuing encouragement during the writing of this thesis.

I would like to thank a number of people at the Draper Laboratory whose assistance, advice, and technical knowledge helped make this thesis possible: Mr. Jerold Gilmore originally suggested the topic of research.

I had numerous discussions with Mr. Tom Thorvaldsen about various topics in numerical analysis. Mr. Thorvaldsen also provided assistance with the inertial navigation simulation program used in obtaining all of the numerical results.

Mr. Harry McOuat did an outstanding job of programming all of the calibration equations and procedures used in the numerical simulations.

Mr. George Bukow provided important information about the LCIGS accelerometers and their utilization in the inertial reference unit.

Mr. Robert Booth provided the needed information about the LCIGS gyros and how they fit into the mechanical configuration of the system.

Messrs. Dan Dunn and Del Pike designed and built the hardware for the accelerometer linear extrapolation method.

Capt. Alan Roberts performed all of the hardware testing of the linear extrapolator.

Messrs. Martin Landey and Roscoe Cooper proof-read the thesis draft and provided editorial assistance.

Ms. Jean Publicover typed the bulk of the thesis. Ms. Patricia Bibby and Ms. Julie Merrell also assisted in the typing.

Mrs. Linda Willy did all of the illustrations.

This report was prepared at The Charles Stark Draper Laboratory, Inc. under Contract F08635-78-C-0306 with the Air Force Armament Laboratory.

Publication of this report does not constitute approval by the Draper Laboratory or the U.S. Air Force of the findings or conclusions contained herein. It is published for the exchange and stimulation of ideas.

### Table of Contents

<u>Chapter No.</u>		<u>Page No.</u>
1	Introduction.....	11
	1.1 Introduction.....	12
	1.2 Low Cost Inertial Guidance Subsystem (LCIGS).....	12
	1.3 Current Calibration Techniques.....	15
	1.4 A New Calibration Technique.....	19
2	Calibration of Accelerometers.....	25
	2.1 Introduction.....	26
	2.2 Accelerometer Alignment.....	28
	2.3 Linearized Solutions for Accelerometer Error Model Coefficients.....	31
	2.4 Solution of the Linear Equation Set.....	36
	2.5 Iterative Solutions.....	45
	2.6 Prediction of Estimation Errors for the LCIGS....	48
3	Accelerometer Quantization.....	54
	3.1 Introduction.....	55
	3.2 Overview of Quantization Effects.....	57
	3.3 A Method for Reducing Accelerometer Quanitzation- Linear Extrapolation.....	68
	3.4 Analysis of Linear Extrapolation Method.....	71
	3.5 Requirement for an External Bias.....	80
4	Alignment and Estimation of Lumped Drifts and Leveling Errors.....	83
	4.1 Introduction.....	84
	4.2 Definition of a Local Level Reference Frame.....	85
	4.3 Derivation of Error Equations.....	92
	4.4 Kalman Filter Equations.....	105
	4.5 Kalman Filter Error Corrections.....	109

6  
Table of Contents (Cont.)

<u>Chapter No.</u>		<u>Page No.</u>
5	Estimation of Gyro Parameters.....	122
	5.1 Introduction.....	123
	5.2 Solution for Static Error Parameters.....	126
	5.3 Convergence of the Iterative Solution.....	140
	5.4 Effect of Gyro Axis Misalignments on Estimated Static Gyro Drift Parameters.....	152
	5.5 Measurement and Estimation Errors for Static Drifts.....	159
	5.6 Solution for Dynamic Error Parameters.....	171
	5.7 Summary of Gyro Calibration Procedure.....	189
6	Numerical Results.....	192
	6.1 Introduction.....	193
	6.2 Calibration of Accelerometers.....	196
	6.3 Linear Extrapolation Method.....	201
	6.4 Newton-Raphson Iterations.....	204
	6.5 Complete Gyro Calibration Simulations.....	211
7	Conclusions and Recommendations.....	227
	7.1 Summary of Thesis Results.....	228
	7.2 Recommendations for Testing Hardware and Test Procedures.....	232
	7.3 Suggested Future Research Topics.....	235

Appendices

2A	Matrix Norms and the Condition Number of a Matrix....	239
2B	The LCIGS Accelerometer Module.....	246
2C	Compensation for Scale Factor Assymetry and Quadratic Errors in the V/F Converter.....	258

## Table of Contents (Cont.)

<u>Appendices</u>		<u>Page No.</u>
5A	Matrices and Norms for Gyro Static Parameter Estimation Procedure.....	262
5B	Solutions for Input Axis Mass Unbalance Drifts.....	275
5C	Perturbations of the Elements of Matrix $C_A$ .....	276
5D	Error Due to Unmodeled Dynamic Drift in a Two State Kalman Filter.....	284
	References.....	286

## Illustrations

<u>Figure No.</u>		<u>Page No.</u>
2.2-1	Definition of System Orthogonal Reference Triad.....	29
2.6-1	Representative Vibration Environment of an Urban Test Laboratory.....	50
3.1-1	Linear Extrapolation Principle.....	56
3.2-1	Gyro Drift Measurement Model.....	58
3.2-2	Drift Measurement Model in the Absence of Accelerometer Quantization.....	58
3.2-3	Drift Measurement Model in the Absence of Gyro Quantization.....	63
3.3-1	Representation of Accelerometer Quantization.....	69
4.2-1	Nominal Static Orientations for Body Reference Axes...	90
4.5-1	Kalman Filter Static Drift Error Corrector for Dynamic Errors.....	114
4.5-2	Kalman Filter Static Drift Error Corrector for Variations in $C_L^{Ba}$ .....	117
4.5-3	Full Correction Procedure for Misalignment Estimates During a Rotation.....	119
4.5-4	Rotation About Body Reference Axis #1.....	121
5.2-1	LCIGS Geometrical Configuration.....	130
5.4-1	Gyro Orthogonal Axes.....	153
5.6-1	Worst Case Rotation.....	186
5.7-1	Block Diagram of Gyro Calibration Procedure.....	190
6.1-1	Simulation Program Block Diagram.....	194
6.3-1	Uniform Probability Function for Non Linear Extrapolation.....	203
2B-1	LCIGS Accelerometer Module Block Diagram.....	246
2B-2	Bi-Polar V/F Converter Block Diagram.....	247
2C-1	Accelerometer Module Output Characteristic.....	260

## Tables

<u>Table No.</u>		<u>Page No.</u>
1.2-1	LCIGS Accuracy Requirements.....	14
2.6-1	LCIGS Composite Standard Deviations for 9 Nominal Orientations.....	52
4.2-1	Choice of Zeroed Element of $C_{Ba}^L$ .....	91
5.3-1	Maximum Measurement Error in °/hr for Initial Covariances.....	152
5.5-1	Recommended Sequence of Nominal Orientations.....	163
5.5-2	Upper Bounds on Standard Deviations of Estimates of Static Drifts.....	170
5.6-1	Nominal Coefficients Dynamic Parameter Estimation Equations.....	181
6.1-1	LCIGS Gyro Specifications.....	197
6.2-1	Accelerometer Simulation Parameters.....	198
6.2-2	Bias Estimation Errors. 10 µg Measurement Errors Alternating in Sign.....	200
6.2-3	Scale Factor Error Estimation Errors. 10 µg Measurement Errors Alternating in Sign.....	200
6.3-1	Quantization Error for Positive Biases.....	202
6.3-2	Quantization Error for Negative Biases.....	202
6.3-3	Comparison of Measured Standard Deviations with Theoretical Bounds Due to Timing Errors.....	203
6.4-1	Description of Newton-Raphson Iteration Runs.....	205
6.4-2	Deviations of Estimated Earth Rate Components from Final Values.....	207
6.4-3	Sum of Squares of Final Earth Rate Component.....	207
6.4-4	Final Estimation Errors for Gyro Drift Terms.....	209
6.4-5	Measurement Errors for Run #1.....	210
6.4-6	Largest Computed Magnitude of the Deviation From North.....	212
6.5-1	Gyro Drift Terms and Dynamic Error Parameters.....	214
6.5-2	Accelerometer Biases and Scale Factor Errors.....	216
6.5-3	Key to Simulation Runs.....	217
6.5-4	Base Line Runs - No Vibration Environment.....	219

10  
Tables (Cont.)

<u>Table No.</u>		<u>Page No.</u>
6.5-5	Accelerometer Quantization Effects.....	220
6.5-6	Effect of Accelerometer Bias and Scale Factor Error.....	221
6.5-7	Monte Carlo Runs with Expected Vibrations.....	222
6.5-8	Means and Standard Deviations for Monte Carlo Runs...	224
6.5-9	Runs with High Vibration Environment.....	225
7.1-1	Calibrated Parameters.....	229
7.1-2	Calibration Position Accuracies.....	229
7.1-3	LCIGS Calibration Time.....	231
2B-1	Pertinent LCIGS Accelerometer Specifications - Uncalibrated Instrument.....	250
2B-2	Pertinent LCIGS V/F Converter Specifications - Uncalibrated Unit.....	250
5A-1	Values for $ L^{-1} _{\infty}$ and $ M _{\infty}$ .....	271
5A-2	Values of $1/(1 -  L^{-1} _{\infty}  M _{\infty})$ .....	271
5A-3	Upper Bounds on $ \Delta H_1 H_1^{-1} _{\infty}$ and $ \Delta H_2 H_1^{-1} _{\infty}$ .....	272
5A-4	Upper Bounds on $ S/2 _2$ with $W_1(n-1) = I$ .....	272
5A-5	Upper Bounds on $ T/2 _2$ with $W_1(n-1) = I$ .....	272

## Chapter 1

### Introduction

### 1.1 Introduction

This thesis originates a set of techniques for calibration of the inertial instruments of a Low Cost Inertial Guidance Subsystem (LCIGS). The calibration procedure is at the inertial reference unit level. The inertial reference unit consists of a complete set of inertial instruments assembled into an inertial measurement unit package. Additional test software for calibrating the unit including attitude and velocity algorithms is supplied external to the package.

Related to the logistical aspects of the system, described in the next section, is the need for a set of procedures for calibrating a large number of inertial reference units having large drift and dynamic error parameters with inexpensive calibration equipment, a minimum of on-site surveying or other such measurements, simplified methods for setting up the equipment and for running it. The calibration should also take place in the minimum possible time. A series of techniques has, therefore, been developed which takes into account all of the above considerations. There are described below after presentation of the low cost system description. The techniques are, of course, applicable to all strapdown systems with the same attendant advantages. However, they are illustrated very well by specific application to the LCIGS, presented here, for which they were originally intended.

### 1.2 Low Cost Inertial Guidance Subsystem (LCIGS)<sup>1</sup>

The LCIGS is a new concept for inertial measurement units being developed at The C.S. Draper Laboratory. It is designed to be competitively produced at a unit cost goal of \$10,000 in fiscal year 1976 dollars for 2,000 systems in one buy. In order to achieve this goal, the system is designed in modular form so that different manufacturers' single-degree-of-

freedom (SDF) inertial instruments (gyros and accelerometers) of the same class can be used interchangeably without affecting the electronics, mechanical configuration, or data processing of the system. Therefore, if a vendor's proprietary instrument meets the LCIGS basic normalized specification, it can be used in the system by all LCIGS manufacturers. Thus, all manufacturers will be able to compete for production at every procurement level including repair and sparing.

The modular concept is also applied to the electronics which is functionally partitioned into replaceable electronic modules with corresponding normalized specifications. The electronics modules are replaceable at the depot level and are consistent with the same concepts of interchangeability, throw-away replacement, and upgrading of internal module design as apply to the inertial instrument modules.

The main advantages of the interchangeable module configuration are that reliability and performance improvements are easily incorporated; obsolescence of parts is easily circumvented, and new technology is easily introduced into already purchased systems without the need for major new systems designs and reopening of major production lines.

The modular design is, of course, largely made possible by use of microprocessors for data processing and control.

With large numbers of low cost systems in storage at the depot level, it is imperative to have a rapid calibration procedure in order to obviate the need for frequent large scale periodic recalibration of the stored systems. The calibration should not only be consistent with LCIGS performance goals, but should also have the qualities mentioned in Section 1.1 in order to be compatible with the low cost goals of the entire LCIGS program.

Calibration accuracy goals are modest because LCIGS performance goals have been specified in the context of an aided inertial mid-course guidance mode using typical aids such as Radiometric Area Correlation (RAC), Terrain Correlation (TERCOM), Tactical Global Positioning (GPS), or Loran.

Table 1.2-1 below is a listing of LCIGS accuracy requirements.

Error Term	Nominal Value ( $1\sigma$ )	Worst Case Value ( $1\sigma$ )
<u>Gyro Errors</u>		
bias	$0.5^0/\text{hr}$	$2^0/\text{hr}$
g-sens drift along input axis	$1^0/\text{hr/g}$	$2^0/\text{hr/g}$
g-sens drift along spin axis	$0.8^0/\text{hr/g}$	$2^0/\text{hr/g}$
scale factor error	150 ppm	300 ppm
misalignment error	60 arc-sec	100 arc-sec
<u>Accelerometer Errors</u>		
bias	$100 \mu\text{g}$	$200 \mu\text{g}$
scale factor error	150 ppm	300 ppm

Table 1.2-1 LCIGS Accuracy Requirements<sup>1</sup>

Raw instrument errors can, however, be quite large because of the low cost of the instruments.<sup>2</sup> Raw gyro bias can be as high as  $100^0/\text{hr}$ , misalignment errors (because of low cost system mechanical construction) as high as 2000 arc-sec, scale factor errors can be as high as 60,000 ppm. Similarly,<sup>3</sup> accelerometer raw bias can be as high as 10,000  $\mu\text{g}$  and scale factor error

as high as 60,000 ppm. The calibration procedures must be sufficiently accurate over this range of parameters.

### 1.3 Current Calibration Techniques

Classically, calibration of the inertial instruments assembled into an inertial reference unit was achieved by the obvious procedure of directly measuring the outputs of the inertial instruments for different orientations of the system. The outputs were corrected for gravity and earth rate by means of precise optical measurements of the orientation of the system with respect to the gravity and earth rate vectors.

Not long after the application of optimal data processing techniques to terrestrial inertial navigation system by Brock<sup>4</sup>, these same techniques were specifically applied to alignment and calibration of both gimballed and strapdown inertial navigation systems on a stationary base. The technique used by Brock and Schmidt<sup>5</sup> was to derive a linear error model for a gimballed inertial navigation system to be used in a Kalman filter formulation with the assumption that, on a stationary base, the true average velocity and the average deviation from the true position are both zero. Deviations from zero velocity and from the true position were handled by a third order linear model driven by white noise. Dependence on external measurements was thereby avoided. Ballantoni and Koenke<sup>6</sup> applied the same general principles used by Schmidt and Brock to the launch pad alignment and calibration of a strapdown system with the exception that deterministic external measurements of vehicle sway were used rather than treating the sway as noise. Somewhat later Ryan<sup>7</sup> developed the calibration of a strapdown system using Kalman filtering but with the system in a gyrocompassing mode and not

as a complete inertial navigator. External measurements were also avoided by again modeling vehicle sway as a disturbance noise. Whereas the procedure outlined by Schmidt and Brock readily lends itself to calibration of a limited number of error parameters of each inertial instrument through rotation of the instrument package via commands to the gimbal torquers, in Ryan's scheme only the north component of gyro drift can be accurately calibrated. Expansion of the technique to calibrate more error parameters is limited because the strapdown system is visualized as mounted on a simple hinge in a stationary vehicle rather than on a set of gimbals. Extending the calibration procedure to more instrument parameters was accomplished for the floating ball type inertial system by greatly expanding the states of the Kalman filter linear error model as reported in Strunce<sup>8</sup>. [Here attitude changes for the instrument package are easily commanded as with gimballed systems.] More recently, Widnall, Grundy, and Murch<sup>9</sup> also expanded the linear error model for both strapdown and gimballed systems' instrument error parameters. Here the strapdown system (when doing a laboratory calibration) is mounted on a set of gimbals in order to make all of the error model parameters cleanly observable through proper rotations and orientations of the system. The associated Kalman filter has a total of 48 states. [In addition to all of the instrument error model parameters dealt with in this thesis, Widnall, et al, also include 3 gyro spin-input  $g^2$  error terms, gravity deflections, and the gravity anomaly.] As before, the true average velocity and average deviation from the known laboratory position are assumed to be zero and the deviations are assumed to be statistically modeled. All of the preceding calibration techniques depend upon

knowledge of the orientation of the inertial instrument package with respect to the gravity and earth rate vectors for their nominal behavior but precise knowledge is not required. However, implicit in each of the above calibration procedures are the assumptions that the gyro and accelerometer error parameters are quite small compared to the LCIGS parameter values presented in the previous section. In particular, gyro drifts are assumed to be on the order of several tenths of a degree per hour and accelerometer biases less than 100  $\mu g$ . Therefore, the gyrocompassing and leveling procedures performed to initialize the system can be achieved with great enough accuracy to allow tracking of the gravity and earth rate vectors during calibration without the need of an external measurement of attitude. This cannot be done when, for example, initial gyro bias is on the order of 100°/h as postulated for LCIGS. To surmount this problem, accurate external reference to the earth rate and gravity vectors could be made through the classical complicated optical procedures developed by McKern et al<sup>10</sup> and Garmer et al<sup>11</sup>. More recently a simplified procedure has been developed by Morgan<sup>12</sup> which requires testing on a nearly level slab on which is mounted a precision edge surveyed with respect to north. The system is held in a fixture having six calibrated orthogonal surfaces. Thus, some precise external measurement is also needed as well as the extra requirement for the precision slab and orthogonal surfaces.

This thesis originates a set of techniques which does allow the calibration of very large instrument error parameters, unlike the self-contained methods described above (such as those developed by Widnall et al) and at the same time does not need a precise measurement of the orientation of the

system with respect to gravity and earth rate as is done with the optical methods or those of Morgan. A detailed description of the methods is presented in the following section. It will also be seen that one by-product of the set of procedures developed in this thesis (whereby accelerometer calibration, static gyro error parameter calibration and dynamic gyro error parameter estimation are decoupled) is greatly reduced software over the conventional self-contained calibration techniques.

There is some connection between the work reported in this thesis and the independent developments reported by Torrey and Boyland<sup>13</sup>, Savage<sup>14</sup>, and Taylor, Pasik, and Fish<sup>15</sup>. Torrey and Boyland separate accelerometer and gyro calibration to save software. Measurement of accelerometer errors is through the deviation from the squared magnitude of gravity for convenience of the Kalman filter formulation and not as a means of avoiding a precise tracking of the gravity vector as is done in this thesis since in the former work precise tracking of gravity is still required.

Savage's technique is somewhat similar to the method developed in this thesis for calibration of the gyro dynamic parameters in that changes in the velocity processed in the computed frame due to rotations of the system are used to derive a set of linear equations for the solution of error parameters. Savage also includes accelerometer bias and misalignment calibration as part of the procedure. However, the gyro biases are assumed to be precisely calibrated at the start of the calibration by some other method. Since no provision is made for gyro bias calibration, the method is sensitive to gyro bias errors.

The technique presented by Taylor et al appears to be quite similar to that reported by Savage.

#### 1.4 A New Calibration Technique

The calibration procedure measures all of the gyro and accelerometer parameters listed in Table 1.2-1. Three single-degree-of-freedom dynamic terms: spin axis cross-coupling, anisoinertia drift, and output axis coupling are considered to be directly determined from the physical characteristics of the instruments and are not calibrated with our procedure.

The calibration sequence permits relatively loose tolerances on system orientations in spite of the large instrument error parameters. Six orientations are used for the accelerometer calibration and eight for the gyros. Precision optics are not required to measure the orientations. A survey to find north is also not needed. A positioning tolerance of the level axes to within  $\pm 1/2^\circ$  ( $\pm 10^\circ$  for the accelerometers) is more than adequate as is a tolerance of  $\pm 20^\circ$  with respect to north for one of the nominally level axes. The time for the entire calibration sequence is estimated to be less than 1/2 hour.

The test technique is at the inertial reference unit level (i.e., the full instrument package with attitude, velocity, and other necessary algorithms for software supplied by the test equipment) with the accelerometer and gyro outputs being used to implement a computed local level frame during the gyro calibration sequence. Use of the computed transformation between the body frame (established by the accelerometer input axes) and a local level reference frame used for the gyro calibration eliminates the need for precision test orientation fixturing and reduces test time since the local

reference frame provides angular base motion isolation. The base motion isolation eliminates the need for averaging gyro outputs over a long time period.

Accelerometers are calibrated separately from the gyros using the time averaged outputs of each accelerometer for 6 system orientations. The gravity component sensed by each accelerometer is, in conjunction with the accelerometer bias and scale factor error, treated as an unknown. Additional relationships for the sensed gravity components in the solution for the bias and scale factor are obtained from the constraint

$$g_{ij}^2 + g_{2j}^2 + g_{3j}^2 = g^2 \quad (1.4-1)$$

where  $g$  is the gravity magnitude at the test location and  $g_{ij}$  is the gravity sensed by the  $i^{th}$  accelerometer in the  $j^{th}$  system orientation. The technique is completely self-contained in that system orientations need not be precisely known. There is a tolerance of  $\pm 10^0$  from the nominal system test orientations.

Because the large unknown accelerometer bias and scale factor errors are known to be small with respect to the magnitude of gravity, the equations given by (1.4-1) lead to readily linearized equations forming a set of 6 simultaneous equations for the 6 unknown values of bias and scale factor error.

There is an additional capability to determine accelerometer misalignments to within 40 arc-sec if three more system orientations are used. However, this is not necessary for LCIGS because of the prepackaging of the accelerometers as a fixed triad that is described in Chapter 2.

A linear extrapolation technique is used to reduce the effective accelerometer quantization in order to reduce the averaging time for each orientation. The extrapolator is based on the precise measurement of the time of occurrence of an accelerometer output pulse with respect to the actual readout time of the accelerometer output. The resulting quantization error standard deviation is reduced with this method by a factor of over 17.

Gyros are calibrated using estimated lumped drifts along the two horizontal reference axes of a computed frame that is aligned with a local level reference frame. The lumped drifts are the projections of the drift terms of each gyro onto the reference axes so that knowledge of the direction cosine matrix relating body axes to the reference axis is necessary at each orientation. In order to have a loose tolerance on the azimuth direction of the principal horizontal reference axis, the horizontal components of earth rate along the two horizontal reference axes are treated as unknowns that are added to the lumped drifts. The total drift (gyro lumped errors and the unknown earth rate component) on each horizontal reference axis is measured with a 3-state Kalman filter. Therefore, there are 16 equations relating 8 unknown gyro parameters and 16 unknown earth rate components to the measured drifts for the 8 static system orientations that are used. Thus, there are 16 equations for the 24 unknown earth rate components and gyro parameters. An additional set of 8 non-linear equations is obtained from the earth rate magnitude constraints for each position which are:

$$\omega_{1g}^2 + \omega_{2g}^2 = \omega_h^2 \quad (1.4-2)$$

where  $w_{1j}$  is the horizontal component of earth rate along the principal horizontal reference axis (that nominally points north) for the  $j^{\text{th}}$  system orientation,  $w_{2j}$  is the horizontal component of earth rate along the other horizontal reference axis and  $w_h$  is the magnitude of the horizontal value of earth rate at the test location latitude. For the case of gyro calibration, linearization of the non-linear equations is not possible as with accelerometer calibration because the value of the unknown drifts can be of the same order of magnitude (and higher) as the horizontal earth rate. Hence, the 24 set of equations for gyro parameters and earth rate components is solved iteratively by a Newton-Raphson technique. The particular Newton-Raphson iteration used is quite stable even for measurement errors of several degrees per hour and for deviations from north as high as  $\pm 30^{\circ}$  (although a  $\pm 20^{\circ}$  tolerance is recommended for good numerical conditioning).

The eight gyro parameters solved through this iterative method are the three gyro biases, three spin axis mass unbalance terms, and two  $\Delta$  input axis mass unbalance terms. The two  $\Delta$  input axis mass unbalance terms are defined as follows:

$$\begin{aligned}\Delta_{13} &\stackrel{\Delta}{=} M_{IA_1} - M_{IA_3} \\ \Delta_{23} &\stackrel{\Delta}{=} M_{IA_2} - M_{IA_3}\end{aligned}\quad (1.4-3)$$

where  $M_{IA_i}$  is the input axis mass unbalance coefficient of the  $i^{\text{th}}$  gyro. These definitions are necessary because the three input axis mass unbalance coefficients are not separately observable as projections on the horizontal plane. A separate estimate must be made for the third input axis mass unbalance coefficient.

Calibration of dynamic gyro parameters (scale factor error and misalignment angles) is accomplished using a two state Kalman filter estimate of the angular errors between the computed and level reference frames during a rotation of the system. The dynamic parameters have a large effect only during a rotation of the system from one static orientation to another. Thus, estimation of static parameters is largely decoupled from estimation of dynamic parameters although there is an interaction between these two calibration procedures because the potentially large (10 mrad) misalignment angles result in small earth rate errors and g-sensitive errors during the static calibration procedure. These errors are dealt with in the following iterative manner. (See Section 5.7, Chapter 5.)

Initially, the principal level reference axis is assumed to point due north and preliminary estimation errors will not be large enough to introduce any appreciable errors when these static estimates are used to compensate for the static drifts in the initial estimates of gyro scale factor errors and misalignment angles. These initial dynamic parameter estimates along with separately made estimates of the input axis mass unbalance coefficient of the 3rd gyro are used in turn to compensate for the gravity and earth rate due to the misalignments. This is done by appropriately modifying the known coefficients of the unknown static parameters and the measurements that are to be used in the full Newton-Raphson iteration. The Newton-Raphson procedure is then used to obtain accurate estimates of the gyro static parameters as described above. The accurate static parameters, in turn, are then used in the estimation procedure for obtaining the final set of dynamic parameter estimates.

**Accuracy of the final results for both static and dynamic parameters**

depends mainly on the Kalman filter measurement accuracy which is a function of Kalman filter gains, filtering time, and the environmental vibrations. For the environment of a typical test laboratory (see Chapter 2), the Kalman filter gains were adjusted to yield drift estimates after 1 minute in a static position and angle estimates after a 10 second rotation in order to minimize total calibration time. Resulting accuracies for a simulation of the entire gyro calibration procedure are listed in Table 6.5-8, Chapter 6, and are well within the required accuracies listed in Table 1.2-1. Prediction of accelerometer estimation errors based on LCIGS data (Chapter 2) also leads to the conclusion that these estimates are within the requirements of Table 1.2-1.

## Chapter 2

### Calibration of Accelerometers

## 2.1 Introduction

In order to avoid the need for precise test fixture orientations during inertial reference unit calibration, use is made of the non-linear constraint equations, relating the known magnitude of local gravity to the magnitudes sensed by each accelerometer, to derive a linear set of equations whose solution is a set of approximations to the desired accelerometer parameters. These are bias, scale factor error and misalignment of the input axis with respect to an orthogonal reference frame. (Successive solutions of the equation set, whose coefficients are modified by the preceding solutions, approach the true solution.) The technique is completely self-contained (i.e., there is no need of external measurements of system orientation with respect to gravity). It is also relatively insensitive to angular base motion because non-linear constraints hold instantaneously regardless of angular base motion.

A set of 9 nominal orientations is chosen on the basis of good numerical conditioning of the linear equation set. Numerical conditioning of the 9 resulting equations remains good for perturbations of  $\pm 1/2^0$  from the nominal positions.

The Low Cost Inertial Guidance Subsystem (LCIGS) described in Chapter 1 is used as a bench mark in assessing the accuracies and required operational details of the accelerometer calibration procedure described above. A detailed description of the LCIGS accelerometer module is presented in Appendices 2B and 2C of this chapter. These modules present the added complication to the calibration of scale factor assymetry and significant

quadratic error terms introduced by the accelerometer module readout electronics (i.e., voltage-to-frequency (V/F) converter). Fortunately, this scale factor assymetry and the quadratic error can be handled with the aid of an external test current source without the need for additional system test orientations which would adversely affect the numerical conditioning of the calibration equations. A detailed presentation of these additional calibration procedures is given in Appendices 2B and 2C.

Starting with an initial bias error of  $\pm 10,000 \mu g$  and scale factor error of  $\pm 60,000$  ppm for the entire accelerometer module (accelerometer and V/F converter), it is shown that iterative solution of the linear calibration equations results in bounds on the standard deviations for the estimated bias, positive and negative scale factor errors, and misalignment angles of  $50 \mu g$ ,  $50$  ppm,  $84$  ppm,  $36$  arc-sec, respectively.

Derivation of these error estimates took into account the translational accelerations and angular vibrations described in Section 2.6 as well as the postulated error uncertainties of the accelerometer and V/F converter listed in Appendix 2B. (Also included were the errors inherent in the special V/F converter estimates presented in Appendix 2B.) Accelerometer quantization errors were not considered because it is assumed that their effect will be negligible with the use of the quantization reduction method to be introduced in Chapter 3.

Calibration time for the accelerometers, if done independently of the gyros in the system, can be as low as 3 minutes for only 6 orientations (with misalignments and the V/F converter pre-calibrated and the vibration spectra as presented in Section 2.6) to obtain bias

and scale factor estimates within the LCIGS specified tolerances (100  $\mu$ g, 150 ppm, respectively). The time for a full calibration procedure is difficult to determine at this time because of lack of information on the minimum time required to adequately calibrate the V/F converters. A tentative upper limit of 1/2 hour is chosen.

The misalignment bound of 36 arc-sec is substantially above the LCIGS 20 arc-sec tolerance. However, the potential of the full calibration method can be appreciated in other applications where reduction in the electronics errors would certainly lead to a far lower misalignment error bound. Also, with regard to LCIGS, misalignment errors will be predetermined at the accelerometer module level<sup>16</sup>. The full calibration procedure can, however, serve as a useful check on misalignments in the field.

## 2.2 Accelerometer Alignment

In any practical strapdown system, the gyro and accelerometer input axis triads each form a non-orthogonal set. Furthermore, the corresponding axes of the two sets will not be parallel. It is therefore necessary to define a single body reference frame consisting of a right-handed orthogonal triad of axes<sup>17</sup>. The accelerometer and gyro input axes are considered to be misaligned with respect to these reference axes. Appropriate misalignment angle corrections to the gyro and accelerometer outputs can then be made which will result in a common body reference frame for all system calculations. Choice of suitable reference axes (resulting in small misalignment angles) is somewhat arbitrary. In some previously developed systems<sup>18</sup>, a reference cube

is physically mounted to the system structure and misalignments with respect to the axes defined by the cube have to be determined optically. Twelve misalignment angles are needed - two for each input axis of the gyros and accelerometers. Optical determination of misalignment angles can be avoided and the number of specified misalignment angles can be reduced by defining an orthogonal body reference triad by three misalignment angles with respect to the true accelerometer input axes. Estimation of these three angles becomes a natural part of the approach toward estimating the accelerometer error model coefficients presented in succeeding sections.

Figure 2.2-1 shows the relations between the accelerometer input axes and a particular set of reference triad axes.

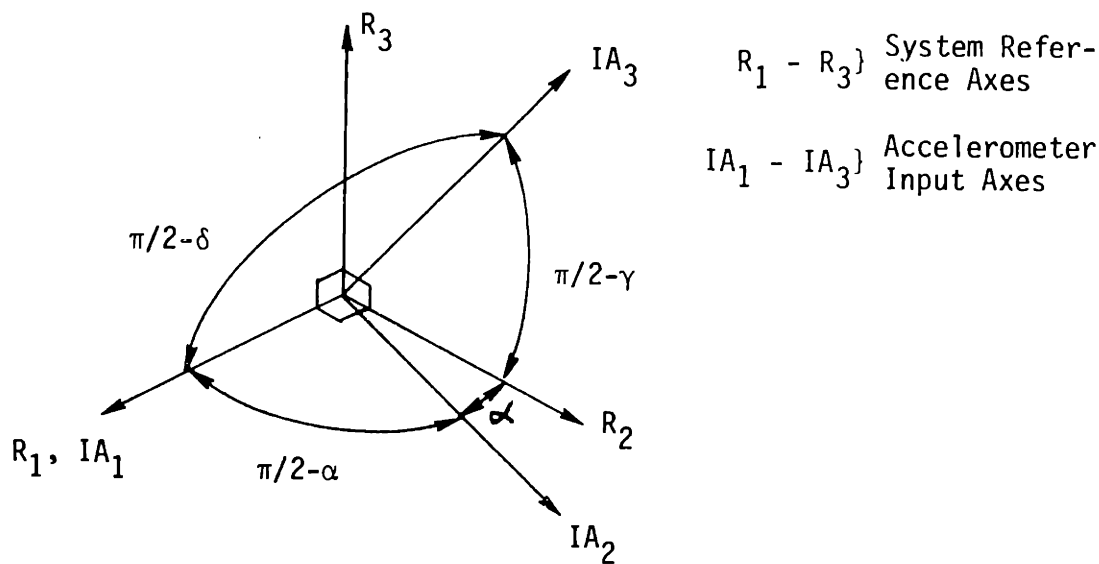


Figure 2.2-1 Definition of System Orthogonal Reference Triad

Reference axis  $R_1$  is chosen to be the same as accelerometer input axis  $IA_1$ . Reference axis  $R_2$  is chosen to be orthogonal to input axis  $IA_1$  in the plane defined by axes  $IA_1$  and  $IA_2$ . Reference axis  $R_3$  is defined as the axis that is perpendicular to the  $IA_1$ ,  $IA_2$  plane. More formally, with  $\underline{R}_1 \perp \underline{R}_3$ ,  $\underline{IA}_1 \perp \underline{IA}_3$  being defined as unit vectors:

$$\underline{R}_1 \triangleq \underline{IA}_1 \quad (2.2-1)$$

$$\underline{R}_3 \triangleq \frac{\underline{IA}_1 \times \underline{IA}_2}{|\underline{IA}_1 \times \underline{IA}_2|} \quad (2.2-1)$$

$$\underline{R}_2 \triangleq \underline{R}_3 \times \underline{R}_1$$

$$\alpha \triangleq \arccos(\underline{IA}_2 \cdot \underline{R}_2) \quad (2.2-2)$$

$$\gamma \triangleq \pi/2 - \arccos(\underline{IA}_3 \cdot \underline{R}_2)$$

$$\delta \triangleq \pi/2 - \arccos(\underline{IA}_3 \cdot \underline{R}_1)$$

The relations between the components of a vector defined in the reference frame and the respective measurements by the three accelerometers are:

$$\underline{g}_i^A = \underline{g}_i^R \quad (2.2-3)$$

$$\underline{g}_2^A \approx \underline{g}_2^R + \alpha \underline{g}_1^R$$

$$\underline{g}_3^A \approx \underline{g}_3^R + \delta \underline{g}_1^R + \gamma \underline{g}_2^R$$

where A denotes the non-orthogonal accelerometer frame (axes  $IA_1$  -  $IA_3$ ) and R denotes the orthogonal reference frame (axes  $R_1$  -  $R_3$ ), and small angle assumptions are used.

### 2.3 Linearized Solutions for Accelerometer Error Model Coefficients

A set of equations for obtaining an estimate of the accelerometer error model coefficients and the misalignment angles is derived by making use of the non-linear constraint equation relating the components of gravity coordinatized in the orthogonal reference frame to the magnitude of gravity,  $g$ , at the test location.

At any angular orientation of the system

$$g_{ij}^2 + g_{2j}^2 + g_{3j}^2 = g^2 \quad (2.3-1)$$

where  $g_{ij}$  represents the gravity component along the  $i^{th}$  orthogonal reference frame axis at the  $j^{th}$  orientation.

Use of these equations obviates the need for precise external determination of the system orientation with respect to gravity.

The outputs of the involved integrating accelerometers will be averaged over a specified measurement interval  $T$ . Therefore, the average gravity component,  $\bar{g}_{ij}$ , over a measurement interval must be used rather than the instantaneous values in Equation (2.3-1).

That is,

$$\bar{g}_{ij} \triangleq \frac{1}{T} \int_{t_0}^{t_0+T} g_{ij} dt \quad (2.3-2)$$

where  $T$  is the measurement interval and  $t_0$  the initial time of measurement. Thus, at time  $t$

$$\bar{g}_{ij} = \bar{\bar{g}}_{ij} + \Delta g_{ij}(t) \quad (2.3-3)$$

where  $\Delta g_{ij}(t)$  is a small zero average variation with respect to  $\bar{g}_{ij}$  due to angular base motion. Substitution of (2.3-3) into (2.3-1) and averaging yields the constraint equation in terms of average values.

$$\sum_{i=1}^3 (\bar{\bar{g}}_{ij}^2 + \overline{\Delta g_{ij}^2}) = \bar{g}^2 \quad (2.3-4)$$

$$\overline{\Delta g_{ij}^2} \triangleq \frac{1}{T} \int_{t_c}^{t_c+T} \Delta g_{ij}^2 dt \quad (2.3-5)$$

For any orientation  $j$ , the average outputs  $r_{ij}$  of accelerometers 1, 2, 3 (whose input axes are IA<sub>1</sub>, IA<sub>2</sub>, IA<sub>3</sub>, respectively) over time interval T are:

$$\left. \begin{aligned} r_{1j} &= b_1 + SF_1 (\bar{\bar{g}}_{1j} + \bar{g}_{1j} + \Delta r_{1j}) \\ r_{2j} &= b_2 + SF_2 (\bar{\bar{g}}_{2j} + \alpha \bar{g}_{1j} + \bar{g}_{2j} + \alpha \bar{\bar{g}}_{1j} + \Delta r_{2j}) \\ r_{3j} &= b_3 + SF_3 (\bar{\bar{g}}_{3j} + \delta \bar{g}_{1j} + \gamma \bar{g}_{2j} + \bar{g}_{3j} + \delta \bar{\bar{g}}_{1j} + \gamma \bar{\bar{g}}_{2j} + \Delta r_{3j}) \end{aligned} \right\} \quad (2.3-6)$$

where

$b_i$  = bias of the  $i^{\text{th}}$  accelerometer

$SF_i$  = scale factor error of the  $i^{\text{th}}$  accelerometer

$\alpha, \delta, \gamma$  = misalignment angles defined in Section 2.2

$\bar{n}_{ij}$  = average output over time interval T of the  $i^{\text{th}}$  accelerometer at the  $j^{\text{th}}$  system orientation

$\Delta n_{ij}$  = average output error over time interval T of the  $i^{\text{th}}$  accelerometer at the  $j^{\text{th}}$  orientation due to unmodeled accelerometer errors and translational accelerations.

The squares of  $\bar{g}_{ij}$  are next obtained from equations (2.3-6) and substituted into the constraint equation (2.3-4) to yield an equation for the  $j^{\text{th}}$  orientation that relates terms that are linear in the unknown values of the modeled error coefficients and misalignments to the squares of the averaged outputs and to non-linear terms which will be neglected in any linear solution for the unknowns.

The result is:

$$\sum_{i=1}^3 n_{ij}(b_i + SF_i \bar{g}_{ij}) + \alpha n_{2j} \bar{g}_{1j} + \delta n_{3j} \bar{g}_{1j} + \gamma n_{3j} \bar{g}_{2j} = \frac{1}{2} \left( \sum_{i=1}^3 n_{ij}^2 - g^2 \right) + e_j \quad (2.3-7)$$

where  $e_j$  includes the average output errors, the non-linear terms, and the  $\Delta g_{ij}^2$  terms.

In order to have computable coefficients for all of the unknowns in (2.3-7) the substitution

$$\bar{g}_{ij} = n_{ij} + (\bar{g}_{ij} - n_{ij}) \quad (2.3-8)$$

is made and all terms containing the coefficient ( $\bar{g}_{ij} - r_{ij}$ ) are included among the non-linear terms.

The resulting equations are given by

$$\sum_{i=1}^3 (r_{ij} b_i + \gamma_{ij}^2 SF_i) + r_{1j} r_{2j} \alpha + r_{1j} r_{3j} \delta \\ + r_{2j} r_{3j} \gamma = \frac{1}{2} \left( \sum_{i=1}^3 \gamma_{ij}^2 - g^2 \right) + E_j \quad (2.3-9)$$

where

$$E_j = \sum_{i=1}^3 \left( \frac{\Delta a_{ij}^2}{2} + \frac{\Delta g_{ij}^2}{2} + r_{ij} SF_i \Delta a'_{ij} - r_{ij} \Delta r_{ij} \right) \\ + r_{2j} \alpha \Delta a_{1j} + r_{3j} \delta \Delta a_{2j} + r_{3j} \gamma \Delta a_{1j} \quad (2.3-10)$$

and

$$\Delta a_{ij} \triangleq r_{ij} - \bar{g}_{ij} \\ \Delta a'_{ij} \triangleq \Delta a_{ij} \\ \Delta a'_{2j} \triangleq \Delta a_{2j} - SF_2 \alpha \bar{g}_{1j} \\ \Delta a'_{3j} \triangleq \Delta a_{3j} - SF_3 \delta \bar{g}_{1j} - SF_3 \gamma \bar{g}_{2j} \quad (2.3-11)$$

Substitution of the expressions for  $r_{ij}$  given by equations (2.3-6) into equations (2.3-11) shows that all of the  $\Delta a_{ij}$  and  $\Delta a'_{ij}$  terms in (2.3-10) do involve only non-linear combinations of the unknowns. Equation (2.3-10) will be numerically evaluated in Section 2.6.

Equation (2.3-9) is normalized by division by  $g^2$  leading to

$$\sum_{i=1}^3 \left( C_{ij} \left( \frac{b_i}{g} \right) + C_{ij}^2 SF_i \right) + C_{1j} C_{2j} \alpha \\ + C_{1j} C_{3j} \delta + C_{2j} C_{3j} \gamma = \frac{1}{2} \left( \sum_{i=1}^3 C_{ij}^2 - 1 \right) + \frac{E_j}{g^2} \quad (2.3-12)$$

with

35

$$c_{ij} \triangleq \frac{r_{ij}}{g} / g \quad (2.3-13)$$

A linear solution for  $b_i$ ,  $SF_i$ ,  $\alpha$ ,  $\delta$ ,  $\gamma$  is obtained from a set of 9 linear equations given by (2.3-12) with  $E_j$  set to zero and  $j = 1, \dots, 9$  for 9 orientations.  $\frac{E_j}{g^2}$  terms are, of course, unknown contributors to the linear solution errors.

A set of only 6 equations from 6 orientations need be solved if the 3 misalignment angles are predetermined. Reference 9 presents an arrangement whereby all three accelerometers are mounted on one separate block that is then affixed to the system frame. In this case, the accelerometer misalignment angles with respect to an orthogonal reference triad that is defined in the separate block can be predetermined and will remain as stable as the mechanical rigidity of the block and the inherent stability of the accelerometer input axes (10 arc-sec<sup>19</sup>). In this case (the arrangement for LCIGS), equation (2.3-12) reduces to

$$\sum_{i=1}^3 (\Delta_{ij} \left( \frac{b_i}{g} \right) + \Delta_{ij}^2 SF_i) = \frac{1}{2} \left( \sum_{i=1}^3 \Delta_{ij}^2 - 1 \right) + E_j / g^2 \quad (2.3-14)$$

where (referring to (2.2-3))

$$\begin{aligned} \Delta_{1j} &\triangleq c_{1j} \\ \Delta_{2j} &\triangleq c_{2j} - \alpha c_{1j} \\ \Delta_{3j} &\triangleq c_{3j} - \delta c_{1j} - \gamma c_{2j} \end{aligned} \quad (2.3-15)$$

( $\alpha, \delta, \gamma$  are predetermined)

and

$$\frac{E_{ij}^1}{g^2} = \sum_{i=1}^3 \left( \frac{\Delta e_{ij}^2}{2} + \frac{\Delta g_{ij}^2}{2g^2} + d_{ij} S F_i \Delta e_{ij} - d_{ij} \frac{\Delta n_{ij}}{g} \right) \quad (2.3-16)$$

with

$$\Delta e_{ij} \triangleq d_{ij} - \bar{g}_{ij}/g^2 \quad (2.3-17)$$

Extension of the above procedures to account for scale factor assymetry introduced by the V/F converter is presented in Appendices 2B and 2C.

#### 2.4 Solution of the Linear Equation Set

Use of equation sets (2.3-12) or (2.3-14) to estimate the unknown accelerometer parameters is predicated upon specifying a set of nominal test orientations for the system (leading to nominal values for the  $C_{ij}$  coefficients) and a maximum deviation tolerance from these positions (resulting in deviations which can be computed for the  $C_{ij}$  coefficients). Errors in the parameter solutions for the nominal orientations and for the maximum deviations from the nominal can then be predicted with the aid of standard accelerometer data and the knowledge of expected angular and translational test fixture motions. (Note that in the real test sequence, only the actual  $C_{ij}$  measurements are used. These will fall within the range of tolerances specified through the calculations described above.).

Intuitively, it would seem that some of the "best" nominal orientations are the ones that follow the standard "up-down" positions used

when the system orientations are adjusted within very close tolerances by optical means. This will be borne out subsequently. However, a general strategy for determining "good" (but not necessarily optimal) nominal orientations can be based on a more detailed argument. The condition number,  $k(A)$ , is a numerical analysis criterion<sup>20</sup> for a well-conditioned set of linear equations. This number is defined in terms of matrix spectral norms by

$$k(A) = |A|_2 |A^{-1}|_2 \quad (2.4-1)$$

where the equation set is

$$A \underline{x} = \underline{y} \quad (2.4-2)$$

for  $A$  an  $n \times n$  matrix,  $\underline{x}$  an  $n \times 1$  vector of unknowns and  $\underline{y}$  an  $n \times 1$  vector of known values.

Appendix 2A presents definitions of appropriate matrix norms, the condition number, and a summary of the theory of numerical conditioning of linear simultaneous equations.

A high value of  $k(A)$  implies that small perturbations in the elements of  $A$  can lead to a large magnification of errors in the solution  $\underline{x}$ . In the case under discussion, the norm of  $A$  will be on the order of 1 (because the maximum values of  $C_{ij}$  cannot be more than 1). Therefore, a well-conditioned set of equations is obtained only when the norm of  $A^{-1}$  is small. A large value of  $|A^{-1}|_2$  directly implies the magnification of errors in  $\underline{x}$  due to errors in the elements of  $\underline{y}$  in equation (2.4-2). Nominal orientations should, therefore lead to relatively small values of  $|A^{-1}|_2$ . A more easily computed upper bound

on  $|A^{-1}|_2$  is the  $p = \infty$  norm,  $|A^{-1}|_\infty$ , which will be used to deduce the strategy for selecting nominal orientations (i.e.,  $|A^{-1}|_\infty$  should be as small as possible).

Examination of the Gauss elimination procedure<sup>20,21</sup> which can be used, given the  $C_{ij}$  elements, to solve equation (2.4-2) or to obtain  $A^{-1}$  shows that the sum of the absolute values of the elements in any row of  $A^{-1}$  is minimized (i.e.,  $|A^{-1}|_\infty$  is minimized), when each row of  $A$  has only one dominant element (or as few as possible) with the remaining elements zero or small with respect to the dominant elements. Also, dominant elements should be distributed among the rows so that no row is a linear combination or "close" to a linear combination of any of the other rows. Therefore, each orientation should be selected to maximize the coefficient  $C_{ij}$  of as few parameters ( $b_i, SF_i, \alpha, \delta, \gamma$ ) as possible and to minimize all the rest. Each orientation should excite a new set of coefficients that is not a linear combination of any of the other sets. The above strategy for selecting orientations is consistent with the goal of having the nominal matrix  $A$  approximate an orthogonal matrix as closely as possible. (The condition number of an orthogonal matrix has the minimum possible value of 1.)

Equation (2.3-12) is rewritten in matrix form where

$$\underline{x} \triangleq \left( \frac{b_1}{g}, \frac{b_2}{g}, \frac{b_3}{g}, SF_1, SF_2, SF_3, \alpha, \delta, \gamma \right)^T \quad (2.4-3)$$

$$\underline{y} \triangleq \left( \dots, \frac{1}{2} \sum_{i=1}^3 (C_{i,j}^2 - 1) + \frac{E_j}{g^2}, \dots \right)^T \quad (2.4-4)$$

$$A \underline{x} = \underline{y} \quad (2.4-5)$$

and A is the appropriate matrix containing elements  $c_{ij}$ ,  $c_{ij}^2$ ,  $c_{1j}c_{2j}$ ,  $c_{1j}c_{3j}$ , and  $c_{2j}c_{3j}$ .

Nominal orientations are chosen to yield the following nominal matrix, A.

$$A \equiv \begin{bmatrix} 1 & 0 & 0 & 1 & 0 & 0 & 0_{3 \times 3} \\ 0 & 1 & 0 & 0 & 1 & 0 & 0_{3 \times 3} \\ 0 & 0 & 1 & 0 & 0 & 1 & 0_{3 \times 3} \\ -1 & 0 & 0 & 1 & 0 & 0 & 0_{3 \times 3} \\ 0 & -1 & 0 & 0 & 1 & 0 & 0_{3 \times 3} \\ 0 & 0 & -1 & 0 & 0 & 1 & 0_{3 \times 3} \\ .71 & .71 & 0 & .5 & .5 & 0 & .5 & 0 & 0 \\ .71 & 0 & .71 & .5 & 0 & .5 & 0 & .5 & 0 \\ 0 & .71 & .71 & 0 & .5 & .5 & 0 & 0 & .5 \end{bmatrix} \quad (2.4-6)$$

(Note with regard to the goals discussed above that the first 6 rows of A are mutually orthogonal and are easily made orthonormal by the same change of scale for each row.)

The orientations for the accelerometer input axes are, with respect to the horizontal, (according to the rows of A)

- 1) Accelerometer 1 up at  $90^\circ$ , other accelerometers level
- 2) Accelerometer 2 up at  $90^\circ$ , other accelerometers level
- 3) Accelerometer 3 up at  $90^\circ$ , other accelerometers level

- 4) Accelerometer 1 down at  $90^\circ$ , other accelerometers level
- 5) Accelerometer 2 down at  $90^\circ$ , other accelerometers level
- 6) Accelerometer 3 down at  $90^\circ$ , other accelerometers level
- 7) Accelerometers 1 and 2 up at  $45^\circ$ , accelerometer 3 level
- 8) Accelerometers 1 and 3 up at  $45^\circ$ , accelerometer 2 level
- 9) Accelerometers 2 and 3 up at  $45^\circ$ , accelerometer 1 level

Orientations 7 through 9 were chosen so that the coefficients of the misalignments are as large as possible.

The inverse of A is given by

$$A^{-1} = \begin{bmatrix} \frac{1}{2} & 0 & 0 & -\frac{1}{2} & 0 & 0 & 0_{3 \times 3} \\ 0 & \frac{1}{2} & 0 & 0 & -\frac{1}{2} & 0 & 0_{3 \times 3} \\ 0 & 0 & \frac{1}{2} & 0 & 0 & -\frac{1}{2} & 0_{3 \times 3} \\ \hline \frac{1}{2} & 0 & 0 & \frac{1}{2} & 0 & 0 & 0_{3 \times 3} \\ 0 & \frac{1}{2} & 0 & 0 & \frac{1}{2} & 0 & 0_{3 \times 3} \\ 0 & 0 & \frac{1}{2} & 0 & 0 & \frac{1}{2} & 0_{3 \times 3} \\ \hline -1.21 & -1.21 & 0 & .21 & .21 & 0 & 2 & 0 & 0 \\ -1.21 & 0 & -1.21 & .21 & 0 & .21 & 0 & 2 & 0 \\ 0 & -1.21 & -1.21 & 0 & .21 & .21 & 0 & 0 & 2 \end{bmatrix} \quad (2.4-7)$$

Nominal positions (1) - (6), only, are required for the case where misalignments are pre-computed (equation (2.3-14)). Here the relevant nominal matrix labeled B is given by the upper left  $6 \times 6$  submatrix of A. Its inverse in the upper left  $6 \times 6$  submatrix of  $A^{-1}$ .

It is necessary to examine the effect of perturbations in A and in B designated as  $\Delta A$  and  $\Delta B$  respectively on the inverses  $A^{-1}$  and  $B^{-1}$ . Let the matrix K denote either A or B. Denote the change in matrix K by  $\Delta K$ . The inverse of the new matrix  $K + \Delta K$  is given by

$$(K + \Delta K)^{-1} = (I + K^{-1} \Delta K)^{-1} K^{-1} \quad (2.4-8)$$

It can be shown that if <sup>22</sup>

$$|K^{-1} \Delta K|_\infty < 1$$

then

$$(I + K^{-1} \Delta K)^{-1} = I - K^{-1} \Delta K + K^{-2} \Delta K^2 - \dots \quad (2.4-9)$$

For an optimistic prediction of estimation errors, we can truncate the series after the second term and obtain

$$\begin{aligned} (K + \Delta K)^{-1} &\approx (I - K^{-1} \Delta K) K^{-1} \\ &= K^{-1} - K^{-1} \Delta K K^{-1} \end{aligned} \quad (2.4-10)$$

and use (2.4-10) and appropriate values for  $E_j$  or  $E'_j$  to calculate the estimation errors. We, of course, assign, in our analysis, the signs of each element perturbation such that the perturbation matrix causes an increase in the magnitudes of all the elements in  $(K + \Delta K)^{-1}$  over the corresponding elements of K.

A very conservative approach is to calculate an upper bound on  $|(K + \Delta K)^{-1}|_\infty$  from (2.4-8) and (2.4-9) as follows:

$$\begin{aligned}
 |(K + \Delta K)^{-1}|_\infty &\leq |K^{-1}|_\infty |(I + K^{-1} \Delta K)^{-1}|_\infty \\
 &< |K^{-1}|_\infty (1 + |K^{-1} \Delta K|_\infty \\
 &\quad + |K^{-1} \Delta K|_\infty^2 + \dots) \\
 &= |K^{-1}|_\infty \left( \frac{1}{1 - |K^{-1} \Delta K|_\infty} \right)
 \end{aligned} \tag{2.4-11}$$

Equation (2.4-11) is then used to calculate a single worst case upper bound on all of the errors in the estimates. However, some of the actual errors may be much smaller than others. (Compare the first 6 rows of A nominal with the last three rows.) Also the upper bound given by (2.4-11) may be too pessimistic. Therefore, both (2.4-10) and (2.4-11) will be used to gauge estimation errors.

The perturbation matrices  $\Delta A$  and  $\Delta B$  to be used in formula (2.4-10) are obtained by assuming small displacements in angle,  $\Delta\theta$ , about each accelerometer input axis and neglecting any products such as  $\Delta\theta^2$ . The signs of the perturbations are neglected. Hence, we define at this point for any matrix K

$\text{abs } K \stackrel{\Delta}{=} \text{matrix whose elements are the absolute values of the corresponding elements of } K$ .

Thus,

$$\text{abs } \Delta A = \begin{bmatrix} 0 & 1 & 1 & 1 & 1 & 0 \\ 1 & 0 & 1 & 0 & 1 & 1 \\ 1 & 1 & 0 & 1 & 0 & 1 \\ 0 & 1 & 1 & 0 & 1 & 1 \\ 1 & 0 & 1 & 1 & 0 & 1 \\ 1 & 1 & 0 & 1 & 1 & 0 \end{bmatrix} | \Delta \theta | \quad (2.4-12)$$

$\text{abs } \Delta B$  is the upper left  $6 \times 6$  submatrix of  $\text{abs } \Delta A$ .

Also

$$(\text{abs } A^{-1})(\text{abs } \Delta A)(\text{abs } A^{-1})$$

$$= \begin{bmatrix} 2.4 & 1.7 & 1.7 & .4 & .7 & .7 & 2 & 2 & 0 \\ 1.7 & 2.4 & 1.7 & .7 & .4 & .7 & 2 & 0 & 2 \\ 1.7 & 1.7 & 2.4 & .7 & .7 & .4 & 0 & 2 & 2 \\ 2.4 & 1.7 & 1.7 & .4 & .7 & .7 & 2 & 2 & 0 \\ 1.7 & 2.4 & 1.7 & .4 & .7 & .7 & 2 & 0 & 2 \\ 1.7 & 1.7 & 2.4 & .7 & .7 & .4 & 0 & 2 & 2 \\ 12 & 12 & 9.3 & .4 & .4 & .4 & 9.7 & 5.7 & 5.7 \\ 12 & 9.3 & 12 & .4 & .4 & .4 & 5.7 & 9.7 & 5.7 \\ 9.3 & 12 & 12 & .4 & .4 & .4 & 5.7 & 5.7 & 9.7 \end{bmatrix} | \Delta \theta | \quad (2.4-13)$$

and

$$(\text{abs } A^{-1})(\text{abs } \Delta A) \approx$$

$$\left[ \begin{array}{ccc|ccc} 0 & 1 & 1 & 1 & 1 & 0 \\ 1 & 0 & 1 & 0_{3 \times 3} & 1 & 0 & 1 \\ 1 & 1 & 0 & & 1 & 0 & 1 \\ \hline 0 & 1 & 1 & 1 & 1 & 0 \\ 1 & 0 & 1 & 0_{3 \times 3} & 1 & 0 & 1 \\ 1 & 1 & 0 & & 1 & 0 & 1 \\ \hline 2.8 & 2.8 & 4.8 & 2 & 2 & 0 & 4.8 & 2.8 & 2.8 \\ 2.8 & 4.8 & 2.8 & 2 & 0 & 2 & 2.8 & 4.8 & 2.8 \\ 4.8 & 2.8 & 4.8 & 0 & 2 & 2 & 2.8 & 2.8 & 4.8 \end{array} \right] |\Delta\theta| \quad (2.4-14)$$

Here  $(\text{abs } B^{-1})(\text{abs } \Delta B)$ ,  $\text{abs } B^{-1}$  and  $(\text{abs } B^{-1})(\text{abs } \Delta B)$  are the upper left  $6 \times 6$  matrices of (2.4-13) and (2.4-24), respectively.

Existence of an inverse for the perturbed A matrix is guaranteed by

$$|(\text{abs } A^{-1})(\text{abs } \Delta A)|_{\infty} \approx 25 |\Delta\theta| < 1$$

or

$$|\Delta\theta| < \frac{1}{25} \text{ rad} = 2.28^\circ$$

By contrast, the limit on  $|\Delta\theta|$  for the perturbed B matrix is given by

$$|(\text{abs } B^{-1})(\text{abs } \Delta B)|_{\infty} \approx 2 |\Delta\theta| < 1$$

(2.4-16)

or

$$|\Delta\theta| < \frac{1}{2} \text{ rad} = 26.5^\circ$$

The 10:1 reduction in the allowed perturbation limit in going from the nominal B matrix to the nominal A matrix is the penalty paid when introducing the last 3 non-orthogonal rows (orientations 7-9 listed previously) needed to estimate misalignments.

Choice of operating values for  $|\Delta\theta|$  within the limits prescribed by (2.4-15) or (2.4-16) depends on an analysis of predicted estimation errors using the expressions introduced in this section and expected accelerometer errors.

## 2.5 Iterative Solutions

When, for any one accelerometer, the normalized parameters in the error  $E_j/g^2$  (equation (2.3-10)) are on the order of 1000 ppm, their resultant contribution to the non-linear terms in  $E_j/g^2$  will be on the order of 1 ppm. In this case, the linear set (2.3-12) can be safely solved without any appreciable error due to the neglect of the non-linear terms. This situation would certainly hold if the accelerometer modules were pre-calibrated, even roughly, before installation in the strapdown system. If there is no such pre-calibration, the solution for accelerometer parameters outlined in the two preceding sections must be able to accommodate especially large values of  $b_i/g$  and  $SF_i$ . Tables 2B-1 - 2B-2 presented in Appendix 2B yield system specifications for the LCIGS accelerometers and V/F converters. From these tables, it is concluded that installation of uncalibrated accelerometer modules would require accommodation of a normalized bias of 10,000 ppm (combining accelerometer and V/F converter biases) and a combined

accelerometer and V/F converter scale factor error of 60,000 ppm for each module.

A simple iterative procedure for the solution of the linearized equations (2.3-12) will account for these large initial values in bias and scale factor error.

The first 6 equations ( $j = 1, \dots, 6$ ) are solved iteratively with any coupling of the misalignment parameters ignored. The contribution of the misalignment errors to any of the first 6 equations is of second order. (See the first 6 rows of the nominal A matrix, equation (2.4-6).) Any perturbation to matrix A represented by a deviation  $\Delta\theta$  from the perfectly leveled orientation will result in only a small coupling of the misalignment parameters. The 6 equations are first solved to yield initial estimates of  $SF_i$  and  $b_i$ . The  $C_{ij}$  coefficients are then corrected using these values. That is: Let  $\hat{SF}_i(n)$ ,  $b_i(n)$  represent incremental bias and scale factor error estimates at the  $n^{\text{th}}$  iteration. Then, the coefficients  $C_{ij}(n+1)$  for the next iteration are given by

$$C_{ij}(n+1) = \frac{C_{ij}(n) - b_i(n)/g}{1 + SF_i(n)} \quad (2.5-1)$$

which are substituted into the linearized equation set. The set is then solved for  $b_i(n+1)$  and  $SF_i(n+1)$  and the process is continued.

After  $N$  iterations, the overall scale factor error,  $\hat{SF}_i(N)$  that we have compensated during the iteration procedure is given by

$$1 + \hat{SF}_i(N) = \prod_{n=0}^N (1 + SF_i(n)) \quad (2.5-2)$$

whereas the overall compensated bias,  $b_i(N)$ , is given by

$$\hat{b}_i(N) = \frac{1}{1 + \hat{SF}_i(N)} \left\{ b_i(0) + b_i(1)(1 + SF_i(0)) + b_i(2)(1 + SF_i(0))(1 + SF_i(1)) + \dots + b_i(N) \left[ (1 + SF_i(0)) \dots (1 + SF_i(N-1)) \right] \right\} \quad (2.5-3)$$

The full set of 9 equations is then used to solve for the incremental scale factor error  $SF_i(N+1)$ , the incremental bias  $b_i(N+1)$  and the misalignments  $\alpha$ ,  $\gamma$ ,  $\delta$ . The equation coefficients are  $C_{ij}(N+1)$ .

Finally, we obtain

$$1 + \hat{SF}_i(N+1) = (1 + \hat{SF}_i(N))(1 + SF_i(N+1))$$

$$\hat{b}_i(N+1) = b_i(N) + (b_i(N+1))(1 + \hat{SF}_i(N))(1 + \hat{SF}_i(N+1))^{-1} \quad (2.5-4)$$

and  $\hat{\alpha}$ ,  $\hat{\delta}$ ,  $\hat{\gamma}$  the misalignment estimates from the 9 equation solution.

At the end of the  $n^{\text{th}}$  iteration, the error in estimating the  $n^{\text{th}}$  incremental values of  $SF_i$  and  $b_i$ , due to neglect of non-linearities is easily determined from the expression for  $E_j/g^2$  given by equations (2.3-10), (2.3-11) and (2.3-6). That part of  $E_j/g^2$  due solely to neglect of the non-linear terms that involve only  $SF_i$  and  $b_i$  is given to a close approximation by

$$\left\{ \begin{array}{l} \text{Non-linear} \\ \text{terms} \\ \text{in } SF_i \text{ and } b_i \\ \text{in the} \\ \text{expression } E_j/g^2 \end{array} \right\} \approx \sum_{i=1}^3 \left[ \frac{1}{2} \left( \frac{b_i(n)}{g} + SF_i(n) \frac{\bar{g}_{ij}}{g} \right)^2 + C_{ij} SF_i(n) \left( \frac{b_i(n)}{g} + SF_i(n) \frac{\bar{g}_{ij}}{g} \right) \right] \quad (2.5-5)$$

The neglected non-linear terms will, therefore, decrease as the squares of the incremental estimates  $SF_i(n)$ ,  $b_i(n)$ . Convergence will, therefore, be extremely fast. A numerical example is presented in Section 2.6

## 2.6 Prediction of Estimation Errors for the LCIGS

A prediction of estimation errors using the iterative technique illustrated in the previous section and the equations developed in Sections 2.3 and 2.4 is made below for the LCIGS.

There is a lack of data for representative field environments. Therefore, the hypothesized angular and translational vibration spectra are presented by H. Weinstock in Reference 23. Figure 2.6-1 depicts these spectra. It is assumed that the vertical translational spectrum is the same as the horizontal spectrum shown in the Figure.

Expected accelerometer non-orthogonality based on machining practices used with the LCIGS<sup>24</sup> should be well within the 3 mrad value used in the subsequent analysis.

Specifications of the LCIGS accelerometer module including the V/F converter are listed in Appendix 2B, Tables 2B-1 and 2B-2. The bias and scale factor stability estimates in these tables are standard deviations over 1 hour periods. In order to be conservative, these values and the values for the V/F calibration estimates described in Appendix 2B will be used as the standard deviations for each new orientation of the system.

At this point, the nominal and perturbed matrices in Section 2.4 must be re-examined in order to correctly utilize the preceding data. Selection of a perturbation value of  $1/2^{\circ}$  is well below the upper limit of  $2.28^{\circ}$  (equation (2.4-15)) and also results in a quite loose tolerance for positioning and leveling the calibration fixture. Substitution of

$$|\Delta\theta| = \frac{1}{2}^{\circ} \approx 0.01 \text{ rad} \quad (2.6-1)$$

into the appropriate equations in Section 2.4 yields.

$$|\text{abs } A^{-1}) (\text{abs } \Delta A)|_{\infty} \approx 0.25 \quad (2.6-2)$$

$$|(A^{-1} + \Delta A)^{-1}|_{\infty} \leq |A^{-1}|_{\infty} / |I - A^{-1} \Delta A|_{\infty} = 6.45 \quad (2.6-3)$$

$$\text{abs } (A + \Delta A)^{-1} \approx \text{abs } A^{-1} + (\text{abs } A^{-1}) (\text{abs } \Delta A) \quad (\text{abs } A^{-1}) =$$

$$\left[ \begin{array}{cccccc|cccccc} .524 & .017 & .017 & 1.504 & .007 & .007 & .02 & .02 & 0 \\ .017 & .524 & .017 & 1.007 & .504 & .007 & 1.02 & 0 & .02 \\ .017 & .017 & .524 & 1.007 & .007 & .504 & 1.02 & 0 & .02 \\ \hline .524 & .017 & .017 & 1.504 & .007 & .007 & 1.02 & .02 & .02 \\ .017 & .524 & .017 & 1.007 & .504 & .007 & 1.02 & .02 & 0 \\ .017 & .017 & .524 & 1.007 & .007 & .504 & 1.02 & 0 & .02 \\ \hline 1.33 & 1.33 & .093 & 1.25 & .25 & .25 & .036 & 2.097 & .057 \\ 1.33 & .093 & 1.33 & 1.25 & .036 & .25 & .057 & 2.097 & .057 \\ .093 & 1.33 & 1.33 & .036 & .25 & .25 & .057 & 2.097 & .057 \\ \hline \end{array} \right] \quad (2.6-4)$$

The approximation given by (2.6-4) has a  $p = \infty$  norm of 5.5 which is only 19% below the pessimistic bound of 6.45 given by (2.6-3). We, therefore, use the approximation given by (2.6-4) with the confidence that it will not yield results that are too optimistic.

The following error assessments are made for use with the approximate matrix (2.6-4) in evaluating the iteration sequence.

Initially,  $E_j$  (equation (2.3-10)) is dominated by the large initial scale factor and bias uncertainties. Nominal orientations (1) - (6) yield

$$E_j/g^2 \approx \frac{1}{2} \left( SF_i + \frac{b_i}{g} \right)^2 + \left( \sum_{i=1}^3 \frac{b_i^2}{2g^2} \right) - \frac{b_i^2}{2g^2} + SF_i \left( SF_i + \frac{b_i}{g} \right) \quad (2.6-5)$$

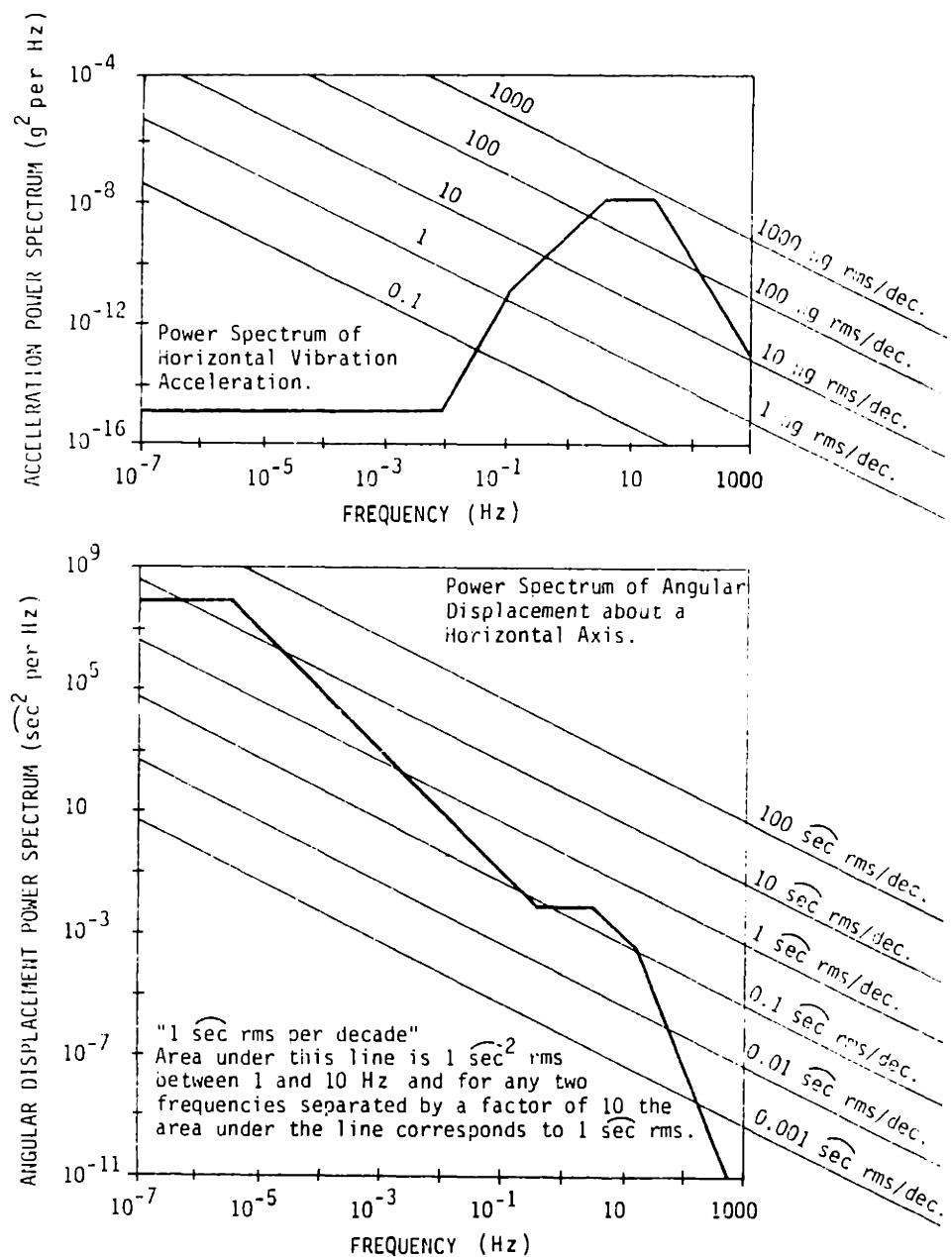


Figure 2.6-1 Representative Vibration Environment of an Urban Test Laboratory

where

$i = \text{either 1 or 2 or 3}$

$j = 1, \dots, 6$

Substituting the values from Tables 2B-1 and 2B-2, in Appendix 2B, into the above yields a maximum value for  $E_j$  of

$$\max E_j/g^2 \approx 0.00675 \quad (2.6-6)$$

A glance at the first 6 rows of (2.6-5) shows that the initial solution would yield maximum errors of 6750 ppm for the scale factor and 6750  $\mu\text{g}$  for the bias. After the next iteration, that portion of  $E_j/g^2$  involving only the bias and scale factor errors is again given by (2.6-5). Substituting the above errors from the first solution into (2.6-5) yields a value of

$$\max \frac{E_j}{g^2} \approx 230 \text{ ppm} \quad (2.6-7)$$

Estimation of solution errors can now proceed with the non-linear error terms neglected provided the terms (eq. (2.3-10))

$$\frac{\overline{\Delta g_{ij}^2}}{g^2} \quad \frac{\Delta \bar{n}_{ij}}{g^2}$$

are much smaller than 230 ppm. This is shown in the following evaluations.

For a minimum averaging time of 30 seconds, it is deduced from Figure 2.6-1 by Weinstock that the horizontal translational acceleration standard deviation is 0.67  $\mu\text{g}$ . We will use 10 times this figure or 6.7  $\mu\text{g}$ . Also, over the low frequency range of interest in

the angular spectrum that the  $1\sigma$  value of  $\Delta g_{ij}$  is 0.01 milli-g. We will use .1 milli-g. It is immediately seen that even for .1 milli-g,

$$\frac{\overline{\Delta g_{ij}^2}}{g^2} = 0.1 \text{ ppm}$$

Errors due to accelerometer quantization are neglected because it is assumed that the effects of any quantization will be practically eliminated through use of the quantization reduction scheme presented in Chapter 3.

Composite standard deviations for the linear portion,  $\sum_{i=1}^3 r_{ij} \Delta r_{ij}$ ,

of the error given by (2.3-10) corresponding to the nominal orientations (1) - (9) defined in Section 2.4 are listed below. Each value was computed with the data presented above in this section and the data in Appendix 2B. For any one orientation, the errors due to a separate source (e.g., scale factor, error, V/F converter calibration errors, etc.) were considered to be statistically independent. However, no assumptions are made about statistical correlations between orientations.

Nominal Orientation	Composite Standard Deviation (ppm)	
1	51.5	
2	51.5	
3	51.5	Table 2.6-1 -
4	47.4	<u>LCIGS Composite</u>
5	47.4	<u>Standard Deviations</u>
6	47.4	<u>for 9 Nominal</u>
7	33.6	<u>Orientations</u>
8	33.6	
9	33.5	

These standard deviations are also assumed to hold accurately for the perturbed orientations since additional errors introduced by the perturbations are multiplied by small values ( $\leq 0.01$  as given by Equation (2.6-1)).

The composite errors for orientations (7) - (9) are, of course, strongly correlated with the errors for orientations (1) - (3) and this is taken into account in computing the standard deviations of the estimates obtained through multiplication of the linear error vector

$$\left[ \begin{array}{c} \vdots \\ -\sum_{i=1}^3 n_{ij} \Delta n_{ij} \\ \vdots \end{array} \right]$$

by the perturbed nominal matrix inverse given by Equation (2.6-4). [The small matrix elements are ignored.] The results are approximate bounds of 50  $\mu g$ , 50 ppm, 36 arc-sec on the bias, positive scale factor error and misalignment estimate standard deviations respectively.

A bound of 84 ppm is put on the negative scale factor error estimate standard deviation to account for the error in the V/F scale factor ratio  $\frac{K_-}{K_+}$  described in Appendix 2B.

**Chapter 3**  
**Accelerometer Quantization**

### 3.1 Introduction

An advantage in reducing accelerometer quantization during gyro calibration procedures is deduced from examining simple gyro drift estimation models that are compatible with the more representative but complicated models presented in Chapter 4. Little is gained by reducing the planned LCIGS accelerometer velocity quantum of 1 cm/sec if white noise can always be used to represent the effects of gyro and accelerometer quantization. However, whether or not the white noise hypothesis is valid, we are guaranteed that gyro drift estimation errors and errors in the estimated error angles will be sufficiently small over acceptable filtering times when the effects of accelerometer quantization are appreciably reduced. Furthermore, it is demonstrated that regardless of the applicability of the white noise hypothesis, there is a large reduction in accelerometer calibration time when the velocity quantum is reduced.

Quantization can be reduced through the linear extrapolation technique presented in Section 3.3. The supposition is that the integral of the accelerometer analog loop output is converted to digital form with a staircase type quantizer such as the combination of a V/F converter feeding into a counter. The basic principle used is that the quantizer output is a true representation of the input at the exact time at which the quantizer output has just changed from a previous value. (At this time the input is exactly equal to the known quantizer input threshold.) Knowing the times at which the quantizer output has changed (i.e., the time of occurrence of the V/F converter output pulses) allows computation of a slope and prediction of the output at update times occurring between output steps. See Figure 3.1-1.

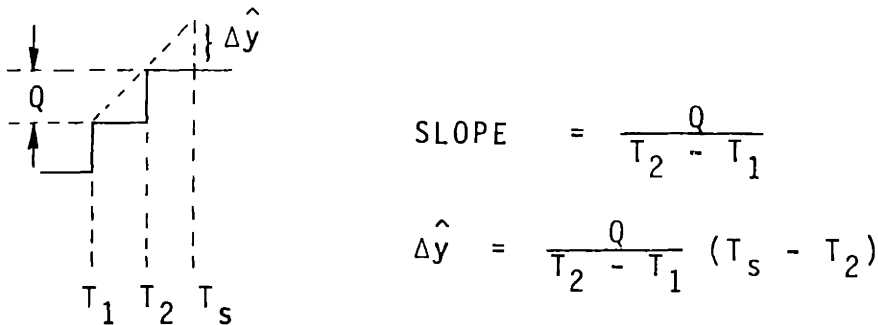


Figure 3.1-1 Linear Extrapolation Principle

Also note that for linear extrapolation to work with inputs having a high bandwidth, the input to the quantizer must be biased whether by actually introducing an external bias (e.g., 1000 cm/sec<sup>2</sup> at the V/F converter input) or by properly orienting the input axis of the accelerometer to pick up a large component of g. This requirement results in frequent enough exact samples (at  $T_1$ ,  $T_2$ , etc.) for linear extrapolation.

An example is given in Section 3.4 to demonstrate that with the application of sufficient external bias, the linear extrapolation error can be negligible for a sinusoidal input due to rotation of the accelerometer. In any event the linear extrapolation error is zero for a constant input to the V/F converter integrator (Figure 3.3-1, Section 3.3) and errors result only from the measurement errors of the times  $T_1$ ,  $T_2$ ,  $T_s$  illustrated in Figure 3.1-1. On the basis of the timing frequency of 192 KHz used in the LCIGS hardware<sup>25</sup> to verify the linear extrapolation concept, it is predicted that quantization will be reduced from 1 cm/sec to a value on the order of .01 cm/sec for constant inputs to the integrator. Actual results from hardware testing will be presented in Chapter 6. Finally, it is suggested in Section 3.5, that addition of a bias is not necessary during

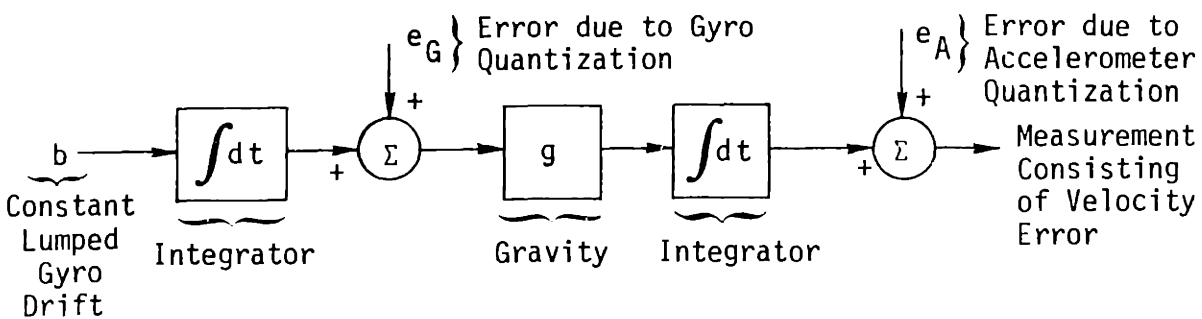
accelerometer calibration but should be done when estimating gyro static lumped drift. The question of adding a bias during large rotation of the system is more complex and it is briefly concluded that the accelerometer modules whose inputs are not parallel to the axis of rotation may not need the additional bias because they are subjected to relatively large values of gravity for 90% of the rotation.

### 3.2 Overview of Quantization Effects

The effects of gyro and accelerometer quantization on estimates of both lumped gyro drifts and error angles that are obtained by means of the Kalman filters described in the next chapter can be accurately ascertained only through numerical computations or simulations. However, valuable insight into the likely results and into what must be done, if anything, about the quantization is easily obtained through the simple computations given below. As a byproduct the effects of accelerometer quantization on the accelerometer calibration procedure of the last chapter and the consequent need for a method to reduce the quantization during accelerometer calibration are also determined in this chapter.

Gyro quantization for the integrating gyro modules used by the LCIGS is characterized by a positive or negative quantum of angle (approximately 3 arc-sec). The gyro output is considered to be the sum of these quanta or a net accumulation of angle. Similarly, accelerometer quantization is characterized by a quantum of velocity (approximately 1 cm/sec).

The simple model for measuring gyro drift illustrated below is directly introduced in place of deducing the relatively complicated model resulting from the mechanizations of strapdown attitude, velocity, and alignment algorithms, as will be done in the next chapter.



Although this model is simpler than the more realistic model shown in Chapter 4, it is consistent with that model.

The effects of errors on the drift estimate due to gyro and accelerometer quantization will be considered separately. The results will be optimistic when compared with a Kalman filter estimation in the presence of both error sources and therefore represent lower bounds on the estimation error.

In the absence of accelerometer quantization, it is theoretically possible to differentiate without error the measurement shown in Figure 3.2-1, divide by  $g$ , and so obtain an equivalent measurement, contaminated only by gyro quantization noise, from which estimates of the constant gyro drift are to be made. The model for this situation is shown below.

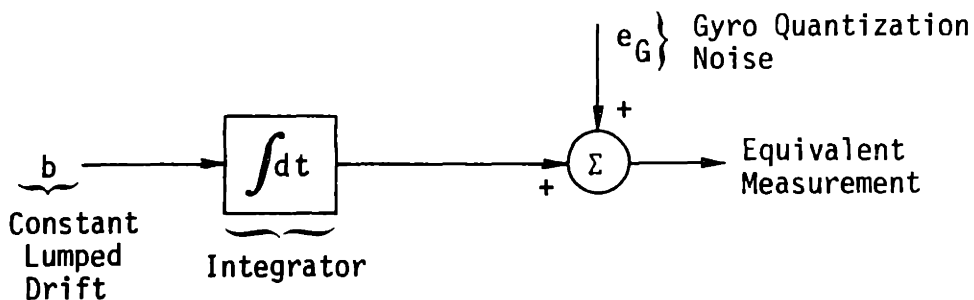


Figure 3.2-2 Drift Measurement Model in the Absence of Accelerometer Quantization

For measurements  $m_i$  at discrete times  $t_i$ , where  $i$  denotes the measurement sample,

$$m_i = b t_i + e_{G_i} \quad (3.2-1)$$

assuming a zero initial condition on the integrator. Estimation of the constant lumped drift,  $b$ , is obtained using the standard least squares fit<sup>26</sup> to the measurement data. This estimate is

$$\hat{b} = \frac{\sum_{i=1}^N m_i t_i}{\sum_{i=1}^N t_i^2} = b + \frac{\sum_{i=1}^N e_{G_i} t_i}{\sum_{i=1}^N t_i^2} \quad (3.2-2)$$

Evaluation of the error term

$$e_b = \frac{\sum_{i=1}^N e_{G_i} t_i}{\sum_{i=1}^N t_i^2} \quad (3.2-3)$$

depends on the assumptions made about the nature of the gyro quantization error  $e_{G_i}$ . A common assumption<sup>27,28</sup> almost always used in designing Kalman filters, is that the quantization errors are well approximated by a zero average "white noise" sequence having a uniform probability distribution. For a quantum of angle  $Q$ , the statistical characteristics of  $e_{G_i}$  would then be given by

$$\begin{aligned} \bar{e}_{G_i} &= 0 \\ \bar{e}_{G_i} e_{G_j} &= 0, \quad i \neq j \\ \bar{e}_{G_i}^2 &= Q^2 / 12 \end{aligned} \quad (3.2-4)$$

Use of equations (3.2-4) in evaluating (3.2-3) yields

$$\bar{e}_b = 0$$

$$\bar{e_b^2} = \bar{e_{G_i}^2} \sum_{i=1}^N t_i^2 / \left( \sum_{i=1}^N t_i^2 \right)^2 = \bar{e_{G_i}^2} / \sum_{i=1}^N t_i^2 \quad (3.2-5)$$

The sum in (3.2-5) is closely approximated by

$$\sum_{i=1}^N t_i^2 \approx \frac{T^3}{3\Delta t} \quad (3.2-6)$$

where

$$T = t_N = \text{total estimation time}$$

$$\Delta t = \text{period between successive measurements}$$

$$t_N = N\Delta t$$

Substituting (3.2-6) and (3.2-4) into (3.2-5) and taking the square root results in a standard deviation for  $e_b$  given by

$$\bar{\sigma}_{e_b} \triangleq \sqrt{\bar{e_b^2}} \approx \frac{1}{2} \sqrt{\frac{\Delta t}{T}} \frac{Q}{T} = \frac{1}{2\sqrt{N}} \frac{Q}{T} \quad (3.2-7)$$

An alternative to the preceding statistical approach is to place the following bound on the magnitude of the estimation error

$$|e_b| \leq \frac{Q}{2T} \quad (3.2-8)$$

This bounds holds when, in place of the least squares fit, the estimate of the drift,  $b$ , is obtained by dividing the total accumulated angle  $m_N$  by the accumulation time  $T$ . If a least squares fit is used, then it

is easily shown that the bound on  $|e_b|$  is closely approximated by

$$|e_b| \leq (1.5) \frac{Q}{2T} \quad (3.2-9)$$

with the assumption that

$$|e_{G_i}| \leq \frac{Q}{2} \quad (3.2-10)$$

The difference in magnitude between the statistical figure of merit given (3.2-7) and the bounds given by (3.2-8) and (3.2-9) is large even for modest values of  $T$  and  $\Delta t$ . For example, a sample period of 0.1 sec and a total accumulation time of only 1 minute results in  $N = 600$  samples so that

$$\bar{e}_b \approx \frac{1}{25} \left( \frac{Q}{2T} \right), \quad N = 600 \quad (3.2-11)$$

for a statistical figure of merit that is 25 times smaller than the more intuitive figure given by (3.2-8). A common source of concern about the validity of (3.2-11) arises from a confusion between the minimum drift that is measurable over a fixed interval and the accuracy to which a drift can be estimated when it is greater than the measurable minimum. Obviously, for an angle quantum of  $Q$  and a measurement interval equal to  $T$ , the bound given by (3.2-8) is also 1/2 the minimum possible constant drift that is detectable during the interval.

However, if the assumptions about the statistics of the quantization errors given by (3.2-4) are valid, then the standard deviation of the zero mean estimation error can be 50 times smaller than the minimum detectable drift as in the above example.

Covariance analysis of Kalman filter estimation errors will, of course,

yield results that are closer to the much smaller statistical figure of merit, (3.2-11), than to the intuitive upper bound because the white noise assumption is used in designing the filter. On the other hand, direct Monte-Carlo type simulations of the filter may not yield small estimation errors. This depends on how the quantization noise is generated in the simulation model as opposed to merely introducing a white noise sequence in the simulation to directly represent the hypothesis implied by equations (3.2-4). The white noise quantization error hypothesis is based on the assumption that the gyros (in the case under discussion) will be subject to more than just the constant drifts represented in Figure 3.2-2. In particular, it is expected that random angular base motion (such as described for a typical urban test laboratory in the last chapter) and perhaps gyro module electronics noise will be sufficient to cause the quantization error to approximately resemble white noise without the need for any external artificial dither.

In the absence of any such additional excitations in either the simulations or the actual situation, the quantization error becomes highly dependent on the magnitude of the lumped drift input (Figure 3.2-2). Estimation error due to gyro quantization would therefore, be a function of this magnitude but in any event could not exceed the worst case bound given by (3.2-9) for our example.

In the absence of gyro quantization error, the model shown below is appropriate for measuring lumped drift.

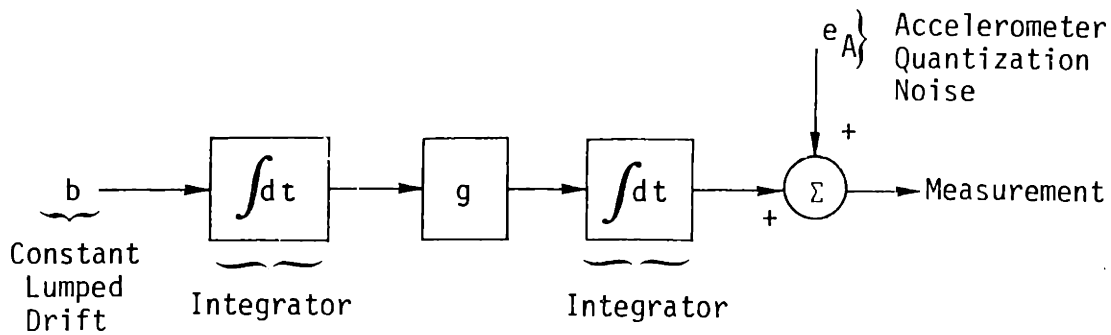


Figure 3.2-3 Drift Measurement Model in the Absence of Gyro Quantization

For measurements  $m_i$  at discrete times  $t_i$  and zero initial conditions on both integrators, the standard least squares fit to the measurement data results in the following estimate for the drift.

$$\hat{b} = \frac{2 \sum_{i=1}^N m_i t_i^2}{g \sum_{i=1}^N t_i^4} = b + \frac{2 \sum_{i=1}^N e_{Ai} t_i^2}{g \sum_{i=1}^N t_i^4} \quad (3.2-12)$$

The error term

$$e_b = \frac{2 \sum_{i=1}^N e_{Ai} t_i^2}{g \sum_{i=1}^N t_i^4} \quad (3.2-13)$$

has a standard deviation closely approximated by

$$\sigma_{eb} \approx \frac{1.3 Q_A}{g T^2 \sqrt{N}} \quad (3.2-14)$$

where  $Q_A$  is the accelerometer quantum of velocity when the accelerometer quantization errors  $e_{Ai}$  are assumed to be zero average white noise sequences

with a uniform probability distribution.

An alternative measure of drift estimation error is given by the bound

$$|\epsilon_b| \leq 1.7 Q_A / gT^2 \quad (3.2-15)$$

for a bound of

$$|\epsilon_{A,i}| \leq \frac{Q_A}{2} \quad (3.2-16)$$

Applicability of either figure of merit ((3.2-14) or (3.2-15)) is based on the same considerations presented for estimation of gyro drift in the presence of only gyro quantization error except for the expectation that random linear acceleration of the base in addition to random angular base motion will be sufficient to cause the accelerometer quantization error to resemble white noise.

Comparison of the respective figures of merit (3.2-7) versus (3.2-14) and (3.2-9) versus (3.2-15) suggests the following definition of an equivalent quantum of angle,  $Q_{eq}$ , in terms of the accelerometer velocity quantum,  $Q_A$ , which approximately results in the same figures of merit for drift estimation error due only to accelerometer quantization.

$$Q_{eq} \triangleq 2Q_A / gT \quad (3.2-17)$$

The above equivalent angle quantum thus allows a direct comparison between the effects of a particular gyro angular quantum and a particular accelerometer velocity quantum. For example, one minute of estimation time and the LCIGS velocity quantum of 1 cm/sec results in

$$Q_{eq} \cong \frac{(2)(1)}{(980)(60)} = 0.034 \text{ mrad} \cong 7 \text{ sec.} \quad (3.2-18)$$

compared to a true gyro angular quantum of 3 arc-sec. If the white noise hypothesis were true for both the gyro and accelerometer quantizations, the standard deviations of drift estimation errors for each noise source after one minute are approximately.

$$\sigma_{eb} \approx 0.001^\circ/\text{hr}, Q = 3 \text{ sec}$$

$$\sigma_{eb} \approx 0.0024^\circ/\text{hr}, Q_{eq} = 7 \text{ sec} \quad (3.2-19)$$

and neither quantum value is a cause for concern. On the other hand, the respective bounds on drift estimation error (using the least squares method) are approximately

$$|e_b| \leq 0.038^\circ/\text{hr}, Q = 3 \text{ sec} \quad (3.2-20)$$

$$|e_b| \leq 0.088^\circ/\text{hr}, Q_{eq} = 7 \text{ sec}$$

and some benefit in reducing  $Q_{eq}$  (i.e., accelerometer quantization) is apparent.

Introduction of a suitable simplified model for a measurement of error angle during a rotation of the strapdown system is not as clear cut as for the drift measurement models presented above because of the presence of unmodeled drifts driving the build up of the error angle. The Kalman filters described in the next chapter that are used to estimate the error angle accommodate these drifts through the use of white noise random drivers. A procedure for correcting the angle estimates in order to account for the effect of the unmodeled true drifts can be implemented after completion of the entire sequence of static system positions and rotations. However, if the unmodeled drift were a constant, then an optimum estimate of error angle (with zero initial conditions on the integrators) which would serve as a

standard of comparison with the actual corrected angle estimate is given by

$$\hat{e}_a = \hat{b}T \quad (3.2-21)$$

where  $\hat{b}$  is the optimal estimate of the drift given by (3.2-12) when considering only the effects of accelerometer quantization errors. (Obviously if only gyro quantization error was being considered, then the optimal error angle estimate is equivalent to merely differentiating the measurement in Figure 3.2-1, and dividing the result by g. The error in this ideal estimate is therefore the quantum of angle itself.)

The error in  $\hat{e}_a$  can thus be characterized by multiplying each of (3.2-14) and (3.2-15) by T to yield

$$\sigma_{\hat{e}_a} \approx \frac{1.3 Q_A}{gT\sqrt{N}}, \text{ white noise assumption for accelerometer quantization} \quad (3.2-22)$$

$$|\hat{e}_a| \leq \frac{1.7 Q_A}{gT}, \text{ bound on error angle estimation error due to accelerometer quantization} \quad (3.2-23)$$

Comparison of (3.2-22) and (3.2-23) with the corresponding estimation error measures present with only gyro quantization

$$\sigma_{\hat{e}_a} \approx \frac{Q}{\sqrt{2}}, \text{ white noise assumption for only gyro quantization} \quad (3.2-24)$$

$$|\varepsilon| \leq Q, \text{ bound on error angle estimation} \quad (3.2-25)$$

due only to gyro quantization

suggests the continued applicability of the equivalent quantum of angle defined by (3.2-17) for only the upper bound figures of merit given by (3.2-23) and (3.2-25).

For the following estimation period recommended in Chapter 5,

$$T = 10 \text{ second} \quad (3.2-26)$$

the equivalent angle quantum is

$$Q_{eq} \approx \frac{(2)(1)}{(10)(980)} = 0.2 \text{ mrad} \approx 42 \text{ sec} \quad (3.2-27)$$

when the velocity quantum is 1 cm/sec. The accelerometer quantization influence on error is not well matched with the gyro quantization influence for the 10 second rotation duration and there is a much stronger indication here for the desirability of reducing accelerometer quantization. Although as before, if the white noise sequence hypothesis actually holds, the comparatively large value of  $Q_{eq}$  above will still have little consequence on the estimation procedures in Chapter 5.

An unequivocal necessity for reducing accelerometer quantization is found upon examining the accelerometer calibration procedure in Chapter 2. This procedure utilizes the direct average of the accelerometer outputs over a specified estimation period. The two figures of merit for the averaged acceleration when dealing only with accelerometer quantization

are therefore

$$\overline{\sigma_{ae}} = \frac{Q_A}{T\sqrt{12}}, \text{ white noise sequence assumption} \quad (3.2-28)$$

$$|\sigma_{ae}| \leq \frac{Q_A}{2T} \rightarrow \text{bound on error in average acceleration} \quad (3.2-29)$$

where  $\sigma_{ae}$  is the error in the computed average acceleration. These error measures would have to be on the order of 1  $\mu\text{g}$  in order to be negligible compared to say the 15  $\mu\text{g}$  bias uncertainties cited in Chapter 2. Setting

$\sigma_{ae} = 1 \mu\text{g}$  yields a required value for  $T$  of

$$T = \frac{(1 \text{ cm/sec})}{(\sqrt{12})(980 \times 10^{-6} \frac{\text{cm}}{\text{sec}^2})} \approx 295 \text{ sec} \approx 5 \text{ minutes} \quad (3.2-30)$$

A bound of 1  $\mu\text{g}$  results in a required value for  $T$  of

$$T = \frac{(1)}{(2)(980 \times 10^{-6})} \approx 510 \text{ sec} \approx 8.5 \text{ minutes} \quad (3.2-31)$$

Clearly, averaging times on the order of the above are out of the question when implementing the procedure in Chapter 2 for fast calibration.

### 3.3 A Method for Reducing Accelerometer Quantization-Linear Extrapolation

A summary of the properties of the LCIGS accelerometer module described in Appendix 2B, Chapter 2 is as follows.

We are dealing specifically with a quantizer consisting of a V to F

converter whose output is a succession of pulses occurring at a frequency that is directly proportional to the accelerometer measurement. (This measurement is obtained from the accelerometer analog torque to balance loop.) The accumulation of these pulses (i.e., counting them) as the final output of the quantizer can be represented by an integrator feeding directly into a staircase non-linear element. See Figure 3.3-1. The accumulated output of the more conventional integrating accelerometer pulse torquing loop can be represented by the same configuration.

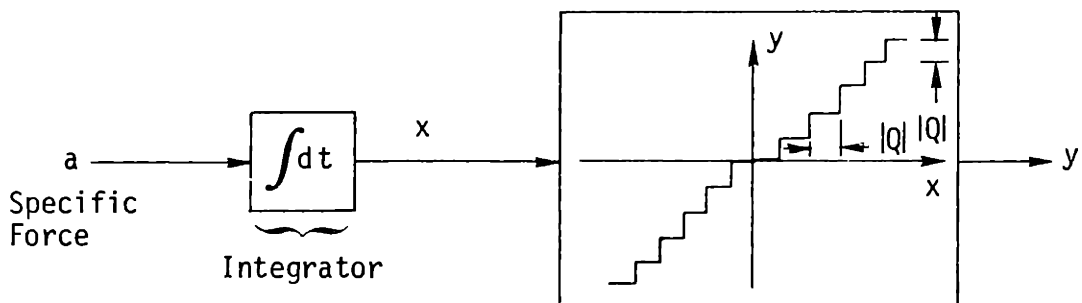


Figure 3.3-1 Representation of Accelerometer Quantization

Reduction of the inherent quantization  $Q$  (the height of a step in Figure 3.3-1) is based on the fact that if we knew exactly (in time) when a change in the accumulated pulse count occurred, then at that point in time we have an exact sample of the input to the non-linear element (i.e., the velocity). In terms of Figure 3.3-1, this means that when  $y$  has just changed, we know that the input  $x$  must be exactly at one of the staircase levels in order to have caused the change. However, even if we knew the exact times for all of the changes in the non-linear output, there is no guarantee that these exact samples will occur frequently enough with respect to an input having a high frequency content. This limitation may be overcome by ensuring that the output of the integrator in Figure 3.3-1 is com-

posed of the desired velocity (e.g., due to base motion) and a ramp. The ramp can be artificially introduced, if necessary, by adding a known bias to the input of the integrator or will naturally occur during a calibration when the accelerometer input axis is sufficiently tilted away from the horizontal plane. The ramp will ensure that the "exact" samples we are obtaining at the Q transition times will occur rapidly in time. If the ramp slope is too small, we will not get enough "true" samples per second. If the ramp slope is too high, Q changes occur too frequently with respect to the "time strobe" that is used to indicate the correct sample. Analysis leading to the proper range of ramp slopes for a particular case is presented in Section 3.4. Another serious problem in using the exact samples is that they occur asynchronously with respect to the algorithms that require them as inputs. This limitation can be overcome by the use of the following linear extrapolation scheme. By means of a fine enough time strobe, the time between the last two "true" samples can be measured and the corresponding average slope of these samples computed. Thus,

$$\text{slope} = \frac{Q}{\Delta t_N} = \frac{Q}{t_N - t_{N-1}} \quad (3.3-1)$$

where  $\Delta t_N$  = time between two  $\pm Q$  transitions occurring respectively at  $t_N$  and  $t_{N-1}$ .

At a later time  $t_{N+\delta}$  when the quantizer output is actually required a linear extrapolation is performed as follows:

$$y(t) = y(t_N) + \underbrace{f_{t_N} \delta}_{\text{linearly extrapolated term}}$$

$$\delta = t_{N+\delta} - t_N = t - t_N \quad (3.3-2)$$

$\Delta t$  = fixed time interval between required samples

An analysis of the above method for reducing quantization is presented in Sections 3.4 and 3.5.

### 3.4 Analysis of Linear Extrapolation Method

An upper bound on the linear extrapolation errors is derived as follows.

Maintaining all of the assumptions presented in the previous section results in the following relation.

$$f(t_N) - f(t_{N-1}) = Q \quad (3.4-1)$$

$f(t)$  = quantizer input

$t_N$  = time at which  $f(t)$  crosses  $N^{\text{th}}$  quantizer level

$Q$  = quantization

Expanding  $f(t_{N-1})$  in a Taylor series with remainder yields

$$f(t_{N-1}) = f(t_N) - f'(t_N) \Delta t_N + \frac{f''(t_N - \xi)}{2} \Delta t_N^2$$

$$\Delta t_N \stackrel{\Delta}{=} t_N - t_{N-1}$$

$$0 \leq \xi \leq \Delta t_N \quad (3.4-2)$$

Substituting (3.4-2) into (3.4-1) yields

$$f'(t_N) \Delta t_N - \frac{f''(t_N - \xi)}{2} \Delta t_N^2 = Q \quad (3.4-3)$$

A first order approximation for  $\Delta t_N$  is given by

$$\Delta t_N \approx Q/f'(t_N) \quad (3.4-4)$$

For  $\Delta t_N$  sufficiently small a closer approximation is obtained by substituting (3.4-4) into the second term of the left hand side of (3.4-3). (This expression can also be obtained through a series representation of the quadratic solution.<sup>29</sup>)

$$\Delta t_N \approx \frac{Q}{f'(t_N)} + \frac{f''(t_N - \xi)}{2 f'(t_N)} \left( \frac{Q}{f'(t_N)} \right)^2 \quad (3.4-5)$$

The error in the above approximation can be numerically evaluated for a specific  $f(t)$ <sup>29</sup>. Its effect on the upper bound we are deriving is negligible. The calculated slope for linear interpolation is given by

$$\begin{aligned} \left\{ \begin{array}{l} \text{Measured} \\ \text{Slope} \end{array} \right\} &= \frac{Q}{\Delta t_N} \\ &= f'(t_N) \left( 1 + \frac{f''(t_N - \xi)}{2} \left( \frac{Q}{f'(t_N)} \right) \left( \frac{1}{f'(t_N)} \right) \right) \end{aligned} \quad (3.4-6)$$

where, for now, infinite resolution in measuring  $\Delta t_N$  is also assumed.

If  $\frac{f''(t_N - \xi)}{2} \left( \frac{Q}{[f'(t_N)]^2} \right)$  is sufficiently small, then (3.4-6) is well approximated by

$$R_N \triangleq \frac{Q}{\Delta t_N} \approx f'(t_N) \left( 1 - \frac{f''(t_N - \xi)}{2} \left( \frac{Q}{[f'(t_N)]^2} \right) \right) \quad (3.4-7)$$

Linear extrapolation by an increment  $\delta_N$  into the next interval  $\Delta t_N$  is given by

$$\Delta \hat{y}_N = R_N \delta_N \approx f'(t_N) \left( 1 - \frac{f''(t_N - \xi)}{2} \left( \frac{Q}{[f'(t_N)]^2} \right) \right) \delta_N \quad (3.4-8)$$

This linearly extrapolated increment  $\hat{\Delta y}_N$  must be compared to the true increment  $\Delta y_N$  which is given by

$$\Delta y_N = f(t_N + \delta_N) - f(t_N) \quad (3.4-9)$$

Equation (3.4-9) is transformed using Taylor series with remainder

$$\Delta y_N = f'(t_N) \delta_N + \frac{f''(t_N + \theta)}{2} \delta_N^2 \quad (3.4-10)$$

$$0 \leq \theta \leq \delta_N$$

The linear extrapolation error,  $e_N$ , (with perfect measurement of  $t_N$ ) is thus given approximately by

$$\begin{aligned} e_N &\stackrel{A}{=} \Delta y_N - \hat{\Delta y}_N \\ &\cong \frac{f''(t_N - \xi)}{2} \left( \frac{Q}{f'(t_N)} \right) \delta_N + \frac{f''(t_N + \theta)}{2} \delta_N^2 \end{aligned} \quad (3.4-11)$$

An approximate upper bound on  $e_N$  is obtained by maximizing the right hand side of (3.4-11) over  $t_N, \xi, \theta, \delta_N$

i.e.,

$$\tilde{e}_N \leq \max_{t_N, \xi, \theta, \delta_N} \left( \left( \frac{Q \delta_N}{f'(t_N)} \right) \frac{f''(t_N - \xi)}{2} + (\delta_N)^2 \frac{f''(t_N + \theta)}{2} \right) \quad (3.4-12)$$

where

$\tilde{e}_N$  is the approximate value of  $e_N$  given by equation (3.4-11)

By definition of  $\delta_N$ ,

$$\text{Max } \delta_N = \text{Max } \Delta t_N = \frac{Q}{\text{Min } f'(t_N)} \quad (3.4-13)$$

Hence,  $\tilde{e}_N$  is bounded as follows:

$$\tilde{e}_N < \frac{Q^2}{[\text{Min}_P f'(r)]^2} \left| \text{Max}_{\theta} f''(\theta) \right| \quad (3.4-14)$$

The following example illustrates use of the bound given by (3.4-14).

The input to the integrator of the V/F converter is a positive bias  $b$  and a sinusoid ( $a \sin \omega t$ ) (due to rotation of the system). The function  $f(t)$  is thus given by

$$\begin{aligned} f(t) &= bt - \frac{a}{\omega} \cos \omega t \\ f'(t) &= b + a \sin \omega t \\ f''(t) &= a \omega \cos \omega t \end{aligned} \quad \left\{ \begin{array}{l} 0 \leq \omega t \leq \pi/2 \\ b > 0, a > 0 \end{array} \right. \quad (3.4-15)$$

$$\begin{aligned} (\text{Min}_P f'(r))^2 &= b^2 \\ \left| \text{Max}_{\theta} f''(\theta) \right| &= a \omega \end{aligned} \quad (3.4-16)$$

Substituting (3.4-16) into (3.4-14) yields

$$\tilde{\epsilon}_N < Q \left( \frac{Q\omega}{b} \right) \left( \frac{a}{b} \right) \quad (3.4-17)$$

The coefficient of  $Q$  in (3.4-17) determines how much improvement in quantization there is over the conventional scheme when using linear extrapolation. For a 10 second duration in rotating the system  $90^\circ$

$$\begin{aligned} \omega &\approx .15 \text{ rad/sec} \\ a &\approx 980 \frac{\text{cm}}{\text{sec}^2} \end{aligned} \quad (3.4-18)$$

Also it is assumed that

$$b = 980 \frac{\text{cm}}{\text{sec}^2} \quad (3.4-19)$$

Substituting (3.4-18) and (3.4-19) into (3.4-17) along with  $Q = 1 \text{ cm/sec}$  yields

$$\tilde{\epsilon}_N < 0.000153 \frac{\text{cm}}{\text{sec}} \quad (3.4-20)$$

Large reductions in accelerometer quantization can also be shown for small base motion perturbations such as would occur for gyro static calibration and accelerometer calibration.

The preceding analysis yields the result of zero quantization error for a constant bias at the integrator input in Figure 3.3-1 and derives bounds on the quantization error for non-constant integrator inputs. Errors

in measuring time intervals  $\Delta t_N$  and  $\delta$ , used in the reduction of quantization errors through equations (3.3-1) and (3.3-2), were neglected. A detailed examination of timing errors is presented below.

Let  $t_N$  = time of occurrence of  $N^{\text{th}}$  pulse output of V/F converter

$\delta_N$  = extrapolation interval from  $t_N$  to next update time

$t_N^m$  = measured time of occurrence of  $N^{\text{th}}$  pulse output

$\delta_N^m$  = measured extrapolation interval

$\epsilon_N$  = error in measuring true time of occurrence of the  $N^{\text{th}}$  pulse

We assume that  $\epsilon_N$  cannot exceed  $E$  where

$E$  = timing quantization size (in seconds)

Thus,

$$|\epsilon_N| \leq E \quad (3.4-21)$$

We assume a uniform probability distribution for  $\epsilon_N$ . Thus,

$$\bar{\epsilon}_N = E/2 \quad (3.4-22)$$

$$\overline{\epsilon_N^2} = E^2/3 \quad (3.4-23)$$

$$\overline{(\epsilon_N - \bar{\epsilon}_N)^2} = E^2/12$$

Also as usual,

$Q$  = V/F quantization size in cm/sec

$b$  = ramp slope at the V/F input in  $\text{cm/sec}^2$

$\Delta t_N = t_N - t_{N-1}$  time between the  $N^{\text{th}}$  and  $(N-1)^{\text{th}}$  V/F converter output pulses

$$\Delta t_N \approx Q/b \quad (3.4-24)$$

(with perfect equality for a constant bias to the V/F integrator).

The measured values  $t_N^m$ ,  $\delta_N^m$  are related to the true values as follows:

$$\begin{aligned} t_N &= t_N^m + \epsilon_N \\ \delta_N &= \delta_N^m - \epsilon_N \\ \Delta t_N &= \Delta t_N^m + \epsilon_N - \epsilon_{N-1} \end{aligned} \quad (3.4-25)$$

The error,  $y_\epsilon$  in the linearly extrapolated output due to timing quantization is

$$y_\epsilon = \frac{Q(\delta_N + \epsilon_N)}{\Delta t_N - \epsilon_N + \epsilon_{N-1}} - \frac{Q\delta_N}{\Delta t_N} \quad (3.4-26)$$

where the above definitions and (3.4-25) have been used to obtain (3.4-26).

Simplification of (3.4-26) results in

$$y_\epsilon \approx Q \left[ \frac{\epsilon_N}{\Delta t_N} \left( 1 + \frac{\delta_N}{\Delta t_N} \right) - \frac{\epsilon_{N-1}}{\Delta t_N} \left( \frac{\delta_N}{\Delta t_N} \right) \right] \quad (3.4-27)$$

Substituting (3.4-24) into (3.4-27) yields

$$y_{\epsilon} \approx b \left[ \epsilon_N \left( 1 + \delta_N / \Delta t_N \right) - \epsilon'_{N-1} \left( \frac{\delta_N}{\Delta t_N} \right) \right] \quad (3.4-28)$$

Assuming  $\epsilon_N$  and  $\epsilon'_{N-1}$  are uncorrelated so that

$$\overline{(\epsilon_N - E/2)(\epsilon'_{N-1} - E/2)} = 0 \quad (3.4-29)$$

and taking the mean and mean square values of  $y_{\epsilon}$  results in

$$\begin{aligned} \bar{y}_{\epsilon} &\approx b \left[ \bar{\epsilon}_N \left( 1 + \delta_N / \Delta t_N \right) - \bar{\epsilon}'_{N-1} \left( \frac{\delta_N}{\Delta t_N} \right) \right] \\ \overline{(y_{\epsilon} - \bar{y}_{\epsilon})^2} &\approx b^2 \left[ \overline{\epsilon'^2_N} \left( 1 + \frac{\delta_N}{\Delta t_N} \right)^2 + \overline{\epsilon'^2_{N-1}} \left( \frac{\delta_N}{\Delta t_N} \right)^2 \right] \end{aligned} \quad (3.4-30)$$

$$\epsilon'_N \triangleq \epsilon_N - \bar{\epsilon}_N$$

We can bound (3.4-30) by noticing that  $\delta_N$  is a maximum when

$$(\delta_N)_{\max} = \Delta t_N \quad (3.4-31)$$

Hence using (3.4-31) in conjunction with (3.4-30) and (3.4-23) leads

to

$$\begin{aligned} \overline{y}_{\epsilon} &\leq b E/2 \\ \overline{(y_{\epsilon} - \bar{y}_{\epsilon})^2} &\leq 5/12 E^2 b^2 \end{aligned} \quad (3.4-32)$$

In place of the above statistical measure,  $y_{\epsilon}$  can also be bounded as follows using (3.4-28), (3.4-31) and (3.4-21).

$$|y_{\epsilon}| \leq 3E b \quad (3.4-33)$$

Both equations (3.4-32) and (3.4-33) hold for constant biases or constant biases with small base motion induced perturbations. Large base motions require going back to (3.4-27) and using a more exact expression for  $\Delta t_N$ . Equivalently we can increase or decrease  $b$  from its nominal value to account for the additional non-constant input at a particular instant of time.

Hardware<sup>25</sup> built for testing the quantization reduction for LCIGS has a timing frequency of 192 KHz so that

$$E = \frac{1}{192 \text{ sec}} = 5.21 \times 10^{-6} \text{ sec} \quad (3.4-34)$$

For  $b$  given by (3.4-19), equations (3.4-32) and (3.4-33) yield

$$\begin{aligned} \bar{y}_e &\leq \frac{bE}{2} = 0.0025 \frac{\text{cm}}{\text{sec}} \\ \sqrt{(y_e - \bar{y}_e)^2} &\leq \sqrt{5/12} E b = 0.0035 \frac{\text{cm}}{\text{sec}} \end{aligned} \quad (3.4-35)$$

$$|y_e| \leq 0.0153 \frac{\text{cm}}{\text{sec}} \quad (3.4-36)$$

The quantization error due to timing errors is therefore small enough to meet the criteria discussed in Section 3.2.

### 3.5 Requirement for an External Bias

As was seen, implementation of the linear extrapolator method, in general, requires addition of a bias at the V/F integrator input. Such a bias was, in fact, included in the numerical example given by equations (3.4-15) - (3.4-20) in the last section. We then have the supplementary requirement of calibrating this bias for each V/F converter with the techniques presented in Appendix 2B, Chapter 2. A review of the accelerometer

calibration procedure in the last chapter and a foreview of gyro calibration techniques in Chapter 5 will reveal when the bias is really needed for these LCIGS tasks.

First, consider accelerometer calibration. For all of the nominal orientations, the nominally horizontal accelerometers have their input axes level within  $1/2^{\circ}$ . All other accelerometers have their input axes either nominally vertical or at  $45^{\circ}$  from the vertical. The resulting coefficients of the quantization errors from the approximately horizontal accelerometers are therefore roughly 1/100 of the non-horizontal accelerometer coefficients. Thus, most of the effective quantization error is from the non-level accelerometers which naturally have a sufficient pulse rate output without the need for an external bias.

In the case of gyro static parameter calibration, nominal system orientations result in the same disposition of accelerometer input axes described above. Unfortunately, the same conclusions on the effect of accelerometer quantization on gyro drift estimation do not apply. That is, the quantization error due to the nominally horizontal accelerometers directly affect gyro drift estimation and are not attenuated in their effect. (See Chapter 4.) However, the calibration uncertainty in the bias applied to the nominally horizontal accelerometer modules (equation (2B-9), Appendix 2B, Chapter 2) will not directly contribute to estimation error uncertainties. Only variations in this bias during an estimation interval will result in error because of the unobservability of constant accelerometer bias during any one static position of the system.

During nominal rotations of the system for calibration of gyro dynamic parameters, the axis of rotation (which is a system body reference axis) is nominally level within our usual  $1/2^{\circ}$  criterion. The other two system body

axes are eventually rotated through  $180^{\circ}$ . The module associated with the accelerometer having its input axis parallel to the axis of rotation should therefore be treated the same as the two accelerometer modules that are nominally horizontal for a static system orientation. The inputs of the other two accelerometers are subject to significant values of gravity for most of the rotation. At a constant rotation rate of .15 rad/sec, gravity sensed by either of these accelerometers is less than 0.1g for a period of less than approximately 1.3 seconds in a rotation lasting 10 seconds. Examination of the error expression (3.4-11) will show that the linear extrapolation error is small under the above conditions. We, therefore, conclude that these two accelerometer modules need not have an applied bias.

**Chapter 4**  
**Alignment and Estimation of**  
**Lumped Drifts and Leveling Errors**

#### 4.1 Introduction

The goal of minimum calibration time dictates the use of any stabilized frame such as a local level reference frame for base motion isolation as an alternative to averaging the direct outputs of the gyros. In addition, use of an attitude algorithm to compute the transformation between the local level frame and the body reference axes allows calibration of gyro scale-factor errors and misalignments without recourse to precise positioning of the system while rotating the system between static positions. The earth rate vector cannot be used to establish an azimuth reference for the local level frame because of the large magnitude of the gyro drift uncertainties. Hence, in Section 4.2 an azimuth reference is defined that is based on the orthogonal body reference frame defined relative to the accelerometer triad in Chapter 2. Section 4.3 derives the error differential equations for the misalignments (i.e., leveling errors) between the frame computed by the attitude and alignment algorithms and the local level reference frame. It is shown that the misalignment angle about each level reference axis is essentially driven by a static lumped drift and what is termed a dynamic lumped drift. The static lumped drift is composed of a horizontal component of earth rate and the projection onto the level axis of those gyro drifts due to static gyro error parameters (bias and mass unbalance drifts). The dynamic lumped drift is defined as the projection onto the level reference axis of those gyro drifts due to dynamic gyro error parameters (scale factor error and gyro misalignments). When the inertial system is at rest, with the exception of incidental base motion, the static drift terms pre-dominate over the dynamic lumped drift terms. These can be estimated by means of the 3 state Kalman filter described in

Section 4.4. The lumped drift estimates so obtained for a sequence of static system positions will then be used to obtain estimates of the gyro static parameters albeit corrupted by a small dynamic lumped drift term. This procedure is described in Chapter 5. These initial static estimates are then used in the determination of the gyro dynamic parameters from misalignment angles estimated by a two state Kalman filter during a sequence of system rotations when the dynamic lumped drift terms predominate. (This is also described in Chapter 5.) The misalignment angle estimates during a rotation, however, are corrupted by the error introduced in not modeling both the static and dynamic drifts in the Kalman filters. It is shown in Section 4.5 how the errors in the Kalman filter estimates of static lumped drift during a static orientation may be corrected afterwards for the small errors induced by the dynamic drifts and by small variations in the direction cosine matrix due to the residual base motion. Furthermore, it is shown that the same technique can also be used later to correct the errors in the Kalman filter estimates of misalignment angles during a rotation due to the unmodeled static and dynamic drifts. With the introduction of these techniques for obtaining estimates of lumped drifts and misalignment angles the foundation is then set for Chapter 5 where the techniques are presented for extracting the individual gyro static and dynamic parameters from the lumped drift and misalignment angle estimates.

#### 4.2 Definition of a Local Level Reference Frame

The earth rate vector cannot be used to establish an azimuth reference for a local level frame because of the large magnitude of the gyro drifts that

is to be accommodated. Hence, the definition of an azimuth reference is based on the orthogonal body reference frame defined relative to the accelerometer triad in Chapter 2, Section 2.2. The azimuth reference for the local level frame is, therefore, defined as the horizontal projection of one of the accelerometer body reference triad axes onto the level plane established by the accelerometer.

A computed frame is said to exist whenever there is a direction cosine matrix or quaternion, computed by means of an attitude algorithm,<sup>30</sup> which represents a transformation between the body reference frame and the computational frame. That is, the computed frame is represented in the computer only by means of a quaternion or direction-cosine matrix rather than by some explicit definition of the frame.

A local level frame is to be implemented. A measure of the leveling error of the computed frame  $C$  with respect to the local level frame is given by the first two components of the vector

$$C_{B_a}^c \underline{g}^{B_a}$$

since

$$C_{B_a}^c \underline{g}^{B_a} = C_L^c C_{B_a}^L \underline{g}^{B_a} = C_L^c \begin{bmatrix} 0 \\ 0 \\ g \end{bmatrix} \quad (4.2-1)$$

where  $C_L^c$  is the direction cosine matrix representing the deviation between the computed frame and the desired level frame.  $[B_a]$  denotes the

the orthogonal body reference frame defined with respect to the accelerometer input axes. L denotes the level frame.  $\underline{g}^{B_a}$  denotes gravity in the body frame. g denotes the magnitude of gravity.] An azimuth reference must also be defined in order to completely specify the level frame. One such choice which is independent of earth rate measurements is the vector  $\underline{u}_\perp^B(t)$  defined in the body frame at time t by

$$\begin{aligned}\underline{u}_\perp^{B_a}(t) &\triangleq \left( \frac{\underline{g}^{B_a} \times \underline{n}^{B_a}}{g_{u_\perp}} \right)_t \\ g_{u_\perp} &\triangleq \left| \left( \frac{\underline{g}^{B_a} \times \underline{n}^{B_a}}{g_{u_\perp}} \right)_t \right|\end{aligned}\quad \left. \right\} \quad (4.2-2)$$

where

$$\underline{n}^{B_a}(t) = \text{unit vector along a body axis at time } t$$

This azimuth reference vector,  $\underline{u}_\perp^{B_a}$ , is expressed in the level frame by

$$\underline{u}_\perp^L = C_{B_a}^L \underline{u}_\perp^{B_a} = \left( \begin{bmatrix} 0 \\ 0 \\ g \end{bmatrix} \times C_{B_a}^L \underline{n}^{B_a} \right) (g_{u_\perp})^{-1} \quad (4.2-3)$$

The following non-normalized azimuth reference vector will suffice for specifying the local level reference frame.

$$\underline{a}_\perp^L \triangleq \left( \begin{bmatrix} 0 \\ 0 \\ 1 \end{bmatrix} \times C_{B_a}^L \underline{n}^{B_a} \right) \quad (4.2-4)$$

Depending on the orientation of the body axes, described below,  $\underline{m}^B_a$  can be one of the following three unit vectors.

$$\begin{bmatrix} i \\ 0 \\ c \end{bmatrix}, \begin{bmatrix} 0 \\ 1 \\ 0 \end{bmatrix}, \begin{bmatrix} 0 \\ 0 \\ 1 \end{bmatrix}$$

To which the corresponding vectors,  $\underline{a}_L^L$  are, using (4.2-4):

$$\begin{bmatrix} -c_{21} \\ c_{11} \\ 0 \end{bmatrix}, \begin{bmatrix} -c_{22} \\ c_{12} \\ 0 \end{bmatrix}, \begin{bmatrix} -c_{23} \\ c_{13} \\ 0 \end{bmatrix}$$

where  $c_{ij}$  is the  $i,j^{\text{th}}$  element of  $C_{B_a}^L$ .

In any of the above three cases, it is desired that the normalized azimuth reference vector in the horizontal plane be given by

$$\begin{bmatrix} 0 \\ 1 \\ 0 \end{bmatrix}$$

which represents an arbitrary choice in establishing the reference for the azimuth orientation of the level frame.

Hence, once the conditions for a level frame given by equation (4.2-1) are met,

$$(C_L^c)_{13} = (C_L^c)_{23} = 0 \quad (4.2-5)$$

where  $(C_L^c)_{ij}$  is the  $i,j^{\text{th}}$  element of  $C_L^c$ .

Thus one of the following conditions of the resultant matrix  $C_{B_a}^L$ , (i.e., frame C is now "equal" to a level frame L),

$$C_{21} = 0 \text{ or } C_{22} = 0 \text{ or } C_{23} = 0 \quad (4.2-6)$$

corresponding to the choice of  $\underline{N}_{B_a}$ , must be met to completely specify the level frame L.

Eight nominal static body axis orientations for calibration of the gyro static parameters are chosen in Chapter 5. These static orientations are specified by two body axes that are nominally level. Furthermore, deviation of these axes from the level position will be small. This leads to the requirement for only fine alignment, described in Section 4.4, in order to satisfy equation (4.2-5). Rotation from one static position to another and for the purpose of dynamic gyro parameter calibration will be about a nominally level axis. Selection of the proper condition in (4.2-6) must, therefore, correspond with this pre-determined sequence of rotations. The rotations for dynamic calibration are fitted within the frame work of the 8 nominal static orientations. Figure 4.2.-1 depicts the nominal sequence.

In each position and during rotations one of the three body reference axes  $\underline{N}_{B_a}^{B_a}$  should be chosen to be the body axis whose projection on the horizontal plane has the largest component in the nominal azimuth direction. Guided by this preceding logic, the proper choice of which element of  $C_{B_a}^L$  to force to zero at each position is indicated in Table 4.2-2.

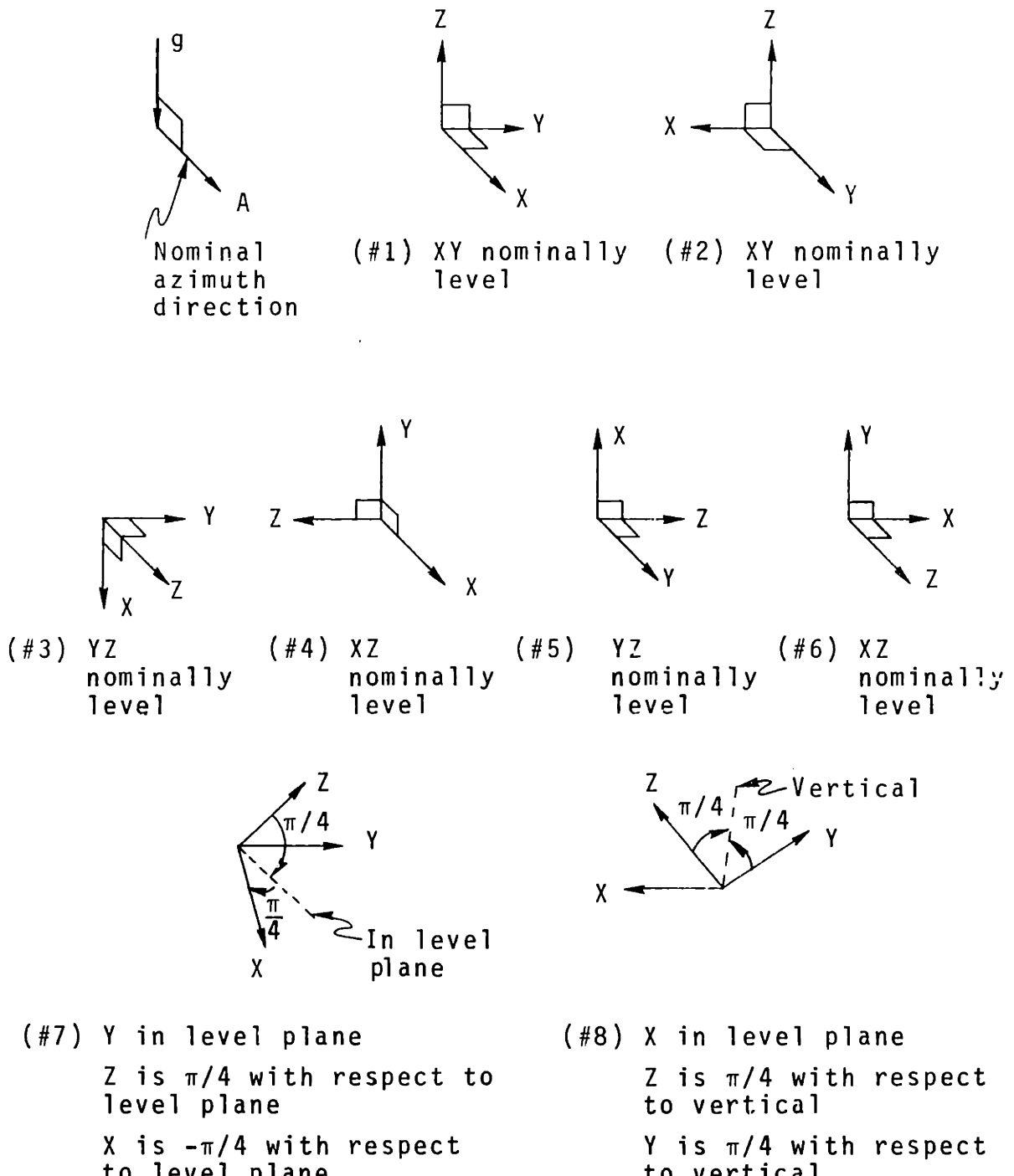


Figure 4.2-1 Nominal Static Orientations for Body Reference Axes

Position	1	2	3	4	5	6	7	8
Element of $C_{B_a}^L$ forced to zero	$c_{21}$	$c_{22}$	$c_{23}$	$c_{21}$	$c_{22}$	$c_{23}$	$c_{21}$	$c_{22}$

Table 4.2-1 Choice of Zeroed Element of  $C_{B_a}^L$

It should be emphasized that the azimuth reference so chosen above is variable with time due to base motion and the rotations of the system. The effects of this variation will be included in the subsequent analyses.

This section is concluded by identifying those elements in  $C_L^C$  that are measures of the leveling and azimuth errors. From equation (4.2-1), it is seen that the two leveling errors  $\varphi_1$ ,  $\varphi_2$  are given by

$$\left. \begin{aligned} \varphi_1 &= (C_L^C)_{13} \\ \varphi_2 &= (C_L^C)_{23} \end{aligned} \right\} \quad (4.2-7)$$

Also the azimuth error, deduced from (4.2-4), where

$$\underline{\alpha}_L = \begin{bmatrix} 0 \\ C_{11} \\ 0 \end{bmatrix}, \alpha_2 \begin{bmatrix} 0 \\ C_{12} \\ 0 \end{bmatrix}, \alpha_3 \begin{bmatrix} 0 \\ C_{13} \\ 0 \end{bmatrix}$$

depending on the choice of  $\underline{n}_{Ba}$ , is given by

$$\varphi_{Az} = (C_L^C)_{12} \quad (4.2-8)$$

### 4.3 Derivation of Error Equations

The error between the computed frame and the level reference frame as a function of various quantities (gyro drift, initial misalignment, etc.) that will be introduced below plays an important part in:

1. Alignment of the computed frame to the level reference frame.
2. Estimation of lumped gyro drifts in the reference frame during static orientations for static gyro calibration.
3. Estimation of misalignments between the computed and reference frames during a rotation for gyro dynamic calibration.

Reference (24) was a pioneering development of the representative error differential equations resulting from an analysis of the errors between the computed and reference frames for a strapdown system. However, this analysis assumed that the dynamic errors: gyro scale factor error and misalignment angles with respect to the reference body frame, were pre-calibrated and were not considered separately. The subsequent derivation of the pertinent error differential equations in this chapter will take these additional factors into account.

Three frames are required for the derivation. First, frame  $B_a$ , defined in Section 2.2, Chapter 2, represents the orthogonal body reference frame. Second, frame  $B_g$  represents the non-orthogonal frame whose axes are parallel to the gyro input axes. Third, frame  $B_s$  represents the non-orthogonal frame whose axes are parallel to the gyro spin axes. A fourth frame to account for the gyro output axes is not needed because the LCIGS considered here is assumed to have negligible output axis mass unbalance drift coefficients.

Frames  $B_g$  and  $B_a$  are related by a non-orthogonal direction cosine matrix such that

$$C_{B_G}^{B_a} \triangleq I - M \quad (4.3-1)$$

where, generally,  $M$  is a matrix of small valued elements.

The nonorthogonal direction cosine matrix relating frames  $B_s$  and  $B_a$  is designated by

$$C_{B_a}^{B_s} \triangleq I + N \quad (4.3-2)$$

The relationships between matrices  $M$  and  $C_{B_a}^{B_s}$  will be given in detail in Chapter 5.

The equivalent angular rate input  $\underline{\omega}_{ALG}$  to the attitude algorithm<sup>30</sup> from the gyros and an external command signal is given by

$$\underline{\omega}_{ALG} = \underline{\omega}_{IB_a}^{B_G} + \underline{\omega}_D^{B_G} + S \underline{\omega}_{IB_a}^{B_G} + S \underline{\omega}_D^{B_G} - \underline{\omega}_{CMD}^{B_G} \quad (4.3-3)$$

where

$\underline{\omega}_{IB_a}^{B_G}$  = angular rate of body frame with respect to inertial space in  $B_G$  frame coordinates. Note that

$$\underline{\omega}_{IB_a}^{B_G} = \underline{\omega}_{IB}^{B_a} + M \underline{\omega}_{IB_a}^{B_G} \quad (4.3-4)$$

using the definition given by (4.3-1)

$\underline{\omega}_p^{B_G}$  = static gyro drift terms in the  $B_G$  frame

where for LCIGS

$$\underline{\omega}_D^{BG} = \begin{bmatrix} B_1 \\ B_2 \\ B_3 \end{bmatrix} + \begin{bmatrix} g_1^{BG} M_{IA_1} \\ g_2^{BG} M_{IA_2} \\ g_3^{BG} M_{IA_3} \end{bmatrix} + \begin{bmatrix} g_1^{BS} M_{SA_1} \\ g_2^{BS} M_{SA_2} \\ g_3^{BS} M_{SA_3} \end{bmatrix} \quad (4.3-5)$$

$B_i$  = bias of  $i^{\text{th}}$  gyro

$M_{IA_i}$  = input axis mass unbalance drift coefficient of  $i^{\text{th}}$  gyro

$M_{SA_i}$  = spin axis mass unbalance drift coefficient of  $i^{\text{th}}$  gyro

The gravity vectors in the  $B_G$  and  $B_S$  frames are given by

$$\underline{g}^{BG} = C_{B_a}^{B_G} C_L^{B_a} \begin{bmatrix} 0 \\ 0 \\ g \end{bmatrix} \quad (4.3-6)$$

$$\underline{g}^{BS} = C_{B_a}^{B_S} C_L^{B_a} \begin{bmatrix} 0 \\ 0 \\ g \end{bmatrix}$$

with

$$C_{B_a}^{B_G} = \left( C_{B_G}^{B_a} \right)^{-1} = (I - M)^{-1} \quad (4.3-7)$$

also

$\underline{\omega}_{\text{cmd}}^{B_a}$  = angular rate external command in the  $B_a$  frame

$S$  = diagonal matrix of gyro scale factor errors.

That is,

$$S \triangleq \begin{bmatrix} SF_1 & 0 & 0 \\ 0 & SF_2 & 0 \\ 0 & 0 & SF_3 \end{bmatrix} \quad (4.3-8)$$

$SF_i$  = scale factor error of  $i^{\text{th}}$  gyro

Substitution of (4.3-4) into (4.3-3) yields

$$\begin{aligned} \underline{\omega}_{ALG} = & \underline{\omega}_{IB_a}^{B_a} - \underline{\omega}_{\text{ind}}^{B_a} + \underline{\omega}_D^{B_G} + S \underline{\omega}_D^{B_G} \\ & + (S+M) \underline{\omega}_{IB_a}^{B_G} \end{aligned} \quad (4.3-9)$$

The gyro drift terms are given by

$$\underline{\omega}_{D_{ALL}}^{B_a} \triangleq \underline{\omega}_D^{B_G} + S \underline{\omega}_D^{B_G} + (S+M) \underline{\omega}_{IB_a}^{B_G} \quad (4.3-10)$$

They are directly integrated by the attitude algorithm which is however defined to integrate the angular rate inputs as if they were in the orthogonal reference frame  $B_a$ . Hence we can validly consider  $\underline{\omega}_{D_{ALL}}^{B_a}$  to be an equivalent drift term in frame  $B_a$ .

With the input to the attitude algorithm given by (4.3-9) and (4.3-10) we can suppose that the algorithm computes the transformation from the  $B_a$  frame to a computed frame, C, with a drift error given by  $\underline{\omega}_{D_{ALL}}^{B_a}$ . The algorithm, in effect, is considered to integrate the following matrix differential equation for direction-cosine matrix  $C_{B_a}^C$

$$\dot{C}_{B_a}^c = C_{B_a}^c \left[ (\underline{\omega}_{I B_a}^{B_a} - \underline{\omega}_{cmd}^{B_a} + \underline{\omega}_{DNL}^{B_a}) x \right] \quad (4.3-11)$$

where

$[(\underline{\omega})x]$  is the skew symmetric matrix form for the vector  $\underline{\omega}$ .

Analysis of equation (4.3-11) can now identically follow that in reference 31 to yield the differential equation for the transformation  $C_L^c$  between the level reference frame defined in Section 4.2 and the computed frame. Extraction of the desired differential equation from (4.3-11) is as follows:

$$C_{B_a}^c = C_L^c C_{B_a}^L \quad (4.3-12)$$

Differentiation of (4.3-12) yields

$$\dot{C}_{B_a}^c = \dot{C}_L^c C_{B_a}^L + C_L^c \dot{C}_{B_a}^L \quad (4.3-13)$$

But  $C_{B_a}^L$  satisfies the usual matrix differential equation

$$\dot{C}_{B_a}^L = C_{B_a}^L \left[ \underline{\omega}_{LB_a}^{B_a} x \right] \quad (4.3-14)$$

Substitution of (4.3-14) into (4.3-13) and equating the result to the right hand side of (4.3-11) yields

$$\dot{C}_L^c C_{B_a}^L = C_L^c C_{B_a}^L \left[ (\underline{\omega}_{IL}^{B_a} - \underline{\omega}_{cmd}^{B_a} + \underline{\omega}_{DNL}^{B_a}) x \right] \quad (4.3-15)$$

or

$$\dot{C}_L^c = C_L^c \left[ (\omega_{IL}^L - \omega_{cmd}^L + \omega_{DALL}^L) x \right] \quad (4.3-16)$$

after applying the appropriate similarity transformation to the skew symmetric matrix.

The base motion term  $\omega_{IB_e}^{B_a}$  has been eliminated from (4.3-16) apart from its inclusion in  $\omega_{DALL}^L$  in the correct coordinates as a coefficient of the dynamic errors (misalignments and scale factor errors).

The term,  $\omega_{xL}^L$ , contains earth rate terms plus the vertical component of motion of the base with respect to the earth fixed frame. This is in accord with the definition of the local level reference frame in Section 4.2. Correspondingly, the eliminated base motion term  $\omega_{LB_e}^{B_a}$  contains only those base motions that cannot be resolved onto the vertical axis of the L frame.

It is obvious that the equivalent quaternion differential equation<sup>30</sup> is given by

$$\dot{q}_L^c = \frac{i}{2} q_L^c (0, \omega_{IL}^L + \omega_{DALL}^L - \omega_{cmd}^L) \quad (4.3-17)$$

Quaternions will prove easier to use in the subsequent development because only 4 elements rather than the 9 of the direction cosine matrix must be handled.

Any command velocity will be calculated in the computed coordinates, where

$$(0, -\omega_{cmd}^L) = q_L^L (0, -\omega_{cmd}^c) q_L^c \quad (4.3-18)$$

Substituting (4.3-18) into (4.3-17) yields

$$\dot{q}_L^c = \frac{1}{2} q_L^c (0, \underline{\omega}_{IL}^L + \underline{\omega}_{DALL}^L) - \frac{1}{2} (0, \underline{\omega}_{cmd}^c) q_L^c \quad (4.3-19)$$

The following abbreviations are used for the following analysis

$$\left. \begin{array}{l} \underline{\omega} = (\omega_1, \omega_2, \omega_3)^T \triangleq \underline{\omega}_{IL}^L + \underline{\omega}_{DALL}^L \\ \underline{\omega}_M = (\omega_{M_1}, \omega_{M_2}, \omega_{M_3})^T \triangleq \underline{\omega}_{cmd}^c \end{array} \right\} \quad (4.3-20)$$

For

$$q_L^c = (\lambda, (\rho_1, \rho_2, \rho_3)^T) \quad (4.3-21)$$

the following linear set of simultaneous differential equations is obtained from (4.3-19) by substitution of (4.3-20) and (4.3-21) and carrying out the indicated quaternion multiplications.

$$\begin{bmatrix} \dot{\lambda} \\ \dot{\rho}_1 \\ \dot{\rho}_2 \\ \dot{\rho}_3 \end{bmatrix} = \frac{1}{2} \begin{bmatrix} 0 & -(\omega_1 - \omega_{M_1}) & -(\omega_2 - \omega_{M_2}) & -(\omega_3 - \omega_{M_3}) \\ (\omega_1 - \omega_{M_1}) & 0 & (\omega_3 + \omega_{M_3}) & -(\omega_2 + \omega_{M_2}) \\ (\omega_2 - \omega_{M_2}) & -(\omega_3 + \omega_{M_3}) & 0 & (\omega_1 + \omega_{M_1}) \\ (\omega_3 - \omega_{M_3}) & (\omega_2 + \omega_{M_2}) & -(\omega_1 + \omega_{M_1}) & 0 \end{bmatrix} \begin{bmatrix} \lambda \\ \rho_1 \\ \rho_2 \\ \rho_3 \end{bmatrix} \quad (4.3-22)$$

Accompanying equation (4.3-22) are the error indicators of (4.2-7) and (4.2-8). Their equivalent quaternion form is given by<sup>30</sup>

$$\left. \begin{array}{l} \varphi_1 = 2(\lambda \rho_1 + \rho_2 \rho_3) \\ \varphi_2 = -2(\lambda \rho_2 - \rho_1 \rho_3) \\ \varphi_3 \triangleq \varphi_{AZ} = 2(\lambda \rho_3 + \rho_1 \rho_2) \end{array} \right\} \quad (4.3-23)$$

Although the differential equations are linear in  $\lambda, \dot{\rho}_1, \dot{\rho}_2, \dot{\rho}_3$ , the measurement equations are non-linear.

The error differential equations we are seeking are derived by differentiating (4.3-23), substituting for  $\lambda, \dot{\rho}_1, \dot{\rho}_2, \dot{\rho}_3$  using (4.3-22), identifying combinations of the resulting variables on the right hand sides of the equations that yield  $\dot{\varphi}_1, \dot{\varphi}_2, \dot{\varphi}_3$ , (equation 4.3-23), and dropping all but 1st order terms in  $\dot{\rho}_1, \dot{\rho}_2, \dot{\rho}_3$ . The latter is permitted because body axis orientations in the static position before initial alignment, will always be close to the local level frame. (This is discussed in Chapter 5) (i.e., for  $1^\circ$  misalignments,  $\dot{\rho}_1 - \dot{\rho}_3$  are on the order of 0.01 and their 2nd order products are on the order of  $10^{-4}$ ). Use of the constraint

$$\lambda^2 + \dot{\rho}_1^2 + \dot{\rho}_2^2 + \dot{\rho}_3^2 = 1 \quad (4.3-24)$$

is also made in the derivation. The result is as follows:<sup>32</sup>

$$\begin{aligned} \dot{\varphi}_1 &\approx \omega_1 - \omega_{M_1} + (-\omega_3 \varphi_2 - \omega_{M_2} \varphi_3) \\ \dot{\varphi}_2 &\approx -\omega_2 + \omega_{M_2} + (\omega_3 \varphi_1 - \omega_{M_1} \varphi_3) \end{aligned} \quad \left. \right\} \quad (4.3-25)$$

$$\dot{\varphi}_3 \approx \omega_3 - \omega_{M_3} \quad \text{for } \varphi_1, \varphi_2 \approx 0 \quad (4.3-26)$$

where the components  $\omega_1 - \omega_3, \omega_{M_1} - \omega_{M_3}$  are defined by equations (4.3-20) and  $\omega_{M_i}$  components are restricted to values which tend to keep the  $\varphi_i$  components close to zero.

Equations (4.3-25), suitably modified to include the uncertainties of random gyro drifts and gyro angle quantization will serve as dynamic models for the Kalman filters described in the next section. These

Kalman filters with suitable error corrections presented in Section 4.5 are used to estimate misalignment angles  $\varphi_1$  and  $\varphi_2$  for alignment of the computed to the level reference frame and for gyro dynamic calibration and also to estimate static drifts. Equation (4.3-26) will not be used because  $\omega_3$  contains the unattenuated vertical component of base motion.

Before applying such estimation theory to measurements that will be subsequently presented, it is desirable to examine the terms comprising  $\omega_1$  and  $\omega_2$  in more detail.  $\underline{\omega}$  is rewritten as below.

$$\underline{\omega} = \underline{\omega}_{IL}^L + C_{B_n}^L (\underline{\omega}_D^{BG} + S \underline{\omega}_D^{BG} + (S+M) \underline{\omega}_{IB_n}^{BG}) \quad (4.3-27)$$

A more compact representation of (4.3-27) is obtained using the following definitions.

$$\left. \begin{aligned} \underline{\omega}_{stat} &\triangleq C_{B_n}^L (\underline{\omega}_D^{BG} + S \underline{\omega}_D^{BG}) + \underline{\omega}_{IL}^L \\ \underline{\omega}_{dyn} &\triangleq C_{B_n}^L (S+M) \underline{\omega}_{IB_n}^{BG} \end{aligned} \right\} \quad (4.3-28)$$

Substituting (4.3-28) into (4.3-27) leads to

$$\underline{\omega} = \underline{\omega}_{stat} + \underline{\omega}_{dyn} \quad (4.3-29)$$

Equation (4.3-29) is in turn substituted into the two differential equations, (4.3-25), representing the dynamics of the misalignment angles about the two axes of the level reference frame. The result is

$$\left. \begin{aligned} \dot{\varphi}_1 &= \omega_{\text{stat}_1} + \omega_{\text{dyn}_1} - \omega_{M_1} + \omega_{\theta_1} \\ \dot{\varphi}_2 &= -\omega_{\text{stat}_2} - \omega_{\text{dyn}_2} + \omega_{M_2} + \omega_{\theta_2} \end{aligned} \right\} \quad (4.3-30)$$

where from (4.3-25)

$$\left. \begin{aligned} \omega_{\theta_1} &= -\omega_3 \varphi_2 - \omega_{M_2} \varphi_3 \\ \omega_{\theta_2} &= \omega_3 \varphi_1 - \omega_{M_1} \varphi_3 \end{aligned} \right\} \quad (4.3-31)$$

$\omega_{\text{stat}_1}$  and  $\omega_{\text{stat}_2}$  are the first and second components, respectively, of the projection of the sum of the earth rate,  $\underline{\omega}_{IL}^L$ , and a static lumped drift,  $\underline{\omega}_D^{B_C} + S \underline{\omega}_D^{B_C}$ , onto the level plane.

$\omega_{\text{dyn}_1}$  and  $\omega_{\text{dyn}_2}$  are the first and second components, respectively, of the projection of a dynamic lumped drift,  $(S + M) \underline{\omega}_{IB..}^{B_C}$ , onto the level plane.

The terms  $\omega_{\theta_1}$  and  $\omega_{\theta_2}$  represent the sum of the cross coupling of the azimuth rate (which includes the vertical component of base motion) and the cross-coupling of the command rates to the level reference axes 1 and 2 respectively.

The gyro dynamic error model parameters are given by the elements of M and S. [The elements of N are only indirectly needed to obtain refined values of the spin axis mass unbalance drifts.]

The general strategy in solving for both the static and dynamic parameters is as follows: during a static orientation  $\omega_{\text{stat}_{1,2}}$  are almost constant and larger in magnitude than  $\omega_{\text{dyn}_{1,2}}$ . The components  $\omega_{\text{stat}_{1,2}}$  are therefore estimated to first order with a single 3 state Kalman filter.

These estimates are in turn used to obtain first order approximations to the gyro static parameters. These static parameter solutions are then used to correct estimates of the dynamic parameters (comprising  $W_{dyn,1,2}$ ) that are obtained from Kalman filter estimates of  $\varphi_1$  and  $\varphi_2$  during a rotation of the system when the terms  $W_{dyn,1,2}$  are greatly magnified. The dynamic parameter estimates are in turn used to modify the first order static parameter estimates to account for the originally neglected dynamic terms  $W_{dyn,1,2}$  during the static estimation procedure, to separate, if desired,  $\underline{W}_D^{BG,1,2}$  from the sum  $(\underline{W}_D^G + \underline{S}\underline{W}_D^G)$ , and to correct errors in the estimates of the g sensitive static coefficients due to the gyro input axis and spin axis misalignments. The possibility of a second iteration and so forth, if required, is obvious. Some of the details of this iteration will be covered in Section 4.5 with the remainder in Chapter 5. Section 5.7, Chapter 5, will summarize the iteration actually simulated and recommended for LCIGS.

Measurement of the two misalignments  $\varphi_1$ ,  $\varphi_2$  between the computed and reference frame is through processing of the accelerometer outputs coordinatized in the computed frame by means of the direction cosine matrix  $C_{Ba}^C$  described previously. Because the outputs of the accelerometer modules are integrals of specific force, the measurements are of two velocity variables  $v_1$  and  $v_2$  such that

$$v_1 = \int \varphi_1 g dt, \quad v_2 = \int \varphi_2 g dt \quad (4.3-32)$$

in the absence of any translational accelerations.

Estimation of  $\omega_{\text{stat}_1}$ , for example, will therefore depend on the three states  $V_1, \varphi_1, \omega_{\text{stat}_1}$ . These states satisfy the differential equation set

$$\left. \begin{aligned} \dot{V}_1 &= \varphi_1 g \\ \dot{\varphi}_1 &= \omega_{\text{stat}_1} + \omega_{\text{dyn}_1} + \omega_\theta - \omega_M \\ \dot{\omega}_{\text{stat}_1} &= 0 \end{aligned} \right\} \quad (4.3-33)$$

The states  $V_2, \varphi_2, \omega_{\text{stat}_2}$  satisfy a similar set of differential equations.

The terms  $\omega_{\text{dyn}_1}, \omega_\theta$ , are unknown drivers of the state derivative  $\dot{\varphi}_1$  in (4.3-32).

In what follows in this section, we will focus on the Kalman filters and state equations relating to  $V_1, \varphi_1, \omega_{\text{stat}_1}$  with the understanding that completely analogous results apply to  $V_2, \varphi_2, \omega_{\text{stat}_2}$ .

Development of the discrete state and measurement equations for design of the Kalman filters will involve the addition of white noise terms to account for uncertainties in the drivers of  $\varphi_1, V_1, \omega_{\text{stat}_1}$  and in the measurement of  $V_1$ . The Kalman filter estimates will then be corrected for some of the true uncertainties in the discrete equation set model used to design the filter by means of the error correction procedure presented in Section 4.5.

The discrete state equations are derived by integrating (4.3-33), ignoring the uncertainties  $\omega_{\text{dyn}_1}, \omega_\theta$ , and adding uncertainty terms representing white noise random sequences. This resulting equation set is:

$$\begin{bmatrix} V_1(n+1) \\ \varphi_1(n+1) \\ \omega_{\text{stat}_1}(n+1) \end{bmatrix} = \bar{\Phi} \begin{bmatrix} V_1(n) \\ \varphi_1(n) \\ \omega_{\text{stat}_1}(n) \end{bmatrix} + \begin{bmatrix} 0 \\ f(n) \\ u(n) \end{bmatrix} + \begin{bmatrix} 0 \\ \omega_M(n) \\ 0 \end{bmatrix} \quad (4.3-34)$$

where

$$\Phi = \text{transition matrix} = \begin{bmatrix} 1 & gat & gat^2 \\ 0 & 1 & at \\ 0 & 0 & 1 \end{bmatrix} \quad (4.3-35)$$

$\Delta t$  = filter update period

$\rho(n)$  = white noise zero mean random sequence variable to account for gyro quantization

$u(n)$  = white noise zero mean random sequence variable to account for variations in gyro lumped drift along level reference axis 1

$w_{M_i}(n)$  = control sequence variable

The associated measurement equation is given by

$$m_i(n+1) = v_i(n+1) + r_i(n+1) \quad (4.3-36)$$

where

$r_i(n+1)$  = white noise zero mean random sequence variable to account for accelerometer quantization and other unmodeled accelerometer uncertainties

Note that accelerometer biases are not included in (4.3-35) since they are indistinguishable from initial values of  $\varphi_i^{26}$  in one static position. It is assumed that the accelerometers are calibrated before this procedure in any event.

During a rotation that state equations used for the filter must be modified because  $\omega_{stat,i}$  varies in an unknown manner and can no longer be used as a state. That is, only  $v_i$  and  $\varphi_i$  are retained as states and a larger uncertainty is assumed for the unknown drift effects on  $\varphi_i$  and  $v_i$ . The details are presented in the next section.

#### 4.4 Kalman Filter Equations

As can be deduced from the discussion in the previous section, the following state equations are to be used as the model for the Kalman filter for each of the two horizontal reference axes.

$$\begin{bmatrix} v_{m+1} \\ \dot{\varphi}_{m+1} \\ (\omega_{\text{stat}})_{m+1} \end{bmatrix} = \Phi \begin{bmatrix} v_m \\ \dot{\varphi}_m \\ (\omega_{\text{stat}})_m \end{bmatrix} + \begin{bmatrix} (1-\alpha) g \frac{\Delta t^2}{2} \\ (1-\alpha) \Delta t \\ \alpha \end{bmatrix} \begin{pmatrix} ((1-\alpha) w_m \\ + \alpha u_n) \end{pmatrix} + \begin{bmatrix} 0 \\ p_m \\ 0 \end{bmatrix} + \begin{bmatrix} 0 \\ w_m(n) \\ 0 \end{bmatrix} \quad (4.4-1)$$

where

$\alpha = 1$  during a static orientation

$\alpha = 0$  during a rotation of the system

$w_m$  is an uncertainty introduced to account for the uncertainties due to  $\omega_{\text{stat}}$  and the much larger value of  $\omega_{\text{dyn}}$  during a rotation. [ $w_m$  is a white noise random sequence variable.]

The transition matrix  $\Phi$  is re-defined by

$$\Phi = \begin{bmatrix} 1 & g \Delta t & \alpha g \frac{\Delta t^2}{2} \\ 0 & 1 & \alpha \Delta t \\ 0 & 0 & \alpha \end{bmatrix} \quad (4.4-2)$$

All other variables in (4.4-1) and (4.4-2) were defined in Section 4.3.

The associated measurement equation is the same as presented in equation (4.3-36). That is,

$$m_{m+1} = v_{m+1} + r_{m+1} \quad (4.4-3)$$

The standard discrete Kalman filter equations<sup>33</sup> are specialized to the model represented by equations (4.4-1) - (4.4-3). The resultant equations are:

$$\begin{aligned} \Pi_{n+1} &= \Phi P_n \Phi^T + G((1-\alpha)w + \alpha u) \\ &\quad + \begin{bmatrix} 0 & 0 & 0 \\ 0 & Q & 0 \\ 0 & 0 & 0 \end{bmatrix} \end{aligned} \quad (4.4-4)$$

$$\underline{\underline{R}}_{n+1} = \begin{bmatrix} \Pi_{11}(n+1) \\ \Pi_{12}(n+1) \\ \Pi_{13}(n+1) \end{bmatrix} \left( \frac{1}{\Pi_{11} + R_2} \right) \quad (4.4-5)$$

$$P_{n+1} = \begin{bmatrix} 1 - \underline{\underline{R}}_{11}(n+1) & 0 & 0 \\ -\underline{\underline{R}}_{12}(n+1) & 1 & 0 \\ -\underline{\underline{R}}_{13}(n+1) & 0 & 1 \end{bmatrix} \Pi_{n+1} \quad (4.4-6)$$

where

$\Pi_{n+1}$  is the 3x3 extrapolated covariance matrix before the  $n+1^{st}$  measurement

$P_n$  is the 3x3 covariance matrix after a measurement

$\Phi$  is the transition matrix defined by (4.4-2)

$G$  is a 3x3 matrix given by

$$G = \begin{bmatrix} (1-\alpha)g^2 \frac{\Delta t^4}{4} & (1-\alpha)g \frac{\Delta t^3}{2} & 0 \\ (1-\alpha)g \frac{\Delta t^3}{2} & (1-\alpha)\Delta t^2 & 0 \\ 0 & 0 & \alpha \end{bmatrix} \quad (4.4-7)$$

$P$  is the covariance of  $\rho_m$ ,  $E[\rho_m^2] \triangleq P$

$W$  is the covariance of  $w_m$ ,  $E[w_m^2] \triangleq W$

$U$  is the covariance of  $u_m$ ,  $E[u_m^2] \triangleq U$

$\Sigma$  is the covariance of  $\pi_m$ ,  $E[\pi_m^2] \triangleq \Sigma$

$\underline{g}_c$  is the vector of gains for the estimation of  $V$ ,  $\varphi$ , and  $\omega_{\text{start}}$

Initially, it is assumed that the system is in the static orientation #1 depicted in Figure 4.2-1. The initial covariance matrix to be inserted in (4.4-4) consists of a diagonal matrix of initially expected covariances of  $V$ ,  $\varphi$ ,  $\omega_{\text{start}}$ .

$$P_0 \triangleq \begin{bmatrix} E[V_0^2] & 0 & 0 \\ 0 & E[\varphi_0^2] & 0 \\ 0 & 0 & E[(\omega_{\text{start}})_0^2] \end{bmatrix} \quad (4.4-8)$$

At the start of a rotation we need only switch from  $\alpha = 1$  to  $\alpha = 0$  in the above equations. After any rotation, at the time  $\alpha$  is switched back to 1, the covariance matrix is modified to account for the expected uncertainties in  $\omega_{\text{start}}$ ,  $\varphi$ , and  $V$  due to the rotation.

Leveling of the computed frame is best done by an impulsive control<sup>7</sup> whereby the estimates of  $\varphi_1$  and  $\varphi_2$  are, at the instant of their determination, transformed to the body reference frame and the resultant immediately subtracted from the gyro angular increments supplied to the attitude algorithm. This procedure prevents the introduction of drift error terms through the control sequence variable  $W_M^{(n)}$ .

When impulsive control is used, the Kalman filter estimates are given by<sup>7</sup>

$$\begin{bmatrix} \hat{v}_{m+1} \\ \hat{\omega}_{stat,m+1} \\ (\hat{\omega}_{stat})_{m+1} \end{bmatrix} = \Phi \begin{bmatrix} \hat{v}_m \\ 0 \\ (\hat{\omega}_{stat})_m \end{bmatrix} + \begin{bmatrix} \kappa_{m+1} (m - \hat{v}_m) \\ -\alpha g \frac{\Delta t^2}{2} (\hat{\omega}_{stat})_m \end{bmatrix} \quad (4.4-9)$$

In concluding the presentation of the above Kalman filter design mention must be made of the way linear accelerations are implicitly handled. Reference (7) takes special care to model the linear accelerations on the basis of vehicle sway in wind gusts. The filter update increment is then adjusted so that measurements are taken far enough apart for the linear acceleration "noise" samples to remain uncorrelated. The model characterizing linear accelerations in this section is based on Weinstock's data in Figure 2.6-1 (Chapter 2) for the power spectrum of horizontal vibration acceleration for a typical urban laboratory. It is easily deduced from this acceleration spectrum that the associated velocity spectrum is flat (to a good approximation) over the frequencies of interest,  $10^{-3}$  Hz to 20 Hz, and then rapidly falls off (as  $f^{-2}$  and then as  $f^{-4}$ ). Therefore, the integrated samples of acceleration can be treated as uncorrelated for sample frequencies at least as high as 20 Hz and are part of the uncorrelated measurement noise modeled by  $\pi_{m+1}$  in equation (4.4-3). For the amplitude in Figure 2.6-1, a 20 Hz sample frequency, for example, yields a standard deviation in the velocity increment of roughly 0.14 cm/sec. Simulation runs in Chapter 6 show that this value has a significant effect on the estimation process for the Kalman filter gains used and one minute estimation periods.

#### 4.5 Kalman Filter Error Corrections

The iteration described in Section 4.3 whereby the dominant terms are estimated from Kalman filter drift estimates during static system orientations and are then used to correct the dominant terms estimated from Kalman filter misalignment angle estimates during rotations of the system can be further refined using the procedures outlined below.

The effect of the small  $\omega_{dyn}$  terms on the Kalman filter estimate of

$\omega_{stat}$  can be computed and used to correct these estimates after the initial values for the gyro dynamic parameters are calculated from the rotational data. Likewise the effect of the unmodeled  $\omega_{dyn}$  and  $\omega_{stat}$  terms on the misalignments estimated during a rotation can be computed and then used to refine the initial dynamic parameter estimates. The same approach can also be used to compute the effects of small changes in the elements of  $C_{Bq}^c$  due to base motion during a static position. The initial focus will be on keeping track of the effect of the unmodeled  $\omega_{dyn}$  terms during a static orientation.

The true state equations in the absence of any random inputs are characterized by equation set (4.3-33). This set is rewritten below as applicable to either level reference axis.

$$\begin{aligned}\dot{\mathbf{r}} &= \mathbf{u}g \\ \dot{\psi} &= \omega_{stat} + \omega_{dyn} + \omega_\theta - \omega_M \\ \dot{\omega}_{stat} &= 0\end{aligned}\tag{4.5-1}$$

Use of impulsive control for alignment of the computational frame to the level reference frame allows dropping the term  $\omega_M$  from further consideration since its effect on drift estimation will be negligible.

The term,  $\omega_\theta$ , given by (4.3-31), clearly tends toward zero at the completion of the initial alignment process. The Kalman filter gains are such that estimates of drift do not occur until completion of the initial alignment.<sup>7</sup> Hence, the term  $\omega_\theta$  is also dropped from current considerations. Only the two principal drift terms  $\omega_{\text{stat}}$  and  $\omega_{\text{dyn}}$  remain and are included in the following version of the "true" discrete state equations.

$$\begin{bmatrix} v_{n+1} \\ q_{n+1} \\ (\omega_{\text{stat}})_{n+1} \end{bmatrix} = \Phi \begin{bmatrix} v_n \\ q_n \\ (\omega_{\text{stat}})_n \end{bmatrix} + \begin{bmatrix} g(P_1)_n \\ (D_2)_n \\ 0 \end{bmatrix} \quad (4.5-2)$$

where

$$\begin{aligned} (D_2)_n &\triangleq \left\{ \int_{t_n}^{t_n + \Delta t} (\omega_{\text{dyn}} + (1-\alpha)\omega_{\text{stat}}) dt \right. \\ (D_1)_n &\triangleq \left. \int_{t_n}^{t_n + \Delta t} \int_{t_n}^t (\omega_{\text{dyn}} + (1-\alpha)\omega_{\text{stat}}) dt \right\} \end{aligned} \quad (4.5-3)$$

and  $\Phi$  is given by (4.4-2)

The error,  $\underline{\epsilon}_n$ , at the  $n^{\text{th}}$  iteration caused by not modeling  $(D_1)_n$  and  $(D_2)_n$  for the Kalman filter (Section 4.4) is defined by

$$\underline{\epsilon}_n \triangleq \underline{x}_n - \hat{\underline{x}}_n \quad (4.5-4)$$

where  $\underline{x}_n$  is the vector of states indicated in (4.5-2) and  $\hat{\underline{x}}_n$  is the estimate of the state vector from the Kalman filter described in Section 4.4.

Substitution of (4.4-3) into (4.4-9) and the result into (4.5-4) along with substitution of (4.5-3) yields the following difference equation for  $\underline{e}_n$  with the effects of measurement noise  $\underline{r}_n$  discounted [i.e., only that part of the error caused by  $D_1$  and  $D_2$  is of interest]:

$$\underline{e}_{n+1} = K_{n+1} \underline{\Phi} \underline{e}_n + K_{n+1} \underline{D}_n \quad (4.5-5)$$

where  $K_{n+1}$  is the following matrix of Kalman filter gains

$$K_{n+1} \triangleq \begin{bmatrix} 1 - R_1(n+1) & 0 & 0 \\ -R_2(n+1) & 1 & 0 \\ -R_3(n+1) & 0 & 1 \end{bmatrix} \quad (4.5-6)$$

$\underline{\Phi}$  is the usual transition matrix and  $\underline{D}_n$  is the vector of driving terms.

$$\underline{D}_n \triangleq \begin{bmatrix} g(D_1)_n \\ (D_2)_n \\ 0 \end{bmatrix} \quad (4.5-7)$$

That part,  $\underline{e}_n$ , of the total error that is due to the  $\underline{D}_n$  driver is, of course, 0 at  $n = 0$ . i.e.,

$$\underline{e}_0 = 0 \quad (4.5-8)$$

The matrix  $\Psi_n$  for the set of equations (4.5-5) where

$$\Psi_n \triangleq K_{n+1} \underline{\Phi} \quad (4.5-9)$$

is the state transition matrix of the Kalman filter<sup>34</sup> so that all of the usual theorems<sup>34</sup> relating observability and controllability properties of the true set of state equations to the stability of the set of error equations (4.5-5) hold.

For the case of a static system orientation,  $D_1$  and  $D_2$  are composed only of the dynamic term  $\underline{\omega}_{dyn}$  which is unknown. However, the set of error equations is linear which allows keeping track of the effects of  $\underline{\omega}_{dyn}$  in the following manner:

From equation set (4.3-28)

$$\underline{\omega}_{dyn} = C_{B_n}^L (S + M) \underline{\omega}_{IB_n}^{BG} \quad (4.5-10)$$

$$\underline{\omega}_{stat} = C_{B_n}^L (\underline{\omega}_D^{BG} + S \underline{\omega}_D^{BG}) + \underline{\omega}_{IL}^L \quad (4.5-11)$$

where  $C_{B_n}^L$  is assumed to be a constant matrix and  $\underline{\omega}_{IL}^L$  and  $\underline{\omega}_D^{BG}$  constant vectors for a fixed orientation of the system. Also, the elements of  $S$  and  $M$  are by definition constants.

$\underline{\omega}_{dyn}$  is rewritten below as derived in Chapter 5, equations (5.6-1) through (5.6-16).

$$\underline{\omega}_{dyn} = C_{B_n}^L (S_{eq} + M_{eq}) (\underline{\omega}_G^{BG} - \underline{\omega}_{D_{eq}}^{BG}) \quad (4.5-12)$$

where  $\underline{\omega}_G^{BG}$  represents the true gyro indication of rate including static drifts.

$$\left. \begin{aligned} \underline{\omega}_G^{BG} &\triangleq \underline{\omega}_{IB_n}^{BG} + \underline{\omega}_{D_{eq}}^{BG} \\ \underline{\omega}_{D_{eq}}^{BG} &\triangleq (I + S) \underline{\omega}_D^{BG} \end{aligned} \right\} \quad (4.5-13)$$

and  $\hat{S}_{eq}$  and  $\hat{M}_{eq}$  are equivalent scale factor and misalignment matrices respectively.

[Variations in  $\underline{\omega}_{dyn}$ , due to small variations in  $C_{B_n}^L$  and in  $\underline{\omega}_D^{BG}$  will be only of second order thereby justifying the above assumptions.]

Each of the first two elements of  $\underline{\omega}_{dyn}$  are linear combinations of the elements of  $\underline{\omega}_G^{BG}$  and  $\underline{\omega}_{Deq}^{BG}$ , i.e.,

$$\begin{aligned}\omega_{dyn_i} = & a_{i1} \omega_G^{BG_1} + a_{i2} \omega_G^{BG_2} + a_{i3} \omega_G^{BG_3} \\ & - (a_{i1} \omega_{Deq}^{BG_1} + a_{i2} \omega_{Deq}^{BG_2} + a_{i3} \omega_{Deq}^{BG_3}), \quad (4.5-14) \\ i = & 1, 2\end{aligned}$$

where

$$a_{ij} \text{ is an element of the matrix } C_{B_n}^L (\hat{S}_{eq} + \hat{M}_{eq})$$

and  $a_{ij}$  and will be computed during the first iteration of the calibration procedure.

Equation (4.5-5) is therefore used to track the effects of the  $\omega_{G_j}^{BG}$ ,  $j = 1, 2, 3$ , elements and the  $\omega_{Deq_i}^{BG}$  elements, and the results are combined using linear superposition as in (4.5-14) to yield estimate on the error due to  $\underline{\omega}_{dyn}$  during a static position. This procedure is illustrated in Figure 4.5-1. Here, the drivers of the four error equation sets are formed respectively from  $\omega_{G_j}^{BG}$ ,  $j = 1, 2, 3$  and 1 (since  $\omega_{Deq_i}$  are constants) as shown below.

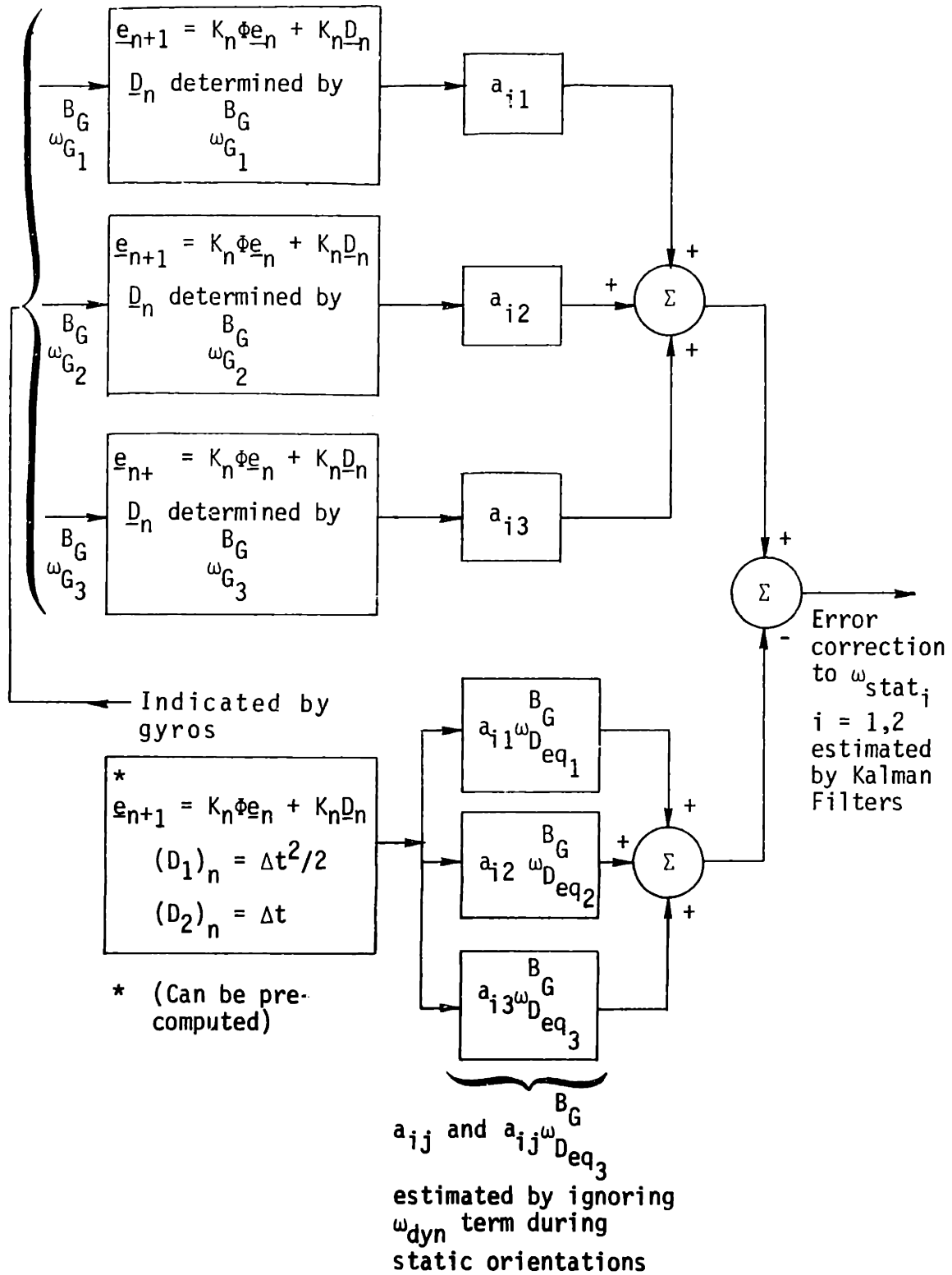


Figure 4.5-1 Kalman Filter Static Drift Error Corrector for Dynamic Errors

$$\left. \begin{aligned}
 (D_2)_m &= \int_{t_n}^{t_n + \Delta t} w_{Gj}^{BG} dt, \quad j = 1, 2, 3 \\
 (D_1)_m &= \int_{t_n}^{t_n + \Delta t} \int_{t_n}^t w_{Gj}^{BG} dt, \quad j = 1, 2, 3 \\
 (D_2)_m &= \Delta t, \quad (D_1)_m = \frac{\Delta t^2}{2}
 \end{aligned} \right\} \begin{array}{l} 1^{\text{st}} \\ 3 \text{ sets} \\ 4^{\text{th}} \\ \text{set} \end{array} \quad (4.5-15)$$

At the price of yet an additional software burden, variations in  $C_{B,i}^L$  in the term

$$\underline{\omega}_{\text{stat}} = C_{B_n}^L (\underline{\omega}_{D_{eq}}^{BG}) + \underline{\omega}_{IL}^L \quad (4.5-16)$$

can be accommodated in a similar way. These variations also mean that the g-sensitive terms are varying. In order to obtain explicit expressions for the form of the drift corrections, the derivation of static drift terms in Chapter 5 is borrowed. There it is shown that  $\omega_{S_{k\ell}^j}$  is, for the  $j^{th}$  static orientation, given by

$$(\omega_{\text{stat}})_{ij} \approx h_{ij} \frac{\nu_s}{s}, \quad i=1,2 \text{ for } j^{\text{th}} \text{ orientation} \quad (4.5-17)$$

where

$$\underline{h}_{ij}^T \triangleq (c_{i1}, c_{i2}, c_{i3}, c_{i1}c_{31}, c_{i2}c_{32}, c_{i1}c_{32}, c_{i2}c_{31}, c_{i3}c_{32}) \quad (4.5-18)$$

$$\underline{\underline{N}}_s^T \triangleq (B_1, B_2, B_3, \Delta_{13}, \Delta_{23}, g_{MSH_1}, g_{MSH_2}, g_{MSH_3}) \quad (4.5-19)$$

and

$C_{ij}$  are the direction cosine elements of  $C_{B_{ix}}^L$

$B_1, B_2, B_3$  are the gyro bias drifts

$\Delta_{13}$  is the difference between the input axis mass unbalance drifts of the first and third gyros

$\Delta_{23}$  is the difference between the input axis mass unbalance drifts of the second and third gyros

$gM_{SA_1}, gM_{SA_2}, gM_{SA_3}$  are the gyro spin axis mass unbalance drifts

Assume that  $\omega_{stat,i}$  for a particular orientation has been estimated without any corrections or with corrections for the dynamic terms obtained from the procedure block diagram in Figure 4.5-1. The solutions for the elements of  $\underline{\chi}_s$  (equation (4.5-19)) are then obtained as presented in Chapter 5 using  $\underline{h}_{ij}^T$  as defined by (4.5-18) but with the elements of  $\underline{h}_{ij}^T$  averaged over the time interval during which  $\omega_{stat,i}$  is estimated. The vector of averaged elements is designated by  $\bar{\underline{h}}_{ij}^T$ . The initial estimate of  $\underline{\chi}_s$  is designated by  $\underline{\chi}_s^0$ . Figure 4.5-2 then shows the correction procedure. As with the procedure in Figure 4.5-1 linear superposition is used to obtain approximate corrections in an estimate of  $\underline{h}_{ij}^T \underline{\chi}_s$  due to variations in the elements of  $\underline{h}_{ij}^T$  from their average values during the Kalman filter estimation period.

In both (Figures 4.5-1 and 4.5-2) of the preceding correction schemes, the errors due to using the initial approximations to  $\omega_{stat,i}$  and  $\underline{\chi}_s$  before any of the corrections are made should be of second order in these corrections provided that the errors due to the initial neglected

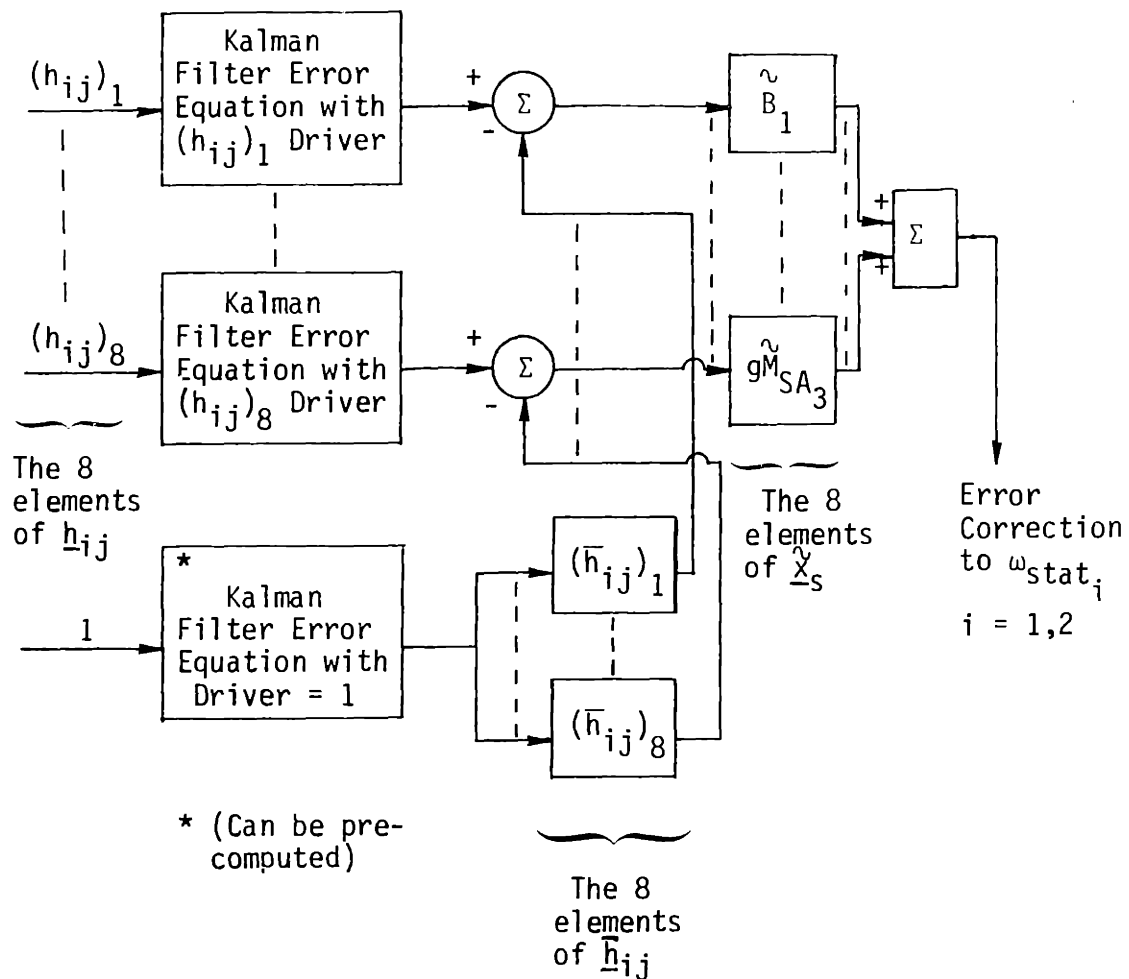


Figure 4.5-2 Kalman Filter Static Drift Error Corrector for Variations in  $C_Ba^L$

118

dynamic term and variations in  $C_{Bq}^L$  are not greatly magnified by the initial estimation procedure.

During a rotation the static and dynamic drifts are not modeled by the Kalman filter equations and both contribute to the errors in the Kalman filter estimates of misalignment angles. Again, correction for these errors is based on linear superposition and is similar to the preceding methods. In order to illustrate this particular procedure some additional information must be borrowed from Chapter 5. The dynamic term,  $\omega_{dynij}$ , for the  $j^{th}$  rotation is given approximately by

$$\omega_{dynij} \approx (c_{i1}, c_{i2}, c_{i3}) \begin{bmatrix} \omega_{A_1j}^{BG} \\ \omega_{A_2j}^{BG} \\ \omega_{A_3j}^{BG} \end{bmatrix} \quad \left\{ i=1,2 \right. \quad (4.5-20)$$

where  $\omega_{A_kj}^{BG}$  is an approximately constant dynamic error induced by the  $j^{th}$  nominal rotation in the  $k^{th}$  gyro. The rotation is nominally at a constant rate (say by use of a motor to rotate the system).

$c_{ij}$  is an element of  $C_{Bq}^L$ .

The full correction procedure for the Kalman filter estimates of misalignment during a rotation of the system is depicted in Figure 4.5-3. Here the same notation  $\delta_{ij}$  for the corrections for static drift errors is used but with the exception that  $j$  denotes the  $j^{th}$  rotation rather than the  $j^{th}$  static orientation. Also  $\tilde{\omega}_{Aij}^{BG}$  represents the initial estimate of  $\omega_{Aij}^{BG}$  made before any corrections have been applied to the initial dynamic parameter estimates. The previous remarks, concerning Figures 4.5-1 and 4.5-2, about the second order effect of initial errors

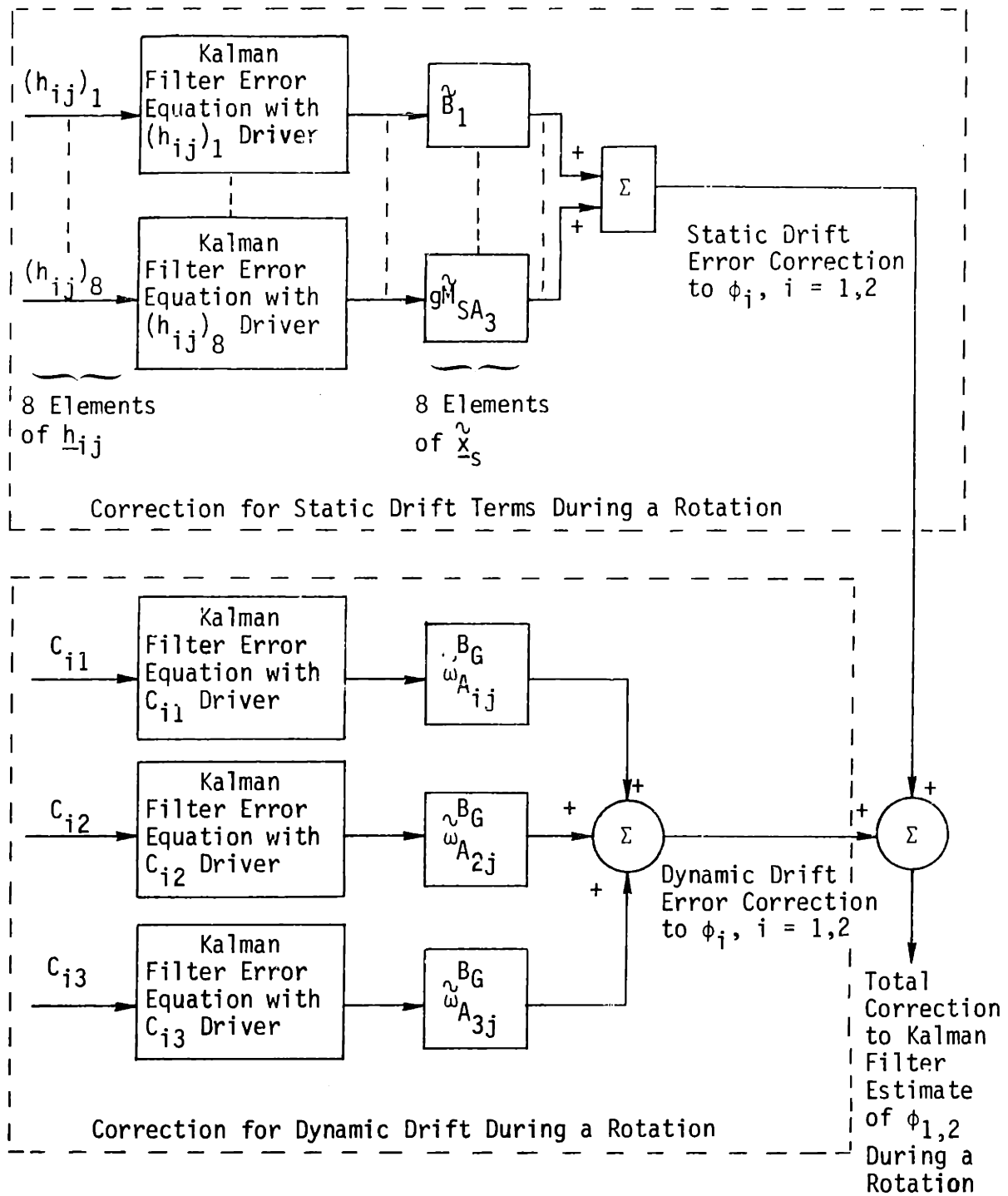


Figure 4.5-3 Full Correction Procedure for Misalignment Estimates During a Rotation

(such as in the estimates  $\hat{x}_s$  and  $\hat{w}_{n_{ij}}^G$ ) on the estimated error correction also apply to the Figure 4.5-3 procedure.

Implementation of the error correction software presented above appears at first to require a great amount of computation. However, all of the Kalman filter error equations use pre-computed gains and involve at most only 3x3 matrices and 3 dimensional vectors. Analysis<sup>32</sup> of the computational requirements for a full 24 state optimal filter which would in effect eliminate need for the correction procedures (if the filter was actually applicable to the requirements discussed in Chapter 1) shows that the computational burden includes 4860 multiplications filter cycle. The maximum computational burden for the error correction procedures presented in this section would occur if the schemes in Figures 4.5-1 and 4.5-2 were implemented together as well as the scheme in Figure 4.5-3. This burden would include roughly 1000 multiplications filter cycles for a considerable savings over the hypothetical optimal Kalman filter.

Approximations to the above correction schemes that are derived from tailoring the corrections more closely to the actual nominal orientations and rotations carry an even lighter software burden. The following example is presented for a particular nominal rotation and the general correction procedure in Figure 4.5-3. Nominal rotation is about body reference axis 1 which is nominally level. (See Figure 4.5-4). Hence body axis 1 is nominally parallel to level reference axis 1. Initially as shown in the figure, body reference axis 2 is parallel to level reference axis 2. A savings in the correction scheme in Figure 4.5-3 is made by assuming that even for small deviations from the nominal rotation shown, the lumped drift (dynamic and static) projected on reference level axis 2 is due only to gyros 2 and 3 and that the lumped

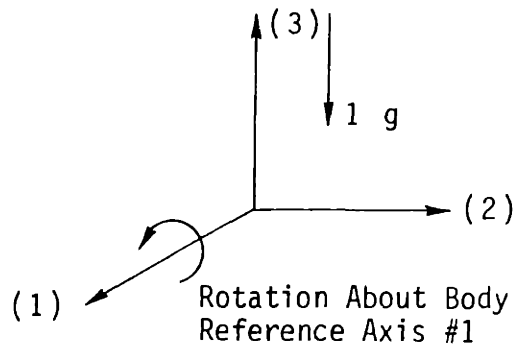


Figure 4.5-4 A Nominal Rotation of the System Body Axes

drift projected on reference level axis 1 is due only to gyro 1. The reference level axis 2 lumped drift drives the misalignment angle about reference level axis 1 and vice-versa. With these assumptions, we can, in Figure 4.5-3, for the misalignment angle correction for reference level axis 1, dispense with drivers  $(h_{1j})_1, (h_{1j})_4, (h_{1j})_6, C_{11}$ , and the error equations fed by these drivers. For the reference level axis 2 misalignment correction we need only retain, in Figure 4.5-3, drivers  $(h_{2j})_1, (h_{2j})_6, C_{21}$ , along with their associated error equations. The total savings over the original scheme is the need to compute an additional 12 error difference equations (i.e., the computational burden is cut in half). Similar savings are possible for all of the nominal rotations and orientations by employing the same kind of assumptions as above tailored to the particular nominal rotation or nominal static orientation.

Chapter 5  
Estimation of Gyro Parameters

### 5.1 Introduction

Extraction of the gyro static parameters from a set of Kalman filter lumped drift estimates and extraction of the gyro dynamic parameters from a set of Kalman filter error angle estimates are the main concerns of this chapter. The relevant Kalman filters and their estimates were described in the previous chapter.

Gyro static parameters are bias, spin axis mass unbalance drift and input axis mass unbalance drift. Because all drift estimates are obtained from the projection of body axis drifts onto two horizontal reference axes, it is shown that the three gyro input axis mass unbalance terms are not separately observable. Instead two new observable variables

$$\begin{aligned}\Delta_{13} &\triangleq M_{IA_1} - M_{IA_3} \\ \Delta_{23} &\triangleq M_{IA_2} - M_{IA_3}\end{aligned}\quad (5.1-1)$$

are defined to take the place of the three input axis mass unbalance terms,  $M_{IA_1}$ ,  $M_{IA_2}$ ,  $M_{IA_3}$ . The requirement is, therefore, for the extraction of 8 gyro static parameters from lumped drift estimates obtained from a series of 8 static orientations of the system. Individual input axis mass unbalance terms can be obtained from (5.1-1) once  $M_{IA_3}$  is known. Appendix 5B suggests two approaches toward separately estimating  $M_{IA_3}$ .

With the azimuth reference tied to the body frame (as defined in Chapter 4), the horizontal earth rate components along the local level reference axes are treated as unknowns to be added to the lumped gyro drift components along these same axes. They are, in fact, included in the Kalman filter lumped drift estimates. Estimation of these earth rate components by, for example, a simple  $180^\circ$  rotation about the vertical averaging technique cannot be done accurately unless the system is "perfectly" leveled

because of the need to accommodate very large mass unbalance drifts for one thing. [Accelerometers, as previously explained, are independently calibrated to allow determination of a local level frame and precise estimation of drifts in that frame.] Therefore, to allow a reasonable tolerance on leveling (and, in general, any positioning of the system), the earth rate components are treated as unknowns in a non-linear equality constraint equation relating the magnitudes of these components to the magnitude of the horizontal component of earth rate. That is, if  $\omega_1$  and  $\omega_2$  are the components, then

$$\omega_1^2 + \omega_2^2 = \omega_h^2 \quad (5.1-2)$$

where  $\omega_h$  is the horizontal component of earth rate.

A minimal data set of the Kalman filter drift estimates obtained from a sequence of 8 static orientations (mentioned above) is used in the iterative solution (of Newton-Raphson type) of 8 simultaneous equations formed by taking into account the non-linear earth-rate component constraint equation (5.1-2) for each static orientation.

It is shown, using a Lyapunov analysis, that it is probable that the iteration converges under the conditions expected for LCIGS (cited throughout this chapter) and the typical urban laboratory environment presented by Weinstock and quoted in Chapter 2. That is, with a tolerance of  $\pm 20^\circ$  in the deviation of the principal reference axis from north, a tolerance of  $\pm 1/2^\circ$  in leveling and in otherwise positioning the system, and always starting the iteration by assuming that the principal reference axis is due north, the iteration should converge for typical LCIGS measurement noise sources.

It is estimated that due only to the gyro random walk term the equiva-

lent parameters for bias and spin axis mass unbalance drifts will be accurate to the order of  $0.1^0/\text{hr}$ . Input axis mass unbalance estimates will be somewhat worse (on the order of  $0.3^0/\text{hr}$  for the  $g\Delta_{13}$  and  $g\Delta_{23}$  drifts). Actual errors due to measurement noise simulations will be assessed in Chapter 6.

The dynamic drifts due to the base motion during a static position as deduced from Weinstock's data are expected to have a negligible effect so that the Kalman filter correction scheme of Figure 4.5-1 in Chapter 4 is not needed in the immediate application of calibrating LCIGS in a laboratory type environment. Similar comments apply to the correction scheme of Figure 4.5-2, in the same chapter, for variations in the computed direction cosine matrix during the static positions.

It is assumed in the above analyses that each static position will be of 1 minute duration.

The estimated static gyro parameters and earth rate components are then used along with the Kalman filter estimates of the change in angle about each reference axis during a rotation in the solution of 9 simultaneous linear equations for the dynamic parameters. These dynamic parameters, originally defined in Chapter 4, consist of 3 gyro scale factor errors and 6 direction cosine values.

Six nominal rotations are defined with tolerances of  $\pm 1/2^0$  in positioning and rotating the system axes. The nine necessary equations are selected from the twelve available equations that can be formulated for the six rotations.

There is a subtlety in that the direction solutions of the 9 simultaneous equations are for equivalent scale factor errors and equivalent direction cosine values defined in Section 5.5. However, it is shown

that the true scale factor errors and direction cosines are readily derived from these initial solutions. Analysis of the dynamic parameter estimation errors due to LCIGS error sources including the accelerometer estimation errors presented in Chapter 2 shows that the LCIGS requirements for scale factor error and gyro misalignments (300 ppm  $1\sigma$  and 100 arc-sec  $1\sigma$ ) can be met provided that the Kalman filter error correction scheme for misalignment estimates during a rotation presented by Figure 4.5-3 in Chapter 4 is implemented and, of course, provides the requisite corrections for angle errors due to unmodeled static and dynamic drifts during a rotation.

A rotation duration of 10 seconds was assumed in the above analyses.

Finally, as mentioned in the introductory chapter, the dynamic terms that can be solely determined from the physical parameters of the gyro, output axis coupling, spin axis cross coupling, and anisoinertia drifts, are not considered here.

## 5.2 Solution for Static Error Parameters

The static lumped drift vector,  $\underline{\omega}_D^{BG}$ , introduced in the last chapter represents the total drift rate introduced into the attitude algorithm (see equation (4.3-1)) due to the static gyro error parameters. It compromises the principal portion of the static lumped drift estimates of the Kalman filters (presented in Chapter 4) that is not due to earth rate. For the gyro static model considered in this and the following section, the gyro misalignments implicitly defined by equations (4.3-1) and (4.3-2) are considered to be zero. Examination of misalignment effects on estimation of static drift parameters is postponed to Section 5.4. Thus the  $i^{\text{th}}$  component of  $\underline{\omega}_D^{BG}$  (i.e., the static drift of the  $i^{\text{th}}$  gyro) is given by

$$(\underline{\omega}_D^{BG})_i = B_i + g_{IA_i}^B M_{IA_i} + g_{SA_i}^B M_{SA_i} \quad (5.2-1)$$

where the superscript B now denotes the common reference frame in the absence of misalignments and

$B_i$  = bias drift of the  $i^{\text{th}}$  gyro

$g_{IA_i}^B$  = gravity along the input axis of the  $i^{\text{th}}$  gyro

$M_{IA_i}$  = input axis mass unbalance drift coefficient of  $i^{\text{th}}$  gyro

$g_{SA_i}^B$  = gravity along the spin axis of the  $i^{\text{th}}$  gyro

$M_{SA_i}$  = spin axis mass unbalance drift coefficient of the  $i^{\text{th}}$  gyro

and the effects of gyro scale factor error on the static drift magnitudes is assumed to be included under these terms.

The two static lumped drift terms estimated by the two Kalman filters are given by equation (4.3-27)

$$\underline{\omega}_{SNT_1} = [1 \ 0 \ 0] \left\{ C_{B_a}^L \underline{\omega}_D^{BG} + \underline{\omega}_{IL}^L \right\} \quad (5.2-2)$$

$$\underline{\omega}_{SNT_2} = [0 \ 1 \ 0] \left\{ C_{B_a}^L \underline{\omega}_D^{BG} + \underline{\omega}_{IL}^L \right\}$$

(Note  $\underline{\omega}_D^{BG}$  is subsumed under the term  $\underline{\omega}_D^{BG}$ )

(where  $\underline{\omega}_{IL}^L$  is the horizontal projection of earth rate)

The direction cosine matrix  $C_{B_a}^L$  in equation (5.2-2) is explicitly written as

$$C_{B_a}^L \triangleq \begin{bmatrix} C_{11} & C_{12} & C_{13} \\ C_{21} & C_{22} & C_{23} \\ C_{31} & C_{32} & C_{33} \end{bmatrix} \quad (5.2-3)$$

Furthermore

$$\begin{bmatrix} g_{IA_1}^B \\ g_{IA_2}^B \\ g_{IA_3}^B \end{bmatrix} = C_L^{B_a} \begin{bmatrix} 0 \\ 0 \\ g \end{bmatrix} = \begin{bmatrix} C_{31}g \\ C_{32}g \\ C_{33}g \end{bmatrix} \quad (5.2-4)$$

If we substitute (5.2-1), (5.2-3) and (5.2-4) into equations (5.2-2), we see that the sum of the terms containing the input axis mass unbalance coefficients in the resulting expressions for  $\omega_{stat_1}$  and  $\omega_{stat_2}$  are given respectively by

$$D_1 \triangleq C_{11}C_{31}gM_{IA_1} + C_{12}C_{32}gM_{IA_2} + C_{13}C_{33}gM_{IA_3} \quad (5.2-5)$$

$$D_2 \triangleq C_{21}C_{31}gM_{IA_1} + C_{22}C_{32}gM_{IA_2} + C_{23}C_{33}gM_{IA_3} \quad (5.2-6)$$

But the orthogonality relations between the rows of  $C_{B_a}^L$  yield

$$C_{11}C_{31} + C_{12}C_{32} + C_{13}C_{33} = 0 \quad (5.2-7)$$

$$C_{21}C_{31} + C_{22}C_{32} + C_{23}C_{33} = 0 \quad (5.2-8)$$

Solving equations (5.2-7) for  $C_{13}C_{33}$  and (5.2-8) for  $C_{23}C_{33}$  and substituting the results into (5.2-5) and (5.2-6) leads to

$$D_1 = C_{11}C_{31}g(M_{IA_1} - M_{IA_3}) + C_{12}C_{32}g(M_{IA_2} - M_{IA_3}) \quad (5.2-9)$$

$$D_2 = C_{21}C_{31}g(M_{IA_1} - M_{IA_3}) + C_{22}C_{32}g(M_{IA_2} - M_{IA_3}) \quad (5.2-10)$$

Equations (5.2-9) and (5.2-10) demonstrate that the three input axis mass unbalance coefficients  $M_{IA_1}$ ,  $M_{IA_2}$ ,  $M_{IA_3}$  are not separately observable in equations (5.2-2).

Therefore, two new coefficients defined by

$$\begin{aligned} \Delta_{13} &\triangleq (M_{IA_1} - M_{IA_3}) \\ \Delta_{23} &\triangleq (M_{IA_2} - M_{IA_3}) \end{aligned} \quad (5.2-11)$$

are used to replace the three input axis mass unbalance coefficients in the expressions for  $\omega_{stat_1}$  and  $\omega_{stat_2}$ . A vector,  $\underline{\chi}_s$ , of static drift terms for the three system gyros can now be defined.

$$\underline{\chi}_s \triangleq (B_1, B_2, B_3, gM_{SA_1}, gM_{SA_2}, gM_{SA_3}, gA_{13}, gA_{23})^T \quad (5.2-12)$$

Using the system (LCIGS) geometry depicted in Figure 5.2-1, two row vectors  $\underline{\chi}_{1j}^T$ ,  $\underline{\chi}_{2j}^T$  are defined by

$$\underline{\chi}_{1j}^T \triangleq [C_{11}, C_{12}, C_{13}, C_{11}C_{32}, C_{12}C_{31}, C_{13}C_{32}, C_{11}C_{31}, C_{12}C_{32}] \quad (5.2-13)$$

$$\underline{\chi}_{2j}^T \triangleq [C_{21}, C_{22}, C_{23}, C_{21}C_{32}, C_{22}C_{31}, C_{23}C_{32}, C_{21}C_{31}, C_{22}C_{32}] \quad (5.2-14)$$

$$\begin{aligned} \omega_{STAT1j} &\approx \underline{\chi}_{1j}^T \underline{\chi}_s + \omega_{1j} \\ \omega_{STAT2j} &\approx \underline{\chi}_{2j}^T \underline{\chi}_s + \omega_{2j} \end{aligned} \quad (5.2-15)$$

where  $j$  denotes the  $j^{th}$  static orientation of the system and

$\omega_{1j} \triangleq (\omega_{IL}^L)_{1j}$  = horizontal projection of earth rate along level reference axis 1 at the  $j^{\text{th}}$  static orientation

$\omega_{2j} \triangleq (\omega_{IL}^L)_{2j}$  = horizontal projection of earth rate along level reference 2 at the  $j^{\text{th}}$  static orientation

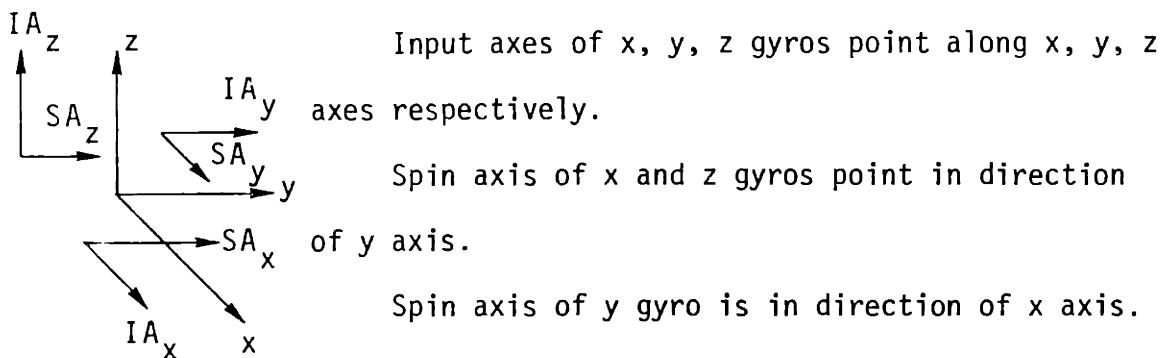


Figure 5.2-1 LCIGS Geometrical Configuration

At each static orientation  $\omega_{1j}$  and  $\omega_{2j}$  are related by the non-linear equality constraint equation

$$\omega_{1j}^2 + \omega_{2j}^2 = (\omega_{ie} \cos L)^2 \quad (5.2-16)$$

where

$\omega_{ie}$  = earth rate

L = latitude at the system location

In the following development, all angular rates are normalized with respect to  $\omega_{ie} \cos L$  so that the constraint equations appear as

$$\omega_{1j}^2 + \omega_{2j}^2 = 1 \quad (5.2-17)$$

The Kalman filter lumped drift estimates for the  $j^{\text{th}}$  static orientation are written as

$$\begin{aligned} m_{1j} &= h_{1j}^T \underline{x}_s + \omega_{1j} + \gamma_{1j} \\ m_{2j} &= h_{2j}^T \underline{x}_s + \omega_{2j} + \gamma_{2j} \end{aligned} \quad (5.2-18)$$

where  $\gamma_{1j}$  and  $\gamma_{2j}$  include the effects of all deviations from the supposed stationary terms ( $\omega_{\text{stat},1j}$ ) and ( $\omega_{\text{stat},2j}$ ) during the Kalman filter estimation interval. These include gyro random walk terms, the residual dynamic drift terms  $\omega_{\text{dyn},1j}$  and  $\omega_{\text{dyn},2j}$ , the additional g-sensitive misalignment error terms discussed in Chapter 4, variations due to small angular base motions, and the Kalman filter estimation errors. Detailed discussion of the effects of these error sources is deferred to Section 5.5 after the basic static estimation procedure is presented and analyzed.

Eight parameters (i.e., components of  $\underline{\chi}_s$ ) are to be estimated from the Kalman filter estimates obtained during each of 8 static orientations. Hence, the following set of 24 equations must be solved for  $\underline{\chi}_s$ .

$$\left. \begin{array}{l} \underline{h}_{11}^T \underline{\chi}_s + \omega_{11} = m_{11} \\ \vdots \\ \underline{h}_{18}^T \underline{\chi}_s + \omega_{18} = m_{18} \end{array} \right\} \quad \begin{array}{l} \text{8 equations for} \\ \text{16 unknowns} \\ \text{(8 components of } \underline{\chi}_s \text{ and} \\ \text{8 values of } \omega_{ij}) \end{array} \quad (5.2-19)$$

$$\left. \begin{array}{l} \underline{h}_{21}^T \underline{\chi}_s + \omega_{21} = m_{21} \\ \vdots \\ \underline{h}_{28}^T \underline{\chi}_s + \omega_{28} = m_{28} \end{array} \right\} \quad \begin{array}{l} \text{8 equations for} \\ \text{16 unknowns} \\ \text{(8 components of } \underline{\chi}_s \text{ and} \\ \text{8 values of } \omega_{2j}) \end{array} \quad (5.2-20)$$

$$\left. \begin{array}{l} \omega_{11}^2 + \omega_{21}^2 = 1 \\ \vdots \\ \omega_{18}^2 + \omega_{28}^2 = 1 \end{array} \right\} \quad \begin{array}{l} \text{8 constraint equations} \\ \text{in 16 unknowns} \end{array} \quad (5.2-21)$$

Solution of the above equation set implies that input axis mass unbalance terms,  $M_{IA_1}$  and  $M_{IA_2}$ , will be solved in terms of  $M_{IA_3}$ .  $M_{IA_3}$  will then have to be obtained by another method in order to obtain distinct values for the input axis mass unbalance coefficients. Two such methods are briefly discussed in Appendix 5B.

The non-linear equality constraint equations lead to the requirement for an iterative technique<sup>35</sup> such as Newton-Raphson iteration to solve the equation set composed of the subsets given by (5.2-19) - (5.2-21).

Any iterative method for solving a set of non-linear equations must start with an initial estimate of the unknown variables. For the equation set being considered, only an initial estimate of the variables involved in the subset of non-linear equations need be made.

Let

$\omega_{1j}(n-1)$  = estimate of  $\omega_{1j}$  at  $(n-1)^{st}$  iteration

$\omega_{2j}(n-1)$  = estimate of  $\omega_{2j}$  at  $(n-1)^{st}$  iteration

then

$$\left. \begin{aligned} \omega_{1j} &= \omega_{1j}(n-1) + \Delta\omega_{1j}(n) \\ \omega_{2j} &= \omega_{2j}(n-1) + \Delta\omega_{2j}(n) \end{aligned} \right\} j = 1, \dots, 8 \quad (5.2-22)$$

Substituting (5.2-22) into (5.2-21) and neglecting products of the deviations  $\Delta\omega_{1j}(n)$  and  $\Delta\omega_{2j}(n)$  yields

$$\begin{aligned} \omega_{1j}(n-1) \delta\omega_{1j}(n) + \omega_{2j}(n-1) \delta\omega_{2j}(n) \\ = \frac{1 - (\omega_{1j}^2(n-1) + \omega_{2j}^2(n-1))}{2} \end{aligned} \quad (5.2-23)$$

for  $j = 1, \dots, 8$ .

where  $\delta\omega_{1j}(n)$  and  $\delta\omega_{2j}(n)$  represent the increments in (5.2-23) and hereafter are estimates of the true deviations  $\Delta\omega_{1j}(n)$  and  $\Delta\omega_{2j}(n)$

Similarly, equations (5.2-19) and (5.2-20) reduce to

$$\underline{\underline{h}}_{1j}^T \underline{\underline{\chi}}_s(n-1) + \delta\omega_{1j}(n) = m_{1j} - \omega_{1j}(n-1) \quad (5.2-24)$$

$$\begin{aligned} \underline{\underline{h}}_{2j}^T \underline{\underline{\chi}}_s(n-1) + \delta\omega_{2j}(n) = m_{2j} - \omega_{2j}(n-1) \\ j = 1, \dots, 8 \end{aligned} \quad (5.2-25)$$

Multiplying (5.2-24) by  $\omega_{1j}(n-1)$  and (5.2-25) by  $\omega_{2j}(n-1)$ , adding the resulting two equations and substituting (5.2-23) into the result

leads to

$$\begin{aligned} (\omega_{1j}(n-1) \underline{\underline{h}}_{1j}^T + \omega_{2j}(n-1) \underline{\underline{h}}_{2j}^T) \underline{\underline{\chi}}_s(n-1) \\ = \omega_{1j}(n-1) m_{1j} + \omega_{2j}(n-1) m_{2j} \\ - \frac{1}{2} (1 + \omega_{1j}^2(n-1) + \omega_{2j}^2(n-1)) \\ j = 1, \dots, 8 \end{aligned} \quad (5.2-26)$$

An iterative solution, therefore, requires taking the inverse of

$$\begin{aligned} C_{m-1} &\triangleq W_1(n-1) H_1 + W_2(n-1) H_2 \\ &= [\omega_{1j}(n-1) \underline{\underline{h}}_{1j}^T + \omega_{2j}(n-1) \underline{\underline{h}}_{2j}^T] \\ &\quad j = 1, \dots, 8 \end{aligned} \quad (5.2-27)$$

on the  $n^{\text{th}}$  iteration, where  $\mathbf{W}'_1(n-1)$  is a diagonal matrix of elements  $\omega_{1j}(n-1)$ ,  $j = 1, \dots, 8$  along the diagonal,  $\mathbf{W}'_2(n-1)$  is a diagonal matrix of elements  $\omega_{2j}(n-1)$ ,  $j = 1, \dots, 8$  along the diagonal and  $H_1$  and  $H_2$  are 8x8 matrices whose rows are, respectively,  $\underline{h}_{1j}^T$ ,  $\underline{h}_{2j}^T$ ,  $j = 1, \dots, 8$ .

Defining,

$$\begin{aligned}\underline{y}(n-1) &\triangleq \mathbf{W}_1(n-1) \underline{m}_1 + \mathbf{W}_2(n-1) \underline{m}_2 \\ &+ \begin{bmatrix} -\gamma_2(1 + \omega_{11}^2(n-1) + \omega_{21}^2(n-1)) \\ \vdots \\ -\gamma_2(1 + \omega_{18}^2(n-1) + \omega_{28}^2(n-1)) \end{bmatrix} \quad (5.2-28)\end{aligned}$$

where  $\underline{m}_1$  and  $\underline{m}_2$  are vectors whose components are  $m_{1j}, m_{2j}$ ,  $j = 1, \dots, 8$  respectively, the solution proceeds as follows (based on equation set (5.2-26)).

$$\underline{x}_s(n-1) = C_{n-1}^{-1} \underline{y}(n-1) \quad (5.2-29)$$

$$\left. \begin{array}{l} \omega_{1j}(n) = m_{1j} - \underline{h}_{1j}^T \underline{x}_s(n-1) \\ \omega_{2j}(n) = m_{2j} - \underline{h}_{2j}^T \underline{x}_s(n-1) \end{array} \right\} \quad j = 1, \dots, 8 \quad (5.2-30)$$

with  $C_{n-1}$  and  $\underline{y}(n-1)$  given by (5.2-27) and (5.2-28) and given initial values of  $\omega_{1j}(0), \omega_{2j}(0)$ ,  $j = 1, \dots, 8$  to start the iteration.

Feasibility of a solution first of all depends on the continued existence of the inverse matrix  $C_{n-1}^{-1}$  throughout the iteration. This obviously depends on the matrices  $H_1, H_2, \mathbf{W}'_1(n-1), \mathbf{W}'_2(n-1)$  in equation (5.2-27) which in turn depend on a set of nominal static orientations for the system, maximum allowed deviations from these orientations, and the convergence properties of the iteration sequences for  $\omega_{1j}(n)$  and  $\omega_{2j}(n)$ .

The nominal orientations are chosen such that, ideally, with the system principal local level reference axis pointed north, the resulting

matrix  $H_1$ , following the same line of reasoning as in Section 2.4, Chapter 2, is close to an orthogonal matrix for good numerical conditioning. Invertibility of  $C_n$  is then examined first for deviations of the principal reference axis from north and then for deviations of the system from the nominal leveling requirements corresponding to the nominal rows of  $H_1$ .

Below is a nominal matrix  $H_1$  and the accompanying matrix  $H_2$  for a nominal set of orientations of a system having the geometry of Figure 5.2-1 as shown in Chapter 4, Figure 4.2-1.

$$H_1 = \begin{bmatrix} 1 & 0 & 0 & 0 & 0 & 0 & 0 \\ 0 & 1 & 0 & 0 & 0 & 0 & 0 \\ 0 & 0 & 1 & 0 & 0 & 0 & 0 \\ 0 & 0 & 0 & 1 & 0 & 0 & 0 \\ 0 & 0 & 0 & 0 & 1 & 0 & 0 \\ 0 & 0 & 0 & 0 & 0 & 1 & 0 \\ 0 & 0 & 0 & 0 & 0 & 0 & 1 \\ 0 & 0 & 0 & 0 & 0 & 0 & 0 \\ .71 & 0 & .71 & 0 & 0 & 0 & -0.5 \\ 0.11 & -0.71 & 0 & 0 & -0.5 & 0 & 0.5 \end{bmatrix}$$

(5.2-31)

$$H_2 = \begin{bmatrix} 0 & 1 & 0 & 0 & 0 & 0 & 0 \\ -1 & 0 & 0 & 0 & 0 & 0 & 0 \\ 0 & 1 & 0 & 0 & -1 & 0 & 0 \\ 0 & 0 & -1 & 0 & 0 & 0 & 0 \\ 0 & 0 & 1 & 0 & 0 & 0 & 0 \\ 0 & 0 & 0 & 1 & 0 & 0 & 0 \\ 1 & 0 & 0 & 0 & 1 & 0 & 0 \\ 0 & 1 & 0 & 0 & 0 & 1 & 0 \\ -1 & 0 & 0 & 0 & 0 & 0 & 1 \end{bmatrix}$$

Accompanying these nominal matrices are the first order level perturbation matrices below. These matrices represent to first order the influence of a small change of angle about the projection of the nominal body axes in the horizontal plane on the elements of the above nominal matrices.  $\Delta H_1$  represents the perturbation to  $H_1$  and  $\Delta H_2$  represents the perturbation to  $H_2$ . The small change of angle is denoted by  $\Delta\theta$  and represents magni-

tudes of the perturbations for both g-sensitive terms and the projections of drift onto the reference axes.

$$\Delta H_1 = \begin{bmatrix} 0 & 0 & 1 & | & 1 & 0 & 0 & | & 1 & 0 \\ 0 & 0 & 1 & | & c & 1 & 0 & | & 0 & 1 \\ 1 & 0 & 0 & | & 0 & 0 & 1 & | & 1 & 0 \\ \hline 0 & 1 & 0 & | & 0 & 0 & 0 & | & 1 & 1 \\ 1 & 0 & 0 & | & 0 & 0 & 0 & | & 1 & 1 \\ 0 & 1 & 0 & | & 0 & 0 & 0 & | & 0 & 1 \\ \hline .71 & 0 & .71 & | & .71 & 0 & .71 & | & .5 & 0 \\ 0 & .71 & .71 & | & 0 & .71 & .5 & | & 0 & .5 \end{bmatrix} |\Delta\theta| \quad (5.2-32)$$

$$\Delta H_2 = \begin{bmatrix} 0 & 0 & 1 & | & c & 1 & 0 & | & 0 & 1 \\ 0 & 0 & 1 & | & 1 & 0 & 0 & | & 1 & 0 \\ 1 & 0 & 0 & | & 0 & 1 & 0 & | & 1 & 1 \\ \hline 0 & 1 & 0 & | & 0 & 0 & 0 & | & 0 & 1 \\ 1 & 0 & 0 & | & 0 & 0 & 1 & | & 1 & 0 \\ 0 & 1 & 0 & | & 0 & 0 & 0 & | & 1 & 1 \\ \hline .71 & 0 & .71 & | & 0 & .71 & 0 & | & .5 & .5 \\ 0 & .71 & .71 & | & .71 & 0 & 0 & | & .5 & .5 \end{bmatrix} |\Delta\theta|$$

In the ensuing calculations it will prove advantageous to express  $C_n^{-1}$  as follows

$$C_{n-1}^{-1} = H_i^{-1} (I + [\alpha_j] H_2 H_i^{-1})^{-1} W_i^{-1} \quad (5.2-33)$$

$$[\alpha_j] \triangleq W_i^{-(n-1)} W_2 (n-1) \quad (5.2-34)$$

Existence of  $C_{n-1}^{-1}$ , therefore, depends on existence of  $\mathbf{W}_1^{-1}$ ,  $\mathbf{H}_1^{-1}$ , and

$$\mathbf{B}(\alpha_j) \triangleq (\mathbf{I} + [\alpha_j] \mathbf{H}_1 \mathbf{H}_1^{-1})^{-1} \quad (5.2-35)$$

Note the significance of the term  $\alpha_j$  where

$$\alpha_j \triangleq \frac{\omega_{2j}(n-1)}{\omega_{1j}(n-1)} \triangleq \tan A_j \quad (5.2-36)$$

represents the tangent of the computed deviation from north,  $A_j$ , for the  $j^{\text{th}}$  system orientation at the  $(n-1)^{\text{th}}$  iteration.

In order to have a numerically well-conditioned solution, more stringent requirements on  $C_n^{-1}$  than mere existence are needed. That is,  $C_n^{-1}$  should have a norm which is within a specified predetermined bound. Examination of (5.2-33) shows that this can be accomplished by restrictions on: (i) the maximum allowed tolerance in the deviation of the principal level reference axis from north, (ii) the maximum deviation from nominal leveling requirements, (iii) the maximum allowable magnitude of the computed value  $\alpha_j(n)$ , (iv) the minimum allowable value of the computed value  $\omega_{1j}(n)$ . It is important to note that restrictions on the computed values of  $\alpha_j(n)$  and  $\omega_{1j}(n)$  during the iteration are logically consistent with having determined allowable tolerances on the nominal system test orientations. Any computation of  $\alpha_j$  and  $\omega_{1j}(n)$  which corresponds to the physical test orientation tolerances' being violated indicates an error in the iteration (due to large measurement errors) which can best be mitigated by holding on only to the computed values of  $\omega_{1j}(n)$  and  $\omega_{2j}(n)$  which are compatible with

those tolerances. Therefore, the iteration sequence defined by (5.2-27) - (5.2-30) is modified by addition of the inequality constraints

$$\omega_{1j}(n) \geq \omega_{c_1}$$

$$\alpha_j(n) \leq \alpha_c, \text{ or equivalently } \omega_{2j}(n) \leq \omega_{c_2} \quad (5.2-37)$$

where  $\omega_{c_1}$ ,  $\omega_{c_2}$ ,  $\alpha_c$  are the tolerance bounds such that

$$\alpha_c = \tan A_c$$

$$\omega_{c_1} = \cos A_c, \omega_{c_2} = \sin A_c \quad (5.2-38)$$

and  $A_c$  is the maximum allowable deviation from north.

Existence of  $W_1^{-1}(n-1)$  is well assured for the inequality constraint on the iteration given by (5.2-37). Appendix 5A is a compilation of matrices encountered in the analysis presented in this chapter for the gyro static parameter estimation procedure.  $H_1^{-1}$ , for zero leveling perturbations is given by (5A-2) in that appendix. Its existence is assured independently of values of  $\omega_{1j}(n-1)$  and  $\omega_{2j}(n-1)$ . The inverse matrix,  $B(\alpha_j)$ , is given by equation (5A-4). It is seen that existence of this matrix directly depends on the conditions

$$1 + \alpha_1 \alpha_2 = \frac{\cos(A_1 - A_2)}{\cos A_1 \cos A_2}$$

$$1 + \alpha_3 \alpha_5 = \frac{\cos(A_3 - A_5)}{\cos A_3 \cos A_5} \quad (5.2-39)$$

$$1 + \alpha_4 \alpha_6 = \frac{\cos(A_4 - A_6)}{\cos A_4 \cos A_6}$$

or

$$\left. \begin{array}{l} A_1 - A_2 \\ A_3 - A_5 \\ A_4 - A_6 \end{array} \right\} < \frac{\pi}{2} \quad (5.2-40)$$

If the system test fixture orientations are precise within, say,  $1/2^0$  and the base motion is slight, it is reasonable to assume that all of the nominal values of  $A_j$ ,  $j = 1, \dots, 8$  are equal in magnitude and of the same sign. Hence  $A_1 - A_2$ ,  $A_3 - A_5$ ,  $A_4 - A_6$  will differ from zero only to the extent that  $\omega_{1j}(n-1)$  differ among themselves and  $\omega_{2j}(n-1)$  differ among themselves during and after the iteration due to non-zero values of the error sources  $\nu_{1j}$  and  $\nu_{2j}$  in equation set (5.2-18). Since the nominal values  $A_j$  are of the same sign, these errors would have to be large enough to cause the effective deviations from north to differ by  $\pi/2$ . This can never happen with the magnitude on  $\alpha_j$  constrained according to (5.2-37) and (5.2-38).

Estimates of upper bounds on matrix norms,  $\|B(\alpha_j)\|_2$  and  $\|H_2 H_1^{-1} B(\alpha_j)\|_2$  used in subsequent analyses, are made in Appendix 5A for various values of  $\alpha_j$ . For nominal values of  $|A_j| \geq 15^0$  it is assumed that all of the calculated values of  $\alpha_j$  will be of the same sign. Hence, the norms can be calculated assuming all  $\alpha_j$  are equal because  $\cos(A_j - A_k)$  is greater in magnitude than either  $\cos A_j$  or  $\cos A_k$  if  $A_j$  and  $A_k$  are the same sign. The upper bounds on the norms are given by equations (5A-10) and (5A-18).

Modifications of these norm upper bounds due to level perturbations of  $1/4^0$  and  $1/2^0$  (in equations (5.2-32)) is also carried out in Appendix 5A. The results are listed in Tables 5A-4 and 5A-5 from which it can be inferred that perturbations equal to or less than  $1/2^0$  still leave the matrix  $C_n^{-1}$  in the iteration numerically well-conditioned.

### 5.3 Convergence of the Iterative Solution

Convergence of the iteration defined by equations (5.2-27) - (5.2-30) and (5.2-37) is examined below. For convenience of reference these iterative equations are repeated in the following form.

$$\begin{aligned} \underline{C}_{n-1} &= [\omega_{1j}(n-1) \underline{\underline{h}}_{1j}^T + \omega_{2j}(n-1) \underline{\underline{h}}_{2j}^T], j = 1, \dots, 8 \\ &= \underline{W}_1(n-1) \underline{H}_1 + \underline{W}_2(n-1) \underline{H}_2 \end{aligned} \quad (5.3-1)$$

$$\begin{aligned} \underline{\underline{y}}(n-1) &= [\omega_{1j}(n-1) \underline{m}_{1j} + \omega_{2j}(n-1) \underline{m}_{2j} \\ &\quad - \frac{1}{2} (1 + \omega_{1j}^2(n-1) + \omega_{2j}^2(n-1))] \\ &\quad j = 1, \dots, 8 \end{aligned} \quad (5.3-2)$$

$$\underline{\underline{v}}_s(n-1) = \underline{C}_{n-1}^{-1} \underline{\underline{y}}(n-1) \quad (5.3-3)$$

$$\omega_1(n) = \underline{m}_1 - \underline{H}_1 \underline{\underline{v}}_s(n-1) \quad (5.3-4)$$

$$\omega_2(n) = \underline{m}_2 - \underline{H}_2 \underline{\underline{v}}_s(n-1) \quad (5.3-5)$$

$$\omega_{1j}(n) \geq \omega_{c1} \quad (5.3-6)$$

$$|\omega_{2j}(n)| \leq \omega_{c2} \quad (5.3-7)$$

where  $\underline{\omega}_1(n), \underline{\omega}_2(n)$  are the vectors with components  $\omega_{1j}(n), \omega_{2j}(n)$  respectively and  $\underline{m}_1, \underline{m}_2$  are the vectors with components  $\underline{m}_{1j}, \underline{m}_{2j}$  respectively, all for  $j = 1, \dots, 8$  and  $\omega_{c1}$  and  $\omega_{c2}$  are predetermined constraint bounds.

Existence of the inverse  $C_{n-1}^{-1}$  throughout the iteration is guaranteed by the constraints (5.3-6), (5.3-7) and constraints on the nominal system orientations.

The iteration stops when either

$$\underline{\omega}_1(n) = \underline{\omega}_1(n-1) \stackrel{\Delta}{=} \underline{u}_1 \quad (5.3-8)$$

$$\underline{\omega}_2(n) = \underline{\omega}_2(n-1) \stackrel{\Delta}{=} \underline{u}_2 \quad (5.3-9)$$

or any of

$$\omega_{1j}(n) = \omega_{c1} \quad (5.3-10)$$

$$\omega_{2j}(n) = \omega_{c2}$$

which are the tolerances in the primary cut-off limits set for the iterations.

Components  $\underline{M}_{1j}$  and  $\underline{M}_{2j}$  and diagonal matrices  $U_1$  and  $U_2$  are defined analogously to the iterated entities,  $\omega_{1j}$ ,  $\omega_{2j}$ ,  $\underline{W}_1$ ,  $\underline{W}_2$ .

Substituting (5.3-8) and (5.3-9) into (5.3-1) - (5.3-5) yields the following equations for the iteration solutions  $\underline{u}_1$ ,  $\underline{u}_2$ .

$$\underline{u}_1 = \underline{m}_1 - H_1 [ U_1 H_1 + U_2 H_2 ]^{-1} \underline{y}(\underline{u}_1, \underline{u}_2) \quad (5.3-11)$$

$$\underline{u}_2 = \underline{m}_2 - H_2 [ U_1 H_1 + U_2 H_2 ]^{-1} \underline{y}(\underline{u}_1, \underline{u}_2) \quad (5.3-12)$$

$$\begin{aligned} \underline{y}(\underline{u}_1, \underline{u}_2) &= U_1 \underline{m}_1 + U_2 \underline{m}_2 \\ &\quad - \frac{1}{2} [ 1 + \underline{u}_{1j}^2 + \underline{u}_{2j}^2 ] \\ j &= 1, \dots, 8 \end{aligned} \quad (5.3-13)$$

If equations (5.3-11) - (5.3-13) do have a solution within the inequality constraint bounds, then it is characterized as follows:

Multiplying (5.3-11) by  $U_1$  and (5.3-12) by  $U_2$  and adding the two equations results in

$$\begin{aligned}
 U_1 \underline{u}_1 + U_2 \underline{u}_2 &= U_1 \underline{m}_1 + U_2 \underline{m}_2 \\
 - [U_1 H_1 + U_2 H_2] [U_1 H_1 + U_2 H_2]^{-1} \underline{y}(\underline{u}_1, \underline{u}_2) \\
 &= U_1 \underline{m}_1 + U_2 \underline{m}_2 - \underline{y}(\underline{u}_1, \underline{u}_2)
 \end{aligned} \tag{5.3-14}$$

Substituting (5.3-13) into (5.3-14) and simplifying yields

$$\underline{\mu}_{1j}^2 + \underline{\mu}_{2j}^2 = 1, \quad j = 1, \dots, 8 \tag{5.3-15}$$

Equation (5.3-15) demonstrates that the iterative solutions  $\underline{u}_{1j}$ ,  $\underline{u}_{2j}$ ,  $j = 1, \dots, 8$  must satisfy the original equality constraint equations (5.2-21) regardless of any errors in the measurements  $\underline{m}_1$  and  $\underline{m}_2$ .

The above suggests use of the following Lyapunov function<sup>36,37</sup> to investigate convergence of the iteration when all of the iterates are within the inequality constraint bounds.

$$V(n) \triangleq \sum_{j=1}^8 |\omega_{1j}^2(n) + \omega_{2j}^2(n) - 1| \tag{5.3-16}$$

where  $||$  indicates absolute value of the enclosed quantity.

The scalar,  $V(n)$ , has the following properties:

- (1) Unless the equality constraints are satisfied,  $V(n) > 0$
- (2)  $V(n) = 0$ , only if the equality constraints are satisfied
- (3) If  $\omega_{1j}(n) \rightarrow \infty$ , or  $\omega_{2j}(n) \rightarrow \infty$ , or both, then  $V(n) \rightarrow \infty$ , independently of the polarities of  $\omega_{1j}(n)$  and  $\omega_{2j}(n)$

At the  $n^{\text{th}}$  stage in the iteration, the change,  $\Delta V(n)$ , in  $V(n)$  is given by

$$\begin{aligned}\Delta V(n) &= V(n) - V(n-1) \\ &= \sum_j | \omega_{1j}^2(n) + \omega_{2j}^2(n) - 1 | \\ &\quad - \sum_j | \omega_{1j}^2(n-1) + \omega_{2j}^2(n-1) - 1 | \quad (5.3-17)\end{aligned}$$

The increments in going from  $\omega_{1j}(n-1)$  to  $\omega_{1j}(n)$  and from  $\omega_{2j}(n-1)$  to  $\omega_{2j}(n)$  are given by

$$\delta \omega_{1j}(n) = \omega_{1j}(n) - \omega_{1j}(n-1) \quad (5.3-18)$$

$$\delta \omega_{2j}(n) = \omega_{2j}(n) - \omega_{2j}(n-1) \quad (5.3-19)$$

Substituting (5.3-18) and (5.3-19) into (5.3-17) yields

$$\begin{aligned}\Delta V(n) &= \sum_j | \omega_{1j}^2(n-1) + \omega_{2j}^2(n-1) - 1 \\ &\quad + 2\delta \omega_{1j}(n) \omega_{1j}(n-1) + \delta \omega_{1j}^2(n) \\ &\quad + 2\delta \omega_{2j}(n) \omega_{2j}(n-1) + \delta \omega_{2j}^2(n) | \\ &\quad - \sum_j | \omega_{1j}^2(n-1) + \omega_{2j}^2(n-1) - 1 | \quad (5.3-20)\end{aligned}$$

Substituting (5.3-18) and (5.3-19) into (5.3-4) and (5.3-5) yields

$$\begin{aligned}\delta \underline{\omega}_1(n) &= \underline{m}_1 - H_1 \left[ W_1(n-1) H_1 + W_2(n-1) H_2 \right]^{-1} \underline{y}(n-1) \\ &\quad - \underline{\omega}_1(n-1) \quad (5.3-21)\end{aligned}$$

$$\begin{aligned}\delta \underline{\omega}_2(n) &= \underline{m}_2 - H_2 \left[ W_1(n-1) H_1 + W_2(n-1) H_2 \right]^{-1} \underline{y}(n-1) \\ &\quad - \underline{\omega}_2(n-1) \quad (5.3-22)\end{aligned}$$

Multiplying (5.3-21) by  $\underline{W}'_1(n-1)$  and (5.3-22) by  $\underline{W}'_2(n-1)$ , adding the two equations and substituting (5.3-2) into the sum results in

$$\begin{aligned}\delta \omega_{ij}(n) \omega_{ij}(n-1) + \delta \omega_{2j}(n) \omega_{2j}(n-1) \\ = \frac{1}{2} \left( 1 - (\omega_{ij}^2(n-1) + \omega_{2j}^2(n-1)) \right) \quad (5.3-23)\end{aligned}$$

Substitution of (5.3-23) into (5.3-20) leads in turn to

$$\begin{aligned}\Delta V(n) &= \sum_j |\delta \omega_{ij}^2(n) + \delta \omega_{2j}^2(n)| \\ &\quad - \sum_j |\omega_{ij}^2(n-1) + \omega_{2j}^2(n-1) - 1| \quad (5.3-24)\end{aligned}$$

Another set of equations in addition to (5.3-23) is needed to relate the first sum in (5.3-24) to the second sum. This set is derived as follows:

For  $n \geq 1$ , equation (5.3-4) is solved for  $\underline{x}_s(n-1)$  and the result substituted into equation (5.3-5) to yield

$$\underline{\omega}_2(n) = \underline{m}_2 - H_2 H_1^{-1} (\underline{m}_1 - \underline{\omega}_1(n)) \quad (5.3-25)$$

For  $n \geq 2$ , equation (5.3-25) can also be expressed as

$$\underline{\omega}_2(n-1) = \underline{m}_2 - H_2 H_1^{-1} (\underline{m}_1 - \underline{\omega}_1(n-1)) \quad (5.3-26)$$

Subtracting (5.3-26) from (5.3-25) leads to the desired additional relationship between the increments.

$$\delta \underline{\omega}_2(n) = H_2 H_1^{-1} \delta \underline{\omega}_1(n) \quad \text{for } n \geq 2 \quad (5.3-27)$$

where  $\delta \underline{\omega}_{1j}(n)$  and  $\delta \underline{\omega}_{2j}(n)$  are defined by (5.3-18) and (5.3-19)

Substituting (5.3-27) into (5.3-23) yields

$$\begin{aligned} & [W_1(n-1) + W_2(n-1)H_2 H_1^{-1}] \delta \underline{\omega}_1(n) \\ &= \frac{1}{2} \left[ 1 - \omega_{1j}^2(n-1) - \omega_{2j}^2(n-1) \right] \\ & \quad j = 1, \dots, 8 \end{aligned} \quad (5.3-28)$$

or

$$\begin{aligned} \delta \underline{\omega}_1(n) &= \frac{1}{2} B(\alpha_j) W_1(n-1) \left[ 1 - \omega_{1j}^2(n-1) \right. \\ &\quad \left. - \omega_{2j}^2(n-1) \right] \\ & \quad j = 1, \dots, 8 \end{aligned} \quad (5.3-29)$$

where  $B'(\alpha_j)$  is given by equation (5.2-35) when matrices  $H_1$  and  $H_2$  also include the leveling perturbations discussed earlier.

Substituting (5.3-29) into (5.3-27) results in

$$\begin{aligned} \delta\omega_2(n) &= \frac{1}{2} H_2 H_1^{-1} B'(\alpha_j) W_1^{-1}(n-1) [1 - \omega_{1j}^2(n-1) \\ &\quad - \omega_{2j}^2(n-1)] \end{aligned} \quad (5.3-30)$$

$j = 1, \dots, 8$

where, again,  $H_1$  and  $H_2$  include the leveling perturbations.

The following definitions are now introduced in order to have a more compact notation.

$$\begin{aligned} S &\triangleq B'(\alpha_j) W_1^{-1}(n-1) \\ T &\triangleq H_2 H_1^{-1} B'(\alpha_j) W_1^{-1}(n-1) \\ \Delta C_j &\triangleq 1 - \omega_{1j}^2(n-1) - \omega_{2j}^2(n-1) \end{aligned} \quad (5.3-31)$$

Substituting (5.3-31) into (5.3-29) and (5.3-30) leads to

$$\delta\omega_1(n) = \frac{1}{2} S [\Delta C_j] \quad (5.3-32)$$

$$\delta\omega_2(n) = \frac{1}{2} T [\Delta C_j] \quad (5.3-33)$$

Taking the  $p = 2$  norm of both sides of (5.3-32) and (5.3-33) yields

$$\|\delta\omega_1(n)\|_2 = \left\| \frac{1}{2} S [\Delta C_j] \right\|_2 \leq \left\| \frac{1}{2} S \right\|_2 \left\| [\Delta C_j] \right\|_2 \quad (5.3-34)$$

$$|\delta \underline{\omega}_2(n)|_2 = |\frac{1}{2}T[\Delta C_j]|_2 \leq |\frac{1}{2}T|_2 |\Delta C_j|_2 \quad (5.3-35)$$

where the norms  $|S|_2$  and  $|T|_2$  are maximized over  $j$ .

Squaring both sides of each inequality, (5.3-34) and (5.3-35), and adding, results in

$$\begin{aligned} \sum_j |\delta \omega_{1j}(n) + \delta \omega_{2j}(n)|^2 &= |\delta \underline{\omega}_1(n)|_2^2 + |\delta \underline{\omega}_2(n)|_2^2 \\ &\leq \left( |\frac{1}{2}S|_2^2 + |\frac{1}{2}T|_2^2 \right) |\Delta C_j|_2^2 \end{aligned} \quad (5.3-36)$$

But

$$|\Delta C_j|_2^2 = \sum_j |\Delta C_j|^2 \quad (5.3-37)$$

Substituting (5.3-37) into (5.3-36) yields the desired relationship required for (5.3-24).

$$\sum_j |\delta \omega_{1j}(n) + \delta \omega_{2j}(n)| \leq \left( |\frac{1}{2}S|_2^2 + |\frac{1}{2}T|_2^2 \right) \sum_j |\Delta C_j|^2 \quad (5.3-38)$$

It is seen from the definition of  $\Delta C_j$  that (5.3-24) can be written as

$$\Delta V(n) = \sum_j \left\{ |\delta \omega_{1j}(n) + \delta \omega_{2j}(n)| - |\Delta C_j| \right\} \quad (5.3-39)$$

Examination of (5.3-38) and (5.3-39) shows that

$$\Delta V(n) < 0 \quad (5.3-40)$$

if

$$(|\frac{1}{2}S|_2^2 + |\frac{1}{2}T|_2^2) |\Delta C_j|^2 < |\Delta C_j| \quad (5.3-41)$$

This is assured for all  $n$  if

$$(|\frac{1}{2}S|_2^2 + |\frac{1}{2}T|_2^2) |\Delta C_j| < 1 \quad (5.3-42)$$

and inequality constraints (5.3-6), (5.3-7) are met.

Equation (5.3-42) is, of course, equivalent to

$$|\Delta C_j| < 1 / (|\frac{1}{2}S|_2^2 + |\frac{1}{2}T|_2^2) \quad (5.3-43)$$

Thus, if the condition given by (5.3-43) is met, then (5.3-40) holds, and standard proofs used in Lyapunov stability theory show that  $\omega_{1j}(n)$  and  $\omega_{2j}(n)$  converge to a set of values  $\omega_{1j}$  and  $\omega_{2j}$  that satisfy constraint equations (5.3-15) provided all iterates meet the inequality magnitude constraints given by (5.3-6) and (5.3-7) which can be violated due to large measurement errors [i.e.,  $V(n)$  defined by equation (5.3-16) is driven toward zero as the iteration proceeds].

Application of (5.3-43) to the specific system test orientations presented in the last section requires either determination of  $|S|_2$  or  $|T|_2$  or of suitably tight upper bounds on these values that hold throughout the iteration. Tables 5A-4 and 5A-5 in Appendix A are upper bounds derived for  $|\frac{1}{2}SW_i(n-1)|$  and  $|\frac{1}{2}TW_i(n-1)|$ , respectively, for values

of the equivalent deviation from north (equation (5.2-36)) ranging from  $15^0$  to  $30^0$  and for leveling perturbations (equations (5.2-32)) of  $1/4^0$  and  $1/2^0$ .

If the iteration is always started by assuming

$$\begin{aligned}\omega_{1j}(0) &= 1 \\ \omega_{2j}(0) &= 0\end{aligned}\quad (5.3-44)$$

then, at the next step in the iteration, equations (5.3-1) - (5.3-5) yield:

$$\begin{aligned}\omega_{1j}(1) &= 1 \quad \text{for } j = 1, \dots, 8 \\ \underline{\omega}_2(1) &= \underline{m}_2 - H_2 H_1^{-1} [\underline{m}_{1j}^{-1}] \\ &\quad j = 1, \dots, 8\end{aligned}\quad (5.3-45)$$

Substituting equations (5.2-18) for  $\underline{m}_{1j}$  and  $\underline{m}_{2j}$  into the above yields

$$\underline{\omega}_2(1) = \underline{\omega}_2 + \underline{\nu}_2 - H_2 H_1^{-1} \left\{ \underline{\nu}_1 + [\omega_{1j}^{-1}] \right\} \quad (5.3-46)$$

$$j = 1, \dots, 8$$

The following definitions are repeated with reference to the above.

$\omega_{1j}$  = earth rate along principal reference axis 1 at  $j^{\text{th}}$  orientation

$\omega_{2j}$  = earth rate along reference axis 2 at  $j^{\text{th}}$  orientation

$\underline{\nu}_1$  = measurement error vector, reference axis 1

$\underline{\nu}_2$  = measurement error vector, reference axis 2

Taking the  $p = \infty$  norm of both sides of (5.3-46) leads to:

$$|\underline{\omega}_2(1)|_{\alpha} \leq |\underline{\omega}_2|_{\alpha} + \left\{ |\underline{\gamma}|_{\alpha} + |H_2 H_1^{-1}|_{\alpha} \right\} |\underline{\gamma}|_{\alpha} + |H_2 H_1^{-1} [\omega_{ij} - i]|_{\alpha} \quad (5.3-47)$$

where it is assumed that

$$\left. \begin{array}{l} |\underline{\gamma}|_{\alpha} \\ |\underline{\gamma}_2|_{\alpha} \end{array} \right\} \leq |\underline{\gamma}|_{\alpha} \quad (5.3-48)$$

Also the signs and magnitudes for each terms of  $[\omega_{ij} - i]$  are the same by virtue of the assumption made in Section 5.2 that the true deviation of the principal reference axis from north for every orientation is the same. Because of this elements along a row of  $H_2 H_1^{-1}$  are added with the signs of each element included when computing  $|H_2 H_1^{-1} [\omega_{ij} - i]|_{\alpha}$ .

The effects of leveling perturbations equal to or less than  $1/2^0$  on  $H_2 H_1^{-1}$  will be small (see Table 5A-3, Appendix A) and are therefore neglected in the following calculations. Using the nominal matrix  $H_2 H_1^{-1}$  presented in Appendix A, equation (5A-2), equation (5.3-47) is reduced to

$$|\underline{\omega}_2(1)|_{\alpha} \leq |\underline{\omega}_2|_{\alpha} + 4 |\underline{\gamma}|_{\alpha} + |[\omega_{ij} - i]|_{\alpha} \quad (5.3-49)$$

The value for  $|\Delta C_j|$  to be used in equation (5.3-43) is therefore given by

$$|\Delta C_j| = \left[ |\underline{\omega}_2|_{\alpha} + 4 |\underline{\gamma}|_{\alpha} + |[\omega_{ij} - i]|_{\alpha} \right]^2 \quad (5.3-50)$$

where  $\Delta C_j$  is defined by equation (5.3-31), keeping in mind that

$$\omega_{ij}(1) = 1 \text{ for } j = 1, \dots, 8$$

Substituting (5.3-50) into (5.3-43) yields a condition which guarantees the iteration to either converge or to result in a reduction of the initial deviation of  $(\underline{\omega}_{ij}^2(1) + \underline{\omega}_{ij}^2(1))$  from 1.

$$\begin{aligned} |\underline{\omega}_2|_\infty + 4|\underline{\Sigma}|_\infty + |[\omega_{ij}-1]|_\infty \\ < \frac{1}{\sqrt{|\frac{1}{2}S|^2_2 + |\frac{1}{2}T|^2_2}} \end{aligned} \quad (5.3-51)$$

or, for a true deviation,  $A$ , of the principal reference axis from north,

$$|\underline{\Sigma}|_\infty < \frac{1}{4} \left[ \frac{1}{\sqrt{|\frac{1}{2}S|^2_2 + |\frac{1}{2}T|^2_2}} - \begin{pmatrix} 1 \sin A + 1 \\ -\cos A \end{pmatrix} \right] \quad (5.3-52)$$

Suppose we wish the computed value for  $A$  to be no more than  $30^\circ$  for the iteration  $n = 2$ . Then, we must have

$$|\underline{\omega}_2(1)|_\infty \leq \tan 30^\circ = 0.577 \quad (5.3-53)$$

since  $\omega_{ij}(1) = 1$

Table 5.3-1 presents values of  $|\underline{\Sigma}|_\infty$  that are compatible with (5.3-53) for various true values of  $A$  and leveling perturbations.

$\Delta\theta$	A	$15^\circ$	$20^\circ$	$25^\circ$	$30^\circ$
$1/4^\circ$		.71	.44	.15	0
$1/2^\circ$		.63	.36	.072	0

Table 5.3-1 Maximum Measurement Error in  $^\circ/\text{hr}$  for Initial Covariances

Measurement errors below these maximum values guarantees only that the iteration at  $n = 2$  will result in a decrease in the deviation  $|(\omega_{ij}(n) - \omega_{ij}^*(n))|$  from its value at  $n = 1$ . For a guarantee of complete convergence of the iteration, it must be shown that the successive computed values  $\alpha_{ij}(n)$  and  $\omega_{ij}(n)$  are within the inequality constraints.

$$|\alpha_{ij}(n)|_\infty \leq \tan 30^\circ \quad (5.3-54)$$

$$|\omega_{ij}(n)|_\infty \geq \cos 30^\circ$$

which were used in computing the bounds  $|\frac{1}{2}S|_2, |\frac{1}{2}T|_2$  in equation (5.3-51) so that the condition for convergence given by equation (5.3-43) continues to hold throughout the remainder of the iteration. It is left up to simulations of the iterations to verify conditions such as (5.3-54).

#### 5.4 Effect of Gyro Axis Misalignments on Estimated Static Gyro Drift Parameters

Gyro axis misalignments are explicitly defined by identifying appropriate elements of the direction cosine matrices specified by equations (4.3-1) and (4.3-2) in Chapter 4. A precise specification of the matrix relating the triad of gyro input axes to the reference frame is made at

the beginning of Section 5.6, for the purpose of gyro dynamic calibration.

This direction cosine matrix is given by

$$C_{BG}^{Ba} = I - M = I - \begin{bmatrix} \beta_1 & \gamma_{12} & \gamma_{13} \\ \gamma_{21} & \beta_2 & \gamma_{23} \\ \gamma_{31} & \gamma_{32} & \beta_3 \end{bmatrix} \quad (5.4-1)$$

To first order the gyro input axes can be assumed to have misalignments given by the off-diagonal elements of  $C_{BG}^{Ba}$  in equation (5.4-1). These can be viewed as the magnitudes of small rotations about the mutually orthogonal gyro spin and output axes. See Figure 5.4-1.

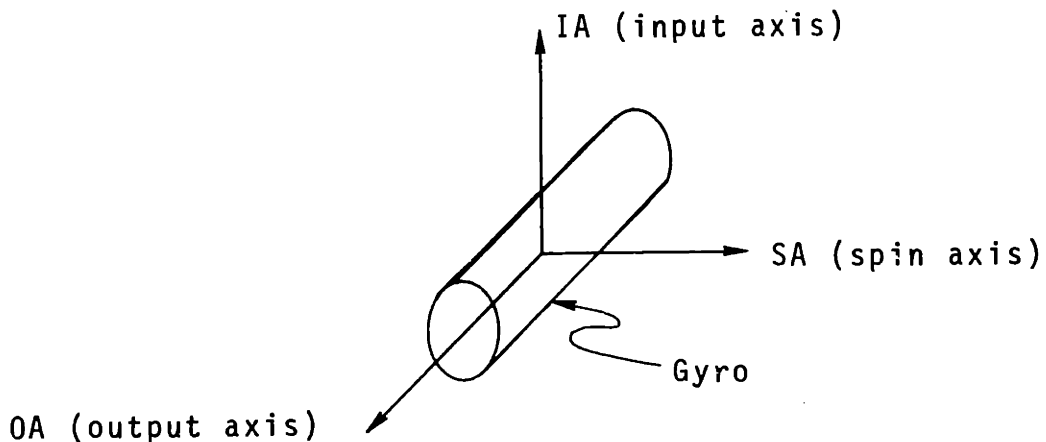


Figure 5.4-1 Gyro Orthogonal Axes

By examining the nominal orientations of the gyro axes in the LCIGS system, (Figure 5.2-1) we can identify  $\gamma_{12}$ ,  $\gamma_{21}$ ,  $\gamma_{32}$  as being associated

with small rotation magnitudes about the output axes of gyros 1, 2, 3, respectively. It then follows that the elements  $\gamma_{13}$ ,  $\gamma_{23}$ ,  $\gamma_{31}$  are associated with respective small rotation magnitudes about the spin axes of the gyros. There is no way of defining the spin axis misalignment components due to rotations about the gyro input axes using the elements of  $C_{BG}^{Ba}$  that are estimated with the dynamic estimation procedures of Section 5.6. Consequently, the transformation symbolized by  $C_{Ba}^{Bs}$  is composed of elements deduced from the dynamic estimation process and of unknown elements  $\theta_1$ ,  $\theta_2$ ,  $\theta_3$  representing small rotations of the spin axes about the gyro input axes. Specifically, for the LCIGS case

$$C_{Ba}^{Bs} \approx \begin{bmatrix} -\gamma_{12} & 1 & \theta_1 \\ 1 & -\gamma_{21} & \theta_2 \\ \theta_3 & 1 & -\gamma_{32} \end{bmatrix} \quad (5.4-2)$$

Since  $\theta_1$ ,  $\theta_2$ ,  $\theta_3$  cannot be estimated separately from the dynamic estimation process of Section 5.6, gravity sensitive errors on the order of  $\theta_i g M_{SA_i}$  will be introduced into the static drift estimation measurements  $m_{1j}$  and  $m_{2j}$  (defined in the two previous sections). These can range from  $0.05^\circ/\text{hr}$  to  $0.5^\circ/\text{hr}$  for  $M_{SA_i}$  equal to  $50^\circ/\text{hr/g}$  and  $\theta_i$  ranging in magnitude from 1 mrad to 10 mrad. Fortunately, there are several possibilities for dealing with  $\theta_i$ . First, control of  $\theta_i$  to small values during manufacture and assembly should be possible even for a low cost system because only one degree of freedom is involved for each instrument. Second, even if  $\theta_i$  is not held to small values, the 8 position static estimation procedure can be expanded to an 11 position

estimation procedure where  $\theta_1, \theta_2, \theta_3$  are subsumed under three additional output axis mass unbalance parameters ( $M_{OA_i}$ ). Because of the desire for fast calibration times in the field, this thesis has concentrated on the shorter 8 static position procedure with the knowledge that an 11 position test can be easily generated if the first option mentioned above does not turn out to be viable for large scale manufacture of LCIGS. The 8 position procedure is also much more tractable analytically and, therefore, allows a clear presentation of the estimation procedure devised in Section 5.2.

Effects of the input axis misalignment values  $\gamma_{ij}$  are known to be relatively large for LCIGS. The latest estimates are for values as high as 10 mrad.<sup>38</sup> The effects are two-fold. First, there is a significant source of error due to the earth rate term in  $\underline{\omega}_{IB_a}^{BG}$  in the expression for dynamic drift given by (4.3-27) in Chapter 4. Specifically, during the static estimation procedure, the drift given by

$$\begin{aligned}\underline{\omega}_{dyn} &= C_{B_a}^L (S + M) \underline{\omega}_{IL}^{BG} \\ &= C_{B_a}^L (S + M) (I - M)^{-1} C_L^{B_a} \underline{\omega}_{IL}^L\end{aligned}\quad (5.4-3)$$

where the scale factor errors in matrix S also contribute to the error as well as the misalignments, will contribute measurement errors on the order of  $1/2^0/\text{hr}$  for, say, a 50,000 ppm scale factor.

The following procedure as a computationally simpler alternative to the post static estimation procedure, presented in Figure 4.5-1, Chapter 4, is recommended for LCIGS in order to account for the above earth rate induced dynamic error.

The static estimation procedure is halted after only the first iteration. This will yield static drift estimates which at most will be in error by  $1 - 2^0/\text{hr}$ . These initial static drift parameter estimates will, therefore, result in dynamic parameter estimates that are accurate within 300 ppm (see Section 5.6). Dynamic estimates after this initial static estimation can then be used to compute correction terms given by

$$(100) \left( C_{Bq}^L \right)_j (S + M) (I - M)^{-1} \left( C_L^{Bq} \right)_j \begin{bmatrix} \omega_{1j} \\ \omega_{2j} \\ \omega_v \end{bmatrix} \quad (5.4-4)$$

$$\triangleq a_{1j} \omega_{1j} + a_{2j} \omega_{2j} + a_{3j} \omega_v$$

and

$$(010) \left( C_{Bq}^L \right)_j (S + M) (I - M)^{-1} \left( C_L^{Bq} \right)_j \begin{bmatrix} \omega_{1j} \\ \omega_{2j} \\ \omega_v \end{bmatrix} \quad (5.4-5)$$

$$\triangleq b_{1j} \omega_{1j} + b_{2j} \omega_{2j} + b_{3j} \omega_v$$

where

$j$  denotes the  $j^{\text{th}}$  static orientation

$\omega_v$  = known vertical component of earth rate

$a_{ij}$  and  $b_{ij}$  are known small numbers

Because  $\omega_{1j}$  and  $\omega_{2j}$  are unknown, the static measurements  $m_{1j}$  and  $m_{2j}$  used in the static iteration procedure that is resumed after obtaining the  $a_{ij}$ ,  $b_{ij}$  dynamic coefficients are compensated as follows:

$$\underbrace{m_{ij} - a_{ij} m_{ij} - a_{2j} m_{2j} - a_{3j} \omega_v}_{\text{compensation for } m_{ij}} \quad (5.4-6)$$

$$= (\underbrace{\underline{h}_{1j}^T - a_{ij} \underline{h}_{1j}^T - a_{2j} \underline{h}_{2j}^T}_{\text{modified } \underline{h}_{ij}^T}) \Psi_s + \omega_{ij} + \left\{ \begin{array}{l} \text{terms that} \\ \text{are 2nd order} \\ \text{in } a_{ij} \end{array} \right\}$$

$$\underbrace{m_{2j} - b_{ij} m_{ij} - b_{2j} m_{2j} - b_{3j} \omega_v}_{\text{compensation for } m_{2j}} \quad (5.4-7)$$

$$= (\underbrace{\underline{h}_{2j}^T - b_{ij} \underline{h}_{1j}^T - b_{2j} \underline{h}_{2j}^T}_{\text{modified } \underline{h}_{2j}^T}) \Psi_s + \omega_{2j} + \left\{ \begin{array}{l} \text{terms that} \\ \text{are 2nd} \\ \text{order in } b_{ij} \end{array} \right\}$$

The modified values of  $\underline{h}_{1j}^T$  and  $\underline{h}_{2j}^T$  indicated above are used along with the compensated static measurements in the resumed iteration. The preceding analysis of convergence (Section 5.3) still holds. Former numerical results should be little affected because of the smallness of  $a_{ij}$ ,  $b_{ij}$ . Second order errors in  $a_{ij}$ ,  $b_{ij}$  will be small. For example, a 50,000 ppm

scale factor error results in a second order earth rate induced error of  $0.025^{\circ}/\text{hr}$  when this computation procedure is used.

The second effect of input axis misalignment is the g-sensitive measurement error arising from the misalignments inherent in the expressions (4.3-5) - (4.3-6) in Chapter 4. These type errors are minimized by modification of  $\underline{h}_{1j}^T$ ,  $\underline{h}_{2j}^T$  and measurements  $\underline{m}_{1j}$  and  $\underline{m}_{2j}$  only after the first static iteration and the initial solutions for the dynamic parameters (see Section 5.7). In  $\underline{h}_{1j}^T$ , the coefficients of parameters  $\Delta_{13}$  and  $\Delta_{23}$  are modified as shown below

$$C_{11} C_{31} \longrightarrow C_{11} [C_{31} + \gamma_{12} C_{32} + \gamma_{13} C_{33}] \quad (5.4-8)$$

$$C_{12} C_{32} \longrightarrow C_{12} [C_{32} + \gamma_{21} C_{31} + \gamma_{23} C_{33}]$$

Measurement  $\underline{m}_{1j}$  must also be modified using the rough estimate of  $\hat{gM}_{IA_3}$  discussed in Appendix 5B since the orthogonality relations of equations (5.2-7) and (5.2-8) no longer apply when there are misalignments from the reference axes. This modification is as follows:

$$\underline{m}_{1j} \longrightarrow \underline{m}_{1j} - \hat{gM}_{IA_3} \left\{ \begin{array}{l} [\gamma_{12} C_{32} + \gamma_{13} C_{33}] C_{11} \\ + [\gamma_{21} C_{31} + \gamma_{23} C_{33}] C_{12} \\ + [\gamma_{31} C_{31} + \gamma_{32} C_{33}] C_{13} \end{array} \right\} \quad (5.4-9)$$

where  $\hat{gM}_{IA_3}$  is the rough estimate of  $gM_{IA_3}$ .

Similar expressions for the  $\Delta_{13}$ ,  $\Delta_{23}$  coefficients in  $\underline{h}_{2j}^T$  and for measurement  $m_{2j}$  are easily obtained from (5.4-8) and (5.4-9) by the replacement of direction cosines indicated below

$$\begin{aligned} C_{11} &\rightarrow C_{21} \\ C_{12} &\rightarrow C_{22} \\ C_{13} &\rightarrow C_{23} \end{aligned} \quad (5.4-10)$$

Similar changes to the coefficients of  $M_{SA_i}$  in both  $\underline{h}_{1j}^T$  and  $\underline{h}_{2j}^T$  are made using the elements of  $C_{Ba}^{Bs}$  given by (5.4-2), except here the  $\theta_i$  elements may be unknown and would therefore constitute error terms.

## 5.5 Measurement and Estimation Errors for Static Drifts

The two purposes of this section are to examine the measurement errors  $\nu_{1j}$ ,  $\nu_{2j}$  (equation (5.2-18)) appearing in the Kalman lumped drift estimates during static orientations and then to examine the effect of the matrix  $C_n^{-1}$  (equation (5.2-33)) in transforming errors in  $\nu_{1j}$ ,  $\nu_{2j}$  due to one source of these measurement errors, gyro random walk in rate, to effective static drift estimation errors at the solution point of the static drift iteration sequence.

A listing of the principal error sources contributing to the total measurement errors  $\nu_{1j}$ ,  $\nu_{2j}$  at each static orientation  $j$  was presented following equation (5.2-18) in Section 5.2. Three of these sources, the residual dynamic drift terms  $\omega_{dyn1j}$  and  $\omega_{dyn2j}$ , variations in  $\omega_{1j}$  and  $\omega_{2j}$ , variations in the coefficient vectors  $\underline{h}_{1j}^T$  and  $\underline{h}_{2j}^T$  (equation (5.2-18)) are all attributable to the incidental random angular base motion present during a static orientation and characterized by the angular power spectrum for an urban test laboratory presented in Figure 2.6-1, Chapter 2.

From that figure, it is deduced that the associated angular velocity

spectrum is roughly flat over frequencies of interest  $10^{-3}$  Hz to 18 Hz and then rapidly falls off as  $f^{-2}$ . The samples of angular velocity can be treated as roughly uncorrelated for sample frequencies at least as high as 20 Hz. For a 20 Hz sample frequency, Figure 2.6-1 yields a standard deviation of approximately  $8^0/\text{hr}$  for each sample of the angular velocity. The dynamic terms  $\omega_{\text{dyn}1j}$  and  $\omega_{\text{dyn}2j}$  defined by equation (4.3-27) are, therefore, on the order of

$$(\text{dynamic error coefficient magnitude}) \times 8^0/\text{hr}$$

For a typical pre-calibrated LCIGS having a dynamic error on the order of 1000 ppm, this yields a standard deviation of  $8 \times 10^{-3} {}^0/\text{hr}$ . A raw uncalibrated system with a dynamic error on the order of 50,000 ppm results in a standard deviation of  $0.4^0/\text{hr}$ . Because these standard deviations apply to measurements before any processing by the Kalman filters, the contribution of the dynamic errors to the processed measurement errors  $\sqrt{\omega_{1j}}$  and  $\sqrt{\omega_{2j}}$  will be considerably smaller.

This is suggested by the following line of reasoning first expounded in Chapter 3. In the absence of any other uncertainties such as gyro and accelerometer quantization, the optimal estimate of a constant drift having an additive white noise source of drift is given by the average value of the total when there is a complete initial uncertainty (i.e., infinite initial variance) in the knowledge of the constant drift. Therefore, for an estimation time of 60 sec, the  $1\sigma$  value of  $0.4^0/\text{hr}$  quoted above, results in the ideal case in standard deviation in the estimate of the constant lumped drift of only  $(0.4^0/\text{hr})(1/\sqrt{1200})$  or  $.01^0/\text{hr}$ . [There are 1200 sample points in the 60 sec interval, because the filter update period is 0.05 sec.] Actual error sensitivities of the Kalman filters will be manifested in the

results presented in Chapter 6.

Variations in  $\omega_{1j}$  and  $\omega_{2j}$  due to base motion angular perturbations constitutes another source error which is quite small for the angular perturbation of  $10^{-5}$  rad introduced in the Chapter 2 analysis. The errors in  $\omega_{1j}$  and  $\omega_{2j}$  will not be more than

$$(10^{-5}) \times 10^0/\text{hr} = 10^{-4} \text{ }^{\circ}/\text{hr}$$

and can be neglected.

Changes in  $\underline{h}_{1j}^T$  and  $\underline{h}_{2j}^T$  due to incidental angular base motion can be interpreted as equivalent drift error measurements  $\Delta\underline{h}_{1j}^T \underline{\chi}_s$  and  $\Delta\underline{h}_{2j}^T \underline{\chi}_s$  where  $\Delta\underline{h}_{1j}^T$  and  $\Delta\underline{h}_{2j}^T$  represent the respective perturbations in  $\underline{h}_{1j}^T$ ,  $\underline{h}_{2j}^T$  and  $\underline{\chi}_s$  is the vector of static drift error parameters. Analysis of these leveling perturbations has already been summarized in Section 5.2 in the form of perturbation matrices  $\Delta H_1$  and  $\Delta H_2$  given by (5.2-32). There the  $j^{\text{th}}$  row of  $\Delta H_1$  represents  $\Delta\underline{h}_{1j}^T$  and similarly for  $\Delta H_2$ . The worst case values of  $\Delta\underline{h}_{1j}^T \underline{\chi}_s$  and  $\Delta\underline{h}_{2j}^T \underline{\chi}_s$  will not exceed  $.002^0/\text{hr}$  for values of  $10^{-5}$  rad for angular base motion and  $50^0/\text{hr}$  for each of the static drifts. Once again it is to be emphasized that these worst case values apply before any Kalman filter processing has been done. Therefore, the contributions of these error sources to  $\dot{\underline{r}}_{1j}$  and  $\dot{\underline{r}}_{2j}$  are also very likely to be much less.

Excessive errors of this kind that are due to incidental angular base motion are always correctable using the procedures presented in Chapter 4, Section 4.5. However, one of the purposes of the above analyses was to show that under the LCIGS conditions, it is plausible that these error sources will not contribute more to the measurement errors than is compatible with the conditions listed in Table 5.3-1, Section 5.3, for con-

vergence of the iteration procedure for deviations of the principal reference axis from north of  $^{\circ}20$  and less.

Additional contributions to the measurement errors are those Kalman filter estimation errors due to gyro quantization, accelerometer quantization, and linear accelerations of the base. Simulation data presented in Chapter 6 will indicate that the gyro and accelerometer quantization-caused errors will not contribute significantly to the Kalman filter estimation errors. However, for the Kalman filter gains and estimation periods chosen, the linear acceleration errors are seen to be significant.

The remaining error source to be examined, gyro random walk in rate, cannot be reduced by any additional practical procedures. The following simplified approach toward analyzing its effect is used:

The bias drift plus random walk in rate in each gyro is viewed as a time varying parameter. Hence, any particular instant of time during the system calibration can be selected as that time at which bias and random walk together are defined as the calibrated bias with zero random walk. At any times prior to or after this baseline point, the "zero error" calibrated bias is assumed to be contaminated by the appropriate random walk increments. Furthermore, in order to simplify the numerical analysis based on this approach, the effect of the Kalman filter processing on each independent random walk increment is neglected.

This definition of a gyro baseline bias clearly brings out the requirement for proper sequencing of the nominal orientations so that the orientations that make the spin axis and  $\Delta$  mass unbalance terms observable for a particular gyro are as close as possible in time to the orientation in which the bias at the zero random-walk baseline is nominally observed. To this end the following sequence of the nominal orientations  $j = 1, \dots, 8$

used in forming the rows of the nominal matrices given by (5.2-31), Section 5.2, is recommended (Table 5.5-1)

j	Description
1	nominal measure of x gyro bias
4	x gyro spin axis mass unbalance made observable
7	$\Delta_{13}$ mass unbalance term made observable
3	nominal measurement of z gyro bias
6	z gyro spin axis mass unbalance made observable
8	$\Delta_{23}$ mass unbalance term made observable
2	nominal measurement of y gyro bias
5	y gyro spin axis mass unbalance made observable

Table 5.5-1 Recommended Sequence of Nominal Orientations

The nominal measurement errors due only to the random walk terms, as postulated in this manner, are listed below by equations (5.5-1).

The random walk increments are indicated by  $\Delta b_k(n)$  where the subscript k denotes the gyro and the argument n denotes the time (in increments of time for each orientation measurement) from the nominally designated zero baseline.

$$\begin{aligned}
 \nu_{11} &= \Delta b_x(0), \quad \nu_{21} = \Delta b_y(-6) \\
 \nu_{12} &= \Delta b_y(0), \quad \nu_{22} = \Delta b_x(+6) \\
 \nu_{13} &= \Delta b_z(0), \quad \nu_{23} = \Delta b_y(-3) \\
 \nu_{14} &= \Delta b_x(1), \quad \nu_{24} = \Delta b_z(-2) \\
 \nu_{15} &= \Delta b_y(1), \quad \nu_{25} = \Delta b_z(4) \\
 \nu_{16} &= \Delta b_z(1), \quad \nu_{26} = \Delta b_x(4) \\
 \nu_{17} &= .71(\Delta b_x(2) + \Delta b_z(-1)), \quad \nu_{27} = \Delta b_y(-4) \\
 \nu_{18} &= .71(\Delta b_y(-1) - \Delta b_z(2)), \quad \nu_{28} = \Delta b_x(5)
 \end{aligned} \tag{5.5-1}$$

From (5.5-1) it is seen that the maximum nominal measurement errors are  $\nu_{21}, \nu_{22}$  which have the standard deviation of 6 random walk increments. For an expected LCIGS gyro random walk in rate<sup>39</sup> having a standard deviation of  $0.2^0/\text{hr}/\sqrt{\text{hr}}$  and consecutive 1 minute intervals for each orientation, these measurement errors have respective standard deviations  $\sigma_{\nu_{21}}, \sigma_{\nu_{22}}$  given by

$$\sigma_{\nu_{21}} = \sigma_{\nu_{22}} = \sqrt{\frac{6}{60}} \times 0.2 = 0.063^0/\text{hr} \tag{5.5-2}$$

However, examination of equations (5.3-45) - (5.3-50) shows that the effect of a measurement error along reference axis 2 on the iteration convergence has at most 1/4 of the effect as the worst case upper bound  $|\underline{v}|_\infty$

defined by equation (5.3-48) and listed in Table 5.3-1 for values which result in convergence of the iteration. Thus, if the value given by (5.5-2) is divided by 4 to yield  $0.016^0/\text{hr}$  and compared with the values in Table 5.3-1, it is seen that the gyro random walk in rate as manifested by a measurement error along reference axis 2 has a negligible effect on the iteration convergence. The maximum error along primary reference axis 1 is given by  $\gamma_{17}$  and  $\gamma_{18}$  in (5.5-1). Their respective standard deviations  $\sigma_{\gamma_{17}}$ ,  $\sigma_{\gamma_{18}}$  are

$$\sigma_{\gamma_{17}} = \sigma_{\gamma_{18}} = 0.71 \frac{\sqrt{5}}{\sqrt{60}} \times 0.2 = 0.041^0/\text{hr} \quad (5.5-3)$$

for the same conditions assumed in calculating the standard deviations in (5.5- ). Again the standard deviation characterizing the random walk in rate contribution to measurement error is small compared with the upper bound values in Table 5.3-1.

Although convergence of the iterative sequence will not be adversely effected by the random walk in rate, it is important to examine the effect of this gyro error source on the errors in the gyro drift estimate at the iteration solution point.

By assuming that the equality constraints (5.3-15) hold at the solution point, it is seen from the iteration equations (5.3-1) - (5.3-7) and the measurement equations (5.2-18) that the errors  $\tilde{x}_s$  in the static drifts  $x_s$  are given by

$$\tilde{x}_s = C_N^{-1} [ u_{1j} (\omega_{1j} + \gamma_{1j}) + u_{2j} (\omega_{2j} + \gamma_{2j}) ] \quad (5.5-4)$$

where  $u_{1j}$ ,  $u_{2j}$  are the estimated horizontal earth rate components at the solution point,  $\omega_{1j}$ ,  $\omega_{2j}$  are the true horizontal components,  $\gamma_{1j}$  and  $\gamma_{2j}$  are the measurement errors and  $N$  denotes the iteration at the solution point.  $C_n$  is defined by (5.3-1).

Let  $A_{uj}$ ,  $A_{wj}$  designate the deviations from north corresponding to the pairs  $U_{1j}$ ,  $U_{2j}$  and  $\omega_{1j}$ ,  $\omega_{2j}$  respectively so that (with angular rates normalized with respect to the magnitude of the horizontal component of earth rate as was done following equation (5.2-16))

$$u_{ij} = \cos A_{uj}, u_{2j} = \sin A_{uj} \quad (5.5-5)$$

$$\omega_{ij} = \cos A_{\omega j}, \omega_{2j} = \sin A_{\omega j}$$

Then, it is easily shown that

$$u_{ij}\omega_{ij} + u_{2j}\omega_{2j} = \cos(A_{uj} - A_{\omega j}) \quad (5.5-6)$$

The contribution to the error in  $\chi_s$  due to the wrong estimates for  $\omega_{1j}$ ,  $\omega_{2j}$  is therefore

$$\tilde{\chi}_s = C_N [\cos(A_{uj} - A_{\omega j}) - 1] \left\{ \begin{array}{l} \text{ignoring} \\ \gamma_{1j}, \gamma_{2j} \end{array} \right\} \quad (5.5-7)$$

Under the conditions for the iteration convergence set up in Section 5.3, this can be very large since  $A_{uj}$  can be as large as  $25^0$  and, of course,  $A_{wj}$  can be zero. In this particular case

$$\cos(A_{uj} - A_{\omega j}) - 1 = \cos 25^c - 1 = -0.937 \quad (5.5-8)$$

for an equivalent drift of  $.937^0/\text{hr}$ . This is not an unexpected result because, for this example, the drift errors are large enough to cause an error in the direction of the principal reference axis of  $25^0$ . However, it has been shown above that in the case under discussion, random walk in rate drift, the measurement errors are small enough for the portion of the error given by (5.5-7) to be neglected. To see this for the above case of  $A_{wj} = 0$ , note that with the measurement error standard deviations given by (5.5-2) and (5.5-3), the worst case standard deviation  $\overline{\sigma}_{\omega_{2j}}$ , of the  $n = 1$  iterate (see equation (5.3-46)) is

$$\overline{\sigma}_{\omega_{2j}} = 0.112^0/\text{hr} \quad (5.5-9)$$

Using a  $\overline{\sigma}_\omega$  value of  $0.336^0/\text{hr}$ , normalized by a horizontal earth rate magnitude of  $10^0/\text{hr}$  yields a maximum value for  $A_{uj}$  given by

$$A_{uj} = \arctan(0.0336) = 1.92^0 \quad (5.5-10)$$

Thus

$$\cos(A_{uj} - A_{wj}) - 1 = \cos 1.92^0 - 1 \\ = -0.00056 \quad (5.5-11)$$

for an equivalent drift of  $0.0056^0/\text{hr}$ , at 3 standard deviations of the measurement error. Therefore, the subsequent analysis will be for the contribution to the error in  $\underline{x}_s$  given by

$$\underline{x}_s = C_N^{-1} [u_{1j} \vec{v}_{1j} + u_{2j} \vec{v}_{2j}] \quad (5.5-12)$$

In considering only the worst case with respect to numerical conditioning, it is assumed that the arguments made at the end of Section 5.2 are valid so that (5.5-12) can be reduced to

$$\tilde{\underline{x}}_s = H_i^{-1} B'(\alpha) \left\{ \underline{\gamma}_i + [\alpha] \underline{\gamma}_2 \right\} \quad (5.5-13)$$

where  $B'(\alpha)$  is defined, using  $B(\alpha)$  in Appendix 5A, by equation (5A-19) and  $B(\alpha)$  is given by equation (5A-5). The matrix  $H_i^{-1}$  is assumed to include the effect of leveling perturbations and its unperturbed form is given by (5A-2). Also  $\underline{v}_1$  is the vector of measurement errors  $v_{1j}$  for level reference 1,  $\underline{v}_2$  is the vector of measurement errors  $v_{2j}$  for level reference axis 2, and  $[\alpha]$  is the diagonal matrix with all elements equal (defined by equation (5.2-36) with all  $\alpha_j$  equal).

The covariance of  $\tilde{\underline{x}}_s$  for zero average values of  $\underline{v}_1$  and  $\underline{v}_2$  is given by

$$\tilde{\underline{\Sigma}}_s = E \left[ \tilde{\underline{x}}_s \tilde{\underline{x}}_s^T \right] = H_i^{-1} B'(\alpha) E \left[ \underline{\gamma}_i \underline{\gamma}_i^T \right] (B'(\alpha))^T (H_i^{-1})^T \quad (5.5-14)$$

with

$$\underline{\gamma}_i \stackrel{\Delta}{=} \underline{\gamma}_i + [\alpha] \underline{\gamma}_2 \quad (5.5-15)$$

Upper bounds on the elements of  $\tilde{\underline{\Sigma}}_s$  are obtained as follows:

The notation following equation (2.4-11) in Chapter 2 is employed whereby

$\text{abs } K \stackrel{\Delta}{=} \text{matrix whose elements are the absolute values of the corresponding elements of } K$

Bounds on the covariance elements are obtained for zero leveling perturbation ( $\Delta\theta = 0^0$ ) from

$$\tilde{\underline{\Sigma}}_s \leq \text{abs}(H_i^{-1} B(\alpha)) K \text{abs}(H_i^{-1} B(\alpha))^T \quad (5.5-16)$$

where the inequality refers to each element of the matrices.  $H_1^{-1}B(\alpha)$  is given in Appendix 5A by equation (5A-25). K is defined by

$$K \triangleq ab \leq E[\underline{v}_T \underline{v}_T^T] \quad (5.5-17)$$

The worst case value of  $\alpha$  at the solution point is taken as  $\alpha = \tan 25^0$ . Corresponding matrices  $abs(H_1^{-1}B(\alpha))$  and K are given by equations (5A-26) and (5A-27) respectively in Appendix 5A. Here the random walk in rate standard deviation<sup>39</sup> is taken as  $0.2^0/\text{hr}/\sqrt{\text{hr}}$ , with assumed 1 minute increments.

For non-zero leveling pertrubations, formulas (5A-20) - (5A-23) are employed, along with the computed results in Tables 5A-2 and 5A-3 of Appendix A to yield

$$abs(H_1^{-1}B'(\alpha)) \leq \frac{abs(H_1^{-1}B(\alpha))}{(1 - |AH_1H_1^{-1}|_\infty)(1 - |L^{-1}|_\infty|M|_\infty)} \quad (5.5-18)$$

with  $H_1$  on the left hand side of (5.5-18) taken to be perturbed.

Perturbations in the elements of K are slight and are therefore ignored.

The final results in the form of standard deviations in  $^0/\text{hr}$  for each of the static drifts are listed below in Table 5.5-2.

It is concluded from the table that except for the input axis mass unbalance terms, the static drift estimates for LCIGS have irreducible standard deviations less than  $0.1^0/\text{hr}$ .

Bounds on $1\sigma$ of Estimates of:		$\Delta\theta = 0$	$\Delta\theta = 1/4^0$	$\Delta\theta = 1/2^0$
Bias	$B_1$	.027	.033	.042
	$B_2$	.027	.033	.042
	$B_3$	.033	.041	.052
Spin Axis Mass Unbalance	$gM_{SA_1}$	.046	.057	.072
	$gM_{SA_2}$	.036	.044	.056
	$gM_{SA_3}$	.056	.069	.088
Input Axis Mass Unbalance	$g\Delta_{13}$	.120	.148	.188
	$g\Delta_{23}$	.140	.173	.219

Table 5.5-2 Upper Bounds on Standard Deviations of Estimates of Static Drifts Due Only to a Gyro Random Walk in Rate of  $0.2^0/\text{hr}\sqrt{\text{hr}}$  for 1 Minute Measurement Intervals and  $\alpha = \tan 25^0$ . Results in deg/hr

### 5.6 Solution for Dynamic Error Parameters

The dynamic error parameters contributing to the dynamic drift vector  $\underline{\omega}_{dyn}$  defined by equations (4.3-28), Chapter 4 are the misalignment angles and the gyro scale factor errors presented respectively in equations (4.3-1) and (4.3-8). The definition of dynamic drift is repeated below

$$\underline{\omega}_{dyn} = \begin{bmatrix} B \\ B_{eq} \end{bmatrix} (S + M) \underline{\omega}_{EBG}^{BG} \quad (5.6-1)$$

with

$$M = \begin{bmatrix} B_1 & \gamma_{12} & \gamma_{13} \\ \gamma_{21} & B_2 & \gamma_{23} \\ \gamma_{31} & \gamma_{32} & B_3 \end{bmatrix} \quad (5.6-2)$$

$\gamma_{ij}$  = off diagonal elements  
in radians

$$B_i = 1 - \sqrt{1 - \sum_{j \neq i} \gamma_{ji}^2}$$

$$S = \begin{bmatrix} SF_1 & 0 & 0 \\ 0 & SF_2 & 0 \\ 0 & 0 & SF_3 \end{bmatrix} \quad (5.6-3)$$

$SF_i$  = scale factor error  
of the  $i^{th}$  gyro

For the purpose of obtaining dynamic error parameter estimates, an equivalent scale-factor error matrix,  $S_{eq}$ , is defined as

$$S_{eq} \stackrel{A}{=} S + \begin{bmatrix} \beta_1 & 0 & 0 \\ 0 & \beta_2 & 0 \\ 0 & 0 & \beta_3 \end{bmatrix} \quad (5.6-4)$$

where

$$(SF_i)_{eq} \stackrel{\Delta}{=} SF_i + \beta_i \quad (5.6-5)$$

and an equivalent misalignment matrix,  $M_{eq}$ , is defined as

$$M_{eq} \stackrel{\Delta}{=} \begin{bmatrix} 0 & \gamma_{12} & \gamma_{13} \\ \gamma_{21} & 0 & \gamma_{23} \\ \gamma_{31} & \gamma_{32} & 0 \end{bmatrix} \quad (5.6-6)$$

A vector of dynamic error coefficients is defined by

$$\underline{\chi}_A \stackrel{\Delta}{=} (SF_{1_{eq}}, \gamma_{21}, \gamma_{31}, SF_{2_{eq}}, \gamma_{12}, \gamma_{32}, SF_{3_{eq}}, \gamma_{13}, \gamma_{23})^T \quad (5.6-7)$$

Substituting equations (5.6-4) and (5.6-6) into (5.6-1) and carrying out the indicated matrix multiplications shows that

$$\begin{aligned} \underline{\omega}_{dyn_{1j}} &= \underline{\Phi}_{A_{1j}}^T \underline{\chi}_A \\ \underline{\omega}_{dyn_{2j}} &= \underline{\Phi}_{A_{2j}}^T \underline{\chi}_A \end{aligned} \quad (5.6-8)$$

with the above two row vectors defined by

$$\begin{aligned} \underline{\Phi}_{A_{1j}}^T &\stackrel{\Delta}{=} (C_{11}\omega_1, C_{12}\omega_1, C_{13}\omega_1, C_{12}\omega_2, C_{11}\omega_2, C_{13}\omega_2, \\ &\quad C_{13}\omega_3, C_{11}\omega_3, C_{12}\omega_3) \end{aligned} \quad (5.6-9)$$

$$\begin{aligned} \underline{\Phi}_{A_{2j}}^T &\stackrel{\Delta}{=} (C_{21}\omega_1, C_{22}\omega_1, C_{23}\omega_1, C_{22}\omega_2, C_{21}\omega_2, C_{23}\omega_2, \\ &\quad C_{23}\omega_3, C_{21}\omega_3, C_{22}\omega_3) \end{aligned}$$

where  $C_{ij}$  are the elements of  $C_{IBa}^L$  as indicated by equation (5.2-3) and  $\omega_i$  is the  $i^{th}$  component of  $\underline{\omega}_{IBa}^{BG}$ .

The static drift equations (5.2-15) are repeated below for reference.

$$\omega_{stat1j} = \underline{h}_{1j}^T \underline{\chi}_s + \omega_{1j} \quad (5.6-10)$$

$$\omega_{stat2j} = \underline{h}_{2j}^T \underline{\chi}_s + \omega_{2j} \quad (5.6-11)$$

where  $j$  now denotes the  $j^{th}$  rotation of the system. The vector of static drifts  $\underline{\chi}_s$  is defined as in equation (5.2-1).  $\underline{h}_{1j}^T$ ,  $\underline{h}_{2j}^T$  are defined by (5.2-13) and (5.2-14) respectively, and  $\omega_{1j}$  and  $\omega_{2j}$  are the horizontal components of earth rate along the two horizontal reference axes in the  $j^{th}$  static orientation.

The true angular velocity,  $\underline{\omega}_{IBa}^{BG}$  is unavailable because of the presence of static and dynamic drifts. The angular rate,  $\underline{\omega}_G^{BG}$ , as measured by the gyros is given by

$$\underline{\omega}_G^{BG} = (I + S) \underline{\omega}_{IBa}^{BG} + \underline{\omega}_D^{BG} \quad (5.6-12)$$

which is a repetition of equation (4.5-13) in Chapter 4. Here  $\underline{\omega}_D^{BG}$  is the vector of static drifts. It is desired to use the available components of  $\underline{\omega}_G^{BG}$  rather than the components of  $\underline{\omega}_{IBa}^{BG}$  in computing the coefficient vectors given by (5.6-9).

Solution of  $\underline{\omega}_{IBa}^{BG}$  in terms of  $\underline{\omega}_G^{BG}$  and  $\underline{\omega}_D^{BG}$  yields

$$\underline{\omega}_{IBa}^{BG} \approx (I + S)^{-1} (\underline{\omega}_G^{BG} - \underline{\omega}_D^{BG}) \quad (5.6-13)$$

Substitution of (5.6-13), (5.6-4) and (5.6-6) into the expression for dynamic drift given by (5.6-1) results in

$$\underline{\omega}_{dyn} = C_{Ba}^L (S_{eq} + M_{eq}) (I + S^-)^{-1} (\underline{\omega}_G^{BG} - \underline{\omega}_D^{BG}) \quad (5.6-14)$$

The matrix expression that is pre-multiplied by  $C_{Ba}^L$  in (5.6-14) can always be written as a sum of a diagonal matrix and a matrix with zero diagonal elements, denoted here respectively by  $\hat{S}$  and  $\hat{M}_{eq}$ , so that

$$(\hat{S}_{eq} + \hat{M}_{eq}) \triangleq (S_{eq} + M_{eq})(I + S^-)^{-1} \quad (5.6-15)$$

and

$$\underline{\omega}_{dyn} \approx C_{Ba}^L (\hat{S}_{eq} + \hat{M}_{eq}) (\underline{\omega}_G^{BG} - \underline{\omega}_D^{BG}) \quad (5.6-16)$$

When, as shown further on, (5.6-16) is used in the solution for  $\hat{S}_{eq}$  and  $\hat{M}_{eq}$ , it is necessary to solve equation (5.6-15) to obtain the true scale factor and misalignment matrices in terms of  $\hat{S}$  and  $\hat{M}_{eq}$ .

Post multiplying both sides of equation (5.6-15) by  $(I + S^-)$  yields

$$S_{eq} + M_{eq} = \hat{S}_{eq} + \hat{S}_{eq} S + \hat{M}_{eq} + \hat{M}_{eq} S \quad (5.6-17)$$

If we at first make the approximation

$$S \approx S_{eq}$$

then

$$S_{eq} + M_{eq} \approx \hat{S}_{eq} + \hat{S}_{eq} S_{eq} + \hat{M}_{eq} + \hat{M}_{eq} S_{eq} \quad (5.6-18)$$

Consequently, the initial approximate solution for  $S_{eq}$  is decoupled from the solution for  $M_{eq}$  and is given by

$$S_{eq}(1) = (\mathbf{I} - \hat{\mathbf{S}}_{eq})^{-1} \hat{\mathbf{S}}_{eq} \quad (5.6-19)$$

where the "1" in parenthesis indicates the first stage in the solution process.

Thus, the solution for  $M_{eq}(1)$  is given by

$$M_{eq}(1) = \hat{M}_{eq}(\mathbf{I} + S_{eq}(1)) \quad (5.6-20)$$

$M$  and  $S$  defined by (5.6-2) and (5.6-3) can be recovered from  $S_{eq}(1)$  and  $M_{eq}(1)$  by means of the equations repeated below

$$\beta_i = 1 - \sqrt{1 - \sum_{j \neq i} \gamma_{ji}^2} \quad (5.6-21)$$

where  $\gamma_{ij}$  is the appropriate element of  $M_{eq}$

$$SF_i = (SF_i)_{eq} - \beta_i \quad (5.6-22)$$

Consideration of the magnitude of  $\beta_i$  for misalignments as large as  $1^0$  shows that the approximation

$$S \approx S_{eq}$$

will yield accurate enough results for  $S_{eq}(1)$  and  $M_{eq}(1)$  so that only this first solution stage need be used for the final extraction of  $M$  and  $S$ .

From the preceding development it is seen that the dynamic coefficient vectors defined by equations (5.6-9) need only be redefined by using the components of  $(\underline{w}_G^{BG} - \underline{w}_D^{BG})$  instead of the components of  $\underline{w}_{IBa}^{BG}$  with the understanding that the dynamic parameter vector  $\underline{x}_A$  originally defined by equation (5.6-7) is redefined to consist of the elements of  $S_{eq}$  and  $M_{eq}$ . That is,

$\underline{x}_A$  is replaced by  $\hat{\underline{x}}_A$  where

$$\hat{\underline{x}}_A \triangleq (\hat{SF}_1, \hat{\delta}_{21}, \hat{\delta}_{31}, \hat{SF}_2, \hat{\delta}_{12}, \hat{\delta}_{32}, \hat{SF}_3, \hat{\delta}_{13}, \hat{\delta}_{23})^T \quad (5.6-23)$$

and

$$\hat{S}_{eq} = \begin{bmatrix} \hat{SF}_1 & 0 & 0 \\ 0 & \hat{SF}_2 & 0 \\ 0 & 0 & \hat{SF}_3 \end{bmatrix} \quad M_{eq} = \begin{bmatrix} 0 & \hat{\delta}_{12} & \hat{\delta}_{13} \\ \hat{\delta}_{21} & 0 & \hat{\delta}_{23} \\ \hat{\delta}_{31} & \hat{\delta}_{32} & 0 \end{bmatrix} \quad (5.6-24)$$

From the development of the error equations (4.3-30) and subsequent description of the equation terms in Chapter 4, it is seen that the two state Kalman filter estimate for the change in angle about horizontal reference axis 1 during the  $j^{th}$  rotation from time  $t_{j-1}$  to  $t_j$  is given by

$$\begin{aligned} \Delta \varphi_{1j} &= \varphi_1(t_j) - \varphi_1(t_{j-1}) \\ &= \int_{t_{j-1}}^{t_j} (I, \underline{h}_{1j}^T, \underline{h}_{A1j}^T) \begin{bmatrix} \omega_{1j} \\ \underline{x}_s \\ \underline{x}_A \end{bmatrix} dt + n_{1j} \end{aligned} \quad (5.6-25)$$

where  $n_{1j}$  represents all of the associated errors in estimating the change in angle. These include errors in estimating the static drift vector and  $w_{1j}$  using the procedure described in Section 5.2 - 5.4, Kalman filter estimation errors not due to the unmodeled deterministic drifts (e.g., errors due to gyro and accelerometer quantization and the linear acceleration noise) and the errors already analyzed above.

Entirely analogous considerations for horizontal reference axis 2 leads to

$$\Delta \varphi_{2j} = \int_{t_{j-1}}^{t_j} (I, \underline{h}_{2j}^T, \underline{h}_{A2j}^T) \begin{bmatrix} \omega_{2j} \\ \underline{x}_s \\ \underline{x}_A \end{bmatrix} dt + n_{2j} \quad (5.6-26)$$

Selection of a set of 9 simultaneous equations from (5.6-5) and (5.6-26) for  $j = 1, \dots, 6$  yields a deterministic solution for  $\underline{x}_A$  assuming  $w_{1j}$  and  $w_{2j}$  remain constant during a rotation. (If not, the error is

assumed to be absorbed by the  $n_{1j}$ ,  $n_{2j}$  error terms.)

Equations (5.6-25) and (5.6-26) are rewritten as

$$\left( \int_{t_{j-1}}^{t_j} h_{A_1j}^T dt \right) \hat{x}_A = \Delta \varphi_{1j} - \int_{t_{j-1}}^{t_j} (I, h_{1j}^T) dt \begin{bmatrix} \omega_{1j} \\ \underline{x}_s \end{bmatrix} - n_{1j} \quad (5.6-27)$$

$$\left( \int_{t_{j-1}}^{t_j} h_{A_2j}^T dt \right) \hat{x}_A = \Delta \varphi_{2j} - \int_{t_{j-1}}^{t_j} (I, h_{2j}^T) dt \begin{bmatrix} \omega_{2j} \\ \underline{x}_s \end{bmatrix} - n_{2j} \quad (5.6-28)$$

in order to explicitly demonstrate the form of the equations to be solved.

Six nominal rotations are chosen below based on the principle of obtaining numerically well conditioned equations that was expounded in Chapter 2, Section 2.4 and in Section 5.2 of this chapter. Resulting coefficients of the elements of  $\hat{x}_A$  are computed from the integrals on the left hand sides of equations (5.6-27) and (5.6-28) for 9 simultaneous equations that are selected from the 12 available equations that can be formulated using (5.6-27) and (5.6-28).

Definition of the rotations is done by listing the associated direction cosine matrix  $C_{Ba}^L$ . Here the components  $w_i'$  are those of  $\underline{\omega}_{LBa}$

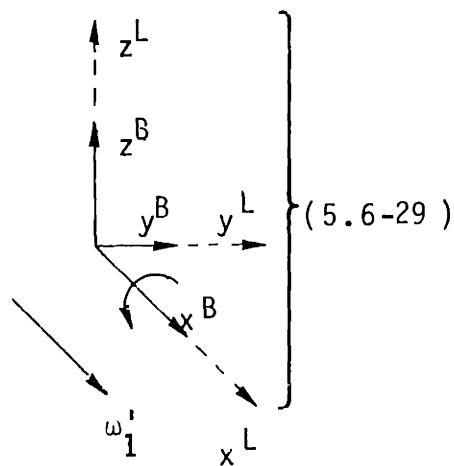
#### Rotations 1 and 2

$$(C_{Ba}^L)_{1,2} = \begin{bmatrix} 1 & 0 & 0 \\ 0 \cos \theta_i & -\sin \theta_i & 0 \\ 0 \sin \theta_i & \cos \theta_i & 0 \end{bmatrix}$$

$$\omega_2' = \omega_3' = 0$$

$$\theta_1 = \int_0^t \omega_1' dt, \quad \theta_1(t_1) = \pi/2.$$

$$\theta_2 = \int_{t_1}^t \omega_1' dt + \theta_1(t_1), \quad \theta_2(t_2) = \pi$$



Rotations 3 and 4

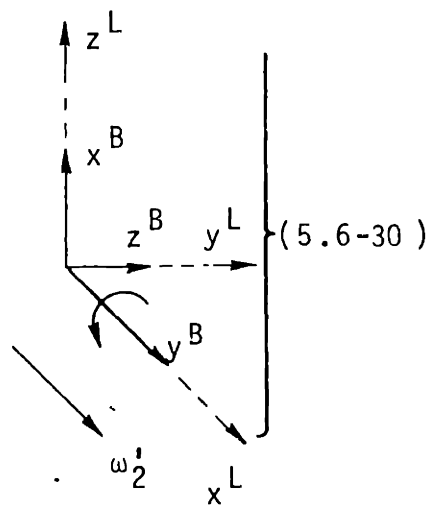
$$(C_{B_0}^L)_{3,4} = \begin{bmatrix} 0 & 1 & 0 \\ -\sin \theta_i & 0 & \cos \theta_i \\ \cos \theta_i & 0 & \sin \theta_i \end{bmatrix}$$

$i = 3, 4$

$$\omega_1' = \omega_3' = 0$$

$$\theta_3 = \int_0^t \omega_2' dt, \quad \theta_3(t_4) = \pi/2$$

$$\theta_4 = \int_{t_4}^t \omega_2' dt + \theta_3(t_4), \quad \theta_4(t_5) = \pi$$



Rotations 5 and 6

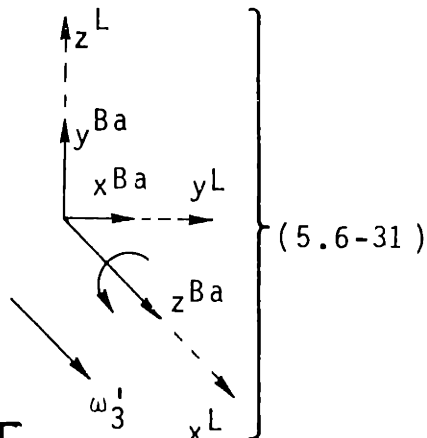
$$(C_{B_a}^L)_{5,6} = \begin{bmatrix} 0 & 0 & 1 \\ 0 & \cos\theta_i - \sin\theta_i & 0 \\ \sin\theta_i & \cos\theta_i & 0 \end{bmatrix}$$

$i=5,6$

$$\omega_1' = \omega_2' = 0$$

$$\theta_5 = \int_0^t \omega_3' dt, \theta_5(t_b) = \pi/2$$

$$\theta_6 = \int_{t_b}^t \omega_3' dt + \theta_5(t_b), \theta_6(t_c) = \pi$$



Substituting the appropriate elements of  $(C_{B_a}^L)_i$  from equations (5.6-29) - (5.6-31) into (5.6-9) and using the approximation

$$\omega_i \approx (\underline{\omega}_{LB_a}^{B_a})_i \quad (5.6-32)$$

where  $\omega_i$  is a component of  $(\underline{\omega}_G^{BG} - \underline{\omega}_D^{BG})$  results in  $\sum_{t_k}^{t_{k+1}} h_i^T A_{ij} dt$   
having only one element of the form

$$\sum_{t_k}^{t_{k+1}} \omega_i dt \approx \int_{t_k}^{t_{k+1}} \omega_i' dt = \theta(t_{k+1}) - \theta(t_k) = \pi/2 \quad (5.6-33)$$

Also  $\int_{t_k}^{t_{k+1}} \underline{b}_j^T A_2 j dt$  has only two elements of the forms

$$\begin{aligned} & \int_{t_k}^{t_{k+1}} \cos \left( \int_{t_k}^t \omega_i' dt + \theta(t_k) \right) \omega_i' dt \\ & \approx \int_{t_k}^{t_{k+1}} \cos \left( \int_{t_k}^t \omega_i' dt + \theta(t_k) \right) \omega_i' dt \end{aligned} \quad (5.6-34)$$

and

$$\begin{aligned} & \int_{t_k}^{t_{k+1}} \sin \left( \int_{t_k}^t \omega_i' dt + \theta(t_k) \right) \omega_i' dt \\ & \approx \int_{t_k}^{t_{k+1}} \sin \left( \int_{t_k}^t \omega_i' dt + \theta(t_k) \right) \omega_i' dt \end{aligned} \quad (5.6-35)$$

Integrating the right hand sides of (5.6-34) and (5.6-35) yields,  
respectively

$$\sin(\theta(t_{k+1})) - \sin(\theta(t_k)) \quad (5.6-36)$$

and

$$\cos(\theta(t_k)) - \cos(\theta(t_{k+1})) \quad (5.6-37)$$

For the odd numbered rotations in (5.6-29) - (5.6-31) these elements are 1 and 1 respectively. For the even numbered rotations they are -1 and 1 respectively.

Below is a listing of the nominal values for  $\left( \int_{t_k}^{t_{k+1}} h^T A_{1j} dt \right)$  and  $\left( \int_{t_k}^{t_{k+1}} h^T A_{2j} dt \right)$  using these nominal elements

Rotation j	$\int_{t_k}^{t_{k+1}} h^T A_{1j} dt$	$\int_{t_k}^{t_{k+1}} h^T A_{2j} dt$
1	$(\pi/2, \underline{0}_{1 \times 8}^T)$	$(0, 1, -1, \underline{0}_{1 \times 6}^T)$
2	$(\pi/2, \underline{0}_{1 \times 8}^T)$	$(0, 1, 1, \underline{0}_{1 \times 6}^T)$
3	$(\underline{0}_{1 \times 3}^T, \pi/2, \underline{0}_{1 \times 5}^T)$	$(\underline{0}_{1 \times 4}^T, -1, 1, \underline{0}_{1 \times 3}^T)$
4	$(\underline{0}_{1 \times 3}^T, \pi/2, \underline{0}_{1 \times 5}^T)$	$(\underline{0}_{1 \times 4}^T, 1, 1, \underline{0}_{1 \times 3}^T)$
5	$(\underline{0}_{1 \times 6}^T, \pi/2, \underline{0}_{1 \times 2}^T)$	$(\underline{0}_{1 \times 7}^T, 1, -1)$
6	$(\underline{0}_{1 \times 6}^T, \pi/2, \underline{0}_{1 \times 2}^T)$	$(\underline{0}_{1 \times 7}^T, 1, 1)$

Table 5.6-1 Nominal Coefficients Dynamic Parameter Estimation Equations

Nine row vectors are selected from Table 5.6-1 to form the following nominal matrix which is the matrix coefficient of the unknown dynamic parameter vector re-defined by equation (5.6-39)

$$C_A \stackrel{\Delta}{=} \left\{ \begin{array}{l} \text{Nominal} \\ \text{Coefficient} \\ \text{Matrix of} \\ \text{Unknown} \\ \text{Vector } \underline{\chi}_A \end{array} \right\} = \begin{bmatrix} \pi/2 & 0 & 0 & 1 & 1 & 1 \\ 0 & \pi/2 & 0 & 0_{3 \times 2} & 0_{3 \times 2} & 0_{3 \times 2} \\ 0 & 0 & \pi/2 & -1 & 1 & -1 \\ 0_{2 \times 3} & -1 & 1 & 0_{2 \times 2} & 0_{2 \times 2} & 0_{2 \times 2} \\ -1 & 1 & 1 & 0_{2 \times 2} & 0_{2 \times 2} & 0_{2 \times 2} \\ 0_{2 \times 3} & 0_{2 \times 2} & -1 & 1 & 1 & 0_{2 \times 2} \\ -1 & 0_{2 \times 2} & 1 & 1 & 1 & 0_{2 \times 2} \\ 0_{2 \times 3} & 0_{2 \times 2} & 0_{2 \times 2} & 1 & -1 & 1 \end{bmatrix} \quad (5.6-38)$$

This nominal matrix is numerically very well conditioned. All of its rows are mutually orthogonal.

$$\underline{\chi}_A \stackrel{\Delta}{=} \begin{bmatrix} \hat{sF}_1 \\ \hat{sF}_2 \\ \hat{sF}_3 \\ \hat{\delta}_{21} \\ \hat{\delta}_{31} \\ \hat{\delta}_{12} \\ \hat{\delta}_{32} \\ \hat{\delta}_{13} \\ \hat{\delta}_{23} \end{bmatrix} \quad \left. \begin{array}{l} \text{Redefinition} \\ \text{of } \underline{\chi}_A \end{array} \right\} \quad (5.6-39)$$

The inverse of  $C_A$  (equation (5.6-40)) is as follows:

$$C_A^{-1} = \begin{bmatrix} 2/\pi & 0 & 0 \\ 0 & 2/\pi & 0 \\ 0 & 0 & 2/\pi \\ \hline 0_{2 \times 3} & \frac{1}{2} & \frac{1}{2} \\ -\frac{1}{2} & \frac{1}{2} & 0_{2 \times 2} \\ \hline 0_{2 \times 3} & 0_{2 \times 2} & -\frac{1}{2} & \frac{1}{2} \\ -\frac{1}{2} & \frac{1}{2} & 0_{2 \times 2} & 0_{2 \times 2} \\ \hline 0_{2 \times 3} & 0_{2 \times 2} & 0_{2 \times 2} & \frac{1}{2} & \frac{1}{2} \\ -\frac{1}{2} & \frac{1}{2} & -\frac{1}{2} & \frac{1}{2} & 0_{2 \times 2} \end{bmatrix} \quad (5.6-40)$$

Worst case perturbations of the elements of  $C_A$  are examined in Appendix 5C where it is concluded that the  $\rho = \infty$  norm of the perturbation  $\delta C_A$  of  $C_A$  is bounded as follows:

$$\|\delta C_A\|_\infty < 18 \Delta \theta \quad (5.6-41)$$

where  $\Delta \theta$  is the maximum of any of the small angle perturbations.

The usual condition for existence of the inverse of the perturbed matrix  $C_A + \delta C_A$  as set forth in Chapter 2 equation (2.4-11) is given by

$$\|C_A^{-1}\|_\infty \|\delta C_A\|_\infty < 1 \quad (5.6-42)$$

also

$$\|(C_A + \delta C_A)^{-1}\|_\infty < \|C_A^{-1}\|_\infty / (1 - \|C_A^{-1}\|_\infty \|\delta C_A\|_\infty) \quad (5.6-43)$$

From (5.6-40) we obtain

$$\|C_A^{-1}\|_\infty = 1 \quad (5.6-44)$$

Substitution of (5.6-44) and  $\|\delta C_A\|_\infty = 18\Delta\varepsilon$  into (5.6-43) yields

$$\|(C_A + \delta C_A)^{-1}\|_\infty < \frac{1}{1 - 18\Delta\varepsilon} \quad (5.6-45)$$

For perturbations of  $1/4^0$ ,  $1/2^0$ ,  $1^0$  we have respectively, 1.09, 1.19, 1.46 for the corresponding bounds on the  $\|\cdot\|_\infty$  norm of the perturbed matrix. This shows that for reasonably small perturbations from the nominal rotations ( $\leq 1^0$ ) the equations formed from (5.6-27) and (5.6-28) that are used to solve for  $\hat{\Sigma}_A$  will be well conditioned.

A rough assessment of the errors subsumed under the terms  $\eta_{ij}, \eta_{2j}$  in equations (5.6-27) and (5.6-28) and their effects follows.

The overall tolerance to all of the dynamic estimation error drivers is obtained by assuming a maximum scale factor error allowance  $1\sigma$  value for LCIGS of 300 ppm and a maximum non-orthogonality error allowance  $1\sigma$  value of 100 arc-sec. In a  $90^0$  rotation, 300 ppm scale factor error is equivalent to an error  $1\sigma$  of 100 arc-sec (or 0.24 mrad). Hence, we will take 100 arc-sec and 300 ppm as the overall maximum  $1\sigma$  tolerances on the dynamic estimation errors.

Unlike the effects of unmodeled dynamic drifts on the 3 state Kalman filter estimates during static drift estimation, which was shown in Section 4 to likely have a small influence, the unmodeled static and dynamic drifts can have a large effect on the two state Kalman filter estimates of angle in the dynamic estimation procedure. This is demonstrated by calculating the error in the angle estimate from a two state Kalman filter for a constant dynamic drift due to a scale factor error of 50,000 ppm. Appendix

5D contains the relevant computations using equations (4.5-3) - (4.5-8) in Chapter 4 and the parameters for a two state filter used in some of the simulations described in the next chapter. The result is an error of 713 arc-sec in the filter estimate of change of angle during a  $90^0$  rotation at a constant rate for 10 sec. This strongly indicates a need for the Kalman filter correction procedure during a rotation presented in Chapter 4 (Figure 4.5-3).

Another considerable source of error in the estimate of angle change is the accelerometer bias uncertainty remaining after performance of the accelerometer calibration procedure presented in Chapter 2. This error is, of course, not correctable. This uncertainty in angle change due to rotation of the accelerometers is, using the estimate of  $50 \mu g$ ,  $1\sigma$  in bias uncertainty made in Chapter 2, roughly  $(\sqrt{2})(50) \mu rad$ ,  $1\sigma$  or equivalently 14 arc-sec. This change is chiefly about the nominal reference axis nominally used only in the estimation of scale factor error. The scale factor error estimate uncertainty due to this cause is

$$\frac{14}{90 \times 3600} = 43.2 \text{ ppm } 1\sigma \quad (5.6-46)$$

for a  $90^0$  rotation.

Two additional possibly significant error sources are the errors in estimating  $\underline{\omega}_s$ ,  $\omega_{1j}$  and  $\omega_{2j}$ . (See equations (5.6-27) and (5.6-28).) Here the error due to an error  $\delta\omega_{ij}$  in estimating  $\omega_{ij}$  is given by a term of the form

$$\int_{t_{k-1}}^{t_k} \delta\omega_{ij} dt = (t_k - t_{k-1}) \delta\omega_{ij} \quad (5.6-47)$$

for  $i=1,2$

The value of  $\delta \omega_{ij}$  is negligible (equation (5.4-16)) for the expected measurement errors occurring during the static estimation procedure. (See Section 5.5.) Variations in  $\omega_{ij}$  during a rotation for system axes  $\pm 1/2^0$  within the nominal are also small ( $0.1^0/\text{hr}$ ).

A worst case error due to the errors  $\delta \underline{\alpha}_s$  in estimating  $\underline{\alpha}_s$  is evaluated for the rotation depicted in Figure 5.6-1 using the geometry shown in Figure 5.2-1. As before, we will assume the rotation occurs at a constant angular rate  $\omega$  so that

$$\theta = \omega t \quad d\theta = \omega dt \quad (5.6-48)$$

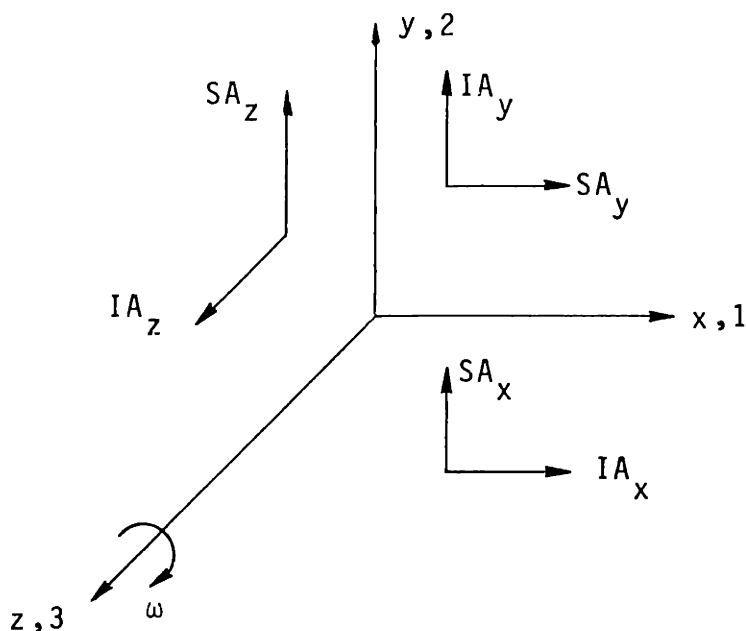


Figure 5.6-1 Worst Case Rotation

For the rotation of Figure 5.6-1, the static error model drift in the level reference frame,  $\underline{\omega}_D^L$ , is given by

$$\underline{\omega}_D^L \triangleq \begin{bmatrix} \omega_{Dz}^L \\ \omega_{Dx}^L \\ \omega_{Dy}^L \end{bmatrix} = \begin{bmatrix} 1 & 0 & 0 \\ 0 & \cos\theta & \sin\theta \\ 0 & -\sin\theta & \cos\theta \end{bmatrix} \begin{bmatrix} B_3 + g \cos\theta M_{SA_3} \\ B_1 - g M_{IA_1} \sin\theta + g M_{SA_1} \cos\theta \\ B_2 + g M_{IA_2} \cos\theta - g M_{SA_2} \sin\theta \end{bmatrix} \quad (5.6-49)$$

where the subscripts 1, 2, 3 are synonymous with x, y, z respectively and the drift terms are defined at the beginning of Section 5.2.

The errors under consideration, neglecting the relatively minor effect of the scale factor errors on the static drift estimates, are therefore approximately given by the following two terms where  $\hat{\cdot}$  denotes the estimation error in the drift.

$$\int_{t_{k-1}}^{t_k} \delta \omega_{Dz}^L dt \approx \int_{t_{k-1}}^{t_k} (\delta B_3 + g \delta M_{SA_3} \cos \hat{\omega} t) dt \quad (5.6-50)$$

$$\int_{t_{k-1}}^{t_k} \delta \omega_{Dx}^L dt \approx \int_{t_{k-1}}^{t_k} \left\{ \delta B_1 \cos \hat{\omega} t + \delta B_2 \sin \hat{\omega} t + g(\delta \Delta_{23} - \delta \Delta_{13}) \sin \hat{\omega} t \cos \hat{\omega} t + g \delta M_{SA_1} \cos^2 \hat{\omega} t - g \delta M_{SA_2} \sin^2 \hat{\omega} t \right\} dt \quad (5.6-51)$$

$$\begin{aligned} &+ g(\delta \Delta_{23} - \delta \Delta_{13}) \sin \hat{\omega} t \cos \hat{\omega} t \\ &+ g \delta M_{SA_1} \cos^2 \hat{\omega} t - g \delta M_{SA_2} \sin^2 \hat{\omega} t \end{aligned} \} dt$$

where

$$\delta \Delta_{23} \triangleq \delta M_{IA_2} - \delta M_{IA_3}$$

$$\delta \Delta_{13} \triangleq \delta M_{IA_1} - \delta M_{IA_3}$$

(The  $\Delta_{mn}$  terms were previously defined in Section 5.2, equations (5.2-11)).

Carrying out the integrations from  $wt_{k-1} = 0$  to  $wt_k = \pi/2$ , and from  $wt_{k-1} = \pi/2$  to  $wt_k = \pi$ , we see that for either integration interval the errors are bounded as follows.

$$\eta_1 \triangleq \int_{t_{k-1}}^{t_k} \delta \omega_D^L dt \leq |\delta B_3| (t_k - t_{k-1}) + \frac{|\delta \delta M_{SA_3}|}{\omega} \quad (5.6-52)$$

$$\begin{aligned} \eta_2 \triangleq \int_{t_{k-1}}^{t_k} \delta \omega_D^L dt &\leq \frac{|\delta B_1|}{\omega} + \frac{|\delta B_2|}{\omega} + \frac{|\delta \delta M_{SA_1}| \pi}{4\omega} \\ &+ \frac{|\delta \delta M_{SA_2}| \pi}{4\omega} + \frac{|\delta \delta \Delta_{23}|}{2\omega} + \frac{|\delta \delta \Delta_{13}|}{2\omega} \end{aligned} \quad (5.6-53)$$

To obtain upper bounds for (5.6-52) and (5.6-53) we assume an error  $\delta B_{UB}$  which is the maximum value of all the error terms in each equation.

Therefore,

$$\eta_1 < \left[ (t_k - t_{k-1}) + \frac{1}{\omega} \right] \delta B_{UB} \quad (5.6-54)$$

$$\eta_2 < \left[ (3 + \pi/2) \left( \frac{1}{\omega} \right) \right] \delta B_{UB}$$

For a rotation interval of 10 seconds where

$$t_R - t_{R-1} = 10 \text{ sec} \quad (5.6-55)$$

the average angular velocity  $\omega$  is given by

$$\omega \cong \frac{90^\circ}{57 \times 10} = 0.16 \frac{\text{rad}}{\text{sec}} \quad (5.6-56)$$

Substituting (5.6-55) and (5.6-56) into (5.6-54) results in

$$\begin{aligned} n_1 &< 16.25 \delta B_{UB} \\ n_2 &< 28.6 \delta B_{UB} \end{aligned} \quad (5.6-57)$$

Using a value of  $0.22^\circ/\text{hr}$  for  $\delta B_{UB}$  (which bounds all of the drifts in Table 5.4-3) yields

$$\begin{aligned} n_1 &< 3.6 \text{ sec} \\ n_2 &< 6.3 \text{ sec} \end{aligned} \quad (5.6-58)$$

These error bounds are well within the 100 arc-sec tolerance suggested earlier. [In fact, if we were to allow all of the 100 arc-sec tolerance to be absorbed by the above errors, the upper bound on drift estimation would from (5.6-57), be  $3^\circ/\text{hr.}$ ]

### 5.7 Summary of Gyro Calibration Procedure

The block diagram of Figure 5.7 summarizes the entire gyro calibration procedure as simulated for the computer runs whose results are presented in the next chapter. Each of the techniques described in the preceding sections is used in the sequence shown in the diagram for calibrating the gyros.

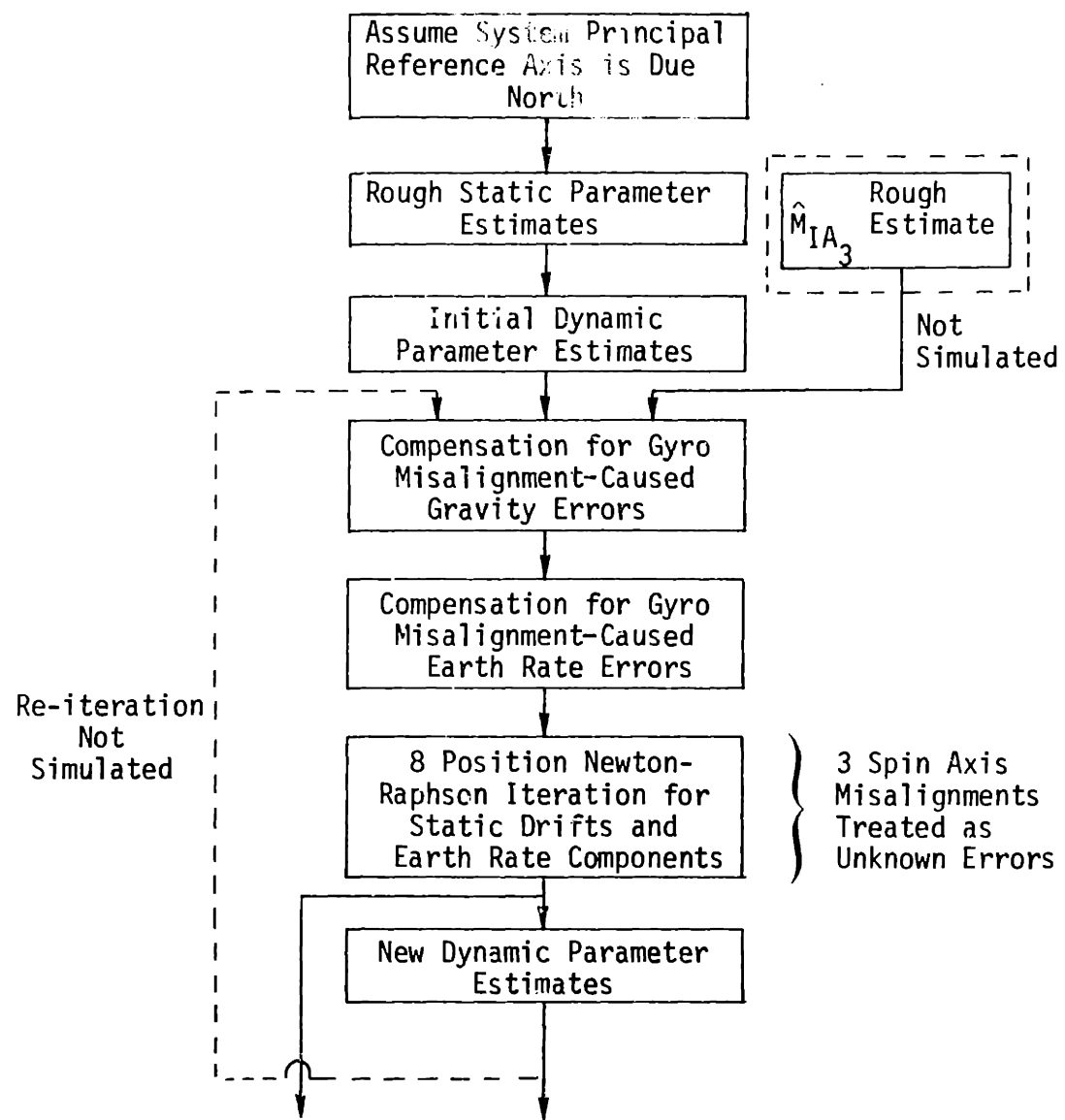


Figure 5.7-1 Block Diagram of Gyro Calibration Procedure

Initially the principal level reference axis, as defined for the system in Chapter 4, Section 4.2, is assumed to point due north. Because the tolerance from due north is  $\pm 20^{\circ}$ , the errors made in forming the initial rough estimates of the gyro static drifts are not high enough to introduce any appreciable errors when these static estimates are used in the initial estimates of gyro scale factor and input axis misalignments. These initial dynamic parameter estimates along with a separately made rough estimates of the input axis mass unbalance coefficient of one of the gyros (arbitrarily gyro number three) are used in turn to compensate for the gravity and earth rate errors caused by these misalignments. This is done by appropriately modifying the known coefficients of the static unknowns and the measurements (outlined in Section 5.4) that are to be used in the Newton-Raphson procedure. The Newton-Raphson procedure as presented in Sections 5.2 and 5.3 is then used to obtain more accurate estimates of the static gyro drift parameters and the horizontal earth rate components. These in turn are used in the new calculations for the gyro dynamic parameters.

If desired, the whole procedure can then be re-iterated as shown by the dashed line and arrow head.

Only 8 static orientations are used in the Chapter 6 simulations so that three spin axis misalignments have to be treated as unknown. The rough estimate of the third gyro input axis mass unbalance term is also not simulated.

Chapter 6  
Numerical Results

### 6.1 Introduction

This chapter is a compendium of all of the numerical simulation results used to verify the calibration techniques developed in Chapters 2, 4 and 5 as applied to the LCIGS described in Chapter 1. Also included are the results of hardware experiments made to verify the linear extrapolation method presented in Chapter 3.

The backbone of the numerical simulation program is the inertial navigation strapdown simulator described in reference 40 to which additional programming was supplied in order to carry out the various calibration procedures. Figure 6.1-1 is a block diagram of those portions of the simulator used and the additional calibration sub-programs. The portion of the diagram within the dashed lines is part of the inertial navigation strapdown simulator. The trajectory module supplies deterministic acceleration and angular velocity to the gyro and accelerometer sub-programs on the basis of specified inertial system orientations with respect to gravity and earth rate and the specified angular velocity of the system itself with respect to a local level frame.

The environment module adds random values of acceleration and angular velocity to the gyro and accelerometer model inputs on the basis of angular velocity and linear velocity environment specifications presented in Section 6.5 that are derived from Weinstock's data (Chapter 2) for a typical urban laboratory. The gyro module has provisions for adding all of the static drift terms and dynamic parameters (misalignments and scale factor errors) needed to demonstrate the full calibration procedure. Also included within the gyro module is a random walk generator for each of the three gyros. The accelerometer module contains similar provisions. The outputs of the three

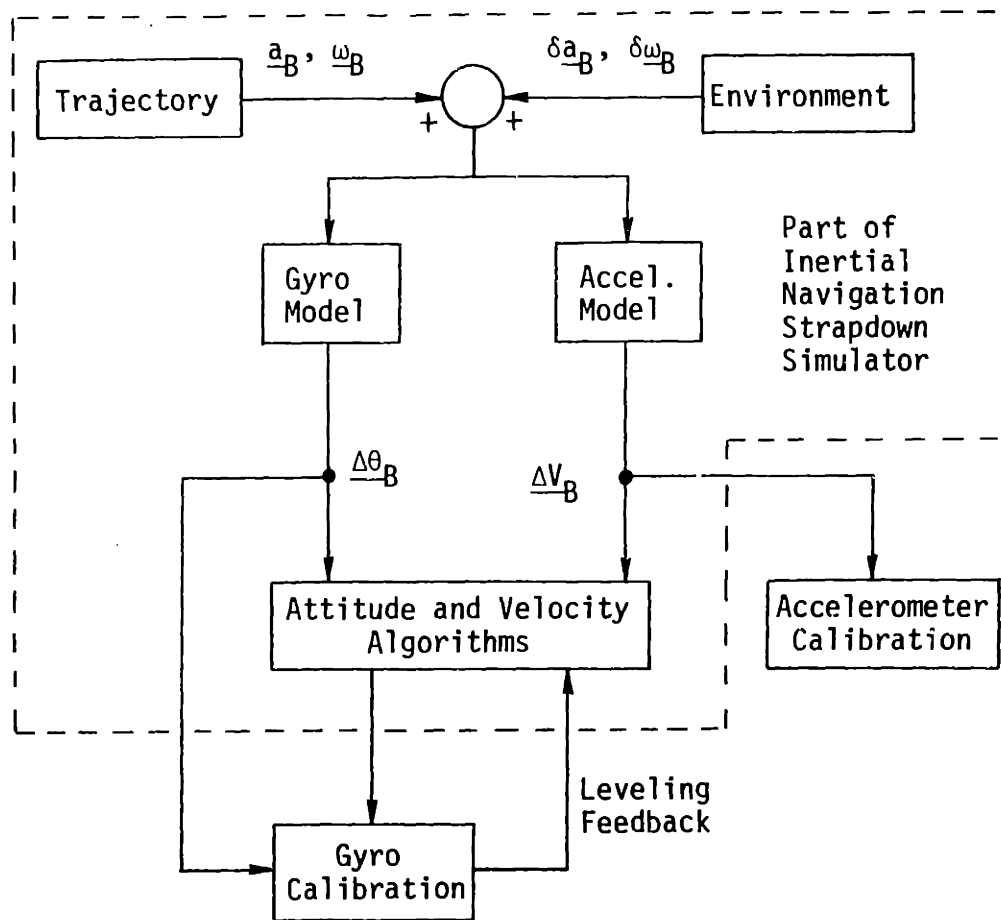


Figure 6.1-1 Simulation Program Block Diagram

gyros are fed to a standard third order quaternion attitude algorithm within the attitude and velocity module. The quaternion is converted to the equivalent direction cosine matrix for use in the calibration procedure and in transforming the body velocity obtained from the accelerometer module into a velocity in the computed frame. The gyro calibration module contains the Kalman filters described in Chapter 4 for processing the transformed velocity. Feedback to the attitude algorithm is applied using the estimated misalignment angles from the Kalman filters in order to maintain the local level reference frame defined at the beginning of Chapter 4. The iterative procedures represented by the block diagram in Figure 5.7-1, Chapter 5, are also included in this module. Outputs of the accelerometers in the body frame are fed to the accelerometer calibration module which carries out the accelerometer calibration procedures derived in Chapter 2.

A summary of the simulation results presented in this chapter is as follows:

In Section 6.2 it is verified that the accelerometer calibration techniques in Chapter 2 can successfully calibrate large biases (10,000  $\mu\text{g}$ ) and scale factor errors (60,000 ppm) with a minimum geometric magnification (approx. 1.4:1) of any measurement errors.

Section 6.3 is a detour from numerical simulations into the results from laboratory measurements made for investigating the linear extrapolation technique introduced in Chapter 3 for reducing the effective accelerometer quantization. With the linear extrapolation timing equipment used, the standard deviation of the accelerometer velocity was reduced from 0.29 cm/sec (due to 1 cm/sec quantization) to 0.013 cm/sec in the worst case.

Section 6.4 presents results from a direct simulation of the Newton-Raphson iterative procedure derived in Section 5.2 of Chapter 5. These re-

sults indicate that the procedure is operative for measurement errors as high as  $2^0/\text{hr}$ , for deviations from north of as much as  $30^0$ , and for leveling deviations of  $1.5^0$ . [The robustness of this procedure was also later confirmed during the simulation of the complete gyro calibration sequence.]

Finally, the results from simulating the complete gyro calibration sequence under various conditions are given in Section 6.5. It is seen that, under a vibration environment modeled using Weinstock's data for a typical urban laboratory (Chapter 2) and Kalman filter gains adjusted for 1 minute static estimation intervals and 10 second rotation intervals, the requirements for LCIGS presented in Chapter 1 and listed again in Table 6.1-1 can easily be met.

## 6.2 Calibration of Accelerometers

A simulation of the critical aspects of the calibration procedure derived in Chapter 2 that are applicable to LCIGS consists of the calibration of large biases and scale factors for varying test position geometries and measurement errors. In view of the common analysis methodology used in Chapter 2, it is felt that verification of the specific LCIGS calibration procedure principles for bias and scale factor only is sufficient indication that the more general calibration procedure which includes misalignment estimates is also viable. Unfortunately, it was not possible at the time the computer simulations were made to verify the V/F converter calibration procedures presented in Appendices 2B and 2C because of appropriate hardware was not available.

Use was made of the accelerometer portion of the inertial navigation strapdown simulator described in the introduction to obtain simulated accelerometer data which was then processed according to equation (2.3-14), Chapter 2, with  $j = 1, \dots, 6$ , and the iterative solution procedure presented in

Parameter	Nominal Value	Allowable Maximum
Gyro Bias, B	$0.5^{\circ}/\text{hr}$ ( $1\sigma$ )	$2^{\circ}/\text{hr}$ ( $1\sigma$ )
Gyro g-sensitive drift along IA, $M_{IA}$	$1^{\circ}/\text{hr/g}$ ( $1\sigma$ )	$2^{\circ}/\text{hr/g}$ ( $1\sigma$ )
Gyro g-sensitive drift along SA, $M_{SA}$	$0.8^{\circ}/\text{hr/g}$ ( $1\sigma$ )	$2^{\circ}/\text{hr/g}$ ( $1\sigma$ )
Gyro Scale Factor Error	150 ppm ( $1\sigma$ )	300 ppm ( $1\sigma$ )
Gyro Input Axis Misalignments	60 arc-sec ( $1\sigma$ )	100 arc-sec ( $1\sigma$ )

Table 6.1-1 LCIGS Gyro Specifications

## Section 2.5

Large enough accelerometer biases and scale factor errors were introduced to test the effectiveness of the iterative procedure. The values of these parameters are listed below in Table 6.2-1.

Accelerometer	X	Y	Z
Bias ( $\mu\text{g}$ )	10,000	-5,000	7,000
Scale Factor Error (ppm)	60,000	30,000	-40,000

Table 6.2-1 Accelerometer Simulation Parameters

The simulated accelerometer outputs were checked directly and it was found that the simulation accuracy for scale factor error was good to 1 ppm. Bias simulation accuracy was better than 0.01  $\mu\text{g}$ . For convenience, it was decided to round the bias estimates to the nearest 1  $\mu\text{g}$ . The scale factor error estimates were rounded to the nearest 1 ppm.

Simulation of the calibration procedure for zero measurement errors for the nominal test positions and for deviations from the nominal (to be described below) yielded zero estimation errors within the accuracy of the simulation.

An equivalent measurement error was added to the time averaged output of each accelerometer. Two cases were implemented. In one case, all of the measurement errors were set equal to +10  $\mu\text{g}$ . Examination of the error expression given by equation (2.3-16), Chapter 2, and the upper left 6x6 submatrix of the nominal inverse matrix given by equation (2.4-7), Chapter 2, shows that this arrangement of measurement errors maximizes the bias estimation errors and yields close to zero scale factor error estimation errors. In the second case, the measurement errors of 10  $\mu\text{g}$  magnitude were alter-

nated in sign from position to position. This arrangement maximizes the scale factor error estimation errors but yields small bias estimation errors.

Accelerometer calibration was simulated for the six nominal "up-down" test positions recommended in Section 2.4, Chapter 2, and for various deviations from these nominal positions. The deviations, in each case, were introduced only in the odd test positions in order to create a dys-symmetry in the deviation of the nominally vertical accelerometer input axis between the two "up-down" test positions which are essentially used to solve for the parameters of a particular accelerometer.

When the constant sign measurement errors were introduced, the bias estimation errors were respectively, +15  $\mu\text{g}$ , +15  $\mu\text{g}$ , +16  $\mu\text{g}$  for the X, Y and Z accelerometers for the nominal test positions and for deviations from the nominal of  $5^\circ$ ,  $10^\circ$ ,  $20^\circ$  and  $40^\circ$ . For the particular deviations chosen, the numerical conditioning of the calibration equations did not result in any appreciable change in the bias estimation errors from the nominal case. Also, scale factor error estimation errors were negligible.

Tables 6.2-2 and 6.2-3 list the calibration errors for the case of measurement errors alternating in sign. Here it can be seen that although there is an increase in both bias and scale factor estimation errors as the magnitude of the perturbations from the nominal positions is increased, the calibration equations remain numerically well conditioned even for perturbations as great as  $40^\circ$ .

For the set of perturbations from the nominal test positions chosen here and for a number of other sets that yielded entirely similar results but are omitted from this presentation, the numerical conditioning of the accelerometer calibration equations yields better results than would be expected from the analysis in Section 2.4 as exemplified by the conclusions

Perturbations to Nominal Test Positions (degrees)	Accelerometer		
	X ( $\mu\text{g}$ )	Y ( $\mu\text{g}$ )	Z ( $\mu\text{g}$ )
0°	0	0	0
5°	-1	+1	0
10°	-2	+2	-1
20°	-5	+3	-3
40°	-14	-7	-14

Table 6.2-2 Bias Estimation Errors. 10  $\mu\text{g}$  Measurement Errors Alternating in Sign

Perturbations to Nominal Test Positions (degrees)	Accelerometer		
	X (ppm)	Y (ppm)	Z (ppm)
0°	+15	-15	-16
5°	+16	-14	-16
10°	+17	-13	-16
20°	+20	-12	-19
40°	+29	-23	-30

Table 6.2-3 Scale Factor Error Estimation Errors. 10  $\mu\text{g}$  Measurement Errors Alternating in Sign

represented by equation (2.4-16). This is because of the inherently conservative nature of that analysis. We can also infer from the simulation results that the accelerometer calibration procedure introduced in Chapter 2, including the iterative technique in Section 2.5, will successfully estimate large values of bias and scale factor error as illustrated in Table 6.2-1. The estimation errors will be on the order of the actual lumped measurement errors for a variety of deviations from the nominal test positions.

### 6.3 Linear Extrapolation Method

The linear extrapolator method developed in Chapter 3, "Accelerometer Quantization", Section 3.3, was tested using the LCIGS V/F converter described in reference 41. The hardware in that reference measures the required  $\delta$  time increment (in equation (3.3-2)) between the time of the last V/F converter pulse and the actual output interrogation time. This time increment is measured with a resolution of 5 microseconds.

A sequence of positive and negative current biases was applied to the V/F converter input. For each bias, both the V/F converter output and the linearly extrapolated output were accumulated and recorded at each interrogation time. The result is a ramp of velocity versus time to which a linear least squares fit was made. The entire least squares fit residual is considered to be the quantization error. This procedure eliminates the problem of measuring the input bias exactly.

Tables 6.3-1 and 6.3-2 list the quantization errors for positive and negative bias values, respectively, with and without the linear extrapolation.

Input Current Bias in g's	Standard Deviation Without Linear Extrap. (cm/sec)	Standard Deviation With Linear Extrap. (cm/sec)
0.432	0.2875	0.003975
0.627	0.2879	0.004373
0.822	0.2869	0.005466
1.017	0.2877	0.007354
1.414	0.2869	0.010434

Table 6.3-1 Quantization Error for Positive Biases

Input Current Bias in g's	Standard Deviation Without Linear Extrap. (cm/sec)	Standard Deviation With Linear Extrap. (cm/sec)
-0.348	0.2880	0.0166
-0.543	0.2874	0.0102
-0.738	0.2875	0.0108
-0.933	0.2878	0.0129
-1.360	0.2879	0.0122

Table 6.3-2 Quantization Error for Negative Biases

The error standard deviations without linear extrapolation for the positive and negative biases are all 0.29 cm/sec rounded to two places. If the bias input is not an exact integral multiple of the quantization divided by the V/F converter sample times, then the errors due to quantization will be uniformly distributed over a long enough test period. Figure 6.3-1 shows the pertinent uniform probability function. The resultant standard deviation computed from this function is 0.289 which matches the pertinent data in Tables 6.3-1 and 6.3-2 very closely. Examination of the standard devia-

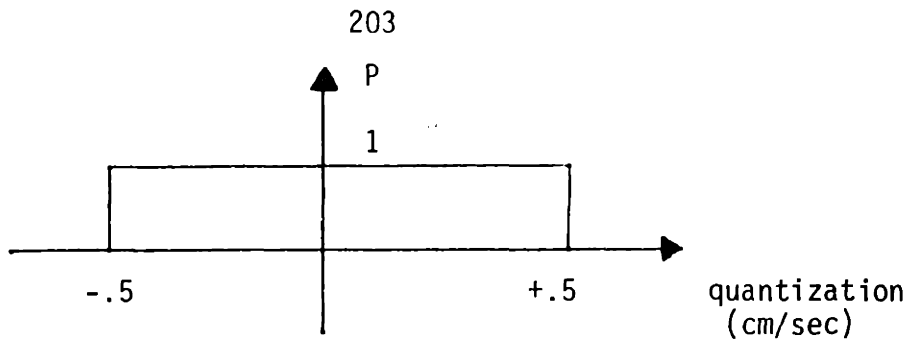


Figure 6.3-1 Uniform Probability Function for No Linear Extrapolation

tions with implementation of the linear extrapolation in Table 6.3-1 immediately shows that the errors for the positive biases are basically due to the timing errors analyzed in Chapter 3. Table 6.3-3 is a side by side comparison of the measured standard deviation values (with linear extrapolation) taken from Table 6.3-1 and the theoretical bounds due to timing errors on the standard deviations calculated directly from equation (3.4-32) in Chapter 3.

Positive Bias in g's	Measured Standard Deviation (cm/sec)	Theoretical Bound On Standard Deviation Due to Timing Errors (cm/sec)
0.432	0.003975	0.001423
0.627	0.004373	0.002069
0.822	0.005466	0.002712
1.017	0.007354	0.003356
1.414	0.010434	0.004666

Table 6.3-3 Comparison of Measured Standard Deviations With Theoretical Bounds Due to Timing Errors

The fact that the measured standard deviations are larger than the theoretical bounds indicates that the statistical assumptions for timing errors made in Chapter 3 are too optimistic. In any case,

the linear extrapolator has succeeded in reducing the standard deviation due to quantization by at least a factor of 28 for the positive biases. Examination of the standard deviations for negative input biases does not reveal a trend that corresponds with equation (3.4-32). This would indicate that for negative biases the linear extrapolation errors due to timing errors are swamped out by V/F converter instabilities. Support for this conclusion comes about through examination of V/F stability data and the V/F circuit design. The V/F converter is asymmetrical in its circuit paths with respect to the polarity of the bias input. A negative bias input would appear to yield a more unstable output than a positive bias. This is borne out by tests made on several V/F converter breadboards in reference 42 where the  $\text{lo}$  output value for negative inputs was as much as four times higher as that for positive inputs over 1 hour averaging times. We note nevertheless from the data in Table 6.3-2, that even for negative bias inputs, the error standard deviation is reduced by at least a factor of 17 when linear extrapolation is used with this particular hardware sample.

#### 6.4 Newton-Raphson Iterations

Preliminary to simulating the full gyro calibration procedure, including processing of the measurements by the Kalman filters, the Newton-Raphson iterative procedure presented in Sections 5.2 and 5.3 was simulated in a fashion analogous to the description of the accelerometer simulation. That is, the true gyro drifts and true earth rate components were introduced directly into gyro simulations whose outputs were then used to calculate the equivalent measurements along the two horizontal reference axes. Lumped measurement errors (in  $^{\circ}/\text{hr}$ ) were then added to these equivalent measurements. The iterative procedure for the 8 static positions (described in Section 5.2) was then carried out.

Run #	Pert. From Level (deg.)	Azimuth Angle (deg.)	Meas. Errors (°/hr)	Instrument Drifts (°/hr)
1	0	20	0	0
2	0	20	0.8	0
3	0.5	20	0	0
4	0.5	20	0.8	0
5	0.5	20	1.5	0
6	0.5	20	2	0
7	1.5	20	0.8	0
8	0.5	-20	0	0
9	0.5	-20	0.8	0
10	0.5	30	0	0
11	0.5	30	0.8	0
12	0.5	30	0	$B_1 = 50, gM_{IA_1} = 40, gM_{SA_1} = 35$ $B_2 = 40, gM_{IA_2} = 20, gM_{SA_2} = 45$ $B_3 = 30, gM_{IA_3} = 10, gM_{SA_3} = 55$
13	0.5	20	0.8	

All values of drift negative

Table 6.4-1 Description of Newton-Raphson Iteration Runs

Table 6.4-1 lists the key descriptions of 13 runs made to evaluate the iterative procedure. As can be seen from the table, runs were made with zero leveling perturbations, others with perturbations of  $0.5^0$  and  $1.5^0$  from the 8 nominal positions. The deviation of the principal reference axis from north is designated by the azimuth angle shown. The angles used were  $+20^0$ ,  $-20^0$  and  $30^0$ . Measurement errors added to the appropriate measurements ranged from 0 to  $2^0/\text{hr}$ . In the first 11 runs, no gyro drifts were introduced in order to simplify the evaluation procedure. The last two runs introduced the large parameters for gyro drifts shown in the table.

In all 13 runs, complete convergence of the iterative procedure occurred in at most 5 iterations. As an illustration of this convergence, the deviations of some representative estimated horizontal earth rate components from their final values in the iteration are shown in Table 6.4-2 for runs 1, 2 and 4. These 3 runs were chosen for the contrasts between them. Run #1 was for zero level perturbation and zero measurement noise. In Run #2, a measurement noise of  $0.8^0/\text{hr}$  was added. Run #4 also included a leveling perturbation of  $0.5^0$ . In each case (and, in fact, for all 13 runs) convergence was extremely rapid as shown by the earth-rate component deviations for each iteration. By the third iteration, the estimation of earth rate components has practically "locked-in" to those values which satisfy the constraint of equation (5.3-15), Section 5.3 and repeated below.

$$w_{1j} + w_{2j} = 1 \quad (6.4-1)$$

where  $w_{1j}$  and  $w_{2j}$  are normalized by a  $10^0/\text{hr}$  magnitude. (However, the deviations in Table 6.4-2 are in deg/hr.) This is illustrated by the accompanying Table 6.4-3, which computes equation (6.4-1) for the normalized final earth rate components of the iterations. It is seen that even for the worst

	Run #1		Run #2		Run #4	
Iteration	$\epsilon_w^x$ (°/hr)	$\epsilon_w^y$ (°/hr)	$\epsilon_w^x$ (°/hr)	$\epsilon_w^y$ (°/hr)	$\epsilon_w^x$ (°/hr)	$\epsilon_w^y$ (°/hr)
0	-.5903	3.3849	-.1207	1.5487	-.125	1.5761
1	-.5903	-.6231	-.1207	-.8593	-.125	-.8706
2	-.0150	-.0545	-.0173	-.0845	-.0173	-.0875
3	$-8 \times 10^{-5}$	$-2.5 \times 10^{-4}$	$-2 \times 10^{-4}$	$-1.07 \times 10^{-3}$	$-2.1 \times 10^{-4}$	$-1.13 \times 10^{-3}$
4	0	0	0	$-6 \times 10^{-7}$	0	0

Table 6.4-2 Deviations of Estimated Earth Rate Components From Final Values

Run #1	$(.94096866)^2 + (.33849369)^2 = 1 - 2.7 \times 10^{-9}$
Run #2	$(.98793446)^2 + (.15487247)^2 = 1 - 2.1 \times 10^{-8}$
Run #4	$(.98750119)^2 + (.15761035)^2 = 1 - 3.8 \times 10^{-7}$

Table 6.4-3 Sum of Squares of Final Earth Rate Component

case of Run #4, the deviation of the sum of the squares from unity is 0.38 parts per million.

Estimation errors for the final gyro drift estimates (at the end of each iterative run) are presented in Table 6.4-4. First of all, note that for those runs (1, 3, 8, 10, 12) where no measurement errors were introduced, there are residual estimation errors ranging from almost zero for  $gMSA_3$  (the spin axis mass unbalance drift of the third gyro) to  $0.065^0/\text{hr}$  for the  $g\Delta_{13}$  mass unbalance drift in Run #8. Note also that errors from one run to another are quite similar regardless of the level perturbation, the azimuth angle, and the magnitude of the gyro drifts being estimated (which range from  $0^0/\text{hr}$  to  $50^0/\text{hr}$ ). These small residual errors are considered to be inherent in the simulation as evidenced, for example, by the inherent measurement errors (with no external measurement errors introduced) listed in Table 6.4-5 for Run #1. These errors range from  $0.027^0/\text{hr}$  to  $0.0063^0/\text{hr}$  and are of the correct magnitude to cause the estimation error magnitudes in Run #1 even though the external noise is zero.

In those runs where fairly large measurement errors are introduced (2, 4, 5, 6, 7, 9, 11, 13), the estimation errors appear to depend mainly on the magnitude of the measurement noise that is introduced and not on the magnitudes of either the leveling perturbation, the azimuth angle or the gyro drift magnitude being estimated. The numerical conditioning of the solution matrix (equation (5.2-27)) at the final iteration is such that the errors for bias and spin axis mass unbalance drifts are not more than approximately twice the measurement errors introduced whereas the  $\Delta_{13}$  mass unbalance drift errors are not more than about five times the measurement error magnitude. As expected, the numerical conditioning results in considerably greater magnification of the measurement errors for the  $\Delta_{13}$  mass unbalance drift esti-

Run #	1*	2	3	4	5	6	7	8	9	10	11	12	13
Drift Error													
$\epsilon B_1$ ( $^{\circ}/hr$ )	.016	0.61	.015	0.58	1.07	1.44	0.57	.035	0.67	.01	0.36	.016	0.59
$\epsilon B_2$ ( $^{\circ}/hr$ )	.034	1.47	.037	1.45	2.93	4.17	1.46	.017	0.39	.035	1.62	.034	1.45
$\epsilon B_3$ ( $^{\circ}/hr$ )	.014	-1.26	.0094	-1.22	-2.01	-2.34	1.1	.025	-0.26	.006	-1.41	.014	-1.21
$\Delta_{13g}$ ( $^{\circ}/hr$ )	.03	-4.05	.028	-3.93	-7.2	-9.31	3.68	.064	-3.71	.019	-4.47	.031	-3.93
$\Delta_{23g}$ ( $^{\circ}/hr$ )	.054	-1.68	.049	1.78	4.56	8.42	1.91	.065	0.94	.054	2.45	.05	1.78
$M_{SA1} g$ ( $^{\circ}/hr$ )	.016	0.86	.02	0.82	1.75	2.57	0.71	-.019	-0.31	.023	1.2	.017	0.82
$M_{SA2} g$ ( $^{\circ}/hr$ )	-.011	-1.21	-.012	-1.20	-2.16	-2.95	-1.25	.020	-1.49	-.0074	-0.62	-.007	-1.2
$M_{SA3} g$ ( $^{\circ}/hr$ )	.0017	1.87	.008	1.81	3.09	3.77	1.66	.009	0.95	.0046	1.79	.0004	1.804

(\*Base line Run - See Table 6.4-5)

Table 6.4-4 Final Estimation Errors for Gyro Drift Terms

Measurement Error Static Position (i)	$\epsilon_{m1i}$ ( $^{\circ}$ /hr)	$\epsilon_{m2i}$ ( $^{\circ}$ /hr)
1	.025	.01
2	.025	.008
3	.027	.01
4	.023	.008
5	.025	.008
6	.025	.0063
7	.024	.0063
8	.027	.008

Table 6.4-5 Measurement Errors for Run #1

mates because of the nonorthogonality of the matrix rows corresponding to the  $45^0$  positions (i.e., non "up-down") used for the  $\Delta_{i3}$  measurements.

In retrospect, it is not surprising that convergence occurred for all thirteen runs in spite of measurement errors all being larger than those listed in Table 5.3-1, Section 5.3. These theoretical values were based on a constraint on the computed maximum deviation from north of  $30^0$ . No such constraint was employed in these iterations. Table 6.4-6 lists the largest computed magnitude of the deviation from north for each run. It is seen that for those runs where noise has been introduced that the maximum computed deviations are all considerably greater than  $30^0$  (for all but Run #9). Also, even for the theoretical case of  $30^0$ , the results in Table 5.3-1 are conservative because of the conservative nature of the bounds  $|S|_2$  and  $|T|_2$  (equation (5.3-52), Section 5.3) obtained in Appendix 5A for leveling perturbations of  $0.5^0$ .

The conclusion to be drawn from the above results is that the Newton-Raphson iteration devised in Section 5.2 is quite robust for the recommended leveling perturbation tolerances of  $.5^0$ , the azimuth tolerances of  $\pm 20^0$ , and for noise values as high as  $2^0/\text{hr}$ . The iteration should, therefore, work well in the simulation of the overall gyro calibration procedure (see block diagram, Fig. 5.7-1 in Chapter 5) and in actual field use.

## 6.5 Complete Gyro Calibration Simulations

The block diagram in Fig. 5.7, Section 5.7 in Chapter 5 represents the overall gyro calibration procedure implemented in the simulation runs used to obtain the data presented in this section. Briefly, the principal reference axis of the local level frame is initially assumed to point due north in order to obtain initial static gyro parameter estimates which are, in turn, used to obtain initial dynamic parameter estimates. The initially

Run # j	Minimum $w_{ij}$	Computed Deviation Magnitude From North (Deg.)
1	0.93839	20.22
2	0.83623	33.26
3	0.93837	20.22
4	0.83696	33.18
5	0.67413	47.61
6	0.45510	62.93
7	0.83493	33.39
8	0.93823	20.24
9	0.89236	26.83
10	0.86375	30.26
11	0.68750	46.57
12	0.93825	20.24
13	0.83701	33.17

Table 6.4-6 Largest Computed Magnitude of the Deviation From North

determined misalignment values (which are included in the dynamic estimates) are, in turn, used to correct any misalignment errors in the full static parameter Newton-Raphson procedure which then follows. The static parameters from the full iteration process are then used in the final dynamic parameter calibration sequence.

The simulations include runs with environment vibrations modeled as white noise sequences for linear velocity and angular velocity having standard deviations of 0.00456 ft/sec and 0.00000217 rad/sec which were roughly estimated from the data in Chapter 2, Fig. 2.6-1 as presented by Weinstock for a typical test laboratory. (Several runs were made with ten times these standard deviations.) The rate of the random sequence samples was taken as 20 Hz since the entire simulation was run at this iteration rate (including the Kalman filters) in order to ensure proper synchronization among all of the separate simulation subprograms. Kalman filter gains were adjusted to yield settled estimates at the end of a 1 minute period for each system static orientation. The strategy used was to try to achieve acceptable gyro parameter estimates for LCIGS in the minimum possible time. In the same vein, Kalman filter gains were adjusted to achieve acceptable estimates of drift angle at the end of a system rotation lasting 10 seconds. Table 6.5-1 lists the considerably large gyro drift terms and dynamic error parameters that were to be calibrated in the simulations. A gyro random walk term of  $0.2^0/\text{hr}/\sqrt{\text{hr}}$  for each gyro was sometimes introduced. The lack of roundedness in the dynamic parameters (scale factor errors and misalignments) stems from the way misalignments were introduced into the simulations. Input misalignments were elements of  $C_{Ba}^{BG}$  (a transformation from the reference frame to the gyro frame) whereas the estimated values were for those of  $S_{eq}$  and  $M_{eq}$  given by equations (5.6-4) and (5.6-6) in Chapter 5. If  $S$  denotes the diagonal

Biases	$B_1$	$50^0/\text{hr}$
	$B_2$	$40^0/\text{hr}$
	$B_3$	$30^0/\text{hr}$
$\Delta$ Mass Unbalance Drifts	$g\Delta_{13}^*$	$40^0/\text{hr}$
	$g\Delta_{23}^*$	$20^0/\text{hr}$
Spin Axis Mass Unbalance Drifts	$gM_{SA_1}$	$35^0/\text{hr}$
	$gM_{SA_2}$	$45^0/\text{hr}$
	$gM_{SA_3}$	$55^0/\text{hr}$
Equivalent Scale Factor Errors, $S_{eq}$	$SF_1$	49,817 ppm
	$SF_2$	39,821 ppm
	$SF_3$	29,828 ppm
Equivalent Misalignments $M_{eq}$	$\gamma_{12}$	9.944 mrad
	$\gamma_{13}$	7.788 mrad
	$\gamma_{21}$	9.368 mrad
	$\gamma_{23}$	11.924 mrad
	$\gamma_{31}$	10.9335 mrad
	$\gamma_{32}$	6.89 mrad

(\* $M_{IA_3}$  set to zero)

Table 6.5-1 Gyro Drift Terms and Dynamic Error Parameters

matrix of scale factors introduced in the simulation program, then the estimated dynamic parameters represented by  $S_{eq} + M_{eq}$  are related to the parameters actually introduced through  $C_{Ba}^{BG}$  and  $S$  by

$$\begin{aligned} C_{Ba}^{BG} &\triangleq I + A \quad C_{Ba}^{Ba} = I - M \\ S_{eq} + M_{eq} &\cong S + A - A^2 \end{aligned} \quad (6.5-1)$$

where  $I - A + A^2$  is the approximate inverse of  $C_{Ba}^{BG}$ .

The squared term in equation (6.5-1) accounts for the lack of roundness in Table 6.5-2 when the actual scale factor values of 50,000 ppm, 40,000 ppm, 30,000 ppm are introduced into matrix  $S$ .

In addition to the above, appropriate values of each gyro spin axis misalignment about the output axis were included. Also, an uncalibratable spin axis misalignment of 1 mrad about the input axis was introduced for each gyro.

Table 6.5-2 is a listing of accelerometer bias and scale factor errors that were sometimes introduced in order to illustrate a typical calibration situation.

Table 6.5-3 is a description of the 14 simulation runs that were made.

Runs 1 - 5 were treated as "base line" runs without any environmental vibrations, gyro random walk terms, or accelerometer bias and scale factor errors being introduced. Table 6.5-4 lists the results for these 5 runs where the prefix  $\epsilon$  in the left most column denotes the error in the estimates made for biases  $B_i$ , etc. The first run was made with no gyro static or dynamic parameters present. Successive inclusion of gyro static parameters only for Run #2, dynamic parameters only for Run #3 and both sets of parameters for Run #4 also result in small estimation errors. In Run #5, additional uncalibratable spin axis misalignments of 1 mrad were introduced. As expected, there are small corresponding increases in the static estimation

Biases	B <sub>1</sub>	50 $\mu$ g
	B <sub>2</sub>	-40 $\mu$ g
	B <sub>3</sub>	30 $\mu$ g
Scale Factor Errors	SF <sub>1</sub>	55 ppm
	SF <sub>2</sub>	45 ppm
	SF <sub>3</sub>	35 ppm

Table 6.5-2 Accelerometer Biases and Scale Factor Errors

Run #	Static Gyro Drifts	Dynamic Gyro Errors	SA Mis-Align. IA	Accel. Bias and Scale Factor Error	Accel. and Gyro Quantization	Environmental Vibrations	Gyro Random Walk
1	0	0	0	0	0	0	0
2	✓	0	0	0	0	0	0
3	0	✓	0	0	0	0	0
4	✓	✓	0	0	0	0	0
5	✓	✓	✓	0	0	0	0
6	✓	✓	0	0	✓ 0.1 cm/sec 3 arc-sec	✓	0
7	✓	✓	0	0	✓ 1 cm/sec 3 arc-sec	✓	0
8	✓	✓	0	✓	✓	✓	0
9 through 16	✓	✓	✓	✓	✓	✓	✓
17 and 18	✓	✓	✓	✓	✓ <u>HIGH</u>	✓	✓

Table 6.5-3 Key to Simulation Runs

errors because of the resulting miscompensation of gravity along the spin axis but, of course, negligible changes in the dynamic parameter estimation errors.

In Runs 6 and 7, the expected environmental vibrations were introduced. Gyro quantization of 3 arc-sec was used for both runs. Run #6 had an accelerometer quantization of 0.1 cm/sec whereas a quantization of 1 cm/sec was included in Run #7. Comparison of the results of these two runs listed in Table 6.5-5 reveals no significant change in estimation errors with the inclusion of the higher accelerometer quantization value. The higher value was, therefore, used in all the following runs.

Another run (#8) with the "normal" environment vibrations was made with the accelerometer errors of Table 6.5-2 inserted. Table 6.5-6 is a side by side comparison of Run #7 without the accelerometer errors and Run #8, having the same conditions as Run #7 but with the additional accelerometer errors. As expected, only the three scale factor error estimates are affected since the estimated leveling error angle is only affected by a change in the effective leveled frame accelerometer bias due to the two accelerometers that are not along the leveled axis of rotation. The changes in scale factor errors due to the accelerometer biases are 6 ppm, -54 ppm, and +58 ppm for gyros 1 through 3, respectively.

The next set of 8 runs (9 through 16) was made with the same set of environmental specifications, but with a gyro random walk term of  $0.2^{\circ}/\text{hr}/\sqrt{\text{hr}}$  added along with the uncalibratable spin axis misalignment of 1 mrad and the accelerometer errors. For each run, different starting numbers for the simulation program random number generators were chosen from a table of random numbers. Errors from these runs are presented in Table 6.5-7. The sample means and standard deviations computed from this data are presented in Table

	RUN	1	2	3	4	5
Static Drift Errors	$\epsilon B_1$ ( $^{\circ}/\text{hr}$ )	.017	.019	-.002	.005	.043
	$\epsilon B_2$ ( $^{\circ}/\text{hr}$ )	.036	.035	.012	.017	.064
	$\epsilon B_3$ ( $^{\circ}/\text{hr}$ )	.013	.013	.013	.009	-.063
	$\epsilon g\Delta_{13}$ ( $^{\circ}/\text{hr}$ )	.036	.036	.033	.027	-.159
	$\epsilon g\Delta_{23}$ ( $^{\circ}/\text{hr}$ )	.051	.053	.038	.035	-.026
	$\epsilon gM_{SA_1}$ ( $^{\circ}/\text{hr}$ )	.018	.016	.013	.005	-.033
Scale Factor Errors	$\epsilon gM_{SA_2}$ ( $^{\circ}/\text{hr}$ )	-.011	-.011	-.005	-.003	-.003
	$\epsilon gM_{SA_3}$ ( $^{\circ}/\text{hr}$ )	.003	.003	.002	.005	.077
	$\epsilon SF_1$ (ppm)	-23	-32	-53	-49	-49
Misalign- ment Errors	$\epsilon SF_2$ (ppm)	1	8	-16	-11	-11
	$\epsilon SF_3$ (ppm)	3	18	-21	58	58
	$\epsilon \gamma_{12}$ (arc-sec)	-1	0	11	18	18
	$\epsilon \gamma_{13}$ (arc-sec)	-13	-11	-20	-23	-23
	$\epsilon \gamma_{21}$ (arc-sec)	-1	-1	3	1	1
	$\epsilon \gamma_{23}$ (arc-sec)	1	3	8	8	8
	$\epsilon \gamma_{31}$ (arc-sec)	1	1	-2	-12	-12
	$\epsilon \gamma_{32}$ (arc-sec)	2	2	-6	-12	-11

Table 6.5-4 Base Line Runs - No Vibration Environment

Run	6	7
$\epsilon B_1$ ( $^{\circ}/\text{hr}$ )	-.017	-.027
$\epsilon B_2$ ( $^{\circ}/\text{hr}$ )	-.094	-.097
$\epsilon B_3$ ( $^{\circ}/\text{hr}$ )	.114	.096
$\epsilon g_{13}^{\Delta}$ ( $^{\circ}/\text{hr}$ )	-.173	-.20
$\epsilon g_{23}^{\Delta}$ ( $^{\circ}/\text{hr}$ )	.082	.085
$\epsilon g_{SA_1}^M$ ( $^{\circ}/\text{hr}$ )	.05	.052
$\epsilon g_{SA_2}^M$ ( $^{\circ}/\text{hr}$ )	-.08	-.1
$\epsilon g_{SA_3}^M$ ( $^{\circ}/\text{hr}$ )	-.216	-.20
$\epsilon SF_1$ (ppm)	-129	-130
$\epsilon SF_2$ (ppm)	-63	-63
$\epsilon SF_3$ (ppm)	44	47
$\epsilon \gamma_{12}$ (arc-sec)	29	28
$\epsilon \gamma_{13}$ (arc-sec)	-31	-30
$\epsilon \gamma_{21}$ (arc-sec)	-6	-5
$\epsilon \gamma_{23}$ (arc-sec)	11	12
$\epsilon \gamma_{31}$ (arc-sec)	-9	-9
$\epsilon \gamma_{32}$ (arc-sec)	-4	-4

Table 6.5-5 Accelerometer Quantization Effects

	Run	7	8
Static Drift Errors	$\epsilon B_1$ ( $^{\circ}/hr$ )	-.027	-.018
	$\epsilon B_2$ ( $^{\circ}/hr$ )	-.097	-.11
	$\epsilon B_3$ ( $^{\circ}/hr$ )	.096	.128
	$\epsilon g\Delta_{13}$ ( $^{\circ}/hr$ )	-.20	-.140
	$\epsilon g\Delta_{23}$ ( $^{\circ}/hr$ )	.085	.117
	$\epsilon gM_{SA_1}$ ( $^{\circ}/hr$ )	.052	.05
Scale Factor Errors	$\epsilon gM_{SA_2}$ ( $^{\circ}/hr$ )	-.1	-.075
	$\epsilon gM_{SA_3}$ ( $^{\circ}/hr$ )	-.20	-.22
	$\epsilon SF_1$ (ppm)	-130	-124
Misalign- ment Errors	$\epsilon SF_2$ (ppm)	-63	-117
	$\epsilon SF_3$ (ppm)	47	105
	$\gamma_{12}$ (arc-sec)	28	29
	$\gamma_{13}$ (arc-sec)	-30	-31
	$\gamma_{21}$ (arc-sec)	-5	-6
	$\gamma_{23}$ (arc-sec)	12	12
	$\gamma_{31}$ (arc-sec)	-9	-9
	$\gamma_{32}$ (arc-sec)	-4	-4

Table 6.5-6 Effect of Accelerometer Bias and Scale Factor Error

Run	9	10	11	12	13	14	15	16
$\epsilon B_1$ (°/hr)	.16	.015	.021	-.209	.114	-.078	.047	.137
$\epsilon B_2$ (°/hr)	.219	-.062	-.079	.002	.382	-.022	-.217	.289
$\epsilon B_3$ (°/hr)	-.218	.045	-.189	-.02	-.22	-.127	.079	-.215
$\epsilon g\Delta_{13}$ (°/hr)	-.98	-.317	-.731	-.284	-.359	.101	-.37	-.734
$\epsilon g\Delta_{23}$ (°/hr)	-.484	.034	.128	.07	-.855	.212	.713	-.682
$\epsilon gM_{SA_1}$ (°/hr)	.025	.02	.054	.582	-.083	.128	.065	-.028
$\epsilon gM_{SA_2}$ (°/hr)	-.079	-.072	-.045	-.303	-.382	.265	-.194	-.241
$\epsilon gM_{SA_3}$ (°/hr)	.210	-.142	.326	-.06	-.019	.233	-.029	.044
$\epsilon SF_1$ (ppm)	-.160	-124	-164	-171	-126	-98	-115	-151
$\epsilon SF_2$ (ppm)	-99	-116	-93	-157	-108	-112	-125	-97
$\epsilon SF_3$ (ppm)	113	105	105	26	39	84	104	66
$\epsilon \gamma_{12}$ (arc-sec)	37	29	36	18	20	26	20	28
$\epsilon \gamma_{13}$ (arc-sec)	-5	-30	-29	-23	7	5	0	-4
$\epsilon \gamma_{21}$ (arc-sec)	-1	-6	-9	-4	0	12	5	-18
$\epsilon \gamma_{23}$ (arc-sec)	11	12	8	17	12	14	14	14
$\epsilon \gamma_{31}$ (arc-sec)	-10	-9	-8	-2	-1	-5	8	-5
$\epsilon \gamma_{32}$ (arc-sec)	3	-5	-8	-16	-6	-8	-8	-12

Table 6.5-7 Monte Carlo Runs with Expected Vibrations

6.5-8. The values for the means and standard deviations of the static parameters are all acceptable for LCIGS with reference to the LCIGS goals presented in Section 6.1. There is a systematic bias for each of the scale factor error estimation errors as evidenced by the sample means for  $\epsilon SF_1$  through  $\epsilon SF_3$  in Table 6.5-8. These biases were traced to an error in the Kalman filter post correction procedure. We conclude that the mean values for the scale factor estimation errors for Runs 9 - 16 in the table can be ignored in measuring the effects of random vibration on the estimation procedure. Therefore, the sample standard deviations can be used as the true measure of dynamic parameter uncertainty. The statistical effect of 50  $\mu g$  ( $1\sigma$ ) accelerometer biases on the scale factor estimation process is given by

$$\frac{(\sqrt{\alpha})(50)}{\pi/2} \cong 45 \text{ ppm } 1\sigma \quad (6.5-2)$$

If this value is root summed squared with the highest sample standard deviation in Table 6.5-8, then the result is 56 ppm ( $1\sigma$ ) for  $\epsilon SF_3$  which shows that the LCIGS maximum allowable requirement of 300 ppm ( $1\sigma$ ) can easily be met. Values (both mean and standard deviations) for the misalignment estimation errors in Table 6.5-8 are all small enough to meet the misalignment error maximum allowable criterion of 100 arc-sec ( $1\sigma$ ) for LCIGS easily.

Two final runs (17 and 18) were made for vibrations having 10 times the standard deviations used in the preceding runs. The results for these runs are listed in Table 6.5-9 and are unacceptable for LCIGS. This means that if a severe vibration regime is encountered rather than the expected one, the Kalman filter gains and estimation times will have to be completely re-adjusted. Note, however, that the Newton-Raphson iteration and all of the other iterative procedures used in the calibration are powerful enough to

Parameter	Sample Mean	Sample Standard Deviation
$\epsilon B_1$ ( $^{\circ}/hr$ )	.026	.122
$\epsilon B_2$ ( $^{\circ}/hr$ )	.064	.208
$\epsilon B_3$ ( $^{\circ}/hr$ )	-.108	.124
$\epsilon g\Delta_{13}$ ( $^{\circ}/hr$ )	-.459	.338
$\epsilon g\Delta_{23}$ ( $^{\circ}/hr$ )	-.108	.522
$\epsilon gM_{SA_1}$ ( $^{\circ}/hr$ )	.095	.206
$\epsilon gM_{SA_2}$ ( $^{\circ}/hr$ )	-.13	.2
$\epsilon gM_{SA_3}$ ( $^{\circ}/hr$ )	.07	.166
$\epsilon SF_1$ (ppm)	-139	26
$\epsilon SF_2$ (ppm)	-113	21
$\epsilon SF_3$ (ppm)	80	33
$\epsilon \gamma_{12}$ (arc-sec)	27	7
$\epsilon \gamma_{13}$ (arc-sec)	-10	15
$\epsilon \gamma_{21}$ (arc-sec)	-3	9
$\epsilon \gamma_{23}$ (arc-sec)	13	3
$\epsilon \gamma_{31}$ (arc-sec)	-4	6
$\epsilon \gamma_{32}$ (arc-sec)	-8	6

Table 6.5-8 Means and Standard Deviations for Monte Carlo Runs

	Run	17	18
Static Drift Terms	$\epsilon B_1$ ( $^{\circ}/\text{hr}$ )	-1.7	-2.5
	$\epsilon B_2$ ( $^{\circ}/\text{hr}$ )	-.9	-.6
	$\epsilon B_3$ ( $^{\circ}/\text{hr}$ )	2.4	1
	$\epsilon g\Delta_{13}$ ( $^{\circ}/\text{hr}$ )	3.7	2.6
	$\epsilon g\Delta_{23}$ ( $^{\circ}/\text{hr}$ )	-1.7	2.3
	$\epsilon gM_{SA_1}$ ( $^{\circ}/\text{hr}$ )	2.7	5.6
Scale Factor Errors	$\epsilon gM_{SA_2}$ ( $^{\circ}/\text{hr}$ )	.5	-1.9
	$\epsilon gM_{SA_3}$ ( $^{\circ}/\text{hr}$ )	2.9	-1.6
	$\epsilon SF_1$ (ppm)	-76	-573
Misalignment Errors	$\epsilon SF_2$ (ppm)	-522	-651
	$\epsilon SF_3$ (ppm)	198	-429
	$\epsilon \gamma_{12}$ (arc-sec)	152	-45
	$\epsilon \gamma_{13}$ (arc-sec)	100	-28
	$\epsilon \gamma_{21}$ (arc-sec)	52	-22
	$\epsilon \gamma_{23}$ (arc-sec)	44	57
	$\epsilon \gamma_{31}$ (arc-sec)	42	12
	$\epsilon \gamma_{32}$ (arc-sec)	34	-90

Table 6.5-9 Runs with High Vibration Environment

226

still yield credible results even when there are large measurement errors.

**Chapter 7**  
**Conclusions and Recommendations**

### 7.1 Summary of Thesis Results

This thesis has introduced and developed a number of techniques for calibrating the inertial reference unit of a low cost inertial guidance strapdown system (LCIGS). The inertial reference unit consists of a complete set of inertial instruments assembled into an inertial measurement unit package. Additional test software including attitude and velocity algorithms is supplied external to the package.

We have demonstrated that by making use of the geometrical properties of the reference unit, including the non-linear pythagorean relationship between the components of gravity in an orthogonal frame to the pre-measured magnitude of gravity at the test location (and analogously for the earth-rate vector), the system can be calibrated for its major parameters without the need for costly test equipment which would ordinarily be needed to precisely position the system during the calibration process. (That is, precise positioning of the system with respect to the gravity and earth-rate vectors is not needed because enough relations between the components of gravity and earth-rate sensed by the instruments and the respective known magnitudes of the gravity and earth-rate vectors at the test location are known in addition to the relations between instrument parameters and measurements to allow solution of the parameters from a complete set of simultaneous equations.) The calibration is for large values of the parameters, consistent with the assembly of a low cost system from inertial components that have only been coarsely pre-calibrated (on, say, a "go-no go" basis). Calibration estimation errors are small and meet the requirements of the particular LCIGS described in the introductory chapter. Table 7-1 lists the range of calibratable parameters and the associated estimation errors obtained from the simulations in Chapter 6.

Accelerometers		
Parameter	Parameter Range	Estimation Error
Bias	$\pm 10,000 \mu\text{g}$	16 $\mu\text{g}$ for 10 $\mu\text{g}$ meas. noise
Scale Factor Error	$\pm 60,000 \text{ ppm}$	17 ppm for 10 $\mu\text{g}$ meas. noise
Gyroscopes		
Parameter	Parameter Range	Estimation Error
Bias	$\pm 50^\circ/\text{hr}$	< $0.5^\circ/\text{hr}$
Spin Axis Mass Unbalance	$\pm 500/\text{hr/g}$	< $0.5^\circ/\text{hr}$
Input Axis Mass Unbalance	$\pm 500/\text{hr/g}$	< $1^\circ/\text{hr}$
Scale Factor Error	$\pm 50,000 \text{ ppm}$	< 150 ppm
Input Axis Misalignment	$\pm 2000 \text{ arc-sec}$	< 60 arc-sec

Table 7.1-1 Calibrated Parameters

Accelerometers $\pm 10^\circ$  with respect to nominal orientationsGyros $\pm 1/2^\circ$  in leveling $\pm 20^\circ$  in azimuth

Table 7.1-2 Calibration Position Accuracies

Positioning accuracies for the system in terms of recommended maximum deviations from the nominal system orientations are given in Table 7.1-2.

The absence of the need for fine tolerances in both constructing the system test hardware and in controlling the test orientations during calibration is obvious.

Concommittant with the use of geometrical properties mentioned above is the organization of the gyro test sequence into a series of static orientations during which the effects of gyro static parameters predominate interspersed with rotations of the system during which the effects of gyro dynamic parameters (scale factor error and input axis misalignments) predominate. This dominance of either class of error source allows use of the post-data-collection corrections described in Chapter 4. This permits use of simple 3-state Kalman filters for estimating lumped static drifts and 2-state Kalman filters for estimating lumped dynamic drifts. Thus, software is appreciably reduced over what would have been needed for Kalman filters that are required to estimate a much larger number of states. A further contribution to the low cost implementation of reference unit calibration is thereby made through greatly reduced software.

The original impetus for research into new calibration techniques for the inertial reference unit was the desire for reduction in calibration time over the more "traditional" methods discussed in Chapter 1. To this end the investigation into accelerometer quantization effects and their reduction, presented in Chapter 3, was conducted as part of the overall strategy of minimizing data collection time. The linear extrapolation method developed in Chapter 3 is capable of reducing the accelerometer module quantization by greater than an order of magnitude according to the results given in Chapter 6. This reduction in quantization definitely helps to lower the accel-

erometer calibration time. It can be expected to lower gyro calibration time (see Chapter 3) depending on the base-motion actually encountered at the calibration test station. Also, a good deal of base motion (i.e., vibration) isolation is obtained from the use of the strapdown system attitude algorithm as explained in Chapter 4. Shortened gyro drift estimation times result because the effective base motion that must be averaged out of the data is much attenuated over the vibration present in the raw gyro outputs. Finally, with respect to minimum calibration time, we can point out that the plan we have followed of obtaining lumped drift estimates through Kalman filter processing and then using this data to solve for the desired parameters from a minimum number of deterministic simultaneous equations always ensures that the minimum possible number of static system orientations and rotations has been employed during the calibration. Table 7.1-3 lists the estimated LCIGS calibration times.

Accelerometers:

1/2 min. each static position

Gyros:

1 min. each static position

10 sec. each nominal rotation

Table 7.1-3 LCIGS Calibration Time

To re-iterate, the above summary of the thesis accomplishments suggests more than a series of interrelated innovations that are convenient to use in calibrating a low cost system with easily operatable low cost test

equipment in the field and in a relatively short period of time. These were the initial goals for the LCIGS described in Chapter 1. The larger implication is that pre-testing and calibration of individual instruments (accelerometers and gyros) can be kept to a bare minimum ("go-no go" type) before assembly of the components into an inertial reference unit. This philosophy of calibrating essentially only at the reference unit level should result in large savings in test time and in the attendant large expenses of testing.

Application of the innovations developed has been to calibrate a real system (LCIGS) having its own particular set of characteristics which obviously is not completely coincident with the set of properties of some other inertial guidance strapdown system. However, it is believed by the author that the major parameters (especially g-sensitive terms) common to any system of the LCIGS generic type have been adequately dealt with by the theory of this thesis. Furthermore, expansion of the calibration techniques to include additional parameters (for example, gyro output axis mass unbalance drift coefficients) at the expense of more system test positions and/or rotations is straightforward although there can be the extra burden of poorer numerical conditioning of calibration equations than is true for the nominal test positions and rotations developed in this thesis. Also, depending on the complexity and sensitivity of the calibration error models, the theory already developed does not rule out any additional procedures after first correcting the system with initial parameter estimates from the coarser but larger magnitude error models dealt with here.

## 7.2 Recommendations for Testing Hardware and Test Procedures

Recommendations for actual LCIGS calibration procedures and a general description of the hardware needed to carry out these procedures are pre-

sented below.

Although some of the nominal system orientations for accelerometer calibration coincide with some nominal orientations for gyro testing, it is advisable to test the accelerometers first (ignoring the gyros) with the complete nominal "up-down" sequence presented in Chapter 2. Corrections using the calibrated accelerometer biases and scale factor errors are then made before starting the gyro test sequence. (Although calibration of the accelerometer misalignments is not needed for LCIGS because of repackaging of the accelerometers described in Chapter 2, there is also the need, in the general case, for accelerometer misalignment calibration.) The reasons for initiating the tests in this manner are two-fold. First, an accurate orthogonal reference frame using only the newly calibrated accelerometers is established for use in gyro calibration. Theoretically, this need not be done but the simplifications in the calibration equations (Chapters 4 and 5) that arise by establishing the accelerometer orthogonal reference frame separately before calibrating the gyros is worth the extra time in carrying out a fully separate accelerometer test sequence. Second, the accelerometer calibration sequence is quite insensitive to large deviations (see Table 7-2) from the nominal positions. This allows use of calibrated accelerometers alone to establish the more stringent leveling conditions for the gyro test sequence even though the test fixture base may not have been initially leveled enough for gyro testing but still leveled well within the requirements for accelerometer testing.

Nominal system test positions for the static orientations are defined in Chapters 4 and 5. These orientations are for the body reference axes of the system. The system itself must be mounted on the inner gimbal of a three gimbal arrangement so that the system body axes can be made to con-

form to the desired arrangement through driving the proper sets of gimbal axes. (It is assumed that the three gimbal set has a motor driving each axis.)

An Euler angle sequence must be set up for driving the system. The sequence is necessary to arrive at each static test position. Note that the dynamic gyro test data is always obtained by driving the system about a single gimbal axis although it is preferable, in order to save test time, to drive the gimbals simultaneously at least about two different axes to get from one static orientation to another when dynamic test data is not involved.

Machining tolerances for the gimbals and other associated equipment for orienting the system need only be compatible with the liberal tolerances listed in Table 7-2.

According to the theory of Chapter 4, it is not strictly necessary to drive the gimbals at a constant speed during a data taking interval for dynamic calibration. However, constancy of angular speed allows simplification of software because we need only then post-correct for unmodeled constant drifts in the Kalman filters. Simplified calculations based on a rotation rate of  $9^0/\text{sec}$  and a 50,000 ppm scale factor error show that motor speed need be constant only to 0.1%.

If the gimbals can be always initialized the same way (say by a suitable use of stops), then the gimbal drive motor commands can be derived open loop and pre-programmed with respect to magnitude and duration. Note that there will be a non-constant speed during the start up and stopping of any particular gimbal rotation. However, dynamic calibration data need only be taken during the constant speed portion of the motion. The azimuth tolerance (Table 7.1-2) of  $\pm 20^0$  for deviation of the principal

reference axis of the test fixture with respect to north allows handling of this alignment in a number of ways. An obvious self-contained method is one of a number of versions of the "east-west averaging" techniques originally used for gimballed inertial measurement units. The author does not recommend this approach because of the additional time and software required for its' implementation. Instead it appears feasible to pre-survey the test-site (in field or laboratory) using only very crude methods (such as a simple magnetic compass) to establish a rough ( $\pm 20^{\circ}$ ) north direction.

### 7.3 Suggested Future Research Topics

For complete theoretical satisfaction it may be desirable to develop a more encompassing set of conditions which guarantees convergence of the Newton-Raphson iteration than was presented in Chapter 5, Section 5.3.

Also, further investigation is required to determine the best method for estimating the input-axis mass unbalance coefficient of the third gyro and its proper combination with the  $\Delta_{i3}$  mass unbalance terms already estimated with the procedures given in Chapter 5.

The simulations in Chapter 6 and theoretical error predictions in the earlier chapters assumed the relatively benign test environment as taken from Weinstock in Chapter 2. In event of much harsher environmental vibrations (as typified by sway of a vehicle in which a system may be mounted), the Kalman filters used in the gyro calibration and the averaging procedure used in accelerometer calibration would have to be suitably modified. Therefore, more information must be assembled about potential environments and the necessary calibration procedure modifications made.

Additional experiments with actual hardware are needed to check the

following concerns about the linear extrapolation technique for reducing accelerometer quantization.

(i) linear extrapolation errors in the presence of sinusoidal inputs plus a large constant bias.

(ii) efficacy of the technique in reducing gyro calibration times.

Furthermore, the error models used in this thesis for both accelerometers and gyros had to neglect (due to scanty data) transient effects in the instruments when rotating the instrument from one static position to another. The effects of temperature and system temperature gradient changes also had to be neglected. It is believed that all of these effects will be second order, but they must be determined from system hardware in order to adequately assess the calibration errors with a real system.

Actual design of the test equipment briefly described in the previous Section 7.2 must be undertaken. Questions of how to maintain low cost for the test equipment in order to take advantage of loose manufacturing tolerances must be carefully considered. For example, would it be cheaper to mold the gimbals out of plastic rather than use aluminum construction? Also, what type of gimbal axis motors should be used? These and other questions can be answered by a systematic design of the test hardware.

With respect to the application of the thesis results to the assembly of systems from "raw" instruments, a number of research questions arise:

(i) What constitutes adequate "go-no go" tests for passing a raw instrument onto final assembly?

(ii) What are the exact economic trade-offs in doing most of the calibration at the inertial reference unit level?

(iii) What are the new operational, logistical and reliability problems and solutions involved?

A concrete concern that is illustrative of the generalities stated in (ii) and (iii) above is how to manage calibration when an inertial instrument has failed while in the system. Will partial testing of the system with the replacement instrument suffice? What should be done with the damaged unit? (Throw it away? Try to repair it with a "go-no go" criterion for successful repair? Have more complete component test facilities for only failed instruments? And so on...)

Research into the means for systematically expanding the calibration procedures to handle additional gyro and accelerometer parameters not directly considered in this thesis is of interest.

Recently some work on a general theory of handling large numbers of inertial instrument parameters has been initiated with as yet no definitive results relating the numerical conditioning of calibration equations to the parameters being calibrated.<sup>43</sup> It can be seen from the analyses made in this thesis that definitive results can be found if, instead of rotating the system continuously to excite all the parameters, the system is rotated to various sets of static orientations so that the effects of gyro (and accelerometer) dynamic and static error parameters are decoupled to first order. During static intervals the statistical aspects of the problem involve processing lumped drifts. Analogous remarks apply to those rotations used to obtain dynamic parameter data. The point is that the resulting sets of non-statistical (deterministic) equations using the pre-statistically processed lumped data can easily be examined using the results of classical numerical analysis. The research needed is to relate those static and dynamic parameters to the necessary static orientations and specific dynamic rotations. This is best done in a systematic way.

There is an obvious example, however, which comes to mind without any

use of any systematic rules, that shows how the calibration procedures can be expanded and how the resulting numerical conditioning is affected. In the case of gyro scale factor error asymmetry, three nominal counter rotations need only be added to the nominal set of rotations already in use (Chapter 5). Numerical conditioning remains excellent (i.e., the same) because each of the additional rows of nominal coefficients introduced into what is now a  $12 \times 12$  matrix (for solving for the dynamic parameters) is orthogonal to any other row. In direct contrast to the preceding, calibration of scale factor asymmetries in the accelerometers (i.e., asymmetries not necessarily due to the V/F converters) can be handled by additional static system test positions but with a decrease in the quality of the numerical conditioning if no scale factor asymmetry had to be calibrated in this manner. The new required test positions in this latter case would appear to best be determined from the systematic general procedure alluded to at the beginning of this discussion.

Extension of the theory proposed here does not, of course, rule out use of two tiered calibration procedures. At the cost of increased calibration time, the system, corrected for its primary error parameters, can then be run through a second (and possibly a different) set of rotations and static orientations for calibration of additional, more subtle parameters.

Appendix 2A - Matrix Norms and the Condition Number of a Matrix<sup>20,21</sup>

The norm of a vector is a generalized concept of length. If  $\underline{x}$  denotes the vector, then the norm  $\|\underline{x}\|$  is a scalar defined to satisfy the following properties:

$$(1) \|\underline{x}\| > 0 \text{ for } \underline{x} \neq \underline{0} \text{ and } \|\underline{0}\| = 0$$

$$(2) \|c\underline{x}\| = |c| \|\underline{x}\| \text{ for any numerical value } c \text{ where } |c| \text{ is the absolute value}$$

$$(3) \|\underline{x} + \underline{y}\| \leq \|\underline{x}\| + \|\underline{y}\|, \text{ triangular inequality}$$

A norm  $\|\underline{x}\|_p$  can be assigned to the vector  $\underline{x}$ , using the following definition

$$\|\underline{x}\|_p \triangleq \left( |x_1|^p + |x_2|^p + \dots + |x_n|^p \right)^{1/p}, \quad p \geq 1 \quad (2A-1)$$

where

$$\underline{x} \triangleq (x_1, x_2, \dots, x_n)^T \quad (2A-2)$$

and  $|x_i|$  denotes the absolute value of  $x_i$ .

Three different vector norms, corresponding to  $p=1, 2, \infty$  are commonly used in numerical analysis.

$p = 1$  vector norm:

$$\|\underline{x}\|_1 \triangleq |x_1| + |x_2| + \dots + |x_n| \quad (2A-3)$$

$p = 2$  vector norm (euclidian norm):

$$\|\underline{x}\|_2 \triangleq \sqrt{x_1^2 + x_2^2 + \dots + x_n^2} \quad (2A-4)$$

$\|\cdot\|_\infty$  vector norm:

$$\begin{aligned} \|\underline{x}\|_\infty &\triangleq \max_i(|x_1|, |x_2|, \dots, |x_n|) \\ &= \lim_{p \rightarrow \infty} (|x_1|^p + |x_2|^p + \dots + |x_n|^p)^{1/p} \end{aligned} \quad (2A-5)$$

The norm  $\|A\|$  of a square matrix A is a scalar defined to satisfy the following properties.

- (1)  $\|A\| > 0$  for  $A \neq 0$  and  $\|0\| = 0$
- (2)  $\|cA\| = |c| \|A\|$  for any numerical value c
- (3)  $\|A+B\| \leq \|A\| + \|B\|$
- (4)  $\|AB\| \leq \|A\| \|B\|$

The norm of a matrix is said to be compatible (or consistent) with a given vector norm when the following inequality holds:

$$\|A\underline{x}\| \leq \|A\| \|\underline{x}\| \quad (2A-6)$$

The matrix norm  $\|A\|_p$  is defined to be compatible with the vector norm  $\|\underline{x}\|_p$  given by (2A-1). i.e.,

$$\|A\underline{x}\|_p \leq \|A\|_p \|\underline{x}\|_p \quad (2A-7)$$

Three matrix norms that are respectively compatible with the  $\rho = 1, 2, \infty$  vector norms given by (2A-3) - (2A-5) are defined as follows, where  $a_{ik}$  denotes an element of A.

$\rho = 1$  matrix norm:

$$|A_1| \triangleq \max_{k=1}^n \sum_{i=1}^m |a_{ik}| \quad \text{the maximum sum of the absolute values of the elements in a column} \quad (2A-8)$$

absolute values of the elements in a column

$\rho = 2$  matrix norm (spectral radius):

$$|A|_2 \triangleq \max_i |\lambda_i(A)| \quad \begin{array}{l} \text{the largest magnitude eigenvalue of } A \\ \lambda_i(A) = i^{\text{th}} \text{ eigenvalue of } A \end{array} \quad (2A-9)$$

$\rho = \infty$  matrix norm:

$$|A|_\infty \triangleq \max_i \sum_{k=1}^n |a_{ik}| \quad \text{the maximum sum of the absolute values of the elements in a row} \quad (2A-10)$$

the absolute values of the elements in a row

An important property of  $|A|_2$  is that it cannot exceed the value of the norms of matrix A. In particular,

$$|A|_2 \leq |A|_\infty \quad (2A-11)$$

A useful theorem concerning the inverse matrix  $(I + A)^{-1}$  is the following.

The equality

$$(I + A)^{-1} = I - A + A^2 - A^3 + A^4 - \dots \quad (2A-12)$$

holds and the series on the right hand side of (2A-12) converges if

$$\|A\|_2 < 1 \quad (2A-13)$$

Thus, the equality is also true if

$$\|A\|_\infty < 1 \quad (2A-14)$$

If (2A-3) is valid, we also have the relation

$$\|(I+A)^{-1}\|_2 \leq \frac{1}{1-\|A\|_2} \quad \|A\|_2 < 1 \quad (2A-15)$$

Likewise

$$\|(I+A)^{-1}\|_\infty \leq \frac{1}{1-\|A\|_\infty} \quad \|A\|_\infty < 1 \quad (2A-16)$$

The condition number  $k(A)$  for a square matrix  $A$  is a measure of the relative change in magnitude of the solution of the linear equation set

$$A \underline{x} = \underline{y} \quad (2A-17)$$

resulting from either perturbations in the elements of  $A$  or in the components of  $\underline{y}$ .

For zero perturbations, the solution of (2A-17) is given by

$$\underline{x} = A^{-1} \underline{y} \quad (2A-18)$$

A perturbation  $\delta \underline{y}$  in  $\underline{y}$  results in a change in the solution given by

$$\delta \underline{x} = A^{-1} \delta \underline{y} \quad (2A-19)$$

Taking the appropriate  $\|\cdot\|_2$  norm yields

$$\|\delta \underline{x}\|_2 \leq \|A^{-1}\|_2 \|\delta \underline{y}\|_2 \quad (2A-20)$$

Also we see from (2A-17) that

$$\|\underline{y}\|_2 \leq \|A\|_2 \|\underline{x}\|_2 \quad (2A-21)$$

Multiplying (2A-20) by (2A-21) results in

$$\|\delta \underline{x}\|_2 \|\underline{y}\|_2 \leq \|A^{-1}\|_2 \|A\|_2 \|\delta \underline{y}\|_2 \|\underline{x}\|_2 \quad (2A-22)$$

or

$$\frac{\|\delta \underline{x}\|_2}{\|\underline{x}\|_2} \leq \|A^{-1}\|_2 \|A\|_2 \frac{\|\delta \underline{y}\|_2}{\|\underline{y}\|_2} \quad (2A-23)$$

The condition number

$$\kappa_2(A) \triangleq \|A^{-1}\|_2 \|A\|_2 \quad (2A-24)$$

is thus a direct measure of the relative change in the solution for a relative change in the right hand side of (2A-18).

In the event of a perturbation  $\delta A$  to the matrix  $A$ , we have

$$\underline{x} + \delta \underline{x} = (A + \delta A)^{-1} \underline{y} \quad (2A-25)$$

Combining (2A-25) and (2A-18) yields

$$\underline{\delta x} = ((A + \delta A)^{-1} - A^{-1}) \underline{y} \quad (2A-26)$$

But

$$\begin{aligned} (A + \delta A)^{-1} - A^{-1} &= A^{-1}(A - (A + \delta A))(A + \delta A)^{-1} \\ &= -A^{-1}\delta A(A + \delta A)^{-1} \end{aligned} \quad (2A-27)$$

as can be verified by direct multiplication of the matrices to the right of the first equal sign in (2A-27).

Substituting (2A-27) into (2A-26) leads to

$$\underline{\delta x} = -A^{-1}\delta A(A + \delta A)^{-1}\underline{y} \quad (2A-28)$$

Substituting (2A-25) into (2A-28) and taking  $\|\cdot\|_2$  norms yield

$$\frac{\|\underline{\delta x}\|_2}{\|\underline{x} + \underline{\delta x}\|_2} \leq \|A^{-1}\|_2 \|\delta A\|_2 \quad (2A-29)$$

or

$$\frac{\|\underline{\delta x}\|_2}{\|\underline{x} + \underline{\delta x}\|_2} \leq \|A^{-1}\|_2 \|A\|_2 \frac{\|\delta A\|_2}{\|A\|_2} \quad (2A-30)$$

so that

$$\frac{\|\underline{\delta x}\|_2}{\|\underline{x} + \underline{\delta x}\|_2} \leq \kappa_2(A) \frac{\|\delta A\|_2}{\|A\|_2} \quad (2A-31)$$

and the condition number is also a direct measure of the relative change in the solution for a relative change in matrix  $A$  (as characterized by the appropriate norms).

The condition number has a minimum value of 1 which occurs for orthogonal matrices. The "numerical conditioning" of a linear system of equations such as (2A-17) is characterized by  $k(A)$ . A smaller condition number means better numerical conditioning.

Appendix 2B - The LCIGS Accelerometer Module

This appendix describes those features of the LCIGS accelerometer module required to evaluate the application of the accelerometer calibration techniques presented in this chapter to the LCIGS.

Figure 2B-1 is a block diagram of the LCIGS accelerometer module<sup>41</sup>

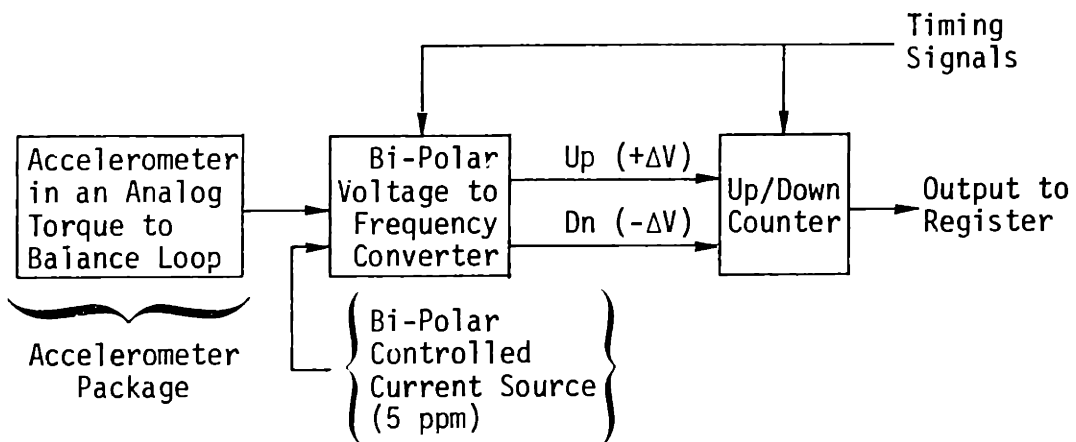
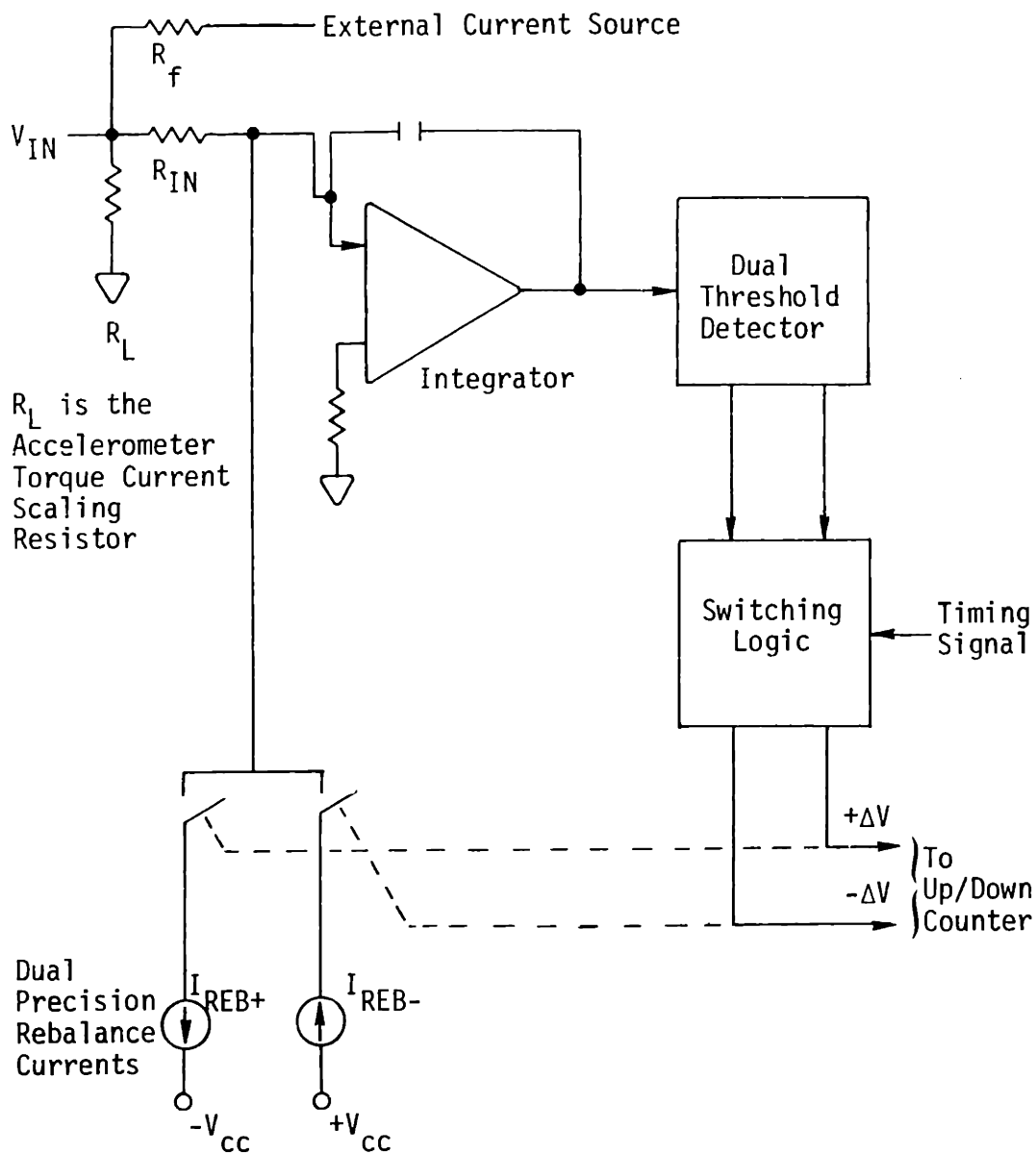


Figure 2B-1 - LCIGS Accelerometer Module Block Diagram

The module consists of a low cost integrating accelerometer in an analog torque-to-balance loop, a bi-polar voltage-to-frequency (V/F) converter, and an up/down counter. The voltage output of the analog torque-to-balance loop is directly proportional to the specific force sensed by the accelerometer. This output is fed to the voltage-to-frequency converter whose dual output yields one of two series of pulses, depending on the polarity of the input, whose frequency is proportional to the input voltage. One series of pulses is counted up when the input to the V/F converter is positive. The other series is counted down. The net result is a digital representation of the integral of the specific force sensed by the accelerometer.

Figure 2B-2 is a block diagram of the V/F converter.

Figure 2B-2 - Bi-Polar V/F Converter Block Diagram

A charge balancing method is employed as the operating principle. The input signal is integrated by an operational amplifier configuration whose output is fed to a dual threshold detector. When either the positive or negative detector threshold is crossed, a positive or negative pulsed current source, depending on the threshold, pulls a

current pulse out of the summing junction to the integrator. The current pulse is controlled by precise timing. The current pulse's magnitude and duration are such that the total charge removed is directly proportional to the nominal weight of the V/F pulse output triggered by the detector. The total count of output pulses, properly weighted, is the accurate integral of the input signal. Reference to this description of the V/F converter will also be made when dealing with the accelerometer module output quantization in Chapter 3.

It is believed that the accelerometer package (accelerometer in a torque-to-balance loop) shown in Figure 2B-1 can be accurately modeled by a bias  $b$ , scale factor error SF, and  $g^2$  sensitive coefficient G in the following equation<sup>3</sup>

$$a_{\text{out}} = b + (1 + SF)a_{\text{in}} + \text{sgn}(a_{\text{in}})G a_{\text{in}}^2 + U_a \quad (2B-1)$$

where

$a_{\text{out}}$   $\triangleq$  specific force indicated by accelerometer package output

$a_{\text{in}}$   $\triangleq$  true specific force sensed by accelerometer

$U_a$   $\triangleq$  uncertainties not accounted for by  $b$ , SF, and G

$\text{sgn}(a_{\text{in}})$   $\triangleq$  sign of  $a_{\text{in}}$

Because of the bi-polar design, the model for the V/F converter is more complicated. In addition to a bias  $b_v$ , there are both positive and negative scale factors designated  $K_+$  and  $K_-$  respectively, and positive and negative quadratic error coefficients designated  $K_{G+}$  and  $K_{G-}$  respectively. The model equations are

$$v_{out} = \begin{cases} K_+ (b_y + v_{in}) + K_{G+} (v_{in} + b_y)^2 + U_v, & (b_y + v_{in}) > 0 \\ K_- (b_y + v_{in}) + K_{G-} (v_{in} + b_y)^2 + U_v, & (b_y + v_{in}) < 0 \end{cases} \quad (2B-2)$$

where

$v_{in}$   $\triangleq$  output frequency of V/F converter normalized to specific force units

$v_{in}$   $\triangleq$  input to V/F converter normalized to units of specific force

$U_v$  = uncertainties not accounted for by  $K_+$ ,  $K_-$ ,  $K_{G+}$ ,  $K_{G-}$ ,  $b_y$ , in units of specific force.

Specifications <sup>3</sup> of the accelerometer and V/F converter pertinent to the error calculations in Section 2.6 are listed below in Tables 2B-1 and 2B-2. The numbers listed are for the uncalibrated case.

The scale factor assymetry and quadratic coefficients of the V/F converter are of obvious concern. Their unaccounted presence in the V/F converter model (Equation 2B-2) would make the calibration procedure presented in Section 2.3 intractable. That is, 9 nominal system orientations are required to calibrate both the coefficients in the accelerometer model (Equation 2B-1) and the misalignment angles. Theoretically, 6 additional orientations would be the required minimum to include calibration of the scale factor assymetry and quadratic terms. Furthermore, the resultant set of linearized equations corresponding to the 18 orientations would necessarily be ill-conditioned because of the obvious difficulty in meeting the requirements for well-conditioned equations outlined in Section 2.4. Fortunately, the scale factor assymetry and large quadratic terms of the V/F converter can be calibrated without

the need for additional system orientations through the use of an available bi-polar controlled current source indicated in both of the above block diagrams. This separate input to the V/F converter adds to any input from the accelerometer. Alternatively, the accelerometer loop torquing current can also be disconnected. A variety of test inputs is, therefore, possible without the need for additional system orientations.

Table 2B-1 - Pertinent LCIGS Accelerometer Specifications<sup>3</sup> -  
Uncalibrated Instrument

Scale Factor Error	$\pm$ 40,000 ppm
Bias (Normalized by 1g)	$\pm$ 5,000 ppm
Non-Linearity (quadratic error coefficient)	< 30 $\mu\text{g/g}^2$
Bias Stability	15 $\mu\text{g}$ ( $1\sigma$ ) over 1 hr.
Scale Factor Stability	15 ppm ( $1\sigma$ ) over 1 hr.

Table 2B-2 - Pertinent LCIGS V/F Converter Specifications<sup>3</sup> -  
Uncalibrated Unit

Scale Factor Error	$\pm$ 20,000 ppm
Bias (Normalized by 1g)	$\pm$ 5,000 ppm
Non-Linearity (quadratic error coefficient)	< 400 $\mu\text{g/g}^2$
Bias Stability*	15 $\mu\text{g}$ ( $1\sigma$ ) over 1 hr.
Scale Factor Stability	15 ppm ( $1\sigma$ ) over 1 hr.

(\*Revised estimate by G. Bukow, Reference 12)

The V/F converter bias term which is given either by  $K_+ b_v$  or  $K_- b_v$ , depending on bias polarity, can be determined by measuring the output of the V/F converter without the input from the accelerometer and with the V/F controlled current source input set to zero. The result is

$$v_{out}^c = \begin{cases} K_+ b_v + K_{G+} b_v^2 + U_v^c, & v_{out}^c > 0 \\ K_- b_v + K_{G-} b_v^2 + U_v^c, & v_{out}^c < 0 \end{cases} \quad (2B-3)$$

Since (Table 2B-2)  $b_v$  is on the order of 5 milli-g magnitude, the  $b_v^2$  terms can be neglected and  $v_{out}^0$  becomes an estimate of either  $K_+ b_v$  or  $K_- b_v$  corrupted by the bias uncertainty  $U_v^0$ , which we take as 15  $\mu g$ ,  $1\sigma$ .

The  $K_{G+}$  coefficient can be estimated using the following procedure<sup>44</sup>.

A minimum of two measurements  $v_{out}^{1+}$  and  $v_{out}^{2+}$  of the V/F converter need be made, with the external current source set for a normalized +1g value in one case and a +2g value in the other case. The bias term, estimated from the procedure previously described (assuming it is positive), is subtracted from each of the two measurements to yield:

$$(v_{out}^{1+} - v_{out}^c) = K_+(I_1 R_v) + K_{G+}(I_1 R_v)^2 + 2 K_{G+}(I_1 R_v) b_v + U_v^{1+} - U_v^c \quad (2B-4)$$

$$(v_{out}^{2+} - v_{out}^c) = K_+(I_2 R_v) + K_{G+}(I_2 R_v)^2 + 2 K_{G+}(I_2 R_v) b_v + U_v^{2+} - U_v^c \quad (2B-5)$$

where

The 5 ppm current source values are in the ratio of 2:1 [ $I_2/I_1 = 2$ ].

$R_v$  is the nominal scaling for currents  $I_1$  and  $I_2$  that converts  $I_1 R_v$  to a nominal +1g value and  $I_2 R_v$  to a 2g value.

$U_v^{1+}$  is the uncertainty in the V/F converter output for the first measurement.

$U_v^{2+}$  is the uncertainty in the V/F converter output for the second measurement.

Solution of (2B-4) and (2B-5) yields

$$\begin{aligned} K_{G+}(I_1 R_v)^2 &= \frac{(V_{out}^{2+} - V_{out}^c)}{2} - (V_{out}^{1+} - V_{out}^c) \\ &- \frac{U_v^{2+}}{2} + U_v^{1+} - \frac{U_v^c}{2} - U_{I_1/I_2} \end{aligned} \quad (2B-6)$$

where the product  $(I_1 R_v)$  is retained as single entity because the scale factor resistor  $R_v$  is not calibrated.

Also

$U_{I_1/I_2}^{\Delta}$  = uncertainty in  $(I_1/I_2) (I_2 R_v)$  due to the uncertainty in the ratio of  $I_1/I_2$ .

If  $I_1$  and  $I_2$  are each considered to have a standard deviation of 5 ppm, then for  $I_1 R_v$  nominally at 2g,  $U_{I_1/I_2}$  has a standard deviation given by

$$\sigma_{U_{I_1/I_2}} = 7 \text{ mg}$$

Also, using the data in Table 2A-2 for bias and scale factor stability,

$$\sigma_{U_v^{1+}} \stackrel{\Delta}{=} \text{standard deviation of } U_v^{1+} = 21 \mu\text{g}$$

$$\sigma_{U_v^{2+}} \stackrel{\Delta}{=} \text{standard deviation of } U_v^{2+} = 33.5 \mu\text{g}$$

$$\sigma_{U_v^0} \stackrel{\Delta}{=} \text{standard deviation of } U_v^0 = 15 \mu\text{g}$$

The standard deviation  $\sigma_{KG+(I_1 R_v)^2}$  in the estimate of  $K_{G+}(I_1 R_v)^2$

is therefore given by

$$\sigma_{KG+(I_1 R_v)^2} \approx 28.5 \mu\text{g} \quad (2B-7)$$

Estimation of  $K_{G-}$  is not as straightforward when the bias is positive as we have chosen. Furthermore, separate calibration of  $K_+$  and  $K_-$  cannot be done accurately because the coefficients of the  $K_+$  and  $K_-$  terms must be known with an error that is far smaller than the error tolerance of the nominal scaling  $R_v$  of the controlled current. Note that  $K_+$  and  $K_-$  are on the order of 1 when normalized with respect to 1g whereas  $K_{G+}$  and  $K_{G-}$  are of sufficiently small magnitude so that we can, without appreciable error, use the nominal value of  $R_v$  when computing their coefficients. Instead, the ratio  $K_+/K_-$  can be estimated. The procedure for then properly employing this ratio in calibrating the accelerometers is presented in Appendix 2C.

Estimates of  $K_+(I_1 R_v)$  and  $K_+(I_2 R_v)$  are required in the next stage

of the V/F converter calibration. Equations (2B-4) and (2B-6) are solved to yield

$$K_+(I_1 R_V) = (V_{out}^{1+} - V_{out}^0) - \left\{ \begin{array}{l} \text{Estimate of} \\ K_{G+}(I_1 R_V)^2 \end{array} \right\} + \frac{U_V^{2+}}{2} + 3/2 U_V^0 + U_{I_1/I_2} - 2K_{G+}(I_1 R_V) b_V \quad (2B-8)$$

The error term  $2K_{G+}(I_1 R_V)$  is, at most,  $4\mu g$  for the  $b_V$  and  $K_{G+}$  values given in Table 2B-2 and is neglected in calculating the standard deviation of  $K_+(I_1 R_V)$ .

The standard deviation  $\sigma_{K_+(I_1 R_V)}$  in the estimate of  $K_+(I_1 R_V)$  is given by

$$\sigma_{K_+(I_1 R_V)} = 27.8 \mu g \quad (2B-9)$$

Once an estimate for  $K_+(I_1 R_V)$  is obtained, an estimate for  $K_{G+}/(K_+)^2$  can be calculated from the estimate of  $K_{G+}(I_1 R_V)^2$  with an error essentially given by (2B-7) but normalized with respect to  $g^2$ .

An estimate of  $K_+(I_2 R_V)$  is obtained by multiplying the estimate of  $K_+(I_1 R_V)$  by  $I_2/I_1$ . The error in this estimate of  $K_+(I_2 R_V)$  is given by twice the error in the estimate of  $K_+(I_1 R_V)$  indicated in Equation (2B-8) plus an additional term  $U_{I_2/I_1}$  representing the uncertainty in  $I_2/I_1$  ( $I_1 R_V$ ) due to the uncertainty in the ratio of  $I_2/I_1$ .

Two additional measurements  $v_{\text{out}}^{1-}$ ,  $v_{\text{out}}^{2-}$  of the V/F converter output are taken with  $I_1$  and  $I_2$  having the same respective magnitudes but opposite polarities from the case presented above. These are (with the bias  $b_v$  assumed positive):

$$\begin{aligned} v_{\text{out}}^{1-} &= -K_-(I_1 R_v) + K_- b_v + K_G (-I_1 R_v + b_v)^2 + U_v^{1-} \\ v_{\text{out}}^{2-} &= -K_-(I_2 R_v) + K_- b_v + K_G (-I_2 R_v + b_v)^2 + U_v^{2-} \end{aligned} \quad (2B-10)$$

where  $U_v^{1-}$  is the uncertainty in  $v_{\text{out}}^{1-}$  and  $U_v^{2-}$  is the uncertainty in  $v_{\text{out}}^{2-}$ .

The equations given by (2B-10) are rewritten below in terms of the quantities  $K_+ I_1 R_v$ ,  $K_+ I_2 R_v$  and  $K_+ b_v$  that were estimated above.

$$v_{\text{out}}^{1-} = -\frac{K_-}{K_+} (K_+(I_1 R_v) - K_+ b_v) + \frac{K_G}{K_+^2} (-K_+(I_1 R_v) + K_+ b_v)^2 + U_v^{1-} \quad (2B-11)$$

$$v_{\text{out}}^{2-} = -\frac{K_-}{K_+} (K_+(I_2 R_v) - K_+ b_v) + \frac{K_G}{K_+^2} (-K_+(I_2 R_v) + K_+ b_v)^2 + U_v^{2-}$$

The terms in the coefficients of the two unknown ratios,  $K_-/K_+$  and  $K_G/K_+^2$  have been estimated as described above. Hence, Equations (2B-11) are readily solved for estimates of  $K_-/K_+$  and  $K_G/K_+^2$ . Denote the combined estimate of  $(K_+(I_1 R_v) - K_+ b_v)$  by

$$\hat{A}_1 \triangleq (\text{estimate of } K_+(I_1 R_v)) - (\text{estimate of } K_+ b_v) \quad (2B-12)$$

and the combined estimate of  $(K_+(I_2 R_v) - K_+ b_v)$  by

$$\hat{A}_2 \triangleq (\text{estimate of } K_+(I_2 R_v)) - (\text{estimate of } K_+ b_v) \quad (2B-13)$$

Then the solution of (2B-11) yields

$$\frac{K_{G^-}}{K_+} \approx (\hat{A}_1, (\hat{A}_2 - \hat{A}_1))^{-1} \left[ \left( \frac{\hat{A}_1}{\hat{A}_2} V_{e^+}^{2-} - V_{e^-}^{1-} \right) \right. \\ \left. - \frac{U_v^{2-} + U_r^{1-} - U_v^0 - U_{I_2}/I_1}{2} \right] \quad (2B-14)$$

and

$$\frac{K_-}{K_+} \approx \hat{A}_1^{-1} \left[ \frac{K_{G^-}}{K_+} \hat{A}_1^2 - V_{e^+}^{1-} - \frac{U_v^{2-}}{2} + \frac{U_v^{2+}}{2} + U_r^{1-} - \frac{U_{I_2}/I_1}{2} \right. \\ \left. + U_{I_1}/I_2 \right] \quad (2B-15)$$

The standard deviations listed in Table 2B-2 yield the following estimates for the standard deviations of  $\frac{K_{G^-}}{K_+}$  denoted by  $\sigma_{K_{G^-}/K_+^2}$

and  $K_-/K_+$  denoted by  $\sigma_{K_-/K_+}$

$$\sigma_{K_-/K_+} = 34 \text{ ppm} \quad (2B-16)$$

$$\sigma_{K_{G^-}/K_+^2} = 28.5 \mu g/g^2$$

The standard deviation  $\sigma_{K_{G^-}/K_+^2}$  of  $K_{G^-}/K_+^2$  given by

$$\frac{K_{G^-}}{K_+^2} = \frac{K_{G^-}}{K_+^2} \left( \frac{K_+^2}{K_-^2} \right) \quad (2B-17)$$

is approximately the same as  $\sigma_{K_{G^-}/K_+^2}$  in view of the small values of  $\sigma_{K_-/K_+}$  and the coefficient  $K_{G^-}/K_+^2$ .

Furthermore, consideration of a compensated negative reading from a module (to be described in Appendix C) leads to a combined error given by

$$\left\{ \begin{array}{l} \text{Combined} \\ \text{error} \end{array} \right\} = \frac{U_v^2 + U_{v/I_1/I_2}^2}{2} \quad (2B-18)$$

$$\sigma_{\text{combined error}} \approx 20 \mu\text{g}$$

for a compensated output of

$$\frac{K_r}{K_s} (R_{ij} - \frac{K_G}{K_s^2} R_{ij}^2), R_{ij} \approx -19$$

Appendix 2C - Compensation for Scale Factor Assymetry and  
Quadratic Errors in the V/F Converter

The quadratic error terms and scale factor assymetry introduced by the V/F converter are calibrated according to the procedures described in Appendix 2B. Treatment of these terms in the calibration effort for the entire accelerometer module is as follows:

For a positive reading, the output  $r_{ij}$  is compensated for the positive quadratic term to yield a compensated output  $r_{ij}^{ct+}$

$$r_{ij}^{ct+} \approx r_{ij} - \frac{K_{G+}}{K_+^2} r_{ij}^2, \quad r_{ij} > 0 \quad (2C-1)$$

For a negative reading, compensation is likewise.

$$r_{ij}^{ct-} = r_{ij} - \frac{K_{G-}}{K_-^2} r_{ij}^2, \quad r_{ij} < 0 \quad (2C-2)$$

Furthermore, the ratio,  $K_+/K_-$ , which characterizes the V/F converter scale factor assymetry is used to normalize the accelerometer module outputs in order to produce the effect of estimating the accelerometer parameters with only one scale factor,  $K_{i+}$  [i.e., all negative values of the module output are multiplied by  $K_{i+}/K_{i-}$ ]. We can then assume that the Equations (2.3-6) in Section 2.3 originally written for the direct outputs of the accelerometers need only be modified by multiplying both sides of each equation by the appropriate  $K_{i+}$  value and redefining  $r_{ij}$  as including the  $K_{i+}$  factor. If it is

understood that  $r_{ij}$  is normalized for units of acceleration, then  $K_{i+}$  can also be represented by

$$K_{i+} \stackrel{\Delta}{=} 1 + \Delta K_{i+} \quad (2C-3)$$

also

$$K_{i-} \stackrel{\Delta}{=} 1 + \Delta K_{i-} \quad (2C-4)$$

where  $K_{i+}$  and  $K_{i-}$  are the scale factor errors for positive and negative accelerometer module outputs respectively. The parameters in Equations (2.3-6) are then interpreted as

$$\begin{aligned} b_i &\rightarrow b_i + \Delta K_{i+} b_i = K_{i+} b_i \\ SF_i &\rightarrow SF_i + \Delta K_{i+} SF_i + \Delta K_{i+} \\ \alpha &\rightarrow \alpha + \alpha \Delta K_{i+} = K_{i+} \alpha \\ \gamma &\rightarrow \gamma + \gamma \Delta K_{i+} = K_{i+} \gamma \\ \delta &\rightarrow \delta + \delta \Delta K_{i+} = K_{i+} \delta \\ \Delta r_{ij} &\rightarrow \Delta r_{ij} + \Delta r_{ij} \Delta K_{i+} = K_{i+} \Delta r_{ij} \end{aligned} \quad (2C-5)$$

with the exception that the second order terms in (2.3-6) are to be interpreted as

$$\begin{aligned} SF_2 \alpha &\rightarrow SF_2 \alpha + \Delta K_{2+} SF_2 \alpha = K_{2+} SF_2 \alpha \\ SF_3 \delta &\rightarrow SF_3 \delta + \Delta K_{3+} SF_3 \delta = K_{3+} SF_3 \delta \\ SF_3 \gamma &\rightarrow SF_3 \gamma + \Delta K_{3+} SF_3 \gamma = K_{3+} SF_3 \gamma \end{aligned} \quad (2C-6)$$

Because separation of  $K_{i+}$  and  $K_{i-}$  from the true accelerometer errors is not practical, the accelerometer module output must be compensated with the products of  $K_{i+}$  and the parameters as depicted

by (2C-5). Similar expressions in terms of  $K_{i-}$  are obtained from (2C-5) with multiplication by the available ratio  $K_{i-}/K_{i+}$ .

As suggested by G. Bukow<sup>16</sup>, a small positive bias can be added in the V/F converters so that the composite bias  $K_{i+}b_i$  which also includes the V/F converter bias is always positive. System compensation using the composite parameters in (2C-5) can then be accomplished according to the accelerometer module output characteristic shown below (Figure 2C-1).

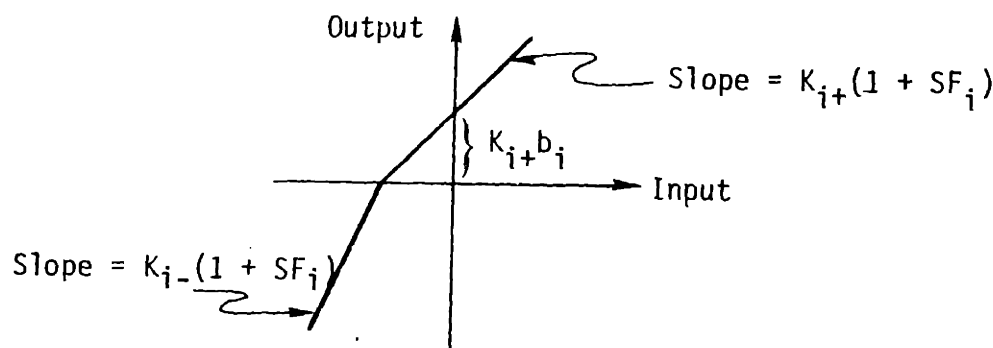


Figure 2C-1: Accelerometer Module Output Characteristic

Composite misalignment terms can be defined as

$$\begin{aligned}\delta' &\triangleq \frac{K_{3+}\delta + K_{3-}\Sigma}{2} \\ \alpha' &\triangleq \frac{K_{2+}\alpha + K_{2-}\alpha}{2} \\ \gamma' &\triangleq \frac{K_{3+}\gamma + K_{3-}\delta}{2}\end{aligned}\tag{2C-7}$$

These composite misalignment estimates are then in error by the terms

$$\frac{(\Delta K_{3+} + \Delta K_{3-})\delta}{2}, \frac{(\Delta K_{2+} + \Delta K_{2-})\alpha}{2}, \frac{(\Delta K_{3+} + \Delta K_{3-})\gamma}{2}$$

respectively.

The irreducible error in estimating  $\delta$ ,  $\alpha$ ,  $\gamma$ , is, therefore, bounded by

$$(2 \times 10^{-2}) (10^{-3}) = 6 \times 10^{-5} \text{ radians}$$

$$= 12 \text{ arc-sec}$$

when  $\delta$ ,  $\alpha$ ,  $\gamma$  are a maximum of 3 mrad and the scale factor error is 20,000 ppm as listed in Table 2B-2 in Appendix 2B.

Matrices and Norms for Gyro Static Parameter Estimation Procedures

Nominal Matrices  $H_1$  and  $H_2$ :

These matrices correspond to the nominal system orientations presented in Section 5.2.

$$H_1 = \begin{bmatrix} I_{3 \times 3} & O_{3 \times 3} & O_{3 \times 2} \\ -I_{3 \times 3} & I_{3 \times 3} & O_{3 \times 2} \\ I_{3 \times 3} & I_{3 \times 3} & O_{3 \times 2} \\ .7 & 0 & .7 \\ 0 & .7 & 0 \\ 0 & 0 & 0 \end{bmatrix} \quad H_2 = \begin{bmatrix} 0 & 1 & 0 & 0 & 0 & 0 \\ -1 & 0 & 0 & 0 & 0 & 0 \\ 0 & 1 & 0 & 0 & -1 & 0 \\ 0 & 0 & -1 & 0 & 0 & -1 \\ 0 & 0 & 1 & 0 & 0 & 0 \\ 1 & 0 & 0 & 0 & 1 & 0 \end{bmatrix}_{3 \times 2} \quad (5A-1)$$

$$H_1^{-1} = \begin{bmatrix} I_{3 \times 3} & O_{3 \times 3} & O_{3 \times 2} \\ -I_{3 \times 3} & I_{3 \times 3} & O_{3 \times 2} \\ 1.4 & 0 & 1.4 \\ 0 & 1.4 & 0 \\ 0 & 0 & 0 \end{bmatrix} \quad H_2 H_1^{-1} = \begin{bmatrix} 0 & 1 & 0 & 0 & 0 & 0 \\ -1 & 0 & 0 & 0 & 0 & 0 \\ 0 & 2 & 0 & 0 & -1 & 0 \\ 0 & 0 & 0 & 0 & -1 & 0 \\ 0 & 0 & 1 & 0 & 0 & 0 \\ 0 & 0 & 0 & 1 & 0 & 0 \end{bmatrix}_{3 \times 2} \quad (5A-2)$$

Matrix  $B(\alpha_j)$ :

$$B(\alpha_j) = (I + [\alpha_j] H_2 H_1^{-1})^{-1}$$

$$= \begin{bmatrix} 1 & \alpha_1 & 0 & 0 & 0 & 0 \\ -\alpha_2 & 1 & 0 & 0 & 0 & 0 \\ 0 & 2\alpha_3 & 1 & 0 & -\alpha_3 & 0 \\ 0 & 0 & 0 & 1 & 0 & -\alpha_4 \\ 0 & 0 & \alpha_5 & 0 & 1 & 0 \\ 0 & 0 & 0 & 0 & \alpha_6 & 0 \\ 0 & 0 & \alpha_7 & 0 & 0 & 1 \\ -3\alpha_8 & 0 & 0 & -7\alpha_9 & 0 & 0 \end{bmatrix}^{-1} \quad (5A-3)$$

$$B(\alpha_j)^{-1} =$$

263

$$\left[ \begin{array}{cccc|ccc} \frac{1}{1+\alpha_1\alpha_2} & 0 & 0 & 0 & 0 & 0 & 0 \\ \frac{\alpha_2}{1+\alpha_1\alpha_2} & 0 & 0 & 0 & 0 & 0 & 0 \\ \frac{-2\alpha_2\alpha_3}{(1+\alpha_1\alpha_2)(1+\alpha_5\alpha_3)} & \frac{-2\alpha_3}{(1+\alpha_1\alpha_2)(1+\alpha_5\alpha_3)} & \frac{1}{1+\alpha_5\alpha_3} & 0 & \frac{\alpha_3}{1+\alpha_5\alpha_3} & 0 & 0 \\ 0 & 0 & 0 & 0 & 0 & 0 & 0 \\ \frac{2\alpha_2\alpha_3\alpha_5}{(1+\alpha_1\alpha_2)(1+\alpha_5\alpha_3)} & \frac{2\alpha_3\alpha_5}{(1+\alpha_1\alpha_2)(1+\alpha_5\alpha_3)} & \frac{-\alpha_5}{1+\alpha_5\alpha_3} & 0 & \frac{1}{1+\alpha_4\alpha_6} & 0 & 0 \\ 0 & 0 & 0 & 0 & 0 & \frac{1}{1+\alpha_5\alpha_3} & 0 \\ \frac{-\alpha_7\alpha_2(1.7+5.1\alpha_5\alpha_3)}{(1+\alpha_3\alpha_5)(1+\alpha_1\alpha_2)} & \frac{-\alpha_7(1.7+5.1\alpha_5\alpha_3)}{(1+\alpha_3\alpha_5)(1+\alpha_1\alpha_2)} & \frac{1.7\alpha_7\alpha_5}{1+\alpha_3\alpha_5} & 0 & 0 & \frac{.7d_7}{1+\alpha_5\alpha_3} & 0 \\ -3\alpha_8 & \frac{.3\alpha_8\alpha_1}{1+\alpha_1\alpha_2} & 0 & 0 & .7d_8 & 0 & .7\alpha_8\alpha_4 \\ \end{array} \right]_{3 \times 2}$$

(5A-4)

Matrix B( $\alpha$ ):

$B(\alpha) =$

$$\left[ \begin{array}{ccc|ccc|c} \frac{1}{1+\alpha^2} & \frac{-\alpha}{1+\alpha^2} & 0 & 0 & 0 & 0 & | & \\ \frac{\alpha}{1+\alpha^2} & \frac{1}{1+\alpha^2} & 0 & 0 & 0 & 0 & | & 0_{3 \times 2} \\ \frac{-2\alpha^2}{(1+\alpha^2)^2} & \frac{-2\alpha}{(1+\alpha^2)^2} & \frac{1}{1+\alpha^2} & 0 & \frac{\alpha}{1+\alpha^2} & 0 & | & \\ \hline 0 & 0 & 0 & \frac{1}{1+\alpha^2} & 0 & \frac{\alpha}{1+\alpha^2} & | & \\ \frac{2\alpha^3}{(1+\alpha^2)^2} & \frac{2\alpha^2}{(1+\alpha^2)^2} & \frac{-\alpha}{1+\alpha^2} & 0 & \frac{1}{1+\alpha^2} & 0 & | & 0_{3 \times 2} \\ 0 & 0 & 0 & \frac{-\alpha}{1+\alpha^2} & 0 & \frac{1}{1+\alpha^2} & | & \\ \hline \frac{-\alpha^2(1.7+5.1\alpha^2)}{(1+\alpha^2)^2} & \frac{-\alpha(1.7+5.1\alpha^2)}{(1+\alpha^2)^2} & \frac{1.7\alpha^2}{1+\alpha^2} & 0 & \frac{.7\alpha}{1+\alpha^2} & 0 & | & 1 \ 0 \\ \frac{-3\alpha}{1+\alpha^2} & \frac{-3\alpha^2}{1+\alpha^2} & 0 & \frac{.7\alpha}{1+\alpha^2} & 0 & \frac{.7\alpha^2}{1+\alpha^2} & | & 0 \ 1 \end{array} \right] \quad (5A-5)$$

Upper Bound on  $|B(\alpha)|_2$

$B(\alpha)$ , (equation (5A-5)), is equal to the sum of a lower triangular matrix  $B_1(\alpha)$  and a very sparse matrix  $B_2(\alpha)$

$$B(\alpha) = B_1(\alpha) + B_2(\alpha) \quad (5A-6)$$

where

$$B_2(\alpha) = \begin{bmatrix} 0 & -\frac{\alpha}{1+\alpha^2} & 0 & 0 & 0 & 0 \\ 0 & 0 & 0 & 0 & 0 & 0 \\ 0 & 0 & 0 & 0 & \frac{\alpha}{1+\alpha^2} & 0 \\ \dots & \dots & \dots & \dots & \dots & \dots \\ 0_{3 \times 3} & 0 & 0 & \frac{\alpha}{1+\alpha^2} & 0 & 0 \\ 0 & 0 & 0 & 0 & 0_{3 \times 2} & 0 \\ 0 & 0 & 0 & 0 & 0 & 0_{2 \times 2} \\ \dots & \dots & \dots & \dots & \dots & \dots \\ 0_{2 \times 3} & 0_{2 \times 3} & 0_{2 \times 2} & & & \end{bmatrix} \quad (5A-7)$$

The  $p = 2$  norm of  $B_1(\alpha)$  upon inspection of the lower triangular matrix obtained from (5A-5) by subtracting  $B_2(\alpha)$  is given by

$$|B_1(\alpha)|_2 = 1 \quad (5A-8)$$

Also

$$|B_2(\alpha)|_2 \leq |B_2(\alpha)|_\infty = \frac{|\alpha|}{1+\alpha^2} \quad (5A-9)$$

Hence

$$|B(\alpha)|_2 \leq |B_1(\alpha)|_2 + |B_2(\alpha)|_2 \leq 1 + \frac{\alpha}{1+\alpha^2} \quad (5A-10)$$

But since

$$\frac{|d_1|}{1+\alpha^2} \leq 1/2 \quad (5A-11)$$

$$|B(\alpha)|_2 \leq 1.5 \quad (5A-12)$$

$$H_2 H_i^{-1} B(\alpha_j) =$$

$$\left[ \begin{array}{ccc|ccc|c} \frac{\alpha_2}{1+d_1\alpha_2} & \frac{1}{1+d_1\alpha_2} & 0 & 0 & 0 & 0 & | \\ \frac{-1}{1+d_1\alpha_2} & \frac{\alpha_1}{1+d_1\alpha_2} & 0 & 0 & 0 & 0 & | \\ \frac{2\alpha_2}{(1+\alpha_1\alpha_2)(1+\alpha_5\alpha_3)} & \frac{2}{(1+\alpha_1\alpha_2)(1+\alpha_5\alpha_3)} & \frac{\alpha_5}{1+\alpha_5\alpha_3} & 0 & \frac{-1}{1+d_5\alpha_3} & 0 & | \\ 0 & 0 & 0 & \frac{\alpha_6}{1+d_4\alpha_6} & 0 & \frac{-1}{1+d_4\alpha_6} & | \\ -2\alpha_2\alpha_3 & -2\alpha_3 & 1 & 0 & \frac{\alpha_3}{1+d_3\alpha_3} & 0 & | \\ (1+\alpha_1\alpha_2)(1+\alpha_5\alpha_3) & (1+\alpha_1\alpha_2)(1+\alpha_5\alpha_3) & 1+\alpha_5\alpha_3 & 0 & 0 & 0 & | \\ 0 & 0 & 0 & \frac{1}{1+d_4\alpha_6} & 0 & \frac{\alpha_4}{1+d_4\alpha_6} & | \\ \frac{1.7\alpha_2-3\alpha_2\alpha_3\alpha_5}{(1+\alpha_1\alpha_2)(1+\alpha_5\alpha_3)} & \frac{1.7-3\alpha_2\alpha_5}{(1+\alpha_1\alpha_2)(1+\alpha_5\alpha_3)} & \frac{.7\alpha_5}{1+d_5\alpha_3} & 0 & \frac{-7}{1+d_5\alpha_3} & 0 & | \\ \frac{-3}{1+d_1\alpha_2} & \frac{.3\alpha_1}{1+d_1\alpha_2} & 0 & \frac{-7}{1+d_4\alpha_6} & 0 & \frac{-7\alpha_4}{1+d_4\alpha_6} & | \end{array} \right] \begin{matrix} 0_{3 \times 2} \\ 0_{3 \times 2} \\ 0_{2 \times 2} \end{matrix}$$

(5A-13)

$$H_2 H_1^{-1} B(\alpha) =$$

$$\left[ \begin{array}{ccc|ccc|c} \frac{\alpha}{1+\alpha^2} & \frac{1}{1+\alpha^2} & 0 & 0 & 0 & 0 & \\ \frac{-1}{1+\alpha^2} & \frac{\alpha}{1+\alpha^2} & 0 & 0 & 0 & 0 & \\ \frac{2\alpha}{(1+\alpha^2)^2} & \frac{2}{(1+\alpha^2)^2} & \frac{\alpha}{1+\alpha^2} & 0 & \frac{1}{1+\alpha^2} & 0 & O_{3 \times 2} \\ \hline 0 & 0 & 0 & \frac{\alpha}{1+\alpha^2} & 0 & \frac{1}{1+\alpha^2} & \\ \frac{-2\alpha^2}{(1+\alpha^2)^2} & \frac{-2\alpha}{(1+\alpha)^2} & \frac{1}{1+\alpha^2} & 0 & \frac{\alpha}{1+\alpha^2} & 0 & O_{3 \times 2} \\ 0 & 0 & 0 & \frac{1}{1+\alpha^2} & 0 & \frac{\alpha}{1+\alpha^2} & \\ \hline \frac{1.7\alpha - 3\alpha^3}{(1+\alpha^2)^2} & \frac{1.7 - 3\alpha^2}{(1+\alpha^2)^2} & \frac{.7\alpha}{1+\alpha^2} & 0 & \frac{- .7}{1+\alpha^2} & 0 & O_{2 \times 2} \\ \frac{- .3}{1+\alpha^2} & \frac{.3\alpha}{1+\alpha^2} & 0 & \frac{- .7}{1+\alpha^2} & 0 & \frac{- .7\alpha}{1+\alpha^2} & \end{array} \right]$$

(5A-14)

As shown with  $B(\alpha)$ , the matrix  $H_2 H_1^{-1} B(\alpha)$  given by equation (5A-14) is equal to the sum of a lower triangular matrix  $(H_2 H_1^{-1} B(\alpha))_1$  and a sparse matrix  $(H_2 H_1^{-1} B(\alpha))_2$

$$H_2 H_1^{-1} B(\alpha) = (H_2 H_1^{-1} B(\alpha))_1 + (H_2 H_1^{-1} B(\alpha))_2 \quad (5A-15)$$

where

$$(H_2 H_1^{-1} B(\alpha))_2 = \begin{bmatrix} 0 & \frac{1}{1+\alpha^2} & 0 & 0 & 0 \\ 0 & 0 & 0 & 0 & 0 \\ 0 & 0 & 0 & \frac{1}{1+\alpha^2} & 0 \\ 0_{3 \times 3} & 0 & 0 & \frac{1}{1+\alpha^2} & 0 \\ 0_{3 \times 3} & 0 & 0 & 0 & 0 \\ 0_{2 \times 3} & 0_{2 \times 3} & 0_{2 \times 2} \end{bmatrix} \quad (5A-16)$$

The  $p = 2$  norm of  $(H_2 H_1^{-1} B(\alpha))_1$  upon inspection of the lower triangular matrix obtained from (5A-14) by subtracting  $(H_2 H_1^{-1} B(\alpha))_2$  is given by

$$\|(H_2 H_1^{-1} B(\alpha))_1\|_2 = \frac{|\alpha|}{1+\alpha^2} \quad (5A-17)$$

Also

$$\|(H_2 H_1^{-1} B(\alpha))_2\|_2 \leq \|(H_2 H_1^{-1} B(\alpha))_2\|_\infty = \frac{1}{1+\alpha^2} \quad (5A-18)$$

Hence

$$\begin{aligned} |(H_2 H_1^{-1} B(\alpha))|_2 &\leq |(H_2 H_1^{-1} B(\alpha))_1|_2 + |(H_2 H_1^{-1} B(\alpha))_2|_2 \\ &\leq \frac{1+|\alpha|}{1+\alpha^2} \leq 1.21 \end{aligned} \quad (5A-19)$$

#### Modification of Preceding Matrices to Account for Leveling Perturbations

$\Delta H_1$  and  $\Delta H_2$ :

Of particular interest is the change in the  $p = 2$  norms for the case of non-zero perturbations  $\Delta H_1$  and  $\Delta H_2$  given by (5.2-32). The following development yields the appropriate formulas for the modified matrices:

The modified matrix corresponding to  $B(\alpha)$  is denoted by  $B'(\alpha)$  where

$$\begin{aligned} B'(\alpha) &\stackrel{\Delta}{=} \left[ \left\{ H_1 + \Delta H_1 + [\alpha] (H_2 + \Delta H_2) \right\} (H_1 + \Delta H_1)^{-1} \right]^{-1} \\ &= (H_1 + \Delta H_1) \left[ \left\{ I + (\Delta H_1 + [\alpha] \Delta H_2) (H_1 + [\alpha] H_2)^{-1} \right\} (H_1 + [\alpha] H_2) \right]^{-1} \\ &= (H_1 + \Delta H_1) (H_1 + [\alpha] H_2)^{-1} \left[ I + (\Delta H_1 + [\alpha] \Delta H_2) (H_1 + [\alpha] H_2)^{-1} \right]^{-1} \\ &= (I + \Delta H_1 H_1^{-1}) B(\alpha) \left[ I + (\Delta H_1 + [\alpha] \Delta H_2) (H_1 + [\alpha] H_2)^{-1} \right]^{-1} \end{aligned} \quad (5A-20)$$

Likewise the modified matrix corresponding to  $H_2 H_1^{-1} B(\alpha)$  is denoted by

$$\begin{aligned} (H_2 H_1^{-1} B(\alpha))' &\stackrel{\Delta}{=} (H_2 + \Delta H_2) (H_1 + \Delta H_1)^{-1} B'(\alpha) \\ &= (H_2 + \Delta H_2) (H_1 + [\alpha] H_2)^{-1} \left[ I + (\Delta H_1 + [\alpha] \Delta H_2) (H_1 + [\alpha] H_2)^{-1} \right]^{-1} \\ &= (H_2 H_1^{-1} + \Delta H_2 H_1^{-1}) B(\alpha) \left[ I + (\Delta H_1 + [\alpha] \Delta H_2) (H_1 + [\alpha] H_2)^{-1} \right]^{-1} \end{aligned} \quad (5A-21)$$

A bound on the  $p = \infty$  norm of the inverse in square brackets in (5A-20) and (5A-21) is obtained as follows.

Define

$$\begin{aligned} \|L'\|_{\infty} &\triangleq \|(H_1 + [\alpha] H_2)^{-1}\|_{\infty} \\ \|M\|_{\infty} &\triangleq \|\Delta H_1 + [\alpha] \Delta H_2\|_{\infty} \end{aligned} \quad (5A-22)$$

then

$$\begin{aligned} &\left\| [I + (\Delta H_1 + [\alpha] \Delta H_2)(H_1 + [\alpha] H_2)^{-1}]^{-1} \right\|_{\infty} \\ &\leq \frac{1}{1 - \|L'\|_{\infty} \|M\|_{\infty}} \end{aligned} \quad (5A-23)$$

The matrix  $(H_1 + [\alpha] H_2)^{-1}$  which is the nominal value of  $C_n^{-1}$  without the  $W_1^{-1}$  factor in the iteration defined by equations (5.2-27) - (5.2-30) is given by

$$(H_1 + [\alpha] H_2)^{-1} = \begin{bmatrix} \frac{1}{1+\alpha^2} & \frac{-\alpha}{1+\alpha^2} & 0 & 0 & 0 & 0 & 1 \\ \frac{\alpha}{1+\alpha^2} & \frac{1}{1+\alpha^2} & 0 & 0 & 0 & 0 & 0 \\ \frac{-2\alpha^2}{(1+\alpha^2)^2} & \frac{-2\alpha}{(1+\alpha^2)^2} & \frac{1}{1+\alpha^2} & 0 & \frac{\alpha}{1+\alpha^2} & 0 & 1 \\ \frac{-1}{1+\alpha^2} & \frac{\alpha}{1+\alpha^2} & 0 & \frac{1}{1+\alpha^2} & 0 & \frac{\alpha}{1+\alpha^2} & 1 \\ \frac{-\alpha}{1+\alpha^2} & \frac{-1}{1+\alpha^2} & \frac{-\alpha}{1+\alpha^2} & 0 & \frac{1}{1+\alpha^2} & 0 & 0 \\ \frac{2\alpha^2}{(1+\alpha^2)^2} & \frac{2\alpha}{(1+\alpha^2)^2} & \frac{-1}{1+\alpha^2} & \frac{-\alpha}{1+\alpha^2} & \frac{-\alpha}{1+\alpha^2} & \frac{1}{1+\alpha^2} & 1 \\ \frac{1.4+2\alpha^2+10.2\alpha^4}{(1+\alpha^2)^2} & \frac{-(.8\alpha+10.2\alpha^2+1.4\alpha^3)}{(1+\alpha^2)^2} & \frac{1.4-3.4\alpha^2}{1+\alpha^2} & 0 & 0 & 0 & 1 \\ \frac{-(2\alpha+8\alpha^2+2\alpha^3)}{(1+\alpha^2)^2} & \frac{-(1.4+.8\alpha+.8\alpha^2-.6\alpha^4)}{(1+\alpha^2)^2} & \frac{4}{1+\alpha^2} & \frac{4}{1+\alpha^2} & \frac{4\alpha}{1+\alpha^2} & \frac{1+1.4\alpha^2}{1+\alpha^2} & 0 \end{bmatrix}_{3 \times 2}$$

(5A-24)

Table 5A-1 lists  $|L^{-1}|_\alpha$  and  $|M|_\alpha$  that appear in (5A-23) for various values of  $\alpha = \tan A$  and perturbation magnitude  $\Delta\theta$ .

$\alpha$	$A$	$15^\circ$	$20^\circ$	$25^\circ$	$30^\circ$
		.268	.364	.466	.5
	$ L^{-1} _\infty$	5.79	5.96	6.03	6.33
	$ M _\infty$ $\Delta\theta=1/4^\circ$	.0183	.0197	.0214	.0233
	$\Delta\theta=1/2^\circ$	.0366	.0394	.0428	.0466

Table 5A-1 Values for  $|L^{-1}|_\infty$  and  $|M|_\infty$

Table 5A-2 presents the resultant values for  $1/(1 - |L^{-1}|_\infty|M|_\infty)$  computed from the Table 5A-1 values.

$A$	$15^\circ$	$20^\circ$	$25^\circ$	$30^\circ$
$\Delta\theta=1/4^\circ$	1.12	1.13	1.15	1.17
$\Delta\theta=1/2^\circ$	1.27	1.31	1.35	1.42

Table 5A-2 Values of  $1/(1 - |L^{-1}|_\infty|M|_\infty)$

Upper bounds on  $|\Delta H_1 H_1^{-1}|_\infty$ , and on  $|\Delta H_2 H_1^{-1}|_\infty$  are given in Table 5A-3.

$\Delta\theta$	$1/4^0$	$1/2^0$
Upper Bound on $ \Delta H_1 H_1^{-1} _\infty$	.069	.138
Upper Bound on $ \Delta H_2 H_1^{-1} _\infty$	.081	.162

Table 5A-3 Upper Bounds on  $|\Delta H_1 H_1^{-1}|_\infty$  and  $|\Delta H_2 H_1^{-1}|_\infty$ 

Finally, the results from Tables 5A-2 and 5A-3 are used in conjunction with equations (5A-20) and (5A-21) to compute the modifications to the upper bounds originally presented by equations (5A-12) and (5A-19). These new upper bounds are in turn used to compute the upper bounds to  $|S/2|_2$  and  $|T/2|_2$  with matrices S and T defined by equation (5.3-31) and  $W_1(n-1) = I$ . These results are listed below in Tables 5A-4 and 5A-5.

A	$15^0$	$20^0$	$25^0$	$30^0$
$\Delta\theta=1/4^0$	.88	.91	.922	.94
$\Delta\theta=1/2^0$	1.08	1.12	1.15	1.21

Table 5A-4 Upper Bounds on  $|S/2|_2$  with  $W_1(n-1) = I$ 

A	$15^0$	$20^0$	$25^0$	$30^0$
$\Delta\theta=1/4^0$	.75	.752	.766	.78
$\Delta\theta=1/2^0$	.923	.95	.98	1.03

Table 5A-5 Upper Bounds on  $|T/2|_2$  with  $W_1(n-1) = I$

Matrix  $H_1^{-1} B(\alpha)$ :

(5A-25)

$$H_1^{-1} B(\alpha) =$$

$$\left[ \begin{array}{cccccc|c} \frac{1}{1+\alpha^2} & \frac{-\alpha}{1+\alpha^2} & 0 & 0 & 0 & 0 & \\ \frac{\alpha}{1+\alpha^2} & \frac{1}{1+\alpha^2} & 0 & 0 & 0 & 0 & 0_{3 \times 2} \\ \frac{-2\alpha^2}{(1+\alpha^2)^2} & \frac{-2\alpha}{(1+\alpha^2)^2} & \frac{1}{1+\alpha^2} & 0 & \frac{\alpha}{1+\alpha^2} & 0 & \\ \frac{-1}{1+\alpha^2} & \frac{\alpha}{1+\alpha^2} & 0 & \frac{1}{1+\alpha^2} & 0 & \frac{\alpha}{1+\alpha^2} & \\ \frac{\alpha^3-\alpha}{(1+\alpha^2)^2} & \frac{\alpha^2-1}{(1+\alpha^2)^2} & \frac{-\alpha}{1+\alpha^2} & 0 & \frac{1}{1+\alpha^2} & 0 & 0_{3 \times 2} \\ \frac{2\alpha^2}{(1+\alpha^2)^2} & \frac{2\alpha}{(1+\alpha^2)^2} & \frac{-1}{1+\alpha^2} & \frac{-\alpha}{1+\alpha^2} & \frac{-\alpha}{1+\alpha^2} & \frac{1}{1+\alpha^2} & \\ \frac{(1.4+2\alpha^2}{(1+\alpha^2)^2} + \frac{10.2\alpha^4}{(1+\alpha^2)^2} & \frac{8\alpha(1.1\alpha^2-1)}{(1+\alpha^2)^2} & \frac{(1.4-3.4\alpha^2)}{1+\alpha^2} & 0 & 0 & 0 & -2 0 \\ \frac{-(2\alpha+8\alpha^2}{(1+\alpha^2)^2} + \frac{2\alpha^3}{(1+\alpha^2)^2} & \frac{-(1.4+8\alpha}{(1+\alpha^2)^2} + \frac{8\alpha^2-6\alpha^4}{(1+\alpha^2)^2} & \frac{.4}{1+\alpha^2} & \frac{.4\alpha}{1+\alpha^2} & \frac{.4\alpha}{1+\alpha^2} & \frac{1+1.4\alpha^2}{1+\alpha^2} & 0 2 \end{array} \right]$$

For  $\alpha = \tan 25^\circ$ :

$$\text{abs}(H_1^{-1} B(\alpha)) = \left[ \begin{array}{ccccccc} .82 & .38 & 0 & 0 & 0 & 0 & 0 \\ .38 & .82 & 0 & 0 & 0 & 0 & 0 \\ .29 & .63 & .82 & 0 & .38 & 0 & 0 \\ .82 & .38 & 0 & .82 & 0 & .38 & 0 \\ .25 & .53 & .38 & 0 & .82 & 0 & 0 \\ .29 & .63 & .82 & .38 & .38 & .82 & 0 \\ 1.56 & .35 & .54 & 0 & 0 & 0 & 2 \\ .912 & 1.33 & .33 & .15 & .15 & 1 & 0 2 \end{array} \right]$$

(5A-26)

$$K = \begin{bmatrix} 1.3 & 0 & .65 & 0 & 0 & 0 & .87 & .33 \\ 0 & 1.3 & 0 & .47 & 0 & .87 & .66 & 1.1 \\ .65 & 0 & .65 & 0 & 0 & 0 & .65 & .33 \\ 0 & .47 & 0 & 1.43 & 0 & .47 & 1 & .47 \\ 0 & 0 & 0 & 1.87 & .47 & 0 & .66 & \\ 0 & .87 & 0 & .47 & .47 & 1.87 & .66 & .16 \\ .87 & .66 & .65 & 1 & 0 & .66 & 2.38 & 1 \\ .33 & 1.1 & .33 & .47 & .66 & .16 & 1 & 2.6 \end{bmatrix} \quad \begin{pmatrix} .04 \\ 60 \end{pmatrix} \quad (5A-27)$$

Where  $K$  is the matrix of absolute values of the elements of the noise covariance matrix defined in (5.5-17).

## APPENDIX 5B

Solutions for Input Axis Mass Unbalance Drifts

It was shown in Section 5.2 that estimation of the input axis mass unbalance terms

$$\begin{aligned}\dot{\gamma} \Delta_{13} &\stackrel{\Delta}{=} \dot{\gamma} M_{IA1} - \dot{\gamma} M_{IA3} \\ \dot{\gamma} \Delta_{23} &\stackrel{\Delta}{=} \dot{\gamma} M_{IA2} - \dot{\gamma} M_{IA3}\end{aligned}\quad (5B-1)$$

is sufficient for estimation of the gyro bias, spin axis mass unbalance, scale factor, in the absence of large input axis non-orthogonality terms. When an estimate of the actual input mass unbalance terms themselves is needed, then the  $M_{IA3}$  term must be estimated separately. This allows solution for  $M_{IA1}$  and  $M_{IA2}$  from (5B-1) above.

There are two possible methods for obtaining  $M_{IA3}$ :

First, the output of the z gyro when its input axis is approximately vertical is directly averaged. Knowledge of the other static parameters previously obtained allows direct solution for the  $M_{IA3}$  parameters. This method is particularly sensitive to base motion about azimuth. For example, with a sinusoidal base motion of 2 arc-min amplitude at a frequency of 1 rad/sec about the vertical axis, the angular velocity disturbance to be filtered out is  $120^0/\text{hr}$ . When the z gyro rate output is averaged over an interval of 2 minutes, the maximum error due to this base motion will be  $1^0/\text{hr}$  or approximately  $1^0/\text{hr/g}$  for  $M_{IA3}$ .

Second, a more accurate estimation of  $M_{IA3}$  can be postponed until the LCIGS is ready for flight. Before flight time, an azimuth reference can be obtained using the aircraft master IMU which would then allow estimation of  $M_{IA3}$  without regard for base motion.

### Perturbations of the Elements of Matrix $C_A$

Perturbations of the elements of  $C_A$  defined in equation (5.6-38) arise in three ways. The first is through deviations of the nominal matrices  $C_L^{Ba}$  in equations (5.6-29) - (5.6-31). The second is through coupling of the angular velocity about the axis of rotation of the test fixture to all three body axes (i.e.,  $w_1 \neq 0$ ,  $w_2 \neq 0$ ,  $w_3 \neq 0$  in any of the rotations). The third is through variation of the rotation angle  $\varphi_i$  from the nominal values given in (5.6-29) - (5.6-31).

#### Deviations from the Nominal

At time  $t_0$ , before a rotation, it is assumed that the system is nominally leveled and aligned in azimuth according to the definitions given in Section 4.2, Chapter 4. The level frame at this time is designated by  $L_0$ . Hence,

$$C_{L_0}^{Ba}(t_0) \stackrel{\Delta}{=} I + \Delta_{L_0}^{Ba}(t_0) \quad (5C-1)$$

$$\Delta_{L_0}^{Ba}(t_0) \stackrel{\Delta}{=} \begin{bmatrix} 0 & 0 & -\psi_2 \\ 0 & 0 & \psi_1 \\ \psi_2 & -\psi_1 & 0 \end{bmatrix} \quad (5C-2)$$

where  $\psi_1$  and  $\psi_2$  are the deviations of the body axes from the level position and there is zero azimuth error for alignment to the azimuth reference defined in Chapter 4.

Also,

$$C_{L_0}^{Ba}(t_0) = C_F^{Ba} C_{L_0}^F(t_0) \quad (5C-3)$$

where F designates the test fixture axes to which the system is mounted.

$$C_F^{B_a} \triangleq I + \Omega_F^{B_a} \quad (5C-4)$$

$$\Omega_F^{B_a} \triangleq \begin{bmatrix} 0 & \beta_3 & -\beta_2 \\ -\beta_3 & 0 & \beta_1 \\ \beta_2 & -\beta_1 & 0 \end{bmatrix} \quad (5C-5)$$

where  $\beta_1, \beta_2, \beta_3$  are the misalignment angles between the system body axes and the test fixtures.

The transformation from the level reference frame to the test fixture axes at time  $t_0$  is obtained by substituting (5C-1) and (5C-4) into (5C-3) and neglecting the products of small angles.

$$\begin{aligned} C_{L_0}^F(t_0) &= I + \Omega_{L_0}^B(t_0) - \Omega_F^B \\ &= I + \begin{bmatrix} 0 & -\beta_3 & \beta_2 - \varphi_2 \\ \beta_3 & 0 & -\beta_1 + \varphi_1 \\ -\beta_2 + \varphi_2 & \beta_1 - \varphi_1 & 0 \end{bmatrix} \end{aligned} \quad (5C-6)$$

When the test fixture is rotated about an axis,

$$\tilde{C}_{L_0}(t) = C_{ROT} C_{L_0}^F(t_0) \quad (5C-7)$$

where  $C_{ROT}$  is the transpose one of the nominal  $C_{Ba}^L$  matrices given in (5.6-29) - (5.6-31).

The transformation between the body axes and frame  $L_0$  is, therefore, given by

$$C_{L_0}^{Ba}(t) = C_F^{Ba} C_{L_0}^F(t) = C_F^{Ba} C_{ROT} C_{L_0}^F(t_0) \quad (5C-8)$$

Substituting (5C-4) and (5C-6) into (5C-8) and neglecting products of small angles results in

$$C_{L_0}^{Ba}(t) \approx C_{ROT} + \Omega_F^{Ba} C_{ROT} + C_{ROT} (\Omega_{L_0}^{Ba}(t_0) - \Omega_F^{Ba}) \quad (5C-9)$$

The following definition is made to condense expression (5C-9)

$$\Omega_{L_0}^{Ba}(t) \triangleq \Omega_F^{Ba} C_{ROT} + C_{ROT} (\Omega_{L_0}^{Ba}(t_0) - \Omega_F^{Ba}) \quad (5C-10)$$

so that

$$C_{L_0}^{Ba}(t) = C_{ROT} + \Omega_{L_0}^{Ba}(t) \quad (5C-11)$$

If the level axes are "clamped" to the horizontal projections of the two nominally level body axes during a rotation, then  $C_{L_0}^{Ba}(t)$  must be corrected for any shifts in azimuth of the  $L_0$  frame. The shifted frame is designated by  $L$  so that

$$C_L^{Ba}(t) = C_{L_0}^{Ba}(t) C_L^{L_0}(t) \approx C_{ROT} + C_{ROT} \Omega_L^{L_0}(t) + \Omega_{L_0}^{Ba}(t) \quad (5C-12)$$

neglecting the products of small angles.

In this expression

$$\Omega_L^{L_0}(t) = \begin{bmatrix} 0 & \delta & 0 \\ -\delta & 0 & 0 \\ 0 & 0 & 0 \end{bmatrix} \quad (5C-13)$$

and  $\delta$  is the azimuth shift.

Substitution of (5C-10) into (5C-12) yields

$$C_L^{Ba}(t) = C_{ROT} + C_{ROT} (\Omega_L^{L_0}(t) + \Omega_{L_0}^{Ba}(t_0) - \Omega_F^{Ba}) + \Omega_F^{Ba} C_{ROT} \quad (5C-14)$$

The perturbation to  $C_L^{Ba}(t)$  is therefore,

$$\delta C_L^{Ba}(t) = C_{ROT} (\Omega_L^{L_0}(t) + \Omega_{L_0}^{Ba}(t_0) - \Omega_F^{Ba}) + \Omega_F^{Ba} C_{ROT} \quad (5C-15)$$

The contribution of this perturbation to the perturbations of the first three rows of  $C_A$  is given by

$$\delta h_{Aij}^T = \int_{t_R}^{t_{R+1}} (100) (\delta C_L^{Ba})_j W_j dt \quad (5C-16)$$

where  $j$  denotes one of the rotations (defined by (5.5-16) - (5.5-18)) made for each of the three rows and

$$W_j \triangleq \begin{bmatrix} w_1' & 0 & 0 & 0 & 0 & w_2' & 0 & 0 & w_3' & 0 & 0 \\ 0 & w_2' & 0 & 0 & w_1' & 0 & 0 & 0 & 0 & w_3' & 0 \\ 0 & 0 & w_3' & 0 & 0 & w_1' & 0 & 0 & w_2' & 0 & 0 \end{bmatrix} \quad (5C-17)$$

with  $w_1, w_2, w_3$  taking on the particular values shown in (5.5-16) - (5.5-18) for each value of  $j$ .

Likewise the contribution to the perturbations of the last six rows of  $C_A$  is given by

$$\delta C_{-A2j}^T = \int_{t_R}^{t_{R+1}} (0 \ 1 \ 0) (\delta C_{B_A}^L)_j w_j dt \quad (5C-18)$$

where  $j$  denotes the rotation made for each of the six rows.

A conservative estimate of the perturbation effects is obtained with  $p = \infty$  norms.

After substituting equation (5C-19), with the appropriate transposition of matrices, into equations (5C-16) and (5C-18), the norms of the perturbation  $\delta C_A$  in matrix  $C_A$  are bounded as follows since  $\delta C_{-A1j}^T$  and  $\delta C_{-A2j}^T$  are the rows of  $\delta C_A$  for particular values of  $j$ .

$$\begin{aligned} |\delta C_A|_\infty &\leq \left| \int_{t_R}^{t_{R+1}} C_{ROT} w_j dt \right|_\infty \\ &\times \left\{ |\Omega_L^L|_\infty + |\Omega_{L0}|_\infty + 2 |\Omega_F^F|_\infty \right\} \end{aligned} \quad (5C-19)$$

If  $\Delta\epsilon$  denotes the maximum value of any of the elements in the  $\Omega$  matrices, then

$$|\delta C_A|_{\infty} \leq (2)(1+1+4)\Delta\epsilon = 12\Delta\epsilon \quad (5C-20)$$

since from Table 5.6-1 we see

$$\left| \int_{t_{k2}}^{t_{k2+1}} C_{Rot} W_j dt \right|_{\infty} = 2 \quad (5C-21)$$

[i.e., the maximum sum of the elements of the row vectors on the right hand side of the table]

and  $\Omega_L^0$ ,  $\Omega_L^B$  have one element per row and  $\Omega_F^B$  has two misalignment elements per row.

The maximum perturbation to  $C_A$  due to  $\delta C_B^L$  is denoted by  $\delta C_{A1}$  so that

$$|\delta C_{A1}|_{\infty} \leq 12\Delta\epsilon \quad (5C-22)$$

### Coupling of Angular Velocity

When the non-orthogonality errors of the test fixture are absorbed in the elements of  $C_F^{Ba}$  given by (5C-4) and (5C-5), the cross coupling of body angular velocity about the axis of rotation is given by

$$\left\{ \begin{array}{l} \text{Cross} \\ \text{Coupling} \\ \text{Terms} \end{array} \right\} \approx \left\{ \begin{array}{l} \Omega_F^B \begin{bmatrix} \omega_1' \\ 0 \\ 0 \end{bmatrix} \quad \text{axis of rotation} \\ \Omega_F^B \begin{bmatrix} 0 \\ \omega_2' \\ 0 \end{bmatrix} \quad \text{axis of rotation} \\ \Omega_F^B \begin{bmatrix} 0 \\ 0 \\ \omega_3' \end{bmatrix} \quad \text{axis of rotation} \end{array} \right. \quad (5C-23)$$

In each case, the coupled velocities will add four extra elements to the two vectors on the right hand side of Table 5.6-1 whose sum has an upper bound of  $4 \Delta\epsilon$  where  $\Delta\epsilon$  is the maximum value of perturbations to  $C_A$ . Two extra elements whose sum has an upper bound of  $\pi\Delta\epsilon$  will be included in the row vectors on the left hand side of Table 5.6-1. The  $4 \Delta\epsilon$  sum is larger; hence

$$|\delta C_{A_1}|_\infty + |\delta C_{A_2}|_\infty < 12\Delta\epsilon + 4\Delta\epsilon = 16\Delta\epsilon \quad (5C-24)$$

where  $\delta C_{A_2}$  is the perturbation in  $C_A$  due to the coupling of angular velocity.

#### Variation of the Rotation Angle $\theta_i$

A small variation  $\Delta\theta_i$  in  $\theta_i$  equations (5.6-29) - (5.6-31) leads to a

small perturbation term  $\Delta\theta_i$  in the unit elements of the row vectors on the right hand side of Table 5.5-1. The sum of these perturbations, in a row, is bounded by  $2 \Delta\epsilon$  where  $\Delta\epsilon$  is now the maximum of all the perturbations classified up to this point in this appendix. Furthermore, the perturbation in the row vectors on the left side of Table 5.5-1 is only  $\Delta\theta_i$ . Hence, the  $p = \infty$  norm of  $\delta C_A$ , the entire perturbation in  $C_A$ , has the bound given below.

$$|\delta C_A|_{\infty} \leq |\delta C_{A_1}|_{\infty} + |\delta C_{A_2}|_{\infty} + |\delta C_{A_3}|_{\infty} \quad (5C-25)$$

$$< 12\Delta\epsilon + 4\Delta\epsilon + 2\Delta\epsilon = 18\Delta\epsilon$$

where  $\delta C_{A_3}$  is the perturbation in  $C_A$  due to the variation in the rotation angle.

Error Due to Unmodeled Dynamic Drift in a Two State Kalman Filter

Parameters used to calculate the filter gains were:

Standard deviation of gyro drift angular rate =  $50^{\circ}/\text{hr}$

Gyro quantization = 3 arc-sec

Accelerometer quantization = 0.1 cm/sec

Filter iteration period = 0.1 sec

The resulting steady-state gains are given by

$$\underline{k}_c = \begin{bmatrix} 0.335 \\ 0.0212 \end{bmatrix} \quad (5D-1)$$

The transition matrix is given by

$$\Phi = \begin{bmatrix} 1 & 3.22 \\ 0 & 1 \end{bmatrix} \quad (5D-2)$$

A constant dynamic drift is denoted by  $M$  and when substituted into (4.5-3), Chapter 4, along with a 0.1 second filter iteration period yields

$$D_2 = 0.1 M \quad D_1 = .005 M \quad (5D-3)$$

for the drivers of error equation (4.5-6)

Substituting (5D-1) - (5D-3) into (4.5-5) and (4.5-6) results in the following error equation

$$\begin{bmatrix} e_1(n+1) \\ e_2(n+1) \end{bmatrix} = \begin{bmatrix} 0.67 & 2.16 \\ -0.0212 & 0.932 \end{bmatrix} \begin{bmatrix} e_1(n) \\ e_2(n) \end{bmatrix} + \begin{bmatrix} .107M \\ .097M \end{bmatrix} \quad (5D-4)$$

A steady-state solution requires that

$$\begin{aligned} e_1(n+1) &= e_1(n) \triangleq e_1 \\ e_2(n+1) &= e_2(n) \triangleq e_2 \end{aligned} \quad (5D-5)$$

Substituting (5D-5) into (5D-4) and solving for  $e_2$  yields

$$e_2 \approx .44 M \quad (5D-6)$$

A rotation of  $90^\circ$  in 10 seconds and a scale factor of 50,000 ppm result in a dynamic drift magnitude of

$$M = 9^\circ/\text{sec} \times .05 \times 3600 = 1620 \frac{\hat{\text{sec}}}{\text{sec}} \quad (5D-7)$$

Substitution of (5D-7) into (5D-6) results in an error given by

$$e_2 \approx 713 \hat{\text{sec}} \quad (5D-8)$$

This error in angle that is caused by the unmodeled gyro drift in the two state Kalman filter used during a rotation of the system would result in an unacceptable dynamic parameter estimation error unless the angle error is corrected through the Kalman filter post correction procedure presented in Figure 4.5-3, Chapter 4.

## References

1. Gilmore, J. P., "LCIGS Design Concept and Operating Features", C-5072, Charles Stark Draper Laboratory, Cambridge, Mass., March 1978.
2. "Critical Item Development Specification for Gyroscope Module, Strapdown, Low Cost", Specification No. SP237053 Code Ident. 18894, Charles Stark Draper Laboratory, Cambridge, Mass., November 1977.
3. "LCIGS Velocity Reference Module Specification SP237054", Preliminary C-4969, Charles Stark Draper Laboratory, Cambridge, Mass., November 1977.
4. Brock, L. D., "Application of Statistical Estimation to Navigation Systems", Ph.D. Thesis T-414, MIT Instrumentation Laboratory, June 1965.
5. Brock, L. D., and G. T. Schmidt, "Statistical Estimation in Inertial Navigation Systems", Journal of Spacecraft, Vol. 5, No. 2, 1968.
6. Bellantoni, J. F., and Koenke, E. J., "Launch Pad Alignment of a Strapdown Navigator by the Kalman Filter". AIAA Paper #68-831 AIAA Guidance, Control, and Flight Dynamics Conference, Pasadena, CA, August 12-14, 1968.
7. Ryan, T. J., "Alignment and Calibration of a Strapdown Inertial Measuring Unit", RE-67, Measurement Systems Laboratory, Massachusetts Institute of Technology, Cambridge, MA, December 1970.
8. Strunce, R. R., "Calibration and Alignment Studies", Report 0173-11433, Honeywell Aerospace Division, St. Petersburg, FL, January 1973.
9. Widnall, W. S., Grundy, P. A., and Murch, W. G., "Inertial Navigation System Tests Having Improved Observability of Error Sources", Journal of Aircraft, Vol. 13, No. 1, January 1976.
10. McKern, R., Swanson, D., and Keenan, J., "SIRU Instrument Calibration", ISS Memorandum No. 849/Rev. A, Charles Stark Draper Laboratory, Cambridge, MA, December 12, 1969.
11. Garmer, D. M., Farrell, E. J., Kau, S., and Bailey, F. N., "Strapdown Calibration and Alignment Study", NASA CR86077, 1968.
12. Morgan, A. A., "Slab Calibration for Strapdown Systems", Proceedings of the Eighth Biennial Guidance Test Symposium, Holloman Air Force Base, New Mexico, May 1977.
13. Torrey, L. W. and Boyland, R. F., "A Partitioned Estimator for the Single Slew Calibration and Alignment Technique", Memorandum T&A-19-71, Charles Stark Draper Laboratory, Cambridge, MA, November 10, 1977.

14. Savage, P. G., "Calibration Procedures for Laser Gyro Strapdown Inertial Navigation Systems", 9th Annual Electro-Optics/Laser Conference and Exhibition, Anaheim, CA, October 1977.
15. Taylor, G. R., D. J. Pasik, and J. W. Fish, "Calibration and Field Testing of a High-Quality Strapped Down Inertial Navigation System", Proceedings of the Eighth Biennial Guidance Test Symposium, Holloman Air Force Base, New Mexico, May 1977.
16. Bukow, G., "Accelerometer Module Calibration and Alignment", LCIGS Memorandum No. 77-10G-10, Charles Stark Draper Laboratory, Cambridge, Mass., 1977.
17. Britting, K. R., Inertial Navigation System Analysis, Wiley Interscience, 1971.
18. Gilmore, J. P., and Cooper, R. J., "SIRU Development Final Report, Volume I, System Development", Report R-746, Charles Stark Draper Laboratory, Cambridge, Mass., July 1973.
19. Bukow, G., Personal Communication, Group 10G Accelerometer Section, Charles Stark Draper Laboratory, Cambridge, Mass., November 18, 1977.
20. Householder, A. S., The Theory of Matrices in Numerical Analysis, Dover, 1964.
21. Fadeeva, V. N., Computational Methods of Linear Algebra, Dover, 1959.
22. Cushing, J. T., Applied Analytical Mathematics for Physical Scientists, Wiley and Sons, 1975.
23. Weinstock, H., "Design of a Precision Tilt and Vibration Isolation System", Doctor of Science Dissertation in Mechanical Engineering, Massachusetts Institute of Technology, Cambridge, Mass., 1968.
24. Merenda, F., "Module Level Test Misalignments", LCIGS Memorandum No. 77-10G-145, Charles Stark Draper Laboratory, Cambridge, Mass., August 2, 1977.
25. Pike, D., "LCIGS System Calibration - Accelerometer Linear Extrapolator", LCIGS Memorandum No. 77-10G-166, Charles Stark Draper Laboratory, Cambridge, Mass., 1977.
26. Carnahan, B., Luther, H. A., and Wilkes, J. O., Applied Numerical Methods, Wiley 1969.
27. Furman, G. G., "Improving Performance of Quantizer Feedback Systems by Use of External Dither", T-201, Electrical Engineering Department, Massachusetts Institute of Technology, Cambridge, Mass., January 1959.
28. "Designers Guide to V/F Converters", Datel Systems, Inc., Canton, Mass.

29. Musoff, H., "Strapdown System Calibration Part I - Base Motion Isolation and Accelerometer Quantization", LCIGS Memorandum No. 76-10G-046, Charles Stark Draper Laboratory, Cambridge, Mass., 1976.
30. McKern, R. A., "A Study of Transformation Algorithms for Use in Digital Computers", MIT/CSDL Report T-493, Charles Stark Draper Laboratory, Cambridge, Mass., 1968.
31. Britting, K. R. and Palsson, T., "Self Alignment Techniques for Strapdown Inertial Navigation Systems with Aircraft Application", Experimental Astronomy Laboratory Report RE-33, Massachusetts Institute of Technology, Cambridge, Mass., November 1968.
32. Musoff, H., "Basic Approach to LCIGS Fast Gyro Calibration", LCIGS Memorandum No. 77-10G-177, Charles Stark Draper Laboratory, Cambridge, Mass., September 1977.
33. Gelb, A., Applied Optimal Estimation, MIT Press, 1974.
34. Jazwinski, A. H., Stochastic Processes and Filtering Theory, Academic Press, 1970.
35. Ortega, J. M. and Rheinboldt, W. C., Iterative Solution of Nonlinear Equations in Several Variables, Academic Press, 1970.
36. Saaty, T. L., Modern Nonlinear Equations, McGraw-Hill, 1967.
37. Ogata, K., State Space Analysis of Control Systems, Prentice-Hall, 1967.
38. Booth, R., Personal Communication, Group 10G System Test Section, Charles Stark Draper Laboratory, Cambridge, Mass., August 28, 1977.
39. Wilkinson, R., "Statistical Properties of Honeywell GG-1111 and Timex IG-10 Gyros", LCIGS Memorandum No. 77-10G-175, Charles Stark Draper Laboratory, Cambridge, Mass., September 16, 1977.
40. Caffery, W., Millard, D., Schmidt, G., Thorvaldsen, T., and Vincent, K., "Inertial Navigation Strapdown Simulator", Report R-969, Charles Stark Draper Laboratory, Cambridge, Mass., February 1977.
41. Tuck, P., "Velocity Reference Digitizer Design Memo", LCIGS Memorandum No. 77-10L-003, Charles Stark Draper Laboratory, Cambridge, Mass., January 5, 1977.
42. Katz, B., "Brassboard Velocity Reference Module - Definition, Calibration and Performance Evaluation Report", LCIGS Memorandum No. 78-10G-76, Charles Stark Draper Laboratory, Cambridge, Mass., May 30, 1978.

43. Friedland, B., "On the Calibration Problem," IEEE Transactions on Automatic Control Vol. AC-22, No. 6, December 1977.
44. Bukow, G., "Accelerometer - V/F Test Equations", LCIGS Memorandum No. 77-10G-165, Charles Stark Draper Laboratory, Cambridge, Mass., September 6, 1977.

Biographical Note

Howard Musoff was born in Brooklyn, New York in 1939. He attended the New York City public schools and received the B.E.E. degree from the City College of New York in 1960. In 1966 he received the M.S. degree in electrical engineering from Northeastern University. He has been employed at The Charles Stark Draper Laboratory since 1960 and has worked on almost every aspect of inertial component and system design. This includes design of electronics for gyroscope assembly and testing, gyro research (involving the invention of a method for transferring wheel motor power to the gyro float by means of radio waves), development and implementation of the key algorithms used in the redundant strapdown SIRU system, application of a strapdown system to synthetic aperture radar motion compensation, and design of new attitude algorithms for strapdown systems. He is a member of IEEE, AIAA, SIAM, and SIGMA XI.